NATIONAL TECHNICAL UNIVERSITY OF ATHENS

SCHOOL OF CIVIL ENGINEERING

DEPARTMENT OF WATER RESOURCES AND ENVIRONMENTAL ENGINEERING

LABORATORY OF HARBOUR WORKS

Wave Input reduction methods combining numerical modelling & Machine Learning for the prediction of the annual coastal bed morphological evolution

PhD Dissertation

Andreas Papadimitriou

Athens, September 2023

ΕΘΝΙΚΟ ΜΕΤΣΟΒΙΟ ΠΟΛΥΤΕΧΝΕΙΟ

ΣΧΟΛΗ ΠΟΛΙΤΙΚΩΝ ΜΗΧΑΝΙΚΩΝ
DEPARTMENT OF WATER ΤΟΜΕΑΣ ΥΔΑΤΙΚΩΝ ΠΟΡΩΝ ΚΑΙ ΠΕΡΙΒΑΛΛΟΝΤΟΣ
ΕΡΓΑΣΤΗΡΙΟ ΛΙΜΕΝΙΚΩΝ ΕΡΓΩΝ

Σχηματοποίηση κυματικού κλίματος με χρήση μαθηματικών μοντέλων και τεχνικών μηχανικής μάθησης για την ετήσια πρόβλεψη της εξέλιξης του παράκτιου πυθμένα

ΔΙΔΑΚΤΟΡΙΚΗ ΔΙΑΤΡΙΒΗ

Για τον Επιστημονικό Τίτλο του «Διδάκτορα Μηχανικού»
στη Σχολή Πολιτικών Μηχανικών του Εθνικού Μετσόβιου Πολυτεχνείου

Ανδρέας Παπαδημητρίου

Αθήνα, Σεπτέμβριος 2023

NATIONAL TECHNICAL UNIVERSITY OF ATHENS
SCHOOL OF CIVIL ENGINEERING
DEPARTMENT OF WATER RESOURCES AND ENVIRONMENTAL ENGINEERING
LABORATORY OF HARBOUR WORKS

Wave Input reduction methods combining numerical modelling & Machine Learning for the prediction of annual coastal bed evolution

PhD THESIS
submitted for the degree of Doctor of Engineering
of the National Technical University of Athens

by
Andreas Papadimitriou

Defended in public, 22 September 2023
Athens, Greece

Members of the Examining Committee

Prof. Vasiliki Tsoukala	Sch. of Civil Eng. NTUA	*Supervisor*
Prof. Theofanis Karambas	Dep. of Civil Eng. AUTh	*Adv. Committee*
Prof. Michel Benoit	Électricité de France (EDF)	*Adv. Committee*
Assist. Prof. Vasiliki Katsardi	Sch. of Civil Eng. UTh	
Assist. Prof. Achilleas Samaras	Dep. of Civil Eng. DUTh	
Assist. Prof. Michalis Chondros	Sch. of Civil Eng. NTUA	
Prof. Christos Makropoulos	Sch. of Civil Eng. NTUA	

What distinguishes a mathematical model from, say, a poem, a song, a portrait or any other kind of "model", is that the mathematical model is an image or picture of reality painted with logical symbols instead of with words, sounds or watercolors.
John L. Casti

The purpose of models is not to fit the data but to sharpen the questions.
Samuel Karlin

Acknowledgements

Dedicated to my parents Giorgos & Afroditi,
my sister Anastasia,
my grandmother Kyriaki
& my partner Efi

Contents

Abstract

Wave Input reduction methods combining numerical modelling & Artificial Intelligence for the prediction of the annual coastal bed morphological evolution

by Andreas Papadimitriou

National Technical University of Athens
School of Civil Engineering
Department of Water Resources and Environmental Engineering
Laboratory of Harbour Works

The numerical prediction of coastal bed evolution has been at the forefront of coastal engineering research for several decades. Even though numerical models are capable of resolving in great detail the coastal processes driving the morphological bed evolution, they are associated with staggering computational burden, rendering a long-term prediction a tedious task. The burden further increases considering the vast amount of input wave characteristics that are used to force the models. To counterbalance this, various wave input reduction methods have been developed and employed in coastal engineering practice.

Despite their widespread usage, a need to further accelerate the morphological simulations, while simultaneously improving the reliability of the wave input reduction methods was identified. This thesis undertakes a systematic effort to thoroughly evaluate various types of wave input reduction methods and provide practical guidelines on the optimal method selection and configuration.

Two new wave binning wave input reduction methods were conceptualized and implemented in the coastal area of Rethymno, in Greece. These methods focus on the elimination of sea-states considered unable to initiate sediment motion, effectively reducing the length of the forcing timeseries. The newly developed methods produced reliable results compared to the widely used energy flux input reduction method but also achieved a significant model run time reduction of up to 62%, compared to a brute force simulation containing the full forcing timeseries.

Additionally, the K-Means clustering algorithm was thoroughly evaluated as a viable alternative to the classical binning input reduction methods and several enhancements were proposed aiming to overturn the unsupervised nature of the clustering algorithm. Implementation of the configurations in the coastal area of Rethymno showcased that the default parametrization of the algorithm can produce satisfactory predictions of annual coastal bed evolution. All the proposed enhancements, exhibited a performance increase compared to the default parametrization, however they added a degree of complexity in the algorithm implementation.

A systematic evaluation of the Representative Morphological Wave Height selection approaches was also carried out, with the development of three new alternative configurations. Notable was the training and validation of an Artificial Neural Network that is included in one of the methods and is tasked with the elimination of lowly energetic sea-states that have little to no effect in the morphological bed evolution. The three proposed enhancements provided a noteworthy performance increase compared to the traditional method, with the best performing one being the method incorporating the Artificial Neural Network.

Last but not least, selected input reduction methods were compared with available field measurements at the coastal area of Eresos, Lesvos in Greece, in an attempt to investigate the reliability of wave input reduction methods in real-life settings. The numerical model forced with three selected input reduction methods reproduced the morphological bed evolution in a very satisfying manner, with the best performing being once again the one incorporating the Artificial Neural Network.

This thesis provides a thorough evaluation of wave input reduction methods, testing several configurations and enhancements, validating their use against both benchmark numerical predictions and field measurements. The incorporation of machine learning in wave input reduction can further increase the reliability of model predictions, leading to a significant reduction of the required computational effort.

Extended Abstract *(in Greek)*

Σχηματοποίηση κυματικού κλίματος με χρήση μαθηματικών μοντέλων και τεχνικών μηχανικής μάθησης για την ετήσια πρόβλεψη της εξέλιξης του παράκτιου πυθμένα

Ανδρέας Παπαδημητρίου

Σχολή Πολιτικών Μηχανικών
Τομέας Υδατικών Πόρων και Περιβάλλοντος
Εργαστήριο Λιμενικών Έργων

1. Εισαγωγή

1.1. Υπόβαθρο, κίνητρα και ερευνητικοί στόχοι

Οι παράκτιες ζώνες συγκεντρώνουν ιστορικά μεγάλο μέρος του παγκόσμιου πληθυσμού, καθώς προσφέρουν ευκαιρίες για ανάπτυξη πολλών οικονομικών δραστηριοτήτων και συνδυάζουν την ταυτόχρονη συνύπαρξη πολύπλοκων οικοσυστημάτων. Συνεπώς η πρόβλεψη της μορφολογικής εξέλιξης του παράκτιου πυθμένα, με απώτερο στόχο την προστασία των ακτών από τη διάβρωση, βρίσκεται στο επίκεντρο της έρευνας της παράκτιας μηχανικής εδώ και αρκετές δεκαετίες.

Παραδοσιακά, η πρόβλεψη της μορφολογικής εξέλιξης του παράκτιου πυθμένα σε ετήσια βάση πραγματοποιείται με μαθηματικά μοντέλα που επικεντρώνονται στην προσομοίωση των παράκτιων διεργασιών. Μεγάλος αριθμός μαθηματικών μοντέλων που επιτελούν αυτό το σκοπό βρίσκονται διαθέσιμα (Roelvink and Renniers, 2011), καθένα με διαφορετικά πλεονεκτήματα και μειονεκτήματα (Afentoulis et al., 2022), ενώ η επιλογή του κατάλληλου μοντέλου εξαρτάται από την χωρική και χρονική κλίμακα καθώς και την περιοχή εφαρμογής. Στην περίπτωση που η εξεταζόμενη παράκτια περιοχή χαρακτηρίζεται από πολύπλοκη βαθυμετρία, που συνδυάζεται και με ταυτόχρονη παρουσία λιμενικών και παράκτιων έργων, τότε μαθηματικά μοντέλα περιοχής (Roelvink and Renniers, 2011) εφαρμόζονται σχεδόν αποκλειστικά.

Ενώ αυτή η κατηγορία μοντέλων μπορεί με μεγάλη ακρίβεια να περιγράψει τις μορφοδυναμικές μεταβολές λόγω της συνδυασμένης δράσης κυματισμών και ρευμάτων, ταυτόχρονα συνδέεται με ιδιαίτερα επαυξημένο υπολογιστικό φόρτο, που κάνει την ετήσια πρόβλεψη της παράκτιας μορφολογίας σχεδόν απαγορευτική για πρακτικές εφαρμογές. Συνυπολογίζοντας την πληθώρα διαθέσιμων ωκεανογραφικών δεδομένων τα οποία είναι διαθέσιμα πλέον σε παγκόσμια κλίμακα, και τα οποία εισάγονται ως οριακές συνθήκες στα μοντέλα περιοχής περαιτέρω προσαυξάνοντας τον υπολογιστικό φόρτο, είναι εμφανής η αναγκαιότητα για την επιτάχυνση των αριθμητικών προσομοιώσεων μορφοδυναμικών μεταβολών σε ετήσια βάση.

Σε αυτή την κατεύθυνση, έχουν αναπτυχθεί μια σειρά μεθόδων σχηματοποίησης του κυματικού κλίματος (Benedet et al., 2016), με σκοπό τη μείωση των διαθέσιμων οριακών συνθηκών και την αντικατάσταση τους με ένα πεπερασμένο αριθμό κυματικών

αντιπροσώπων (6-30 συνήθως) που θα είναι ικανοί να προκαλέσουν αντίστοιχη μορφολογική εξέλιξη πυθμένα με την πλήρη χρονοσειρά κυματικών χαρακτηριστικών. Οι μέθοδοι σχηματοποίησης κυματικού κλίματος μπορούν να ομαδοποιηθούν σε τρεις ευρύτερες κατηγορίες (α) *Ισοδύναμοι κυματισμοί* (Borah and Balloffet, 1985; Brown and Davies, 2009; Chondros et al., 2022; Chonwattana et al., 2005; Karambas et al., 2013; Papadimitriou et al., 2022a; Pletcha et al., 2007) (β) *Μέθοδοι σχηματοποίησης σε κλάσεις* (Benedet et al., 2016; de Queiroz et al., 2019; Papadimitriou et al., 2020; Van Duin et al., 2004; Walstra et al., 2013), (γ) Αλγόριθμοι ομαδοποίησης (de Queiroz et al., 2019; Papadimitriou and Tsoukala, 2022).

Παρά την ευρεία τους διάδοση και εφαρμογή, τα αποτελέσματα των μεθόδων σχηματοποίησης εξαρτώνται από μια σειρά παραμέτρων (π.χ. αριθμός αντιπροσώπων, διάρκεια κυματικού κλίματος, αλληλουχία αντιπροσώπων), ενώ η μείωση του χρόνου προσομοίωσης δεν είναι τόσο εμφανής όταν λαμβάνεται υπόψη η πλήρης αλληλεπίδραση μεταξύ του κυματικού, υδροδυναμικού και μορφολογικού μοντέλου. Ο στόχος της παρούσας διατριβής είναι η συστηματική αξιολόγηση μεθόδων σχηματοποίησης και των τριών κατηγοριών που αναλύθηκαν και η ανάπτυξη νέων με απώτερο σκοπό την περαιτέρω επιτάχυνση των μορφολογικών προσομοιώσεων αλλά και την αύξηση της ακρίβειας των αποτελεσμάτων.

Οι ερευνητικοί στόχοι της παρούσας διατριβής είναι οι εξής:

- Η διερεύνηση και ανάπτυξη νέων μεθόδων σχηματοποίησης κυματικού κλίματος, που θα περιέχουν την εισαγωγή κατάλληλου φίλτρου για την απάλειψη θαλάσσιων καταστάσεων που δεν κρίνονται ικανές να πραγματοποιήσουν έναρξη κίνησης ιζήματος, μειώνοντας έτσι σημαντικά τον απαιτούμενο υπολογιστικό φόρτο.

- Η αξιολόγηση της εφαρμοσιμότητας αλγορίθμων ομαδοποίησης σαν μεθόδους σχηματοποίησης κυματικού κλίματος και η διερεύνηση πιθανών βελτιώσεων τους, σε μια προσπάθεια να εισαχθούν στην αλγοριθμική διαδικασία ποσότητες που είναι απαραίτητες για την μακροχρόνια μορφολογική εξέλιξη του πυθμένα.

- Την εισαγωγή μεθόδων μηχανικής μάθησης μέσω ενός κατάλληλα εκπαιδευμένου Τεχνητού Νευρωνικού Δικτύου, το οποίο θα ενισχύει περαιτέρω την ελάφρυνση του υπολογιστικού φόρτου σε συνδυασμό με την ενίσχυση της ακρίβειας των αποτελεσμάτων.

- Την εφαρμογή των μεθόδων σχηματοποίησης που θα αναπτυχθούν σε δύο παράκτιες περιοχές, εκ των οποίων στη μια θα πραγματοποιηθεί και σύγκριση με μετρήσεις πεδίου, για να αξιολογηθεί η απόδοση των μεθόδων σχηματοποίησης και να προταθούν έτσι κατάλληλες κατευθυντήριες για πρακτικές εφαρμογές.

1.2. Πρωτότυπα σημεία

Η παρούσα διατριβή επικεντρώνεται στην ανάπτυξη και αξιολόγηση μεθόδων σχηματοποίησης κυματικού κλίματος για την επιτάχυνση των απαιτητικών -ως προς

τους υπολογιστικούς πόρους- προσομοιώσεων μορφολογικής εξέλιξης πυθμένα. Τα κυριότερα πρωτότυπα σημεία είναι τα ακόλουθα:

- Εισάγεται μια καινοτόμα προσέγγιση στις κλασικές μεθόδους σχηματοποίησης σε κλάσεις, που επικεντρώνεται στη απαλοιφή θαλάσσιων καταστάσεων που δε θεωρούνται ικανές να θέσουν σε κίνηση τα παράκτια ιζήματα. Το αποτέλεσμα αυτής της προσέγγισης είναι η σημαντική μείωση της υπολογιστικού φόρτου λόγω της μείωσης του χρόνου προσομοίωσης του μαθηματικού μοντέλου.

- Οι αλγόριθμοι ομαδοποίησης αξιολογούνται για πρώτη φορά σε μια εκτεταμένη παράκτια περιοχή με σημαντική μεταβλητότητα, ως ικανοποιητικές μέθοδοι σχηματοποίησης κυματικού κλίματος. Έξι εναλλακτικές διαμορφώσεις του ευρέως χρησιμοποιούμενου αλγόριθμου ομαδοποίησης K-Means αξιολογήθηκαν με στόχο την βελτίωση της απόδοσής του.

- Αξιολόγηση της μεθόδου σχηματοποίησης των ισοδύναμων κυματισμών, με την ταυτόχρονη συμπερίληψη τεχνητού νευρωνικού δικτύου με σκοπό την βελτίωση των αποτελεσμάτων της μεθόδου.

- Συγκριτική αξιολόγηση των μεθόδων σχηματοποίησης κυματικού κλίματος και επαλήθευση των αποτελεσμάτων με διαθέσιμες μετρήσεις πεδίου βαθυμετρίας στην περιοχή της Ερεσού στη Λέσβο.

2. Μαθηματική προσομοίωση μορφολογικής εξέλιξης πυθμένα και βασικές αρχές σχηματοποίησης κυματικού κλίματος

2.1. Μαθηματική προσομοίωσης μορφολογικής εξέλιξης πυθμένα

Οι παράκτιες περιοχές αποτελούν δυναμικά συστήματα που φιλοξενούν διάφορες μορφές ζωής και ανθρώπινες δραστηριότητες. Περίπου ο μισός πληθυσμός του πλανήτη ζει και εργάζεται σε μερικές εκατοντάδες χιλιόμετρα από μια ακτογραμμή. Ωστόσο, παράκτιος πυθμένας και το σχήμα των ακτών μεταβάλλονται συνεχώς λόγω της συνύπαρξης πολλών μηχανισμών. Ο βασικότερος μηχανισμός που θέτει σε κίνηση τα παράκτια ιζήματα προκαλώντας αυτές τις μορφολογικές μεταβολές, είναι τα επιφανειακά κύματα βαρύτητας, ενώ τα κυματογενή ρεύματα αναλαμβάνουν τη συνεπακόλουθη μεταφορά των ιζημάτων.

Για την κατανόηση και την πρόβλεψη της εξέλιξης του παράκτιου πυθμένα υπό τη συνδυασμένη δράση κυματισμών και ρευμάτων, χρησιμοποιούνται αριθμητικά μοντέλα, που βασίζονται στην προσομοίωση των παράκτιων διεργασιών. Αυτά τα μοντέλα μπορούν να χωριστούν σε τρεις βασικές κατηγορίες:

- μοντέλα παράκτιας διατομής (Roelvink and Brocker, 1993), που εστιάζουν κυρίως στην εξέλιξη διατομών του παράκτιου μετώπου λόγω της εγκάρσιας στερεομεταφοράς, αγνοώντας συνήθως την κατά μήκους της ακτής διαφοροποίηση των διατομών.

- μοντέλα εξέλιξης ακτογραμμής (Szmytkiewicz et al., 2000), που εστιάζουν στην εξέλιξη της ακτογραμμής λόγω της κατά μήκους της ακτής στερεομεταφοράς, με

την παραδοχή ότι οι διατομές των παράκτιων μετώπων διατηρούν το σχήμα τους σταθερό.

- μοντέλα παράκτιας περιοχής (de Vriend et al., 1993), στα οποία δεν υπάρχει διάκριση της κατά μήκους και εγκάρσιας στερεομεταφοράς, και αποτελούνται από τη σύζευξη κυματικών, υδροδυναμικών και μοντέλων μορφολογίας, υπολογίζοντας την μεταβολή της βαθυμετρίας σε κάθε κελί του υπολογιστικού πεδίου.

Η επιλογή του κατάλληλου μοντέλου εξαρτάται από την χωρική και χρονική κλίμακα του φαινομένου που εξετάζεται. Για παράδειγμα, τα μοντέλα παράκτιας διατομής χρησιμοποιούνται κυρίως για την αποτίμηση της επίδρασης καταιγίδων στην μορφολογική εξέλιξη μεμονωμένων προφίλ ακτογραμμής, ενώ τα μοντέλα εξέλιξης ακτογραμμής χρησιμοποιούνται για την πρόβλεψη της μακροχρόνια εξέλιξη κυρίως ευθειογενών ακτών, χωρίς πολύπλοκα γεωμορφολογικά χαρακτηριστικά. Σε παράκτιες περιοχές μεγέθους μερικών χιλιομέτρων, με την παρουσία λιμενικών και παράκτιων έργων, σε χρονικό ορίζοντα 1-5 έτη, η πρόβλεψη της μορφολογικής εξέλιξης πραγματοποιείται σχεδόν αποκλειστικά μέσω των μοντέλων παράκτιας περιοχής, λόγω της γεωμορφολογικής πολυπλοκότητας και της αδυναμίας διάκρισης μεταξύ κατά μήκους και εγκάρσιας στερεομεταφοράς.

Τα μοντέλα παράκτιας περιοχής αποτελούνται από ένα κυματικό μοντέλο, που αναλαμβάνει τη διάδοση των κυματισμών, ένα υδροδυναμικό μοντέλο που υπολογίζει τα αναπτυσσόμενα κυματογενή ή άλλων τύπων παράκτια ρεύματα και ένα μοντέλο στερεομεταφοράς μορφολογίας, που δίνει σαν τελικό αποτέλεσμα την εξέλιξη της βαθυμετρίας υπό τη συνδυασμένη δράση κυματισμών και ρευμάτων. Σε αυτό το σημείο είναι σημαντικό να παρουσιαστούν οι δύο προσεγγίσεις που μπορούν να ακολουθηθούν και αφορούν τον τρόπο με τον οποίο λαμβάνεται υπόψη η αλληλεπίδραση των επιμέρους τμημάτων που διαμορφώνουν τα μοντέλα παράκτιας περιοχής:

- Η «Μορφοδυναμική» προσέγγιση, κατά την οποία λαμβάνεται υπόψη η πλήρης αλληλεπίδραση μεταξύ κυμάτων, ρευμάτων και μορφολογίας σε κάθε χρονικό βήμα του μαθηματικού μοντέλου, και στην οποία όλες οι θαλάσσιες καταστάσεις που έχουν επιλεγεί για την προσομοίωση εισέρχονται σαν μια ενιαία χρονοσειρά.
- Η «Μορφοστατική» προσέγγιση, κατά την οποία κάθε θαλάσσια κατάσταση προσομοιώνεται ανεξάρτητα από τις υπόλοιπες, ξεκινώντας από την ίδια αρχική βαθυμετρία. Υπό αυτό το πρίσμα, δε λαμβάνεται υπόψη η πλήρης αλληλεπίδραση μεταξύ κυματικών, υδροδυναμικών διεργασιών και μορφολογικής εξέλιξης.

Και οι δύο προσεγγίσεις των μορφολογικών προσομοιώσεων συνδέονται με ιδιαίτερα αυξημένο υπολογιστικό φόρτο, έχοντας οδηγήσει στην ανάπτυξη διάφορων μεθόδων επιτάχυνσης των μορφολογικών προσομοιώσεων, που μπορούν να διακριθούν στις ακόλουθες κατηγορίες σύμφωνα με τους de Vriend et al., 1993:

- Μείωση μοντέλου, στην οποία οι διεργασίες μικρότερης κλίμακας δεν περιγράφονται με μεγάλη λεπτομέρεια, με εκμετάλλευση της διαφοράς στην κλίμακα που συντελούνται οι μεταβολές στο υδροδυναμικό πεδίο και στη

μορφολογία. Η κυριότερη μέθοδος μείωσης μοντέλου είναι ο συντελεστής μορφολογικής επιτάχυνσης (Lesser, 2009).

- Μοντελοποίηση προσανατολισμένη στη συμπεριφορά, στην οποία δεν λαμβάνεται υπόψη η πλήρης πολυπλοκότητα βασικών παράκτιων διεργασιών, με τη χρήση τεχνικών όπως οι απλοποιητικές οριακές συνθήκες μετακίνησης ακτογραμμής ().

- Σχηματοποίηση κυματικού κλίματος, η οποία βασίζεται στην λογική της κατάλληλης επιλογής ενός περιορισμένου αριθμού αντιπροσωπευτικών κυματικών συνθηκών, που μπορούν να αναπαράγουν με ικανοποιητική ακρίβεια τις μορφολογικές μεταβολές της πλήρους χρονοσειράς κυματικού κλίματος σε ορίζοντα μερικών ετών.

Λόγω της πληθώρας των διαθέσιμων κυματικών χαρακτηριστικών στα ανοιχτά που προέρχονται από ωκεανογραφικές βάσεις δεδομένων, που προσαυξάνουν σημαντικά τα διαθέσιμα δεδομένα εισόδου που απαιτούνται για την ετήσια πρόβλεψη της παράκτιας μορφολογικής εξέλιξης, η παρούσα διατριβή εστιάζει στην αξιολόγηση και περαιτέρω ανάπτυξη των μεθόδων σχηματοποίησης κυματικού κλίματος.

2.2. Βασικές αρχές μεθόδων σχηματοποίησης κυματικού κλίματος

Με την παραδοχή ότι στην παράκτια περιοχή που εξετάζεται είναι μερικές δεκάδες τετραγωνικά χιλιόμετρα και το εύρος παλίρροιας δεν εμφανίζει σημαντικές διακυμάνσεις, ο κύριος παράγοντας που καθορίζει την μορφολογική εξέλιξη του πυθμένα είναι η δράση των κυματισμών. Για την σχηματοποίηση του κυματικού κλίματος συνήθως τα δεδομένα εισόδου είναι μια χρονοσειρά κυματικών χαρακτηριστικών, αποτελούμενη κατ' ελάχιστον από το χαρακτηριστικό ύψος κύματος, την περίοδο κορυφής του φάσματος των κυματισμών και τη γωνία πρόσπτωσης των κυματισμών ως προς την κάθετη στην ακτογραμμή.

Σε περίπτωση απουσίας μετρήσεων παράκτιας βαθυμετρίας στην περιοχή που εξετάζεται, η αποτίμηση της απόδοσης των μεθόδων σχηματοποίησης κυματικού κλίματος συνίσταται στη σύγκριση των αποτελεσμάτων του μοντέλου παράκτιας περιοχής που έχει ως δεδομένα εισόδου τις απομειωμένες κυματικές συνθήκες με μια «προσομοίωση αναφοράς» η οποία διενεργείται λαμβάνοντας υπόψη την πλήρη χρονοσειρά των κυματικών συνθηκών.

Το κύριο στατιστικό μέγεθος για την αποτίμηση της ικανότητας του μορφολογικού μοντέλου να προβλέψει ικανοποιητικά τις μορφολογικές μεταβολές είναι το Brier Skill Score (BSS), που υπολογίζεται από την ακόλουθη εξίσωση:

$$BSS = 1 - \frac{MSE(Y,X)}{MSE(B,X)} = 1 - \frac{\langle (Y-X)^2 \rangle}{\langle (B-X)^2 \rangle} \tag{1}$$

όπου Y είναι η τελική βαθυμετρία όπως προκύπτει από την προσομοίωση των κυματικών αντιπροσώπων, X η τελική βαθυμετρία που έχει προκύψει από την προσομοίωση αναφοράς και B η αρχική βαθυμετρία.

Στη συνέχεια θα αναλυθούν με μεγαλύτερη λεπτομέρεια τα βασικά στοιχεία των τριών βασικών κατηγοριών σχηματοποίησης κυματικού κλίματος.

2.2.1. Μέθοδοι σχηματοποίησης ισοδύναμων κυματισμών

Η συγκεκριμένη κατηγορία αποτελεί την παλαιότερη κατηγορία σχηματοποίησης κυματικού κλίματος, που όμως εφαρμόζεται έως και σήμερα σε ένα μεγάλο πλήθος εφαρμογών (Borah and Balloffet, 1985; Brown and Davies, 2009; Chondros et al., 2022; Chonwattana et al., 2005; Karambas et al., 2013; Papadimitriou et al., 2022a; Pletcha et al., 2007). Η κεντρική ιδέα των περισσότερων μεθόδων αυτής της κατηγορίας είναι ο διαχωρισμός των διαθέσιμων κυματικών χαρακτηριστικών σε κλάσεις σταθερού πλάτους αναφορικά με τη διεύθυνση πρόσπτωσης των κυματισμών. Στη συνέχεια σε κάθε κλάση, υπολογίζεται ένας κυματικός αντιπρόσωπος που έχει το ίδιο δυνητικό «ενεργειακό περιεχόμενο» με τα κυματικά χαρακτηριστικά της κλάσης που ανήκει.

Η μέθοδος των Chonwattana et al., 2005, βασίζεται στην παραδοχή της διατήρησης της κατά μήκος της ακτής ροής ενέργειας των κυματισμών, η οποία συμμετέχει καθοριστικά στη μορφολογική εξέλιξη του πυθμένα σε ένα μεσοπρόθεσμο χρονικό ορίζοντα (μήνες-χρόνια). Με βάση της διατήρησης της ροής ενέργειας κατά μήκους μιας ακτίνας διάδοσης κυματισμών προκύπτει το ακόλουθο σύστημα εξισώσεων για τον υπολογισμό σταθερό ποσοτήτων για όλα τα κυματικά χαρακτηριστικά που ανήκουν στην κάθε κλάση διεύθυνσης πρόσπτωσης:

$$
\begin{cases}
H_s^2 T_p \sin a_o = C_1 \\
H_s^2 T_p \cos a_o = C_2 \\
H_s^{2.5} \cos(a_o^{0.25}) \sin(2a_o) = C_3
\end{cases}
\tag{2}
$$

Στη συνέχεια, σε κάθε κλάση υπολογίζεται μια «ισοδύναμη τιμή» για κάθε έναν από τους συντελεστές C_1, C_2 και C_3, σαν σταθμισμένος μέσο όρος όπου η συχνότητα εμφάνισης (f_i) κάθε θαλάσσιας κατάστασης τίθεται σα συντελεστής βάρους στον υπολογισμό.

$$
\begin{cases}
C_{1,e} = \dfrac{\sum f_i C_{1,i}}{\sum f_i} \\[2ex]
C_{2,e} = \dfrac{\sum f_i C_{2,i}}{\sum f_i} \\[2ex]
C_{3,e} = \dfrac{\sum f_i C_{3,i}}{\sum f_i}
\end{cases}
\tag{3}
$$

Τέλος, σε κάθε κλάση υπολογίζεται ένας αντιπρόσωπος, τα κυματικά χαρακτηριστικά του οποίου υπολογίζονται από την ακόλουθη εξίσωση:

$$
\begin{cases}
a_{o,e} = \tan^{-1} \dfrac{C_{1,eq}}{C_{2,eq}} \\[2ex]
H_{s,e} = \left[\dfrac{C_{3,eq}}{(\cos a_o)^{0.25} \sin(2a_{o,eq})} \right]^{2/5} \\[2ex]
T_{p,e} = \dfrac{C_{2,eq}}{H_{s,eq}^2 \cos a_{o,eq}}
\end{cases}
\tag{4}
$$

όπου $a_{o,e}$, $H_{s,e}$ και $T_{p,e}$ είναι οι ισοδύναμες τιμές της διεύθυνσης διάδοσης, χαρακτηριστικού ύψους κύματος και περιόδου κορυφής των κυματισμών αντίστοιχα.
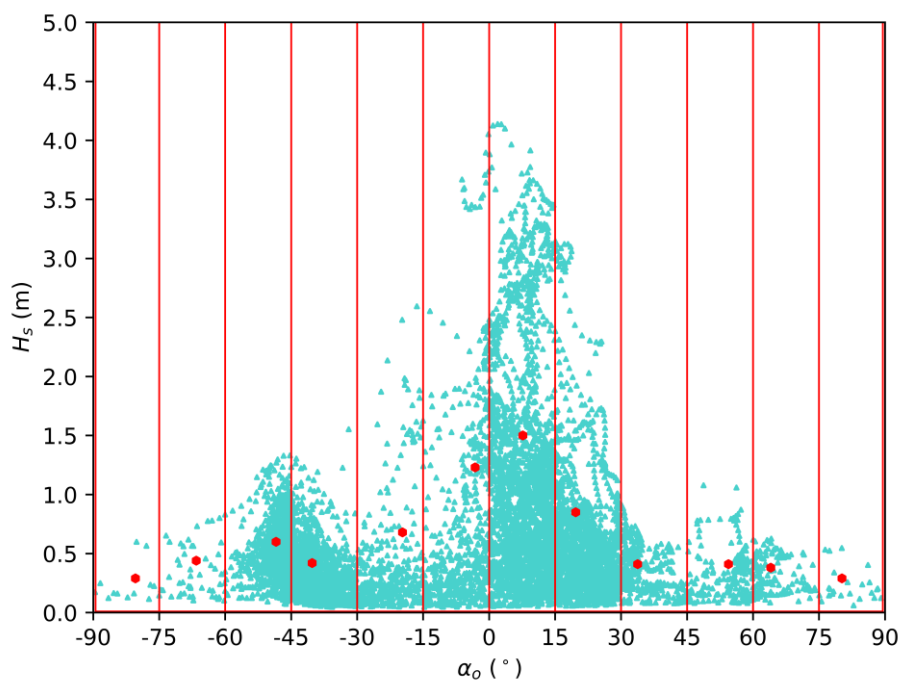
Σχήμα 1. Διαχωρισμός σε κλάσεις και κυματικοί αντιπρόσωποι με τη μέθοδο σχηματοποίησης ισοδύναμων κυματισμών Chonwattana et al., 2005

Η μέθοδος των Chonwattana et al., 2005, αποδίδει καλά αποτελέσματα ακόμη και με ένα μικρό σχετικά (<6) αριθμό αντιπροσώπων, ωστόσο ανά περιπτώσεις το γεγονός ότι οι κλάσεις έχουν σταθερό πλάτος ως προς τη διεύθυνση διάδοσης των κυματισμών, μπορεί δυνητικά να οδηγήσει σε μη ικανοποιητική περιγραφή των κυματισμών με μεγαλύτερο ενεργειακό περιεχόμενο που ίσως επιδρούν σημαντικά στην εξέλιξη της παράκτιας μορφολογίας. Στο Σχήμα 1 παρουσιάζεται ο διαχωρισμός σε 12 κλάσεις και οι κυματικοί αντιπρόσωποι με την εφαρμογή της μεθόδου των Chonwattana et al., 2005 σε ένα σύνολο δεδομένων ωριαίων κυματικών χαρακτηριστικών διάρκειας ενός έτους.

2.2.1. Μέθοδοι σχηματοποίησης κυματισμών σε κλάσεις

Οι μέθοδοι σχηματοποίησης σε κλάσεις αποτελούν μια μετεξέλιξη των μεθόδων ισοδύναμων κυματισμών, που αποτελούν τη πιο διαδεδομένη μορφή σχηματοποίησης κυματικού κλίματος και έχουν εφαρμοστεί σε μια πληθώρα επιστημονικών ερευνών (π.χ. Benedet et al., 2016; de Queiroz et al., 2019; Papadimitriou et al., 2020; Van Duin et al., 2004; Walstra et al., 2013). Οι αντιπρόσωποι καθορίζονται διαχωρίζοντας το κυματικό κλίμα σε κλάσεις μεταβλητού πλάτους, ενώ κάθε κλάση περιέχει το ίδιο ποσοστό μιας ποσότητας που θεωρείται καθοριστική για την εξέλιξη της παράκτιας μορφολογίας σε μεσοπρόθεσμο χρονικό ορίζοντα (π.χ. κατά μήκος της ακτής στερεομεταφορά, ροή ενέργειας των κυματισμών). Με βάση την επιλογή αυτής της ποσότητας, στη διεθνή βιβλιογραφία εντοπίζονται οι ακόλουθες μέθοδοι σχηματοποίησης κυματισμών σε κλάσεις:

- Μέθοδος κλάσεων σταθερού πλάτους
- Μέθοδος ροής ενέργειας
- Μέθοδος κατά μήκος της ακτής στερεομεταφοράς

- Μέθοδος ροής ενέργειας με ακραίες κυματικές συνθήκες
- Μέθοδος Opti

Στο Σχήμα 2, απεικονίζεται ο διαχωρισμός ενός συνόλου δεδομένων ωριαίων κυματικών χαρακτηριστικών διάρκειας ενός έτους, σε 12 κλάσεις με τη μέθοδο της ροής ενέργειας.
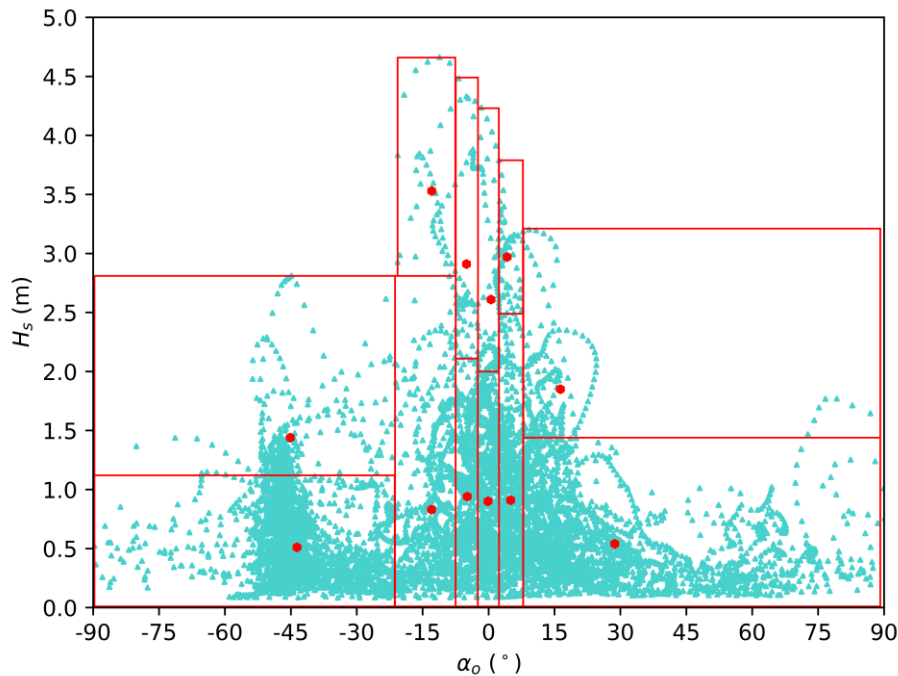
Σχήμα 2. Διαχωρισμός σε κλάσεις και κυματικοί αντιπρόσωποι με τη μέθοδο σχηματοποίησης σε κλάσεις της ροής ενέργειας

Στις έρευνες των Benedet et al., 2016 και de Quieiroz et al., 2019, πραγματοποιήθηκε μια εκτενής συγκριτική αξιολόγηση και ανάλυση ευαισθησίας των μεθόδων σχηματοποίησης κυματισμών σε κλάσεις, με τη μέθοδο ροής ενέργειας και κατά μήκος της ακτής στερεομεταφοράς να δίνουν τα πιο ικανοποιητικά αποτελέσματα.

2.2.1. Μέθοδοι σχηματοποίησης αλγορίθμων ομαδοποίησης

Οι αλγόριθμοι ομαδοποίησης είναι μια κατηγορία μηχανικής μάθησης που χρησιμοποιούνται για την ομαδοποίηση παρόμοιων αντικειμένων ή δεδομένων χωρίς επίβλεψη. Ο στόχος είναι να εντοπιστούν εγγενή μοτίβα ή συγκεκριμένες δομές στα δεδομένα χωρίς να υπάρχει πρότερη γνώση για το πώς αυτά συνδέονται και αλληλεπιδρούν μεταξύ τους. Οι αλγόριθμοι ομαδοποίησης μπορούν να διακριθούν σε τρεις βασικές κατηγορίες:

- Αλγόριθμοι με βάση την επιλογή κεντροειδών
- Αλγόριθμοι ιεράρχησης
- Αλγόριθμοι ομαδοποίησης με βάση την πυκνότητα των δεδομένων

Η πρώτη κατηγορία, είναι αυτή που παρουσιάζει τις περισσότερες δυνατότητες για εφαρμογή σε περιπτώσεις σχηματοποίησης και βασίζεται στη εκχώρηση των δεδομένων σε συστάδες με βάση την εγγύτητα τους στα επιλεγμένα κεντροειδή. Ο καθορισμός των συστάδων και των κεντροειδών γίνεται με μια επαναληπτική διαδικασία που μεταβάλλει τη θέση των κεντροειδών και των αντίστοιχων συστάδων με βάση τις αποστάσεις μεταξύ

των δεδομένων και των κεντροειδών. Ο πιο διαδεδομένος αλγόριθμος αυτού του τύπου είναι ο K-Means (MacQueen, 1967).

Στο Σχήμα 3, απεικονίζεται η ομαδοποίηση ενός συνόλου δεδομένων ωριαίων κυματικών χαρακτηριστικών διάρκειας ενός έτους, σε 12 κλάσεις με χρήση του αλγορίθμου K-Means.
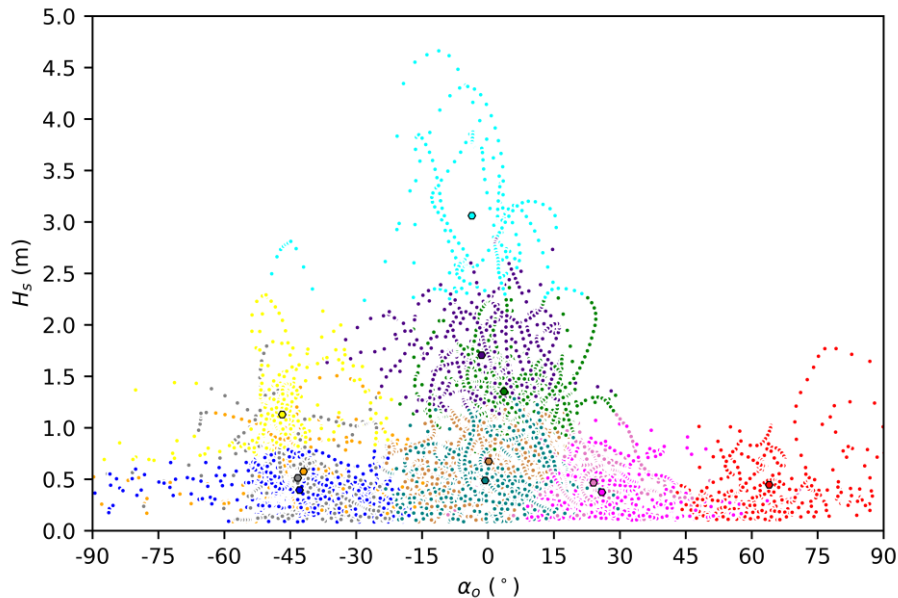
Σχήμα 3. Διαχωρισμός σε κλάσεις και κυματικοί αντιπρόσωποι με τον αλγόριθμο ομαδοποίησης K-Means

Ενώ οι αλγόριθμοι ομαδοποίησης έχουν εφαρμοστεί σε ένα πλήθος εφαρμογών σε πολλές επιστήμες μεταξύ των οποίων και η ωκεανογραφία (Martzikos et al., 2018), η εφαρμογή τους σαν μέθοδος σχηματοποίησης κυματικού κλίματος είναι περιορισμένη (de Queiroz et al., 2019; Papadimitriou and Tsoukala, 2022).

Αναγνωρίζοντας τα εγγενή χαρακτηριστικά των τριών βασικών κατηγοριών σχηματοποίησης κυματικού κλίματος που παρουσιάστηκαν, καθώς και τα πλεονεκτήματα/μειονεκτήματα της εφαρμογής τους, στο πλαίσιο της διδακτορικής διατριβής πραγματοποιήθηκαν βήματα για να προταθούν βελτιώσεις και να αναπτυχθούν νέες μέθοδοι σχηματοποίησης και για τις τρεις προαναφερθείσες κατηγορίες.

3. Μια καινοτόμα προσέγγιση στις μεθόδους σχηματοποίησης σε κλάσεις

Ενώ οι μέθοδοι σχηματοποίησης σε κλάσεις έχουν εφαρμοστεί σε μια μεγάλη πληθώρα εφαρμογών με ικανοποιητικά αποτελέσματα (Walstra et al., 2013; Benedet et al., 2016), όταν οι προσομοιώσεις του μοντέλου παράκτιας περιοχής πραγματοποιούνται με την «Μορφοδυναμική προσέγγιση», η οικονομία χρόνου με την εφαρμογή των μεθόδων σχηματοποίησης δεν είναι τόσο σημαντική σε σύγκριση με την προσομοίωση αναφοράς που περιλαμβάνει την πλήρη χρονοσειρά κυματικών χαρακτηριστικών στα ανοιχτά. Αυτό συμβαίνει γιατί ο συνολικός χρόνος προσομοίωσης πρέπει να είναι ο ίδιος μεταξύ των δύο προσομοιώσεων.

Σε αυτή τη διατριβή αναπτύχθηκαν δύο νέες μέθοδοι σχηματοποίησης σε κλάσεις, που και οι δύο βασίζονται στην αρχή της απαλοιφής θαλάσσιων καταστάσεων που θεωρείται ότι δεν προκαλούν σημαντική κίνηση ιζήματος στα ρηχά και άρα συμμετέχουν ελάχιστα στη μορφολογική εξέλιξη του πυθμένα. Με αυτόν τον τρόπο επιτυγχάνεται η σημαντική εξοικονόμηση του χρόνου των προσομοιώσεων. Αναπτύχθηκαν δύο μεθοδολογίες, η μέθοδος **Pick-up rate** και η μέθοδος **Threshold Current Speed** οι βασικές αρχές των οποίων παρουσιάζονται στη συνέχεια.

3.1. Βασικές αρχές μεθόδου Pick-up rate και Threshold Current Speed

Η βασική αρχή της μεθόδου Pick-up rate είναι η απαλοιφή των θαλάσσιων καταστάσεων που θεωρείται ότι δεν είναι ικανές να προκαλέσουν έναρξη κίνησης ιζήματος στο «βάθος κλεισίματος» (Houston, 1995). Το κριτήριο απαλοιφής είναι η τροχιακή ταχύτητα των κυματισμών κοντά στον πυθμένα να είναι μικρότερη της κρίσιμης τιμής που δίνεται από την ακόλουθη εξίσωση (van Rijn et al., 2007):

$$U_{cr,w} = \begin{cases} 0.24[g(s-1)]^{0.66}d_{50}^{0.33}T_p^{0.33} & \gamma\iota\alpha\ 0.05 \leq d_{50} < 0.5\ mm \\ 0.95[g(s-1)]^{0.57}d_{50}^{0.43}T_p^{0.14} & \gamma\iota\alpha\ 0.5 \leq d_{50} \leq 2.0\ mm \end{cases} \tag{5}$$

Αντίστοιχα, η μέθοδος κρίσιμης ταχύτητας ρεύματος διαφοροποιείται στο μέγεθος που καθορίζει την απαλοιφή των θαλάσσιων καταστάσεων που είναι η κρίσιμη ταχύτητα του ρεύματος (Soulsby, 1997):

$$U_{cr} = \begin{cases} 0.19d_{50}^{0.1}\log_{10}\left(\dfrac{4h}{d_{90}}\right) & \gamma\iota\alpha\ 100 \leq d_{50} < 500\ \mu m \\ 8.50d_{50}^{0.6}\log_{10}\left(\dfrac{4h}{d_{90}}\right) & \gamma\iota\alpha\ 500 \leq d_{50} \leq 2\ mm \end{cases} \tag{6}$$

Ακολούθως, παρουσιάζονται συνοπτικά τα βασικά βήματα εφαρμογής της μεθόδου Pick-up rate.

1. Επιλογή του επιθυμητού αριθμού αντιπροσώπων N_r δεδομένης μιας χρονοσειράς κυματικών χαρακτηριστικών στα ανοιχτά

2. Προσομοίωση με ένα μοντέλο παραβολικής προσέγγισης ήπιας κλίσης για όλα τα δεδομένα της χρονοσειράς και εξαγωγή των κυματικών χαρακτηριστικών ($H_{s,in}$) σε ένα βάθος μεταξύ 8-10 m.

3. Υπολογισμός του «βάθους κλεισίματος» με βάση την εξίσωση Houston, 1995

$$h_{in} = 8.9\overline{H}_{s,in} \tag{7}$$

4. Υπολογισμός της τροχιακής ταχύτητας των κυματισμών κοντά στον πυθμένα στο «βάθος κλεισίματος»

5. Απαλοιφή των κυματικών χαρακτηριστικών για τα οποία η τροχιακή τους ταχύτητα δεν ξεπερνά την κρίσιμη τιμή της Εξ. (5). Απομείωση του μεγέθους της χρονοσειράς στα ανοιχτά

6. Σχηματοποίηση σε κλάσεις στην απομειωμένη χρονοσειρά με βάση την ποσότητα Pick-up (van Rijn et al., 2019)

$$P = 0.00033\rho_s[(s-1)gd_{50}]^{1/2}D_*^{0.3}f_D\left[\left(\frac{\theta-\theta_{cr}}{\theta}\right)\right]^{1.5} \tag{8}$$

Με την εφαρμογή της μεθόδου Pick-up rate επιτυγχάνεται η μείωση του μεγέθους της χρονοσειράς που διαμορφώνει την μορφολογική εξέλιξη του πυθμένα, ενώ ταυτόχρονα αυξάνεται η επιρροή των κυματισμών με μεγαλύτερο ενεργειακό περιεχόμενο, λόγω της απαλοιφής των θαλασσίων καταστάσεων που δεν προκαλούν έναρξη κίνησης ιζήματος.

Η μέθοδος Threshold Current Speed βασίζεται στα ίδια βήματα με τη μέθοδο Pick-up rate με τις εξής διαφοροποιήσεις, (α) στο βήμα 3 υπολογίζεται η μέση ταχύτητα κατά μήκος της ακτής ρεύματος εντός του σημείου έναρξης θραύσης, (β) η απαλοιφή των κυματικών χαρακτηριστικών στο βήμα 5 γίνεται σύμφωνα με την Εξ. (6) και (γ) στο βήμα 6 η σχηματοποίηση γίνεται με βάση τη ροή ενέργειας των κυματισμών.

Όπως γίνεται εμφανές και από την περιγραφή των βημάτων των μεθόδων, αναπόσπαστο τμήμα τους είναι η εφαρμογή ενός μοντέλου παραβολικής προσέγγισης της εξίσωσης ήπιας κλίσης (Chondros et al., 2021), το οποίο αναπτύχθηκε περαιτέρω και επεκτάθηκε στα πλαίσια της διατριβής ώστε να βελτιωθεί το κριτήριο θραύσης των κυματισμών και να μπορεί να προσομοιωθεί η διάδοση σύνθετων μονοκατευθυντικών κυματισμών. Στο Σχήμα 4 παρουσιάζεται η επαλήθευση των αποτελεσμάτων του μοντέλου, που θα καλείται στο εξής PMS-SP, για την περίπτωση Α του πειράματος των Mase and Kirby, 1992, το οποίο αφορά τη θραύση μονοκατευθυντικών κυματισμών σε ακτή ήπιας κλίσης.
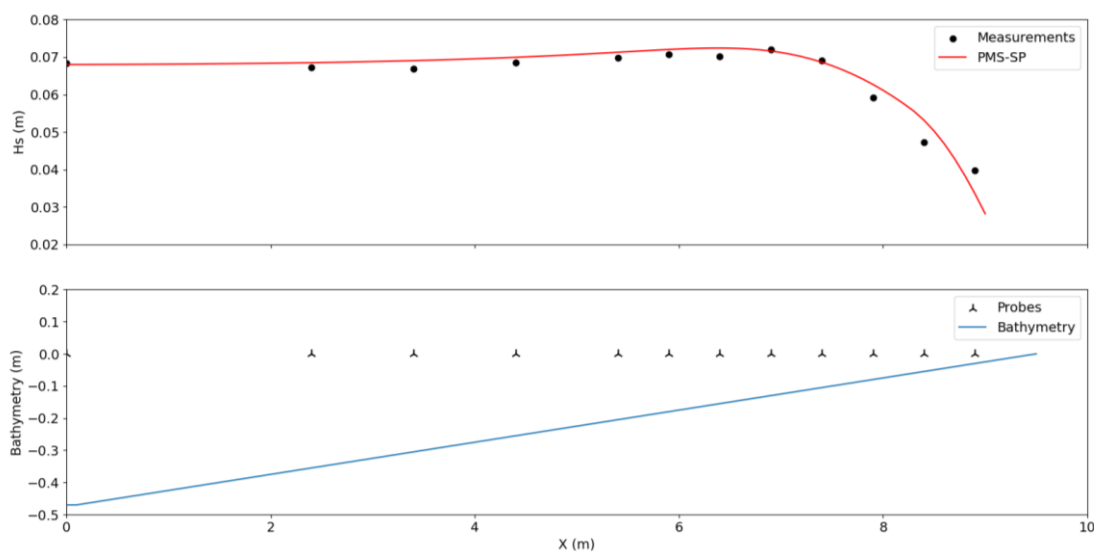
Σχήμα 4. Ύψος κύματος από την προσομοίωση του PMS-SP και σύγκριση με τις πειραματικές μετρήσεις (άνω) και βαθυμετρία και μετρητικοί σταθμοί (κάτω)

3.2. Περιοχή μελέτης και εφαρμογή των μεθόδων

Οι μεθοδολογίες που αναπτύχθηκαν στη συνέχεια εφαρμόστηκαν στην παράκτια περιοχή του Ρεθύμνου στην Κρήτη. Η περιοχή ενδιαφέροντος περιλαμβάνει το λιμάνι και την παρακείμενη ακτή στα ανατολικά, η οποία έχει μήκος περίπου 4 km και συγκεντρώνει πολλές ανθρώπινες δραστηριότητες. Η ακτογραμμή αποτελείται κυρίως από ιζήματα λεπτής άμμου ενώ παρατηρείται συσσώρευση ιζημάτων στην είσοδο του λιμανιού που δυσχεραίνει τη ναυσιπλοΐα.

Για την προσομοίωση της μορφολογικής εξέλιξης του πυθμένα, χρησιμοποιήθηκε το μοντέλο περιοχής MIKE21 CM FM (DHI, 2014) που πραγματοποιεί τους υπολογισμούς

σε ένα μη-δομημένο πλέγμα πεπερασμένων στοιχείων. Οι κυματισμοί εισέρχονται στο υπολογιστικό πεδίο από τα βόρεια, ανατολικά και δυτικά όρια.

Τα κυματικά χαρακτηριστικά στα ανοιχτά ελήφθησαν από τη βάση δεδομένων Copernicus Marine Service, συνολική διάρκειας ενός έτους (2012). Οι προσομοιώσεις διεξήχθησαν με συντελεστή μορφολογικής επιτάχυνσης 50 για την μείωση του χρόνου προσομοίωσης. Επιπρόσθετα, θεωρήθηκε σταθερή μέση διάμετρος ιζήματος 0,15 mm σε όλο το αριθμητικό πεδίο.

Η αξιολόγηση της απόδοσης του μοντέλου επικεντρώθηκε σε μια περιοχή που εκτείνεται έως και 450 m βόρεια της ανατολικής ακτογραμμής, με μέγιστο βάθος περίπου 9 m (Σχήμα 5). Η περιοχή αυτή αποτελείται από αμμώδη ομοιόμορφη κλίνη και παρουσιάζει σημαντικό ενδιαφέρον λόγω τουριστικών και οικονομικών δραστηριοτήτων. Η αξιολόγηση συνίσταται στον υπολογισμό του BSS, για τις μεθόδους σχηματοποίησης Pick-up rate και κρίσιμης ταχύτητα ρεύματος θεωρώντας με την «προσομοίωση αναφοράς» να περιέχει την πλήρη χρονοσειρά για όλο το έτος 2012
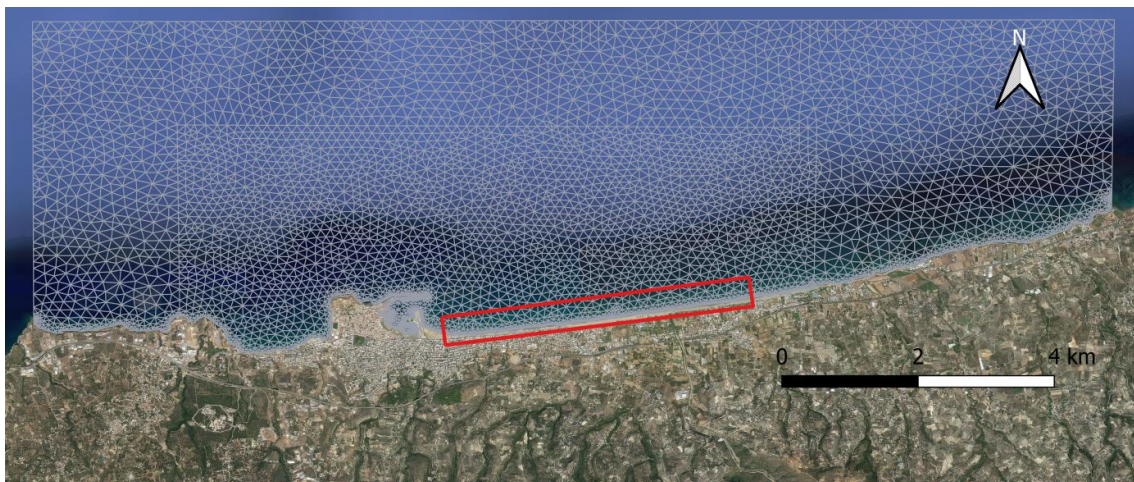
Σχήμα 5. Υπολογιστικό πλέγμα και περιοχή αξιολόγησης αποτελεσμάτων των προσομοιώσεων (εντός του κόκκινου ορθογωνίου)

Με την εφαρμογή της μεθόδου Pick-up rate απαλείφθηκαν 4699 θαλάσσιες καταστάσεις, φτάνοντας σε μείωση 58% της αρχικής χρονοσειράς, ενώ αντίστοιχα με την εφαρμογή της μεθόδου Threshold Current Speed απαλείφθηκαν συνολικά 5082 θαλάσσιες καταστάσεις για μια μείωση 62% της χρονοσειράς. Συνολικά επιλέχθηκαν 12 αντιπρόσωποι και για τις τρεις μεθόδους που εφαρμόστηκαν και συγκρίθηκαν, αριθμός που θεωρείται ικανοποιητικός για την ετήσια πρόβλεψη της μορφολογικής εξέλιξης πυθμένα (Benedet et al., 2016).

Στο Σχήμα 6 παρουσιάζονται οι αντιπρόσωποι που υπολογίστηκαν με τις μεθόδους Pick-up rate, Threshold Current Speed και ροής ενέργειας. Με γαλάζιο χρώμα επισημαίνονται θαλάσσιες καταστάσεις που έχουν απαλειφθεί. Αυτή η απαλοιφή, όπως διακρίνεται και στο Σχήμα 6 οδηγεί στον υπολογισμό αντιπρόσωπων με υψηλότερο ενεργειακό δυναμικό για τις μεθόδους Pick-up rate και Threshold Current Speed σε σχέση με τη μέθοδο ροής ενέργειας.
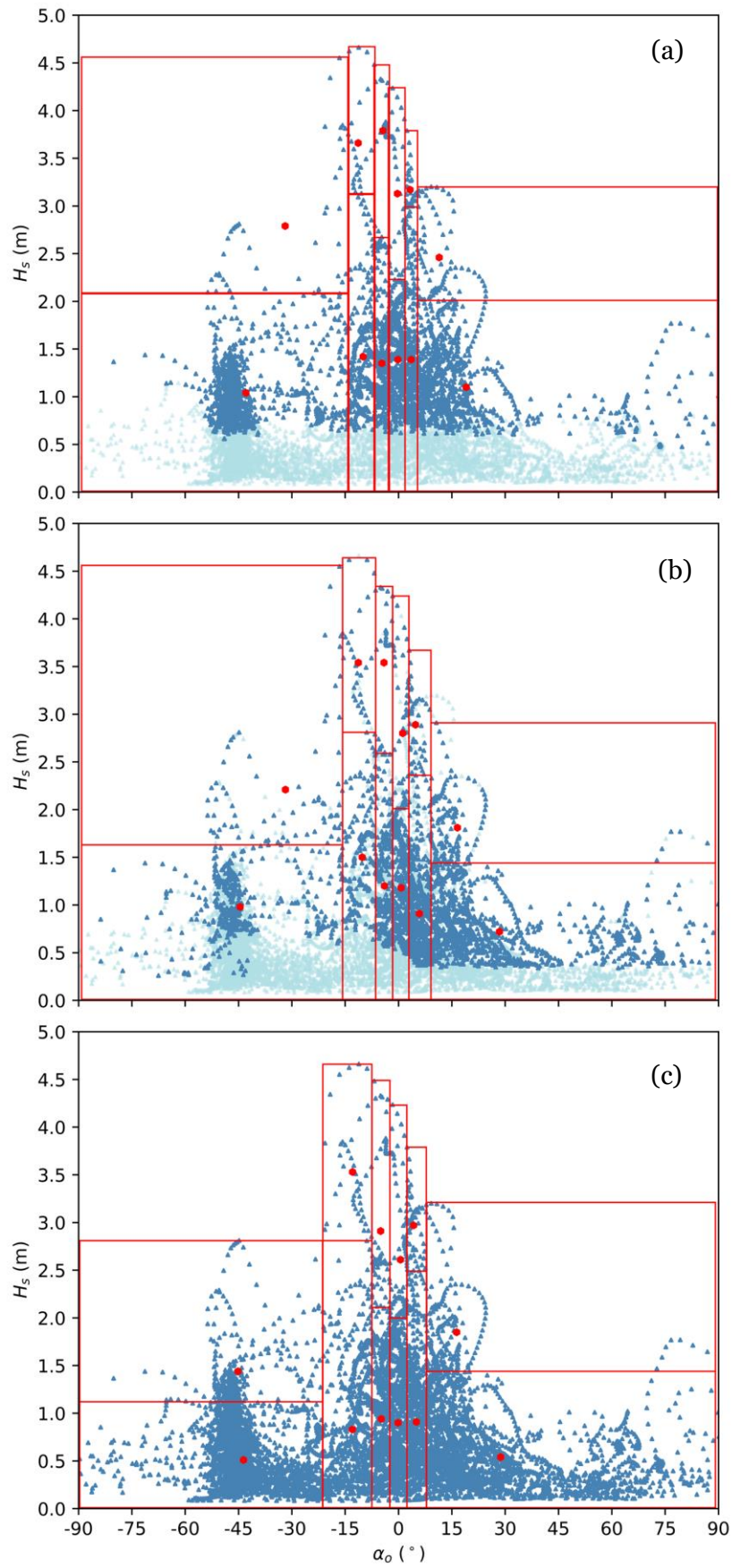
Σχήμα 6. Αντιπρόσωποι και κλάσεις όπως υπολογίστηκαν με τη μέθοδο: (a) Pick-up rate (b) Threshold Current Speed και (c) ροής ενέργειας

3.3. Αποτελέσματα μεθόδων σχηματοποίησης σε κλάσεις

Σε αυτό το σημείο παρατίθενται οι προβλεπόμενες μεταβολές της βαθυμετρίας σε ορίζοντα ενός έτους μετά την εφαρμογή του μοντέλου MIKE21 CM FM, για τις μεθόδους Pick-up rate, Threshold Current Speed και ροής ενέργειας. Τα αποτελέσματα των προσομοιώσεων συγκρίνονται με τα αποτελέσματα της προσομοίωσης αναφοράς για την περαιτέρω αξιολόγηση τους. Η προσομοίωση αναφοράς περιλαμβάνει 8219 ωριαία μεταβαλλόμενες οριακές συνθήκες κυματικών χαρακτηριστικών και με χρήση τιμής συντελεστή μορφολογικής επιτάχυνσης 50, ο συνολικός χρόνος προσομοίωσης φτάνει περίπου 88 ώρες. Η μεταβολή μεταξύ αρχικής και τελικής βαθυμετρίας για την προσομοίωση αναφοράς παρουσιάζεται στο Σχήμα 7. Παρατηρώντας το Σχήμα 7, εντοπίζεται μια εκτεταμένη ζώνη προσάμμωσης κατά μήκος της ακτογραμμής, καθώς και συσσώρευση ιζήματος στον υπήνεμο μώλο του και στην είσοδο του λιμένα. Συνεπακόλουθα, μια ζώνη διάβρωσης μπορεί να εντοπιστεί, νότια της εισόδου του λιμένα.
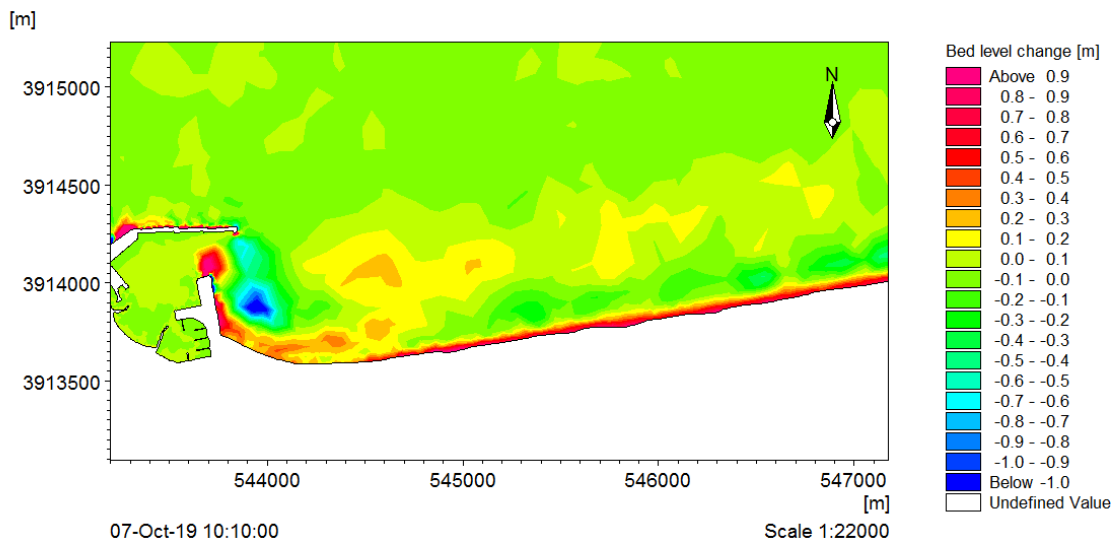
Σχήμα 7. Μεταβολή τελικής βαθυμετρίας ως προς την αρχική για την προσομοίωση αναφοράς

Για τις προσομοιώσεις που πραγματοποιήθηκαν χρησιμοποιώντας τις μεθόδους Pick-up rate και Threshold Current Speed, ένας σημαντικός αριθμός θαλάσσιων καταστάσεων (4699 και 5082, αντίστοιχα) δεν κρίθηκαν ικανές να θέσουν σε έναρξη την κίνηση του ιζήματος. Αυτή η μείωση στο μήκος του συνόλου των δεδομένων και η εξάλειψη των θαλάσσιων καταστάσεων χαμηλής ενέργειας οδήγησαν σε μείωση του συνολικού χρόνου εκτέλεσης της προσομοίωσης κατά 57,2% και 62%, αντίστοιχα. Από την άλλη πλευρά, η μέθοδος ροής ενέργειας δεν απαλείφει καμία θαλάσσια κατάσταση και απαιτεί σχεδόν τον ίδιο χρόνο προσομοίωσης με την προσομοίωση αναφοράς. Τα αποτελέσματα μεταβολής αρχικής και τελικής βαθυμετρίας που προέκυψαν από τις τρεις διαφορετικές μεθόδους σχηματοποίησης παρουσιάζονται στο Σχήμα 7 και γενικά αναπαράγουν τα μοτίβα προσάμμωσης/διάβρωσης που παρατηρήθηκαν στην προσομοίωση αναφοράς.
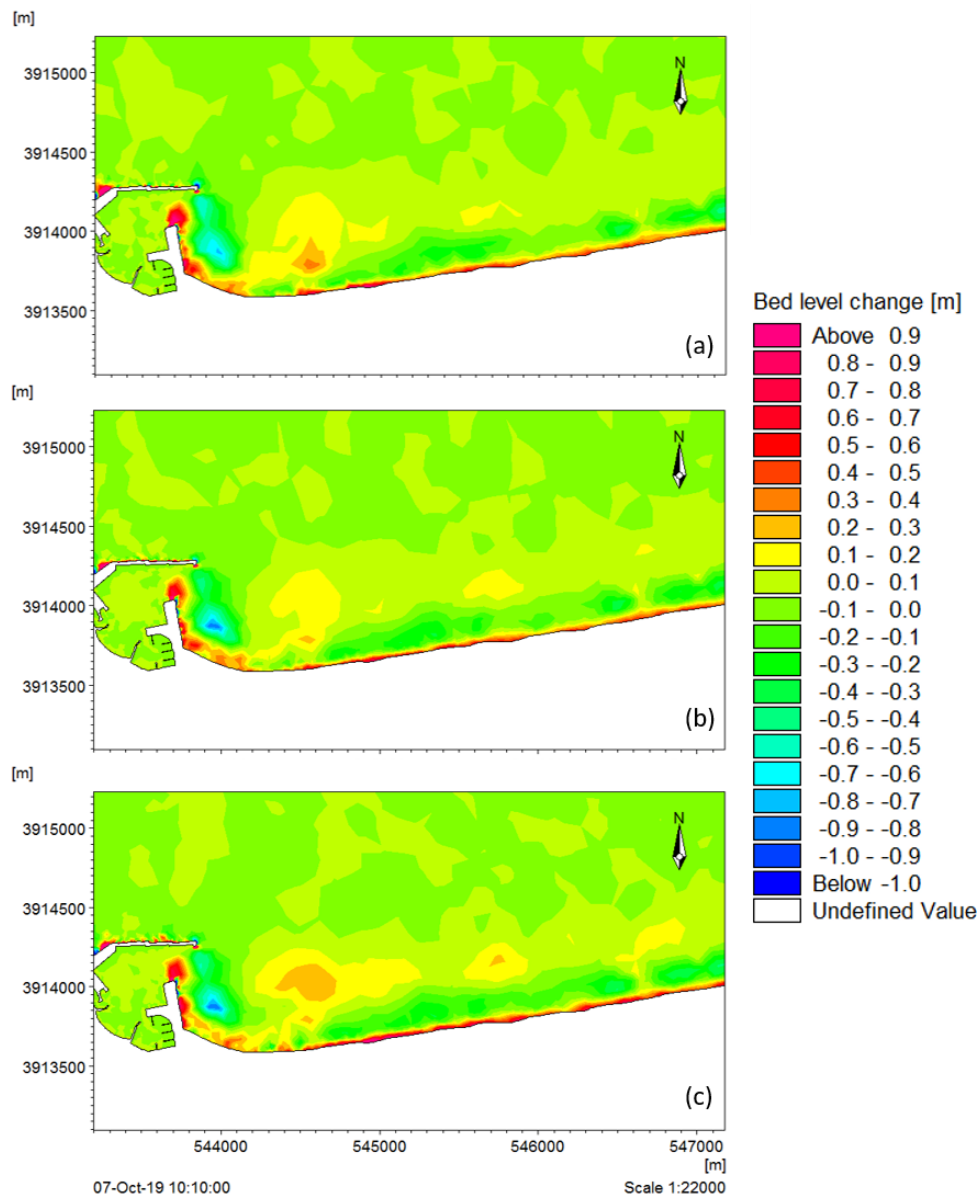
Σχήμα 8. Αποτελέσματα προσομοιώσεων μεταβολής τελικής βαθυμετρίας ως προς την αρχική (a) μέθοδος Pick-up rate, (b) μέθοδος Threshold Current Speed, (c) μέθοδος ροής ενέργειας

Πιο συγκεκριμένα, η μέθοδος ροής ενέργειας αναπαράγει με μεγάλη ακρίβεια τη συσσώρευση ιζήματος κατά μήκος της ακτογραμμής και την προσάμμωση στην είσοδο του λιμανιού. Οι μέθοδοι Pick-up rate και Threshold Current Speed, αν και αναπαράγουν ικανοποιητικά τα μοτίβα προσάμμωσης και διάβρωσης κοντά στην περιοχή του λιμανιού, τείνουν να υποεκτιμούν το μέγεθος των μεταβολών της βαθυμετρίας σε σχέση με την προσομοίωση αναφοράς. Αυτή η υποεκτίμηση μπορεί να αποδοθεί στη μείωση του συνολικού χρόνου εκτέλεσης του μοντέλου που προκύπτει από την εξάλειψη των θαλάσσιων καταστάσεων χαμηλής ενέργειας.

Η αξιολόγηση των αποτελεσμάτων του μοντέλου για τις 3 μεθόδους τελικώς συνίσταται στον υπολογισμό του δείκτη BSS για την περιοχή ενδιαφέροντος. Οι υπολογισθείσες τιμές BSS, συνοδευόμενες από το ποσοστό μείωσης του χρόνου

προσομοίωσης, σε σύγκριση με την προσομοίωση αναφοράς, παρουσιάζονται στον Πίνακα 1.

Πίνακας 1. Υπολογισθείσες τιμές του BSS για τις μεθόδους σχηματοποίησης και ποσοστό μείωσης χρόνου προσομοίωσης σε σχέση με την προσομοίωση αναφοράς

	Μέθοδος Pick-up rate	Μέθοδος Threshold Current Speed	Μέθοδος ροής ενέργειας
BSS	0.74	0.72	0.85
Ποσοστό μείωσης χρόνου προσομοίωσης (%)	57	63	13

Τα αποτελέσματα των προσομοιώσεων κατηγοριοποιούνται ως "Εξαιρετικά" αφού οι τιμές BSS υπερβαίνουν το 0.5 (Sutherland et al., 2004), με τη μέθοδο ροής ενέργειας να έχει την καλύτερη απόδοση (BSS 0.85). Οι μέθοδοι Pick-up rate και Threshold Current Speed δίνουν παρόμοιες τιμές BSS 0.74 και 0.72 αντίστοιχα. Είναι σημαντικό να τονιστεί ότι με την εφαρμογή των νέων μεθόδων, επιτεύχθηκε σημαντική μείωση υπολογιστικού φόρτου, διατηρώντας παράλληλα την αξιοπιστία και την ακρίβεια των αποτελεσμάτων, όπως αποδεικνύεται από την μικρή μείωση του BSS. Συνεπώς, τόσο η μέθοδος Pick-up rate όσο και αυτή της Threshold Current Speed, προβλέπουν την ετήσια εξέλιξη της βαθυμετρίας σε ικανοποιητικό βαθμό, ενώ επιτυγχάνουν αξιοσημείωτη μείωση του χρόνου προσομοίωσης του μαθηματικού μοντέλου.

4. Αξιολόγηση και επέκταση του αλγορίθμου ομαδοποίησης K-Means

Οι αλγόριθμοι ομαδοποίησης έχουν χρησιμοποιηθεί σε πληθώρα εφαρμογών της παράκτιας μηχανικής και ωκεανογραφίας (Camus et al., 2011; Kelpšaitė-Rimkienė et al., 2021; Martzikos et al., 2018; Splinter et al., 2011) ωστόσο η εφαρμογή τους ως εναλλακτικές των πιο διαδεδομένων μεθόδων σχηματοποίησης κυματικού κλίματος είναι περιορισμένη (de Queiroz et al., 2019). Πιο συγκεκριμένα η αξιολόγηση της απόδοσης των αλγορίθμων ομαδοποίησης σε μια παράκτια περιοχή με κατά μήκος της ακτής μεταβλητότητα δεν έχει διερευνηθεί ακόμα. Στο πλαίσιο αυτής της διατριβής εξετάζεται η απόδοση και πιθανές βελτιώσεις του αλγορίθμου K-Means, ενός από τους πιο διαδεδομένους και αξιόπιστους αλγορίθμους. Η επιλογή για τη χρήση αποκλειστικά αυτού του αλγορίθμου ομαδοποίησης, έναντι άλλων διαθέσιμων, βασίζεται στα ακόλουθα βασικά στοιχεία:

- Ο αλγόριθμος διαθέτει μεγάλο εύρος εφαρμογής, υπολογιστική αποδοτικότητα και διαθεσιμότητα σε βιβλιοθήκες ευρέως χρησιμοποιούμενων γλωσσών προγραμματισμού (Python, R, Matlab)
- Σε αντίθεση με άλλους αλγορίθμους (π.χ. Fuzzy C-Means) κάθε στοιχεία έχει μοναδική συμμετοχή σε κάθε συστάδα κάτι το οποίο συνάδει με την μοναδική εμφάνιση κάθε θαλάσσιας κατάστασης στην χρονοσειρά κυματικών χαρακτηριστικών

Σαν δεδομένα εισόδου ο αλγόριθμος λαμβάνει μια χρονοσειρά κυματικών χαρακτηριστικών στα ανοιχτά, που κατ' ελάχιστον πρέπει να περιλαμβάνει το χαρακτηριστικό ύψος κύματος, την περίοδο κορυφής και την διεύθυνση πρόσπτωσης των κυματισμών. Τα δεδομένα κανονικοποιούνται πριν εισαχθούν στον αλγόριθμο.

4.1. Εξεταζόμενες τροποποιήσεις του αλγορίθμου

Στην παρούσα διατριβή εξετάστηκαν συνολικά 5 εναλλακτικές τροποποιήσεις του αλγορίθμου, με διαφορετικά χαρακτηριστικά μεταξύ τους, αλλά με τον κοινό σκοπό να επιτύχουν τη βελτίωση των αποτελεσμάτων που δίνει η πρωταρχική παραμετροποίηση του αλγορίθμου K-Means. Στη συνέχεια παρουσιάζονται συνοπτικά τα βασικά χαρακτηριστικά κάθε εξεταζόμενης περίπτωσης.

- **KM-01**: Βασική παραμετροποίηση του αλγορίθμου. Η αρχικοποίηση των κεντροειδών γίνεται με τον αλγόριθμο K-Means++.

- **KM-02**: Η επαναληπτική διαδικασία εύρεσης των κεντροειδών και συστάδων εκκινεί με βάση τους αντιπροσώπους/κεντροειδή που προκύπτουν από την εφαρμογή της μεθόδου ροής ενέργειας. Με αυτό τον τρόπο αντισταθμίζεται η φύση της «μη-επίβλεψης» του αλγορίθμου K-Means, καθώς η επαναληπτική διαδικασία αρχίζει από τιμές που συμμετέχουν στην εξέλιξη της παράκτιας μορφολογίας.

- **KM-03**: Χρήση της επιμέρους ροής ενέργειας κάθε θαλάσσιας κατάστασης σαν βάρος που εισέρχεται στην αλγοριθμική διαδικασία, με σκοπό να αποφευχθεί η υπερεκτίμηση της επίδρασης των κυματικών χαρακτηριστικών που έχουν μικρότερο ενεργειακό περιεχόμενο.

- **KM-04**: Εναλλαγή των παραμέτρων εισόδου του αλγορίθμου από ύψος κύματος, περίοδο κορυφής και γωνία πρόσπτωσης σε κατά μήκος της ακτής στερεομεταφορά, ροή ενέργειας και γωνία πρόσπτωσης.

- **KM-05**: Αρχικοποίηση των κεντροειδών με βάση τους αντιπροσώπους που έχουν προκύψει από εφαρμογή της μεθόδου σχηματοποίησης κλάσεων Pick-up rate. Η εκκίνηση της αλγοριθμικής διαδικασίας γίνεται από κεντροειδή με μεγαλύτερο ενεργειακό περιεχόμενο σε σχέση με αυτά της περίπτωσης KM-02.

- **KM-06**: Με χρήση του μοντέλου PMS-SP γίνεται κυματική διάδοση στα ρηχά με σκοπό να απαλοιφούν θαλάσσιες καταστάσεις που προσπίπτουν κάθετα στην ακτογραμμή (άρα δεν προκαλούν κατά μήκος της ακτής στερεομεταφορά) και δεν υπόκεινται σε θραύση ως προς το ελάχιστο βάθος που έχει θεωρηθεί για τις προσομοιώσεις. Στη συνέχεια εφαρμόζεται ο αλγόριθμος K-Means σε δύο στάδια: (α) υπολογίζονται τα κεντροειδή του ενδιάμεσου βήματος με εφαρμογή των αρχών της περίπτωσης KM-04, (β) τα κεντροειδή του προηγούμενου ενδιάμεσου βήματος τίθενται σαν αρχικές τιμές σε μια νέα διαμόρφωση του αλγορίθμου K-Means για να προκύψουν οι αντιπρόσωποι του KM-06.

Στον Πίνακα 2 παρουσιάζονται συγκεντρωτικά τα βασικά στοιχεία των εξεταζόμενων εναλλακτικών περιπτώσεων.

Πίνακας 2. Συγκεντρωτική παρουσίαση των εξεταζόμενων εναλλακτικών περιπτώσεων εφαρμογής του αλγορίθμου K-Means

Περίπτωση	Παράμετροι εισόδου	Μέθοδος αρχικοποίησης κεντροειδών	Εφαρμοστέα βάρη
KM-01	H_s, T_p, a_o	K-Means⁺⁺	-
KM-02	H_s, T_p, a_o	Κεντροειδή μεθόδου ροής ενέργειας	-
KM-03	H_s, T_p, a_o	K-Means⁺⁺	Ροή ενέργειας κάθε θαλάσσιας κατάστασης
KM-04	S, E_{fl}, a_o	K-Means⁺⁺	-
KM-05	H_s, T_p, a_o	Κεντροειδή μεθόδου Pick-up rate	-
KM-06	S, E_{fl}, a_o	K-Means⁺⁺	-
	H_s, T_p, a_o	Κεντροειδή προηγούμενου βήματος	-

4.2. Περιοχή εφαρμογής και αντιπροσωπευτικές κυματικές συνθήκες

Οι 6 διακριτές περιπτώσεις εφαρμόστηκαν στην παράκτια περιοχή του Ρεθύμνου, που παρουσιάστηκε στην Ενότητα 3, λαμβάνοντας υπόψη τις ίδιες παραδοχές και την παραμετροποίηση του μαθηματικού μοντέλου MIKE21 CM FM. Σημειώνεται ότι οι προσομοιώσεις πραγματοποιήθηκαν με βάση την «Μορφοδυναμική» προσέγγιση ενώ η αξιολόγηση των αποτελεσμάτων πραγματοποιήθηκε για την περιοχή που παρουσιάζεται εντός του κόκκινου πλαισίου στο Σχήμα 5.

Στο Σχήμα 9 παρουσιάζονται οι κυματικοί αντιπρόσωποι, όπως προέκυψαν για την εφαρμογή των περιπτώσεων KM-01 έως KM-06, σε δισδιάστατο διάγραμμα, όπου στον οριζόντια άξονα τίθεται η γωνία πρόσπτωσης των κυματισμών ως προς την κάθετο στην ακτογραμμή και στον κατακόρυφο άξονα το χαρακτηριστικό ύψος κύματος.

Για τη περίπτωση KM-01, αρκετά κεντροειδή που λαμβάνονται από τον αλγόριθμο ομαδοποίησης βρίσκονται σε κοντινή απόσταση μεταξύ τους, λόγω της χωρικής κατανομής του πλήθους των κυματικών χαρακτηριστικών. Στις περιπτώσεις KM-02, KM-05 και KM-06, στις οποίες επιβλήθηκαν εξωτερικά κεντροειδή για την αρχικοποίηση της επαναληπτικής διαδικασίας, τα τελικά κεντροειδή συστάδας κατανέμονται σε μια ευρύτερη περιοχή, ακολουθώντας την κατανομή των αρχικών κεντροειδών. Η περίπτωση KM-03, η οποία ενσωματώνει βάρη που σχετίζονται με τη ροή ενέργειας των κυματισμών, οδηγεί σε σημαντική μετατόπιση όλων των κεντροειδών προς πιο ενεργητικούς αντιπροσώπους σε σύγκριση με όλες τις άλλες περιπτώσεις. Οι συστάδες της KM-04 ορίζονται με μεγαλύτερη ευκρίνεια, γεγονός που μπορεί να αποδοθεί στη μεταβολή των αρχικών παραμέτρων ομαδοποίησης. Οι περιπτώσεις KM-05 και KM-06, οι οποίες εφαρμόζουν μεθοδολογίες απαλοιφής θαλάσσιων καταστάσεων χαμηλής σχετικά ενέργειας, καταλήγουν σε παρόμοιες τιμές αντιπροσωπευτικών κυματισμών.
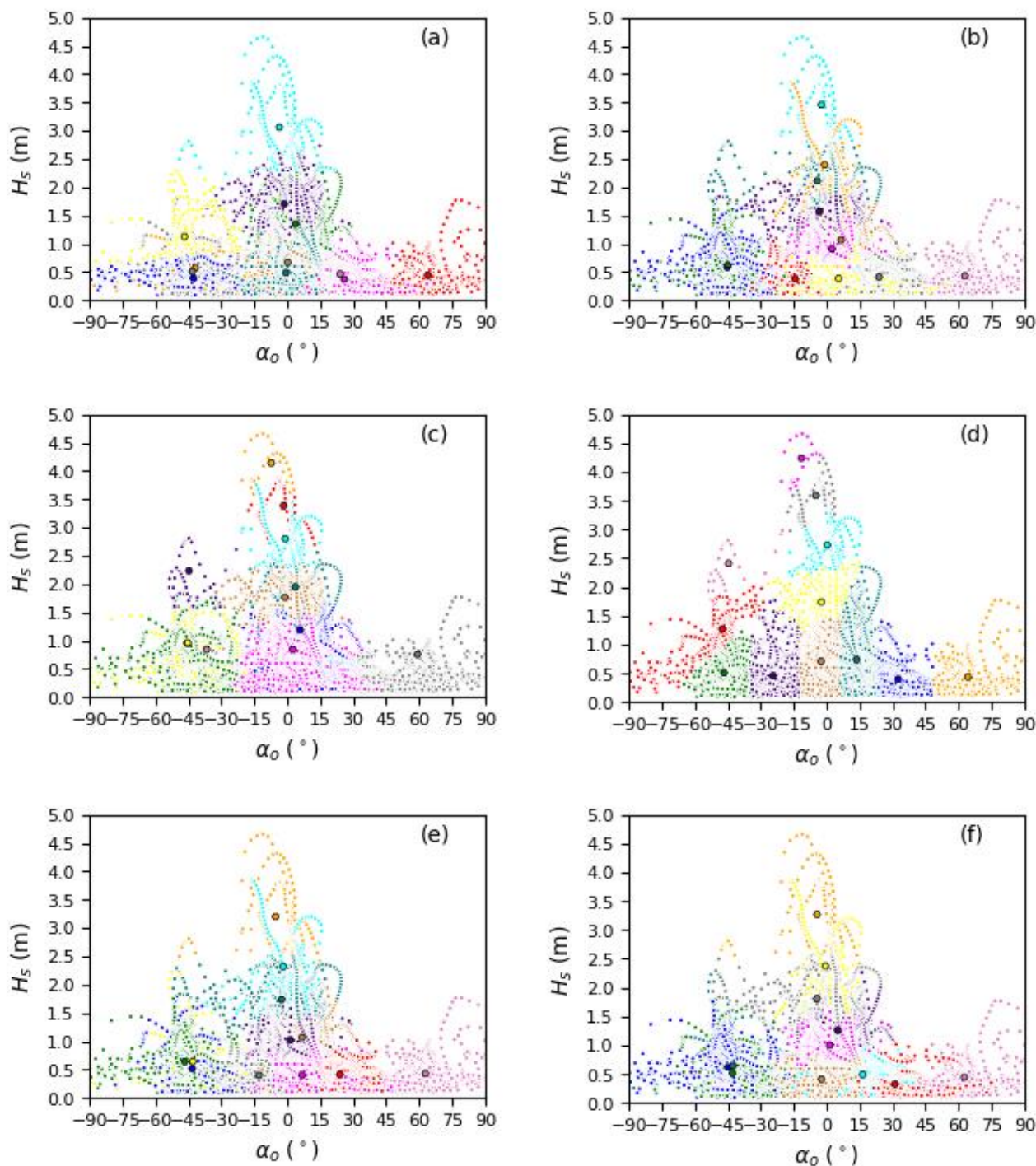
Σχήμα 9. Συστάδες και κυματικοί αντιπρόσωποι με εφαρμογή των μεθόδων (a) KM-01, (b) KM-02, (c) KM-03, (d) KM-04, (e) KM-05, (f) KM-06

4.3. Αποτελέσματα αλγορίθμων ομαδοποίησης

Στη συνέχεια παρατίθενται τα αποτελέσματα μεταβολής της τελικής ως προς την αρχική βαθυμετρία, που προέκυψαν από την εφαρμογή του μοντέλου MIKE21 CM-FM, για τις διαφορετικές διαμορφώσεις του αλγορίθμου KM. Τα αποτελέσματα για κάθε διακριτή περίπτωση παρουσιάζονται συγκριτικά στο Σχήμα 10. Παρατηρείται σε γενικές γραμμές συμφωνία με τα αποτελέσματα της προσομοίωσης αναφοράς (Σχήμα 7) με τον εντοπισμό ζωνών απόθεσης και διάβρωσης κατά μήκος της ακτογραμμής, καθώς και

33

συσσώρευση ιζημάτων στην είσοδο του Λιμένα σε όλες τις προσομοιώσεις. Η συγκριτική αξιολόγηση των αποτελεσμάτων αποκαλύπτει ότι ορισμένες περιπτώσεις εφαρμογής του αλγορίθμου K-Means υποεκτιμούν την ένταση των μορφολογικών μεταβολών, ενώ άλλες αναπαράγουν πιο πιστά την προσομοίωση αναφοράς.
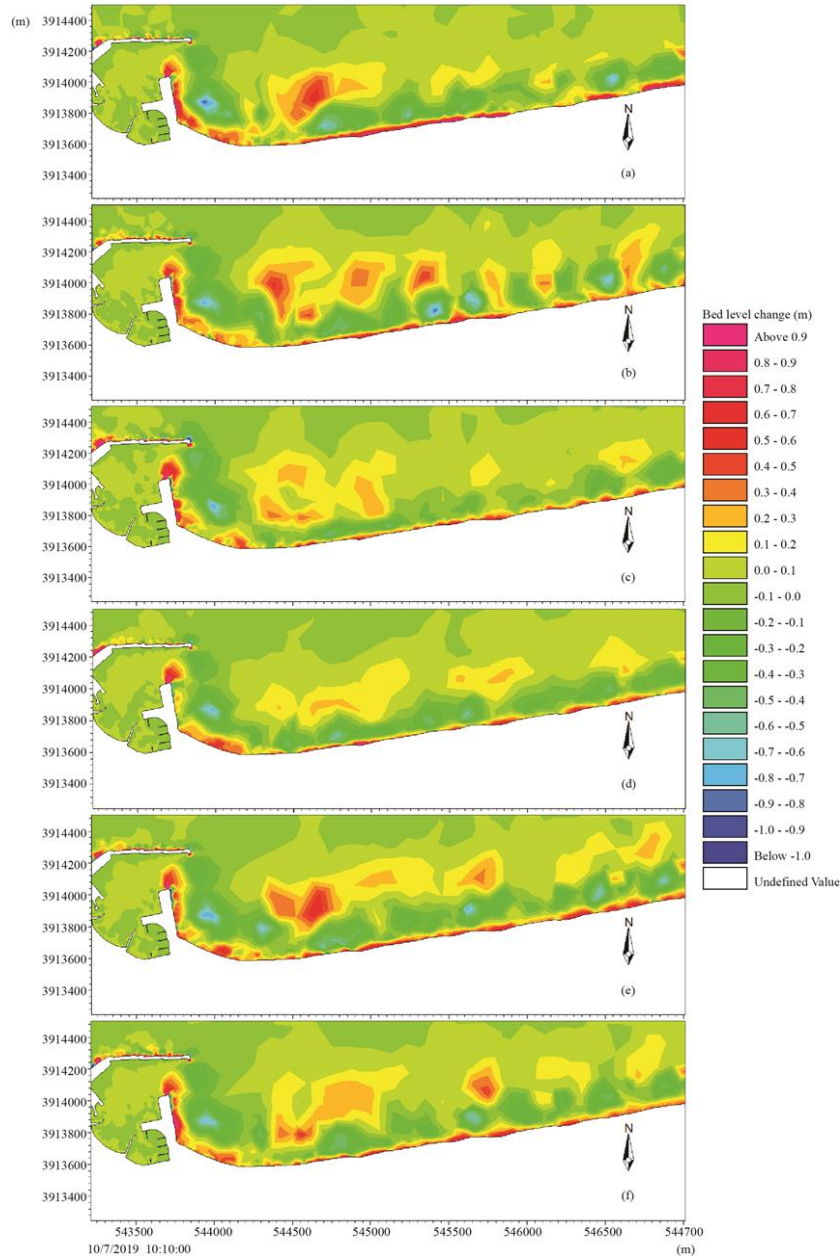
Σχήμα 10. Αποτελέσματα προσομοιώσεων μεταβολής τελικής βαθυμετρίας ως προς την αρχική (a) KM-01, (b) KM-02, (c) KM-03, (d) KM-04, (e) KM-05, (f) KM-06

Από την οπτική συγκριτική αξιολόγηση των αποτελεσμάτων διαφαίνεται ότι η προσομοίωση KM-03 παρουσιάζει την καλύτερη συμφωνία με την προσομοίωση αναφοράς. Ο μετασχηματισμός των μεταβλητών ομαδοποίησης στη δοκιμή KM-04 δείχνει να οδηγεί σε μια υποεκτίμηση των μορφολογικών αλλαγών. Οι δοκιμές KM-05 και KM-06, οι οποίες περιλαμβάνουν διαδικασίες φιλτραρίσματος για την εξάλειψη κυματισμών που θεωρείτε πως δε συμμετέχουν καθοριστικά στη μορφολογική εξέλιξη πυθμένα, προσφέρουν καλή αναπαραγωγή της μορφολογικής εξέλιξης.

Τα αποτελέσματα αξιολογούνται περαιτέρω υπολογίζοντας το δείκτη BSS, και παρουσιάζονται στον Πίνακα 3, ενώ όλες οι προσομοιώσεις ταξινομούνται ως "Εξαιρετικές", ενώ για τις εξεταζόμενες βελτιώσεις (ΚΜ-02 έως ΚΜ-06) παρατηρείται μια έστω και μικρή αύξηση στο δείκτη BSS, ως προς την κλασσική περίπτωση εφαρμογής του αλγορίθμου ΚΜ-01. Οι προσομοιώσεις ΚΜ-05 και ΚΜ-06, φαίνεται πως αποδίδουν καλύτερα, λόγω της συστηματικής απαλοιφής κυματικών συνθηκών χαμηλού ενεργειακού περιεχομένου.

Πίνακας 3. Υπολογισθείσες τιμές του BSS για τις διαφορετικές περιπτώσεις εφαρμογής του αλγορίθμου K-Means

	KM-01	KM-02	KM-03	KM-04	KM-05	KM-06
BSS	0.63	0.64	0.65	0.66	0.71	0.68

Συνοψίζοντας, η δοκιμή ΚΜ-06, δίνει ένα ικανοποιητικό συμβιβασμό ως προς την ακρίβεια των αποτελεσμάτων και την πολυπλοκότητα εφαρμογής της αλγοριθμικής διαδικασίας. Ωστόσο, σημειώνεται πως η κλασσική υλοποίηση του αλγορίθμου ΚΜ (περίπτωση ΚΜ-01) μπορεί να χρησιμοποιείται σε πρακτικές εφαρμογές καθώς υπερισχύει σημαντικά έναντι των λοιπών εξεταζόμενων περιπτώσεων, ως προς την ευκολία εφαρμογής από το χρήστη και δεν απαιτεί την διενέργεια επιπρόσθετων υπολογισμών.

5. Αξιολόγηση και επέκταση των μεθόδων σχηματοποίησης ισοδύναμων κυματισμών

Παρά το γεγονός ότι οι μέθοδοι σχηματοποίησης και υπολογισμού των ισοδύναμων κυματισμών εφαρμόζονται σε μεγάλο πλήθος ερευνητικών εργασιών ακόμα και σήμερα (Borah and Balloffet, 1985; Brown and Davies, 2009; Chondros et al., 2022; Chonwattana et al., 2005; Karambas et al., 2013; Papadimitriou et al., 2022a; Pletcha et al., 2007), εντούτοις δεν έχει πραγματοποιηθεί ακόμα μια συστηματική προσπάθεια αξιολόγησης της διαδεδομένης μεθόδου και διερεύνησης πιθανών βελτιώσεων.

Στην παρούσα διατριβή εξετάστηκαν τρεις επιπλέον πιθανές βελτιώσεις της μεθόδου που παρουσιάστηκε στην εργασία των Chonwattana et al., 2005, μια εκ των οποίων περιλαμβάνει την εκπαίδευση και επαλήθευση ενός Τεχνητού Νευρωνικού Δικτύου (ΤΝΔ).

5.1. Εξεταζόμενες τροποποιήσεις της μεθόδου σχηματοποίησης ισοδύναμων κυματισμών

Όπως προαναφέρθηκε, εξετάστηκαν συνολικά 4 περιπτώσεις εφαρμογής της μεθόδου των ισοδύναμων κυματισμών που θα περιγραφούν συνοπτικά στη συνέχεια.

Η περίπτωση **RMWH-01** αποτελεί την μέθοδο υπολογισμού των ισοδύναμων κυματικών αντιπροσώπων όπως παρουσιάστηκε στην εργασία των Chonwattana et al., 2005. Ομαδοποιώντας τα κυματικά χαρακτηριστικά σε κλάσεις γωνίας πρόσπτωσης σταθερού πλάτους, οι κυματικοί αντιπρόσωποι υπολογίζονται με εφαρμογή των γραμμικών συστημάτων των Εξ. (2), (3) και (4).

Η περίπτωση **RMWH-02** αποτελεί μια σχετικά απλή τροποποίηση της μεθόδου RMWH-01, βασική ιδέα της οποίας είναι η διαμόρφωση δύο υποκλάσεων ανά κάθε κλάση γωνίας πρόσπτωσης. Το κριτήριο για την εκχώρηση των κυματικών χαρακτηριστικών σε κάθε υποκλάση είναι αν η ροή ενέργειας της κάθε θαλάσσιας κατάστασης υπερβαίνει η όχι την μέση αθροιστική ροή ενέργειας κάθε κλάσης. Με αυτό τον τρόπο διαμορφώνονται δυο νέες κλάσεις «υποκρίσιμων» και «υπερκρίσιμων» κυματικών χαρακτηριστικών ως προς τη ροή ενέργειας.

Η περίπτωση **RMWH-03** βασίζεται στην παραδοχή ότι η κατά μήκος και η εγκάρσια στερεομεταφορά επηρεάζουν σε μεγαλύτερο βαθμό τη μορφολογική εξέλιξη του πυθμένα σε μια δεδομένη διατομή του παράκτιου μετώπου, ανάλογα με την γωνία πρόσπτωσης των κυματισμών

Παρατηρώντας μια ακτίνα κυματισμών και εφαρμόζοντας την αρχή διατήρησης της κυματικής ενέργειας στα ανοιχτά, η κατά μήκους της ακτής (κ.μ.α) και εγκάρσια συνιστώσα της ροής ενέργειας υπολογίζεται από την ακόλουθη εξίσωση:

$$\begin{cases} E_{ls} = H_s^2 T_p \sin a_0 \\ E_{cs} = H_s^2 T_p \cos a_0 \end{cases} \tag{9}$$

όπου E_{ls} είναι η κατά μήκους της ακτής και E_{cs} η εγκάρσια συνιστώσα της κυματικής ροής ενέργειας αντίστοιχα.

Υπολογίζοντας τον ισοδύναμο κυματισμό για όλη τη χρονοσειρά κυματικών χαρακτηριστικών στα ανοιχτά, και επιλύοντας την Εξ. (9) για πολλαπλές τιμές της γωνίας πρόσπτωσης των κυματισμών, μπορούν να καθοριστούν ζώνες εναλλασσόμενης κυριαρχίας της κ.μ.α. ή της εγκάρσιας στερεομεταφοράς:

$$\begin{cases} |E_{ls}| \geq 2|E_{cs}|, & \text{υπερισχύσει η κ.μ.α στερεομεταφορά} \\ |E_{cs}| \geq 2|E_{ls}|, & \text{υπερισχύει η εγκάρσια στερεομεταφορά} \\ \text{αλλιώς,} & \text{εναλλασόμενη κυριαρχία των δύο συνιστωσών} \end{cases} \tag{10}$$

Με την παραδοχή μιας σχετικά ευθειογενούς ακτής με παράλληλες ισοβαθείς ως προς την ακτή, οι ακόλουθες έξι ζώνες μπορούν να καθοριστούν, που εξαρτώνται από τη γωνία πρόσπτωσης των κυματισμών αναφορικά με την κάθετο ως προς την ακτογραμμή. Οι έξι ζώνες παρουσιάζονται στο Σχήμα 11.

Ανάλογα με την ζώνη που εξετάζεται, ο υπολογισμός των κυματικών αντιπροσώπων γίνεται με βάση τις αρχές τις μεθόδου RMWH-02, μόνο που οι δύο υποκλάσεις δε διαμορφώνονται με βάση μόνο την ροή ενέργειας. Συγκεκριμένα ο διαχωρισμός σε υποκλάσεις για τις Ζώνες 1 και 6 γίνεται με βάση τη μέση ροή ενέργειας, στις Ζώνες 2 και 5 με βάση την κατά μήκος της ακτής ροή στερεομεταφοράς (Vongvisessomjai et al., 1993), ενώ στις Ζώνες 3 και 4 η κατηγοριοποίηση γίνεται με βάση τη μέση τιμή της παραμέτρου εγκάρσιου προφίλ (Dalrymple, 1992) που υπολογίζεται από την ακόλουθη εξίσωση:

$$P_o = g \frac{H_s^2}{w_f^3 T_p} \tag{11}$$
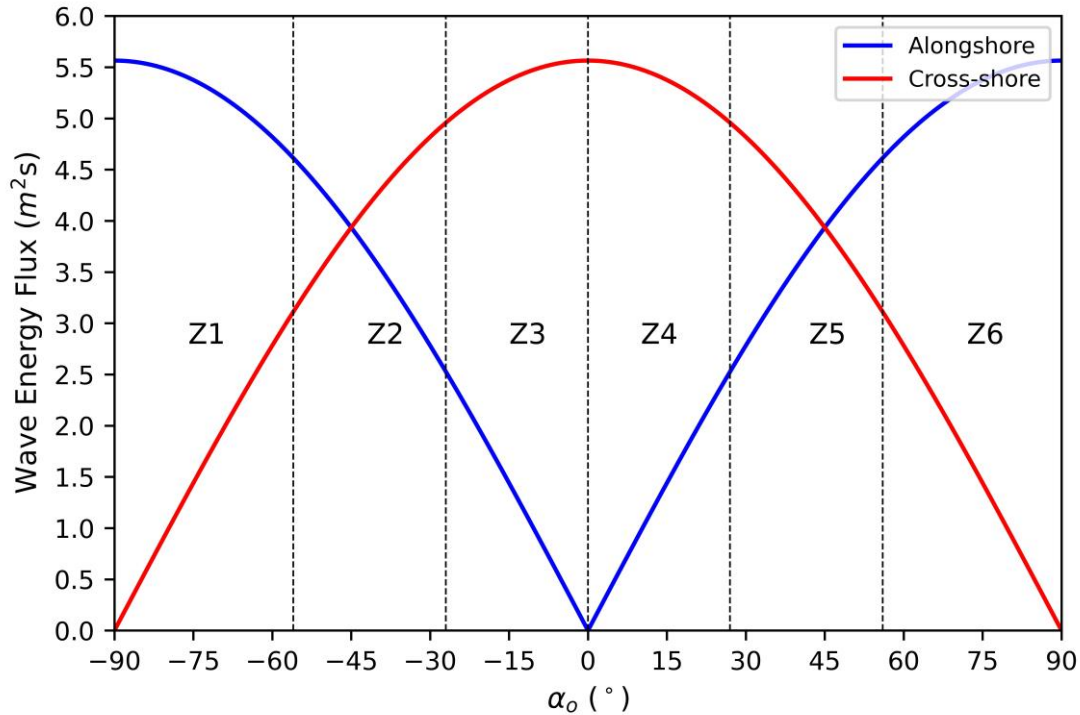
Σχήμα 11. Ζώνες εναλασσόμενης κυριαρχίας της κ.μ.α. και της εγκάρσιας στερεομεταφοράς σχετικά με την γωνία πρόσπτωσης των κυματισμών ως προς την κάθετο στην ακτογραμμή

Τέλος, η περίπτωση **RMWH-04** αφορά στην εκπαίδευση, επαλήθευση και εφαρμογή ενός ΤΝΔ, που αναλαμβάνει την απαλοιφή θαλάσσιων καταστάσεων που θεωρείται ότι δεν είναι ικανές να προκαλέσουν έναρξη κίνησης ιζήματος στα ρηχά νερά. Η μέθοδος RMWH-04 αποτελεί μια μετεξέλιξη της μεθόδου Pick-up rate με την αντικατάσταση των προσομοιώσεων που πραγματοποιούνται με το PMS-SP με το ΤΝΔ.

Οι παράμετροι εισόδου του νευρωνικού δικτύου είναι το χαρακτηριστικό ύψος κύματος, η περίοδος κορυφής και η μέση διεύθυνση διάδοσης κυματισμών στα ανοιχτά καθώς και η μέση διάμετρος κόκκων του ιζήματος και η μέση κλίση πυθμένα, ενώ η παράμετρος εξόδου του νευρωνικού δικτύου είναι η μέση τιμή της τροχιακής ταχύτητας των κυματισμών κοντά στον πυθμένα, υπολογισμένη εντός της ζώνης θραύσης. Συνολικά 3200 συνδυασμοί των παραμέτρων εισόδου, και συνεπακόλουθα 3200 αποτελέσματα προσομοιώσεων του PMS-SP, χρησιμοποιήθηκαν για την εκπαίδευση του νευρωνικού δικτύου.

Αφού εισαχθούν στο ΤΝΔ οι τιμές των κυματικών χαρακτηριστικών στα ανοιχτά για τη δεδομένη χρονοσειρά αναφοράς και καθοριστούν αντιπροσωπευτικές τιμές για τη μέση διάμετρο του ιζήματος και τη μέση κλίση πυθμένα, απαλείφονται κυματισμοί που δεν αναπτύσσουν τροχιακή ταχύτητα μεγαλύτερη από την κρίσιμη τιμή (Εξ. 5), κάτι που έχει ως αποτέλεσμα την μείωση της χρονοσειράς κυματικών χαρακτηριστικών. Στη συνέχεια, εφαρμόζονται τα βήματα της περίπτωσης RMWH-02 στην απομειωμένη χρονοσειρά κυματικών χαρακτηριστικών που προέκυψε και υπολογίζονται οι ισοδύναμοι κυματικοί αντιπρόσωποι.

5.2. Περιοχή εφαρμογής και αντιπροσωπευτικοί ισοδύναμοι κυματισμοί

Οι 4 διακριτές περιπτώσεις (1 περίπτωση εφαρμόστηκαν στην παράκτια περιοχή του Ρεθύμνου, που παρουσιάστηκε στην Ενότητα 3, λαμβάνοντας υπόψη τις ίδιες παραδοχές και παραμετροποίηση του μαθηματικού μοντέλου MIKE21 CM FM. Ωστόσο αυτή τη φορά, οι προσομοιώσεις πραγματοποιήθηκαν με την «Μορφοστατική» προσέγγιση, για 12 κυματικούς αντιπροσώπους. Η προσομοίωση αναφοράς σε αυτή την περίπτωση, αποτελεί μια σχηματοποιημένη μορφή της πλήρους χρονοσειράς κυματικών χαρακτηριστικών (με διακριτοποίηση των υψών κύματος ανά 0.5m και της γωνίας πρόσπτωσης ανά 15˚), και τελικά αποτελείται από 68 θαλάσσιες καταστάσεις. Για μια ακόμα φορά, η αξιολόγηση των αποτελεσμάτων πραγματοποιήθηκε για την περιοχή που παρουσιάζεται εντός του κόκκινου πλαισίου στο Σχήμα 5.

Στο Σχήμα 12 παρουσιάζονται οι κυματικοί αντιπρόσωποι, όπως προέκυψαν για την εφαρμογή των περιπτώσεων RMWH-01 έως RMWH-04. Με γαλάζιο χρώμα σημειώνονται οι θαλάσσιες καταστάσεις που απαλείφονται με την εφαρμογή του νευρωνικού δικτύου.
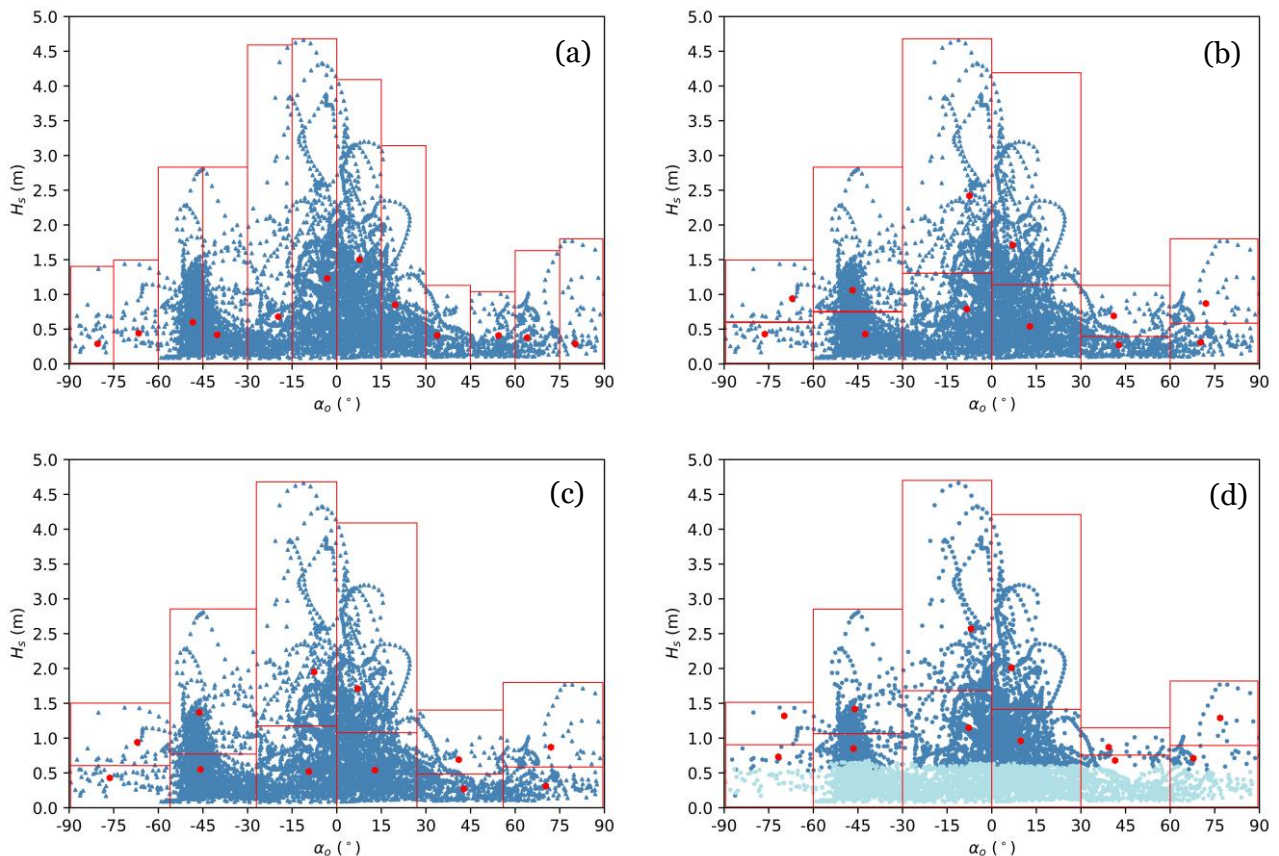
Σχήμα 12. Ισοδύναμοι κυματικοί αντιπρόσωποι και κλάσεις με εφαρμογή των μεθόδων (a) RMWH-01, (b) RMWH-02, (c) RMWH-03, (d) RMWH-04

Η περίπτωση RMWH-01 βασίζεται στην διαδεδομένη προσέγγιση υπολογισμού των ισοδύναμων κυματισμών (Chonwattana et al., 2005). Οι αντιπρόσωποι τείνουν να έχουν χαμηλότερες τιμές ύψους κύματος, λόγω των υψηλών συχνοτήτων εμφάνισης θαλάσσιων καταστάσεων χαμηλού σχετικά ενεργειακού περιεχομένου. Κατά συνέπεια,

οι υψηλότεροι κυματισμοί που εντοπίζονται κυρίως μεταξύ α_o=[-30˚, 15˚], δεν περιγράφονται με τόσο ικανοποιητικό τρόπο από τους ισοδύναμους κυματισμούς.

Στην περίπτωση RMWH-02, λαμβάνοντας υπόψη έξι κλάσεις κατεύθυνσης και δύο υποδιαιρέσεις στον άξονα του ύψους κύματος, επιτυγχάνεται μια καλύτερη αναπαράσταση της ποικιλομορφίας του συνόλου δεδομένων των κυματικών χαρακτηριστικών στα ανοιχτά σε σχέση με την περίπτωση RMWH-01.

Στην περίπτωση RMWH-03 παρά τη χρήση διαφορετικών ποσοτήτων ανάλογα τη ζώνη επιρροής, που εξαρτώνται από την κ.μ.α ή την εγκάρσια στερεομεταφορά, οι αντιπρόσωποι που υπολογίζονται με αυτή τη μέθοδο είναι παρόμοιοι ως προς τις τιμές με εκείνους της RMWH-02. Σημειώνεται επιπρόσθετα ότι η μέθοδος RMWH μπορεί να εφαρμοστεί για να ληφθούν αντιπρόσωποι που είναι ακέραια πολλαπλάσια του αριθμού έξι.

Τέλος η περίπτωση RMWH-04 χρησιμοποιεί ένα τεχνητό νευρωνικό δίκτυο για την εκτίμηση των τροχιακών ταχυτήτων των κυματισμών στα ρηχά και την εξάλειψη των θαλάσσιων καταστάσεων αυτών που δεν υπερβαίνουν το κατώφλι της πυθμενικής τροχιακής ταχύτητας. Κατά συνέπεια, αντιπρόσωποι που λαμβάνονται από την RMWH-04 είναι μετατοπισμένοι σε πιο ενεργητικές κυματικές συνθήκες.

5.3. Αποτελέσματα μεθόδων σχηματοποίησης ισοδύναμων κυματισμών

Κατά αντιστοιχία και με προηγούμενα εδάφια, παρατίθενται οι προβλεπόμενες μεταβολές της βαθυμετρίας σε ορίζοντα ενός έτους με χρήση του μοντέλου MIKE21 CM FM, για τις περιπτώσεις σχηματοποίηση των ισοδύναμων κυματισμών. Η μεταβολή μεταξύ αρχικής και τελικής βαθυμετρίας για την προσομοίωση αναφοράς παρουσιάζεται στο Σχήμα 13. Συγκρίνοντας την με την αντίστοιχη προσομοίωση αναφοράς της «Μορφοδυναμικής» προσέγγισης, παρατηρείται ότι υποεκτιμάται σε ένταση και η διάβρωση που εμφανίζεται νότια της εισόδου του λιμένα όσο και η έκταση της απόθεσης στη ρίζα του υπήνεμου μώλου και στην είσοδο. Ωστόσο η γενική εικόνα των περιοχών απόθεσης ή διάβρωσης που εντοπίζονται στην περιοχή μελέτης βρίσκεται σε συμφωνία μεταξύ της «Μορφοστατικής» και «Μορφοδυναμικής» προσέγγισης.
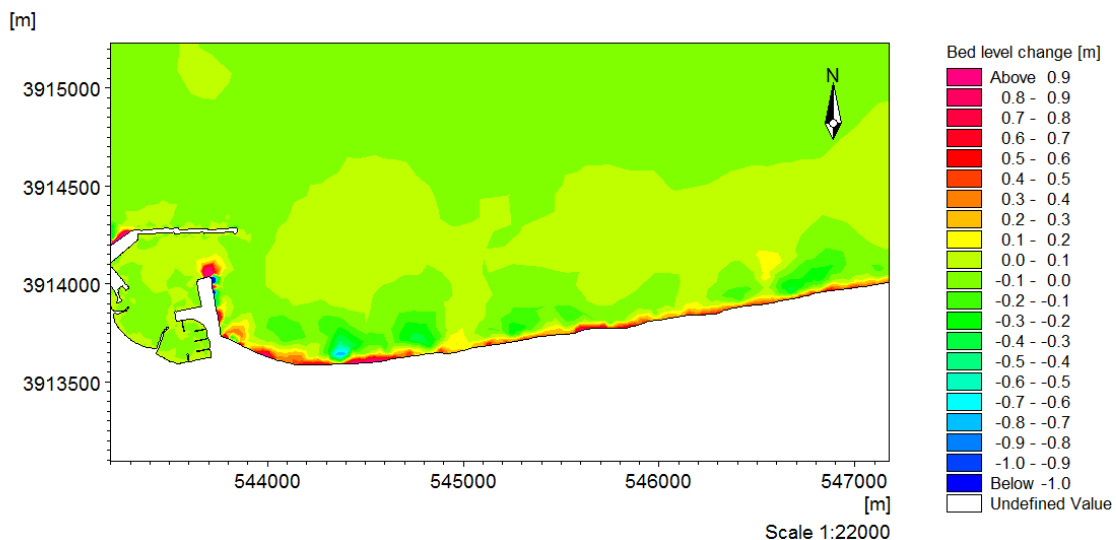
Σχήμα 13. Μεταβολή τελικής βαθυμετρίας ως προς την αρχική για την προσομοίωση αναφοράς της Μορφοστατικής προσέγγισης

39

Τα αποτελέσματα μεταβολής αρχικής και τελικής βαθυμετρίας που προέκυψαν από τις τέσσερις διαφορετικές περιπτώσεις εφαρμογής των μεθόδων σχηματοποίησης ισοδύναμων κυματισμών παρουσιάζονται στο Σχήμα 14.
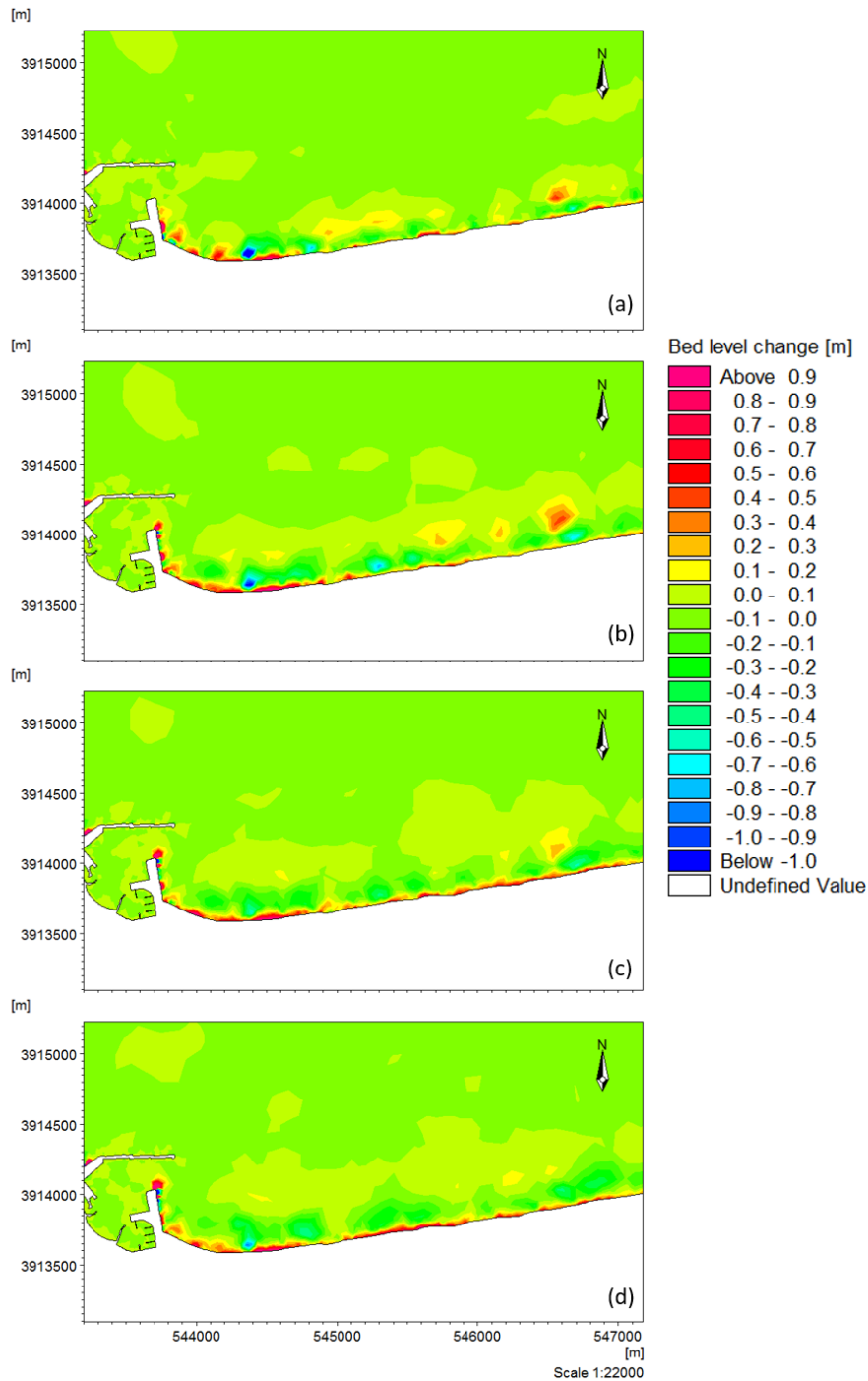
Σχήμα 14. Αποτελέσματα προσομοιώσεων μεταβολής τελικής βαθυμετρίας ως προς την αρχική (a) RMWH-01, (b) RMWH-02, (c) RMWH-03. (d) RMWH-04

Παρατηρείται ότι τα αποτελέσματα προσομοίωσης με τη μέθοδο RMWH-01 υποεκτιμούν σημαντικά την έκταση της προσάμμωσης στην είσοδο του λιμένα, και εμφανίζουν τις μεγαλύτερες αποκλίσεις σε σύγκριση με την προσομοίωση αναφοράς. Αντίθετα, οι περιπτώσεις RMWH-02 και RMWH-03, επιδεικνύουν μια σημαντική βελτίωση των αποτελεσμάτων, και μια ικανοποιητική αναπαραγωγή των μοτίβων

40

απόθεσης και διάβρωσης της προσομοίωσης αναφοράς. Τέλος η περίπτωση RMWH-04, δείχνει από την οπτική αξιολόγηση να βρίσκεται στην καλύτερη συμφωνία σε σχέση με την προσομοίωση αναφοράς.

Για την περαιτέρω αξιολόγηση των αποτελεσμάτων του μαθηματικού μοντέλου Οι υπολογισθείσες τιμές του BSS, συνοδευόμενες από το ποσοστό μείωσης του χρόνου προσομοίωσης σε σύγκριση με την προσομοίωση αναφοράς παρουσιάζονται στον Πίνακα 4.

Πίνακας 4. *Υπολογισθείσες τιμές του BSS για τις μεθόδους σχηματοποίησης και ποσοστό μείωσης χρόνου προσομοίωσης σε σχέση με την προσομοίωση αναφοράς για την περίπτωση των ισοδύναμων κυματισμών*

	RMWH-01	**RMWH-02**	**RMWH-03**	**RMWH-04**
BSS	0.24	0.56	0.58	0.65
Ποσοστό μείωσης χρόνου προσομοίωσης (%)	485	470	462	468

Παρατηρείται ότι εφαρμογή της μεθόδου των Chonwattana et al., 2005 (RMWH-01), στην περιοχή μελέτης του Ρεθύμνου, οδηγεί σε μια «Καλή» κατηγοριοποίηση με βάση την τιμή του BSS, ενώ όλες οι προτεινόμενες βελτιώσεις κατηγοριοποιούνται ως εξαιρετικές, αυξάνοντας σημαντικά τις τιμές του BSS. Η βέλτιστη μέθοδος ως προς τις τιμές του δείκτη BSS είναι η μέθοδος RMWH-04 η οποία εισάγει ένα τεχνητό νευρωνικό δίκτυο που αναλαμβάνει την απαλοιφή θαλάσσιων καταστάσεων που θεωρείται ότι δεν προκαλούν σημαντική μεταφορά ιζήματος στην περιοχή μελέτης. Τέλος, άξια αναφοράς είναι η σημαντική συνεισφορά των μεθόδων σχηματοποίησης στην εξοικονόμηση χρόνου προσομοίωσης, που οφείλεται στη μείωση των σεναρίων προσομοίωσης από 68 σε αυτή την περίπτωση σε 12.

6. Συγκριτική αξιολόγηση μεθόδων σχηματοποίησης και επαλήθευση με μετρήσεις πεδίου

Η επαλήθευση προσομοιώσεων μορφολογικής εξέλιξης πυθμένα με διαθέσιμες μετρήσεις πεδίου, συναντάται περιορισμένες φορές στη διεθνή βιβλιογραφία (Luijendijk et al., 2017a, 2017b), καθώς είναι ιδιαίτερα δύσκολη η διενέργεια τακτικών μετρήσεων βαθυμετρίας, ταυτόχρονα με μετρήσεις κυματισμών και παράκτιων ρευμάτων για την επαλήθευση των μοντέλων παράκτιων περιοχών. Για αυτό το λόγο, οι περισσότερες ερευνητικές προσπάθειες επικεντρώνονται στην επαλήθευση των αποτελεσμάτων προσομοιώσεων των μεθόδων σχηματοποίησης με μια προσομοίωση αναφοράς, η οποία αποτελείται από την πλήρη χρονοσειρά κυματικών χαρακτηριστικών και αντικαθιστά τις μετρήσεις πεδίου. Στο πλαίσιο αυτής της διατριβής, γίνεται η απόπειρα αποτίμησης και συγκριτικής αξιολόγησης επιλεγμένων μεθόδων σχηματοποίησης κυματικού κλίματος που παρουσιάστηκαν στα προηγούμενα εδάφια με διαθέσιμες μετρήσεις πεδίου βαθυμετρίας στην περιοχή της Σκάλας Ερεσού στο νησί της Λέσβου.

6.1. Περιοχή μελέτης και διαθέσιμα δεδομένα

Η παραλία της Ερεσού έχει μήκος περί τα 1.7 km. Στα ανατολικά οριοθετείται από το αλιευτικό καταφυγίου της Σκάλας Ερεσού, ενώ στα δυτικά από το ακρωτήρι του Κοφινά (Σχήμα 15). Στο κέντρο της ακτής εντοπίζεται ο χείμαρρος «Χαλάνδρα», η στερεοαπορροή του οποίου πρακτικά έχει εκμηδενιστεί την τελευταία δεκαετία μετά την κατασκευή φράγματος βόρεια της ακτής. Η παραλία αποτελεί έναν από τους κυριότερους τουριστικούς προορισμούς της Λέσβου, αλλά χαρακτηρίζεται από έντονα φαινόμενα διάβρωσης στο ανατολικό της τμήμα που έχει ενταθεί με την κατασκευή κατακόρυφων προφυλακτήριων τοίχων (Karambas, 2010).

Σχήμα 15. Περιοχή μελέτης στην Σκάλα Ερεσού και σχετική θέση της σε σχέση με το νησί της Λέσβου.

Σε όλη την έκταση της περιοχής μελέτης έχουν διενεργηθεί τακτικές βυθομετρήσεις και συγκεκριμένα στις εξής ημερομηνίες: 03/11/2013, 26/04/2014, 14/02/2015, 19/11/2015, 29/12/2015 (Andreadis, 2021). Επίσης, στην περιοχή έχουν πραγματοποιηθεί ιζηματομετρήσεις, οι οποίες επιβεβαίωσαν ότι τα ιζήματα της παραλίας είναι κατά κύριο λόγο αμμώδη, με το ποσοστό των αργιλο-ιλυώδων αποθέσεων να αυξάνεται εκατέρωθεν της εκβολής του ρέματος Χαλάνδρα. Για την επαλήθευση των μεθόδων σχηματοποίησης επιλέχθηκε να προσομοιωθεί μια περίοδος 9 μηνών μεταξύ των 14/02/2015 και 19/11/2015, με την χρονική έκταση της προσομοίωσης να κρίνεται ικανοποιητική για την επαλήθευση των μεθόδων σχηματοποίησης κυματικού κλίματος.

Λόγω της έλλειψης μετρήσεων κυματικών χαρακτηριστικών στα ανοιχτά, αποκτήθηκαν δεδομένα για την προαναφερθείσα χρονική περίοδο από την Ευρωπαϊκή βάση του Κοπέρνικου. Το κυματικό ροδόγραμμα παρουσιάζεται στο Σχήμα 16, από όπου

διαφαίνεται ότι οι κύριοι κυματισμοί στην περιοχή μελέτης προέρχονται από το Νότιο τομέα.
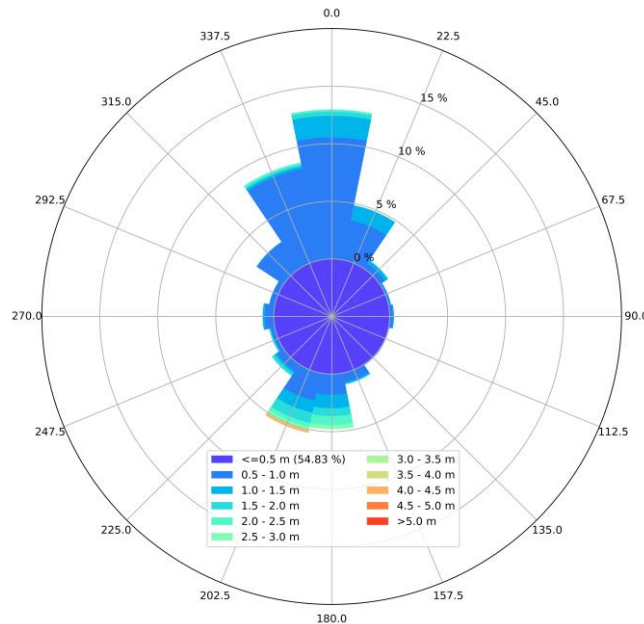
Σχήμα 16. Κυματικό ροδόγραμμα στα ανοιχτά της περιοχής της Σκάλας Ερεσού στη Λέσβο.

Οι μορφολογικές προσομοιώσεις πραγματοποιήθηκαν με το μοντέλο MIKE21 CM FM, ενώ η αποτίμηση των αποτελεσμάτων έγινε σε 4 διακριτά παράκτια προφίλ στο δυτικό τμήμα της περιοχής μελέτης, που χαρακτηρίζεται από μεγαλύτερο μήκος παραλίας και δεν εμφανίζει έντονα φαινόμενα διάβρωσης διαχρονικά. Ο κάνναβος πεπερασμένων στοιχείων και οι διατομές που θα γίνει μετέπειτα η αποτίμηση της απόδοσης των μεθόδων σχηματοποίησης παρουσιάζεται στο Σχήμα 17.
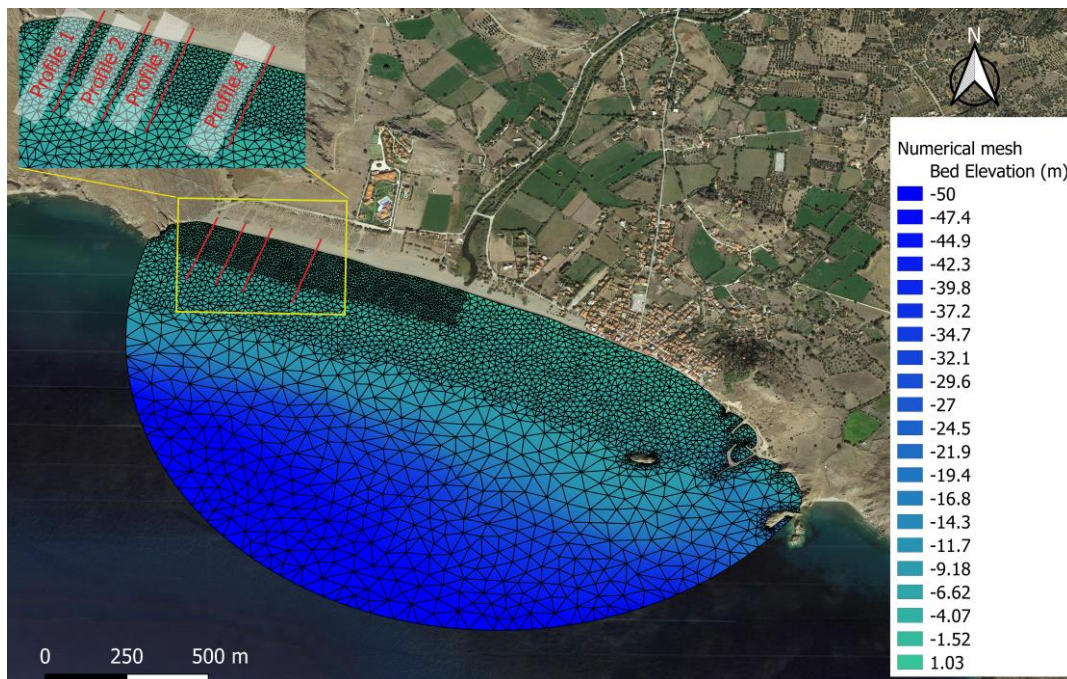
Σχήμα 17. Κάνναβος πεπερασμένων στοιχείων και προφίλ αποτίμησης των αποτελεσμάτων του των αριθμητικών προσομοιώσεων.

43

6.2. Επιλογή βέλτιστων μεθόδων σχηματοποίησης κυματικού κλίματος

Με βάση τα αποτελέσματα των μεθόδων σχηματοποίησης στην περιοχή του Ρεθύμνου θα επιλεγεί για κάθε μια από τις βασικές κατηγορίες μεθόδων σχηματοποίησης (ισοδύναμοι κυματισμοί, μέθοδοι σχηματοποίησης σε κλάσεις, αλγόριθμοι ομαδοποίησης) μια μέθοδος σχηματοποίησης η οποία κρίνεται ως βέλτιστη τόσο ως προς την ακρίβεια των αποτελεσμάτων όσο και ως προς την ευκολία εφαρμογής και εξοικόνομηση υπολογιστικού φόρτου. Σημειώνεται ότι η συγκριτική αξιολόγηση θα γίνει για την «Μορφοστατική» προσέγγιση στις προσομοιώσεις του μοντέλου παράκτιας περιοχής.

Ως προς τις μεθόδους σχηματοποίησης χωρισμού σε κλάσεις, η μέθοδος ροής ενέργειας είχε αποδώσει τα καλύτερα αποτελέσματα σε σχέση με τις μεθόδους Pick-up rate και Threshold Current Speed. Οι τελευταίες προσέφεραν σημαντική εξοικονόμηση χρόνου η οποία όμως είναι σημαντική στη «Μορφοδυναμική» προσέγγιση, ενώ στη «Μορφοστατική» προσέγγιση η εισαγωγή ενός ακόμα μαθηματικού μοντέλου μπορεί να θεωρηθεί ως μειονέκτημα για την ευκολία εφαρμογής. Συνεπώς επιλέγεται στην περιοχή της Ερεσού να χρησιμοποιηθεί η **μέθοδος ροής ενέργειας**.

Για τις εναλλακτικές περιπτώσεις του αλγορίθμου K-Means, οι διαφορές των δεικτών BSS ήταν σχετικά μικρές μεταξύ των εναλλακτικών περιπτώσεων, με τη μέθοδο KM-05 να παρουσιάζει την καλύτερη απόδοση. Ωστόσο οι τροποποιήσεις που εξετάστηκαν πέραν της βασικής εφαρμογής του αλγορίθμου K-Means (KM-01) εισάγουν αρκετά σημαντική πολυπλοκότητα για πρακτικές εφαρμογές. Συναξιολογώντας την ευκολία εφαρμογής και τα ικανοποιητικά αποτελέσματα της μεθόδου **KM-01**, επιλέγεται αυτή ως βέλτιστη από την κατηγορία των αλγορίθμων ομαδοποίησης.

Τέλος, από τις μεθόδους σχηματοποίησης των ισοδύναμων κυματισμών, η μέθοδος **RMWH-04**, που ενσωματώνει κατάλληλα εκπαιδευμένο τεχνητό νευρωνικό δίκτυο για την απαλοιφή θαλάσσιων καταστάσεων που δεν κρίνονται καθοριστικές για την εξέλιξη της παράκτιας μορφολογίας, είναι η βέλτιστη τόσο ως προς την απόδοση με βάση το δείκτη BSS, όσο και ως προς την εξοικονόμηση υπολογιστικού φόρτου.

Στο Σχήμα 18 παρουσιάζονται οι κυματικοί αντιπρόσωποι για τις μεθόδους ροής ενέργειας, KM-01 και RMWH-04 αντίστοιχα στα ανοιχτά της ακτής της Ερεσού. Σημειώνεται ότι επιλέχθηκαν 12 αντιπρόσωποι και για τις 3 μεθόδους και οι προσομοιώσεις πραγματοποιήθηκαν με τη «Μορφοστατική» προσέγγιση.
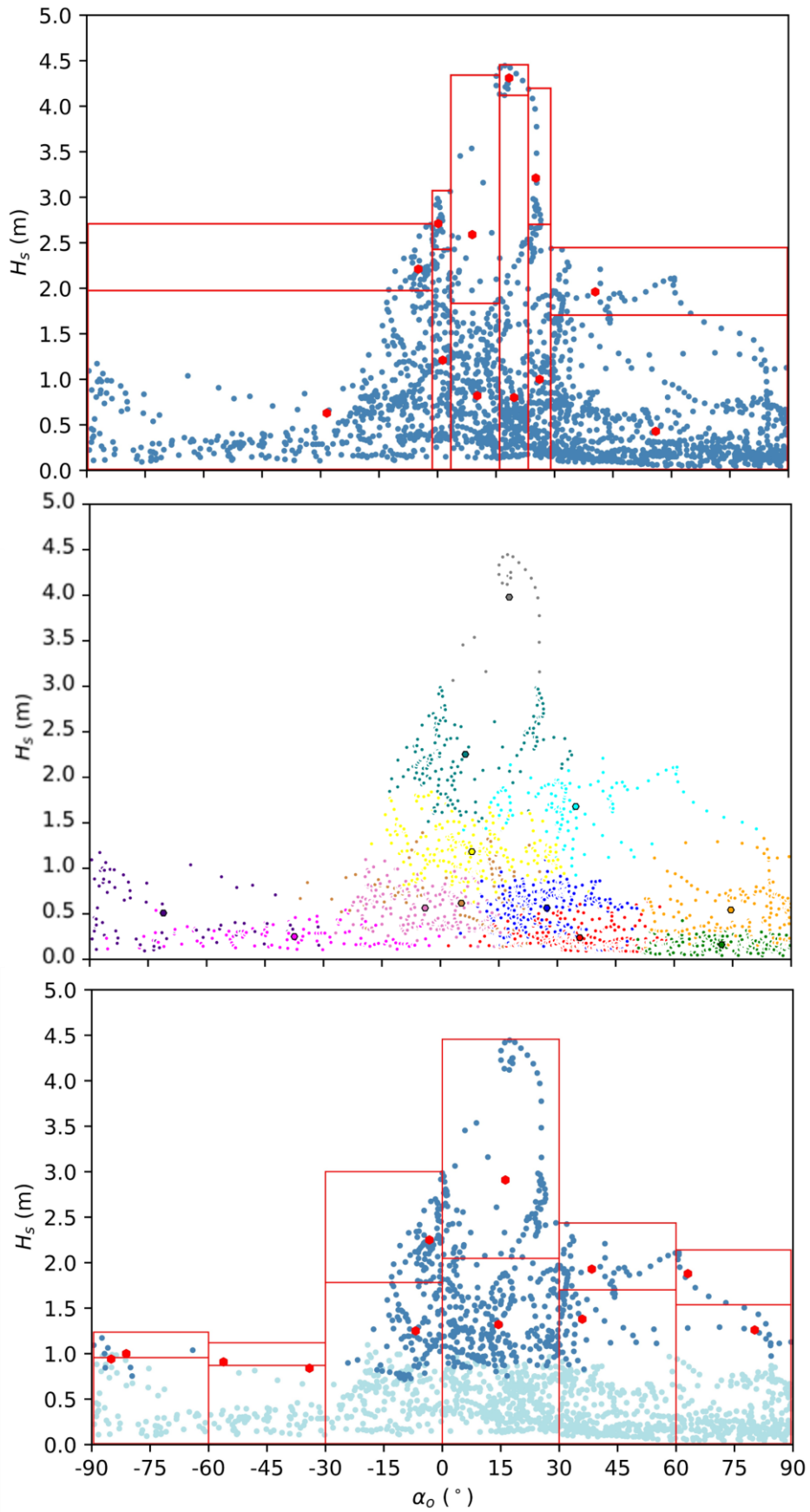
Σχήμα 18. Κυματικοί αντιπρόσωποι και κλάσεις/συστάδες με την εφαρμογή των μεθόδων (a) ροής ενέργειας, (b) ΚΜ-01 και (c) RMWH-04.

6.3. Αποτελέσματα και συγκριτική αξιολόγηση μεθόδων σχηματοποίησης

Η τελική βαθυμετρία που προκύπτει από την προσομοίωση κάθε μεθόδου σχηματοποίησης συγκρίνεται με τις τιμές για κάθε προφίλ ακτής, όπως αυτές προέκυψαν από την τοπο-βαθυμετρική αποτύπωση, και παρουσιάζονται στα Σχήματα 19 και 20.
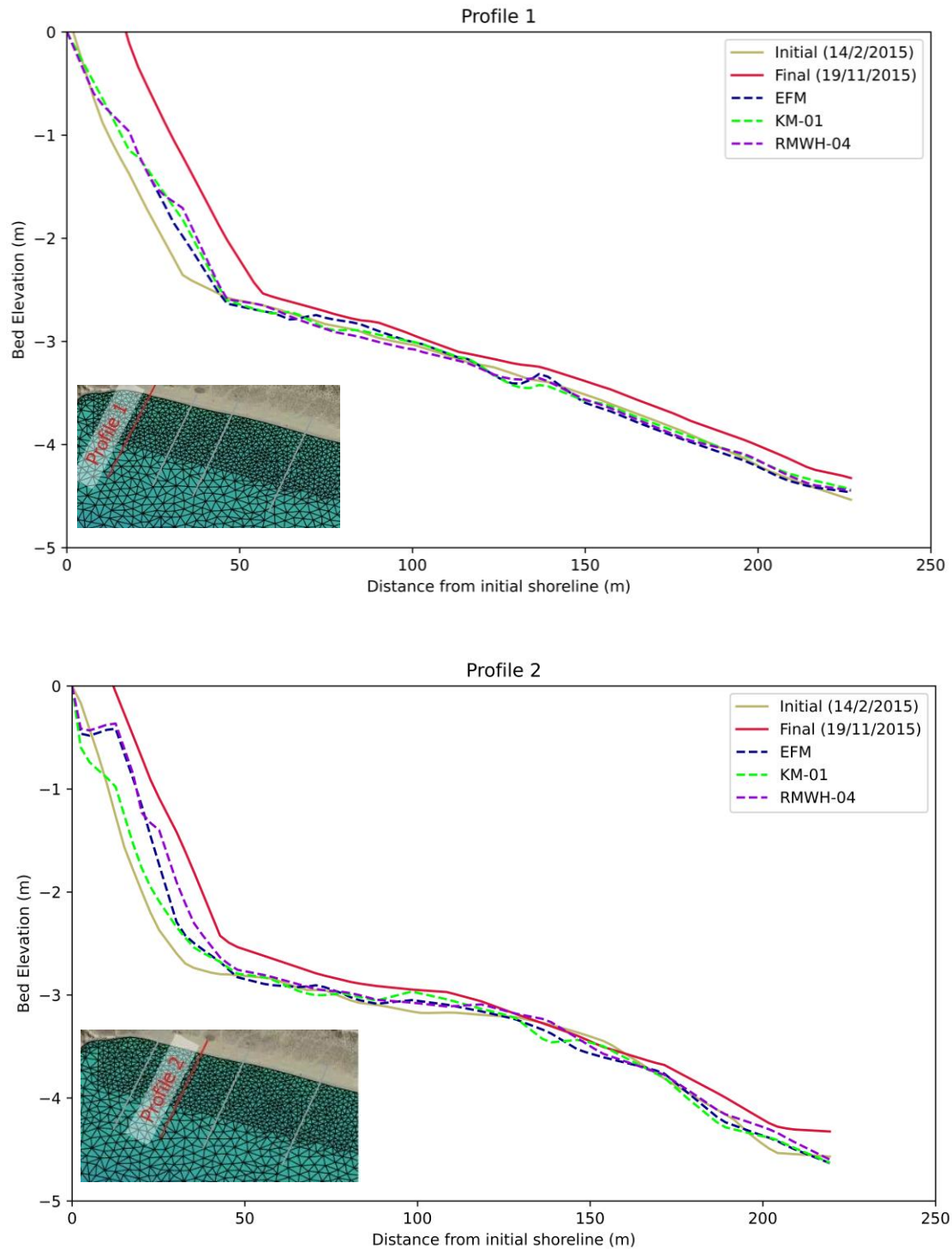
Σχήμα 18. Σύγκριση μετρήσεων πεδίου για την τελική βαθυμετρία (κόκκινη γραμμή) και προβλέψεις μεθόδων σχηματοποίησης για τα παράκτια Προφίλ 1 και 2.
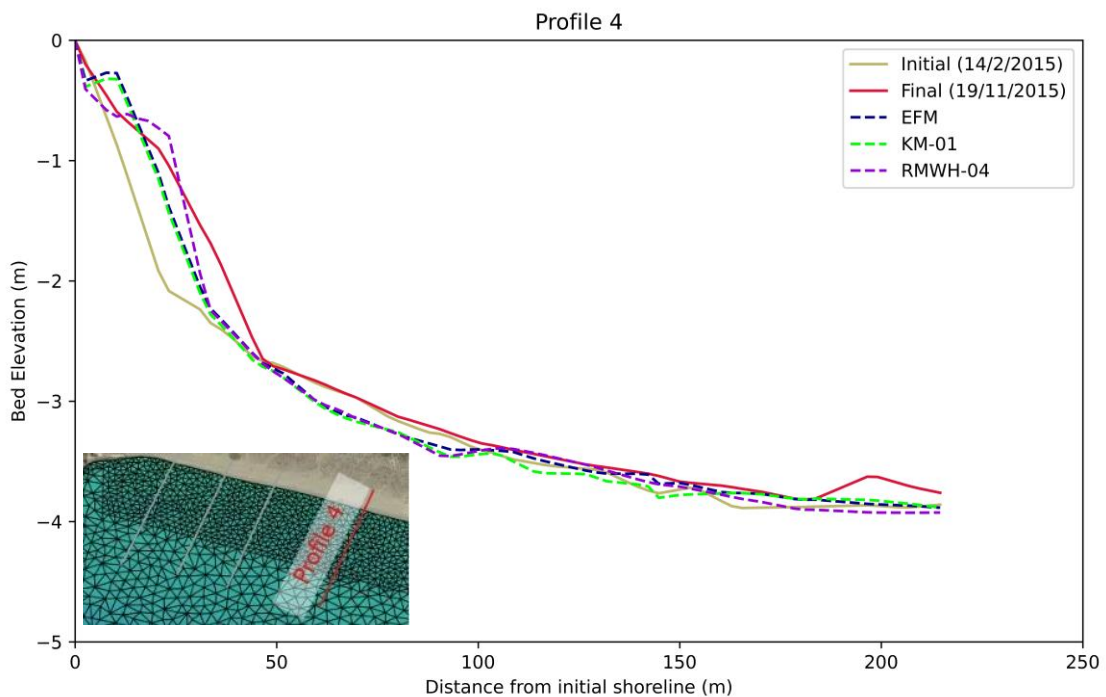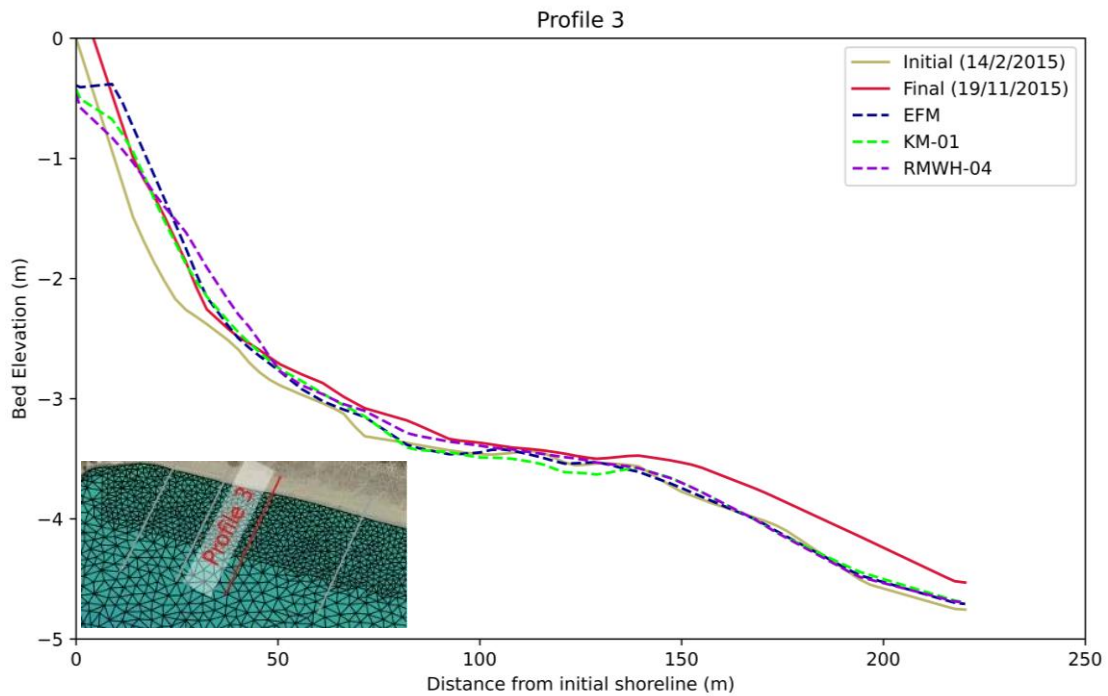
Σχήμα 19. *Σύγκριση μετρήσεων πεδίου για την τελική βαθυμετρία (κόκκινη γραμμή) και προβλέψεις μεθόδων σχηματοποίησης για τα παράκτια Προφίλ 3 και 4.*

Σημαντικοί όγκοι απόθεσης ιζήματος παρατηρούνται από την ακτογραμμή έως και βάθος των -4 m, με τη συσσώρευση άμμου να είναι πιο εμφανής σε βάθος περί τα -2.5 m, υποδεικνύοντας ότι οι παράκτιες διεργασίες συντελούνται κυρίως σε αυτό το εύρος βάθους. Συνολικά, οι τρεις μέθοδοι είναι ικανές να αναπαράγουν τα παρατηρούμενα μοτίβα απόθεσης μεταξύ του βάθους -1.0 και -2.5 m σε όλα τα εξεταζόμενα προφίλ. Ωστόσο, τα αποτελέσματα των προσομοιώσεων δεν περιγράφουν τη συσσώρευση

ιζήματος στο μέτωπο της ακτής (σε βάθη μικρότερα από 0.5 m) καθώς και σε βάθη μεγαλύτερα από 3.0 m στα περισσότερα τμήματα.

Για το Προφίλ 1, παρατηρούνται σημαντικές αποκλίσεις μεταξύ του τελικής βαθυμετρίας των προσομοιώσεων και της αντίστοιχης που προέκυψε από τις επιτόπου μετρήσεις. Συνεπώς, δεν είναι δυνατή η οπτική επιλογή της βέλτιστης μεθόδου. Το προφίλ 2 δίνει παρόμοιες προβλέψεις τελικής βαθυμετρίας μεταξύ RMWH-04 και μεθόδου ροής ενέργειας (EFM), ενώ η μέθοδος KM-01 αποκλίνει περισσότερο από τις μετρούμενες τιμές. Η μέθοδος RMWH-04 έχει καλύτερη απόδοση, προβλέποντας της μετρούμενες ποσότητας απόθεσης στα μεγαλύτερα βάθη.

Στο Προφίλ 3, και οι τρεις μέθοδοι καταγράφουν τη σωστή τάξη μεγέθους στη μεταβολή της βαθυμετρίας. Ωστόσο, καμία από τις μεθόδους δεν αναπαράγει την δημιουργία του ύφαλου αναβαθμού που εντοπίζεται σε βάθη μεγαλύτερα από τα -4 m. Στο Προφίλ 4, η μέθοδος RMWH-04 αναπαράγει πιο αποτελεσματικά τις παρατηρούμενες μεταβολών της στάθμης του πυθμένα, ειδικά σε βάθη μεγαλύτερα των 2.5 m.

Η συγκριτική αξιολόγηση των μεθόδων σχηματοποίησης ως προς το δείκτη BSS παρουσιάζεται στον Πίνακα 5, με τη μέθοδο RMWH-04 να επιτυγχάνει τις υψηλότερες τιμές BSS στα Προφίλ 2 και 4, (που ταξινομούνται ως "Εξαιρετικά"), ακολουθούμενη από τη μέθοδο ροής ενέργειας. Η μέθοδος KM-01 έχει σταθερά χειρότερη απόδοση, με εύρος απόδοσης από "Λογικό/Μέτριο" έως "Καλό", αν και επιτυγχάνει οριακά την υψηλότερη τιμή του δείκτη BSS στο Προφίλ 1.

Πίνακας 5. Υπολογισθείσες τιμές του BSS για τις μεθόδους σχηματοποίησης και κατηγοριοποίηση, Ε: Εξαιρετικό, Κ: Καλό, Λ/Μ: Λογικό/Μέτριο

	EFM	KM-01	RMWH-04
Προφίλ 1	0.25 (Κ)	**0.29** (Κ)	0.28 (Κ)
Προφίλ 2	0.54 (Ε)	0.19 (Κ)	**0.69** (Ε)
Προφίλ 3	**0.23** (Κ)	0.2 (Λ/Μ)	0.22 (Κ)
Προφίλ 4	0.66 (Ε)	0.42 (Κ)	**0.68** (Ε)

Συνοψίζοντας, με βάση τη συγκριτική αξιολόγηση που πραγματοποιήθηκε, διαφαίνεται πως και οι τρεις μέθοδοι μπορούν να προβλέψουν σε ικανοποιητικό βαθμό την εξέλιξη του πυθμένα στην περιοχή της Ερεσού, με τη μέθοδο RMWH-04 να έχει σταθερά την πιο ικανοποιητική απόδοση και να βρίσκεται σε μεγαλύτερη συμφωνία με τις πειραματικές μετρήσεις.

7. Συμπεράσματα

Λόγω του ιδιαίτερα μεγάλου όγκου των διαθέσιμων κυματικών χαρακτηριστικών, καθώς και των αυξημένων υπολογιστικών απαιτήσεων των μαθηματικών μοντέλων προσομοίωσης, οι μέθοδοι σχηματοποίησης κυματικού κλίματος βρίσκονται στο επίκεντρο της έρευνας της παράκτιας μηχανικής. Η παρούσα διατριβή είχε ως στόχο την περαιτέρω ανάπτυξη και αξιολόγηση μεθόδων σχηματοποίησης, με σκοπό τόσο την ενίσχυση της ακρίβειας των αποτελεσμάτων, όσο και τη μείωση του απαιτούμενου χρόνου των προσομοιώσεων.

Αρκετές μέθοδοι σχηματοποίησης εντοπίζονται στη διεθνή βιβλιογραφία και με βάση τα χαρακτηριστικά τους διακρίνονται στις ακόλουθες κατηγορίες:

- *Ισοδύναμοι κυματισμοί*
- *Μέθοδοι σχηματοποίησης σε κλάσεις*
- *Αλγόριθμοι ομαδοποίησης*

Με βάση τους ερευνητικούς στόχους που τέθηκαν στην παρούσα διατριβή, επετεύχθη η βελτίωση της απόδοσης των μεθόδων σχηματοποίησης, με συνεπακόλουθη μείωση του υπολογιστικού φόρτου. Αυτό κατέστη δυνατό με την απαλοιφή δεδομένων κυματικών χαρακτηριστικών που θεωρείται ότι δεν είναι ικανά να προκαλέσουν έναρξη κίνησης ιζήματος. Σημαντική κρίνεται η συμβολή τεχνικών μηχανικής μάθησης (τόσο με τους αλγορίθμους ομαδοποίησης όσο και με την ανάπτυξη τεχνικών νευρωνικών δικτύων) τα που υποβοηθούν τις μεθόδους σχηματοποίησης και παρουσιάζουν υποσχόμενα αποτελέσματα. Στο πλαίσιο της διατριβής αξιολογήθηκαν μέθοδοι σχηματοποίησης και από τις τρεις κύριες κατηγορίες, ενώ τα αποτελέσματα επιλεγμένων μεθόδων επαληθεύθηκαν με διαθέσιμες μετρήσεις πεδίου.

Ως προς τις μεθόδους σχηματοποίησης σε κλάσεις αναπτύχθηκαν 2 νέες μέθοδοι που επικεντρώθηκαν στην απαλοιφή θαλάσσιων καταστάσεων που δεν προκαλούν έναρξη κίνησης ιζήματος στα ρηχά. Συγκεντρωτικά, τα βασικά συμπεράσματα από την αξιολόγηση των μεθόδων σχηματοποίησης σε κλάσεις είναι τα ακόλουθα:

- Η νέα μέθοδος Pick-up rate οδήγησε στην απαλοιφή του 57,2% των καταγραφών της χρονοσειράς κυματικών χαρακτηριστικών και επιτυγχάνοντας το ίδιο ποσοστό μείωσης του χρόνου εκτέλεσης του μαθηματικού μοντέλου, σε σύγκριση με την προσομοίωση αναφοράς που περιλαμβάνει την πλήρη χρονοσειρά. Επιτεύχθηκε τιμή του δείκτη BSS 0.74 ταξινομώντας την προσομοίωση ως «Εξαιρετική».
- Η μέθοδος Threshold Current speed οδήγησε στην απαλοιφή του 62% των δεδομένων της πλήρους χρονοσειράς, με την τιμή του BSS να είναι σε αυτή την περίπτωση 0.72.
- Η μέθοδος ροής ενέργειας (EFM) έδωσε την μεγαλύτερη τιμή του δείκτη BSS (0.85) με μια μείωση του χρόνου προσομοίωσης μόλις 11% σε σχέση με την προσομοίωση αναφοράς.
- Η εφαρμογή τεχνικών φιλτραρίσματος και απαλοιφής κυματικών δεδομένων μειώνει σημαντικά το χρόνο προσομοίωσης με μια μικρή μείωση της τιμής του δείκτη BSS.

Στη συνέχεια εξετάστηκε η ικανότητα του αλγορίθμου ομαδοποίησης K-Means να αποτελέσει μια ικανοποιητική μέθοδο σχηματοποίσης ενώ αξιολογήθηκαν συνολικά 6 περιπτώσεις εφαρμογής του αλγορίθμου, με σκοπό τη βελτίωση της απόδοσής του. Τα βασικά συμπεράσματα από την εφαρμογή του αλγορίθμου K-Means ήταν τα ακόλουθα:

- Όλες οι προσομοιώσεις για τις διάφορες περιπτώσεις (KM-01 έως KM-06) ταξινομούνται ως «Εξαιρετικές» σύμφωνα με την κατηγοριοποίηση του BSS. Κάθε εξεταζόμενη περίπτωση πέρα της βασικής παραμετροποίησης του

αλγορίθμου (KM-01) βελτιώνει οριακά τις τους δείκτες BSS, επικυρώνοντας την καλύτερη απόδοση του αλγορίθμου όταν εισάγονται ποσότητες που είναι καθοριστικές για τη μεταφορά ιζημάτων στην παράκτια ζώνη στην αλγοριθμική διαδικασία.

- Για την περιοχή μελέτης που εξετάστηκε, ο αλγόριθμος ομαδοποίησης K-Means αποδίδει ελαφρώς χειρότερα από τις μεθόδους σχηματοποίησης σε κλάσεις. Επιπλέον, οι περισσότερες δοκιμές είναι εγγενώς πολύπλοκες και απαιτούν είτε τον αρχικό προσδιορισμό αντιπροσωπευτικών συνθηκών μέσω άλλων μεθόδων σχηματοποίησης είτε την αξιοποίηση ενός επιπλέον κυματικού μοντέλου, που αναπτύχθηκε στο πλαίσιο της παρούσας διατριβής.

- Η βασική παραμετροποίηση του αλγορίθμου K-Means (περίπτωση KM-01) δίνει ικανοποιητικά αποτελέσματα με βάση την κατηγοριοποίηση BSS και απαιτεί ελάχιστη παρέμβαση από το χρήστη. Συνεπώς, μπορεί να χρησιμοποιείται σαν εναλλακτική των πιο διαδεδομένων μεθόδων σχηματοποίησης.

Τέλος αξιολογήθηκαν οι μέθοδοι σχηματοποίησης των ισοδύναμων κυματισμών και προτάθηκαν 3 επιπλέον βελτιωτικές τροποποιήσεις. Τα συμπεράσματα από την εφαρμογή των μεθόδων σχηματοποίησης των ισοδύναμων κυματισμών είναι τα ακόλουθα:

- Η «Μορφοστατική» προσέγγιση είναι σημαντικά ταχύτερη από την «Μορφοδυναμική» λόγω της μείωσης του απαιτούμενου αριθμού των θαλάσσιων καταστάσεων που πρέπει να προσομοιωθούν. Για τη συγκεκριμένη μελέτη περίπτωσης και το μοντέλο παράκτιας περιοχής που εφαρμόστηκε, οι χρόνοι προσομοίωσης μειώθηκαν κατά περίπου 400-450% σε σχέση με τους αντίστοιχους που απαιτούνται για την προσομοίωση αναφοράς.

- Η κλασσική μέθοδος υπολογισμού των ισοδύναμων κυματισμών (περίπτωση RMWH-01) είχε τη χειρότερη απόδοση σε σύγκριση με τις άλλες δοκιμές με τιμή BSS 0.24, ταξινομώντας τα αποτελέσματα της προσομοίωσης ως "Καλά".

- Η περαιτέρω υποδιαίρεση σε δύο κλάσεις ύψους κύματος ανά κλάση γωνίας πρόσπτωσης (περίπτωση RMWH-02) είναι σχετικά απλή στη σύλληψη, αλλά βελτίωσε σημαντικά τα αποτελέσματα του μοντέλου σε σχέση με την μέθοδο RMWH-01, ταξινομώντας την προσομοίωση ως «Εξαιρετική».

- Η μέθοδος RMWH-04 παρουσίασε την καλύτερη απόδοση και δεδομένου ότι ενσωματώνει ένα τεχνητό νευρωνικό δίκτυο απαιτεί ελάχιστους υπολογιστικούς πόρους. Η υποδειγματική απόδοση της εν λόγω μεθόδου, επαληθεύτηκε τόσο για τη "Μορφοστατική" όσο και τη "Μορφοδυναμική" προσέγγιση, αποδεικνύοντας πως η απαλοιφή θαλάσσιων καταστάσεων χαμηλής ενέργειας μπορεί να οδηγήσει σε βελτιωμένα αποτελέσματα με ταυτόχρονη μείωση του υπολογιστικού φόρτου.

Τελικά, με βάση τις ληφθείσες τιμές του δείκτη BSS και επίσης συνυπολογίζοντας την ευκολία εφαρμογής και υπολογιστική αποδοτικότητα όλων των εναλλακτικών μεθόδων που εξετάστηκαν σε αυτή τη διατριβή, επιλέχθηκε μία μέθοδος ως η βέλτιστη για κάθε κλάδο σχηματοποίησης. Συγκεκριμένα επιλέχθηκαν ως βέλτιστες επιλογές η μέθοδος ροής ενέργειας, η KM-01 και η RMWH-04. Οι τρεις αυτές μέθοδοι εφαρμόστηκαν στην

παράκτια περιοχή της Ερεσού στη Λέσβο και συγκρίθηκαν με διαθέσιμες μετρήσεις πεδίου. Τα επιμέρους συμπεράσματα από αυτή την συγκριτική αξιολόγηση ήταν τα εξής:

- Δεδομένης της πολυπλοκότητας της βαθμονόμησης των μοντέλων της παράκτιας περιοχής για τη πρόβλεψη της εξέλιξης του πυθμένα, και οι τρεις μέθοδοι αποδίδουν με ικανοποιητικό τρόπο, αποδίδοντας τιμές BSS που κυμαίνονται από "Καλές" έως "Εξαιρετικές".

- Η μέθοδος RMWH-04 είχε σταθερά την πιο ικανοποιητική απόδοση, ακολουθούμενη από τη μέθοδο ροής ενέργειας. Αντίθετα, η μέθοδος KM-01 είχε τη χειρότερη συγκριτική απόδοση.

- Οι αποκλίσεις μεταξύ των μετρήσεων και των αποτελεσμάτων του μαθηματικού μοντέλου μπορούν να αποδοθούν σε ένα ευρύ φάσμα παραγόντων, όπως η έλλειψη ταυτόχρονων μετρήσεων κυμάτων και ρεύματος για τη βαθμονόμηση των μοντέλων, η πιθανή εισροή ιζήματος από εξωτερικές πηγές και η έλλειψη μετρήσεων κυματισμών από πλωτήρες στα ανοιχτά της περιοχής μελέτης.

Συνοψίζοντας, προτείνεται η χρήση της μεθόδου **RMWH-04** με 12 κυματικούς αντιπροσώπους για πρακτικές εφαρμογές, καθώς επέδειξε την καλύτερη συνολικά απόδοση και στις δύο περιπτώσεις μελέτης που εξετάστηκαν στο πλαίσιο της διατριβής. Η ουσιαστική συμβολή των τεχνικών μηχανικής μάθησης στη βελτίωση μεθόδων σχηματοποίησης κυματικού κλίματος αξίζει το ενδιαφέρον της επιστημονικής κοινότητας, προς την κατεύθυνση της περαιτέρω επιτάχυνσης των απαιτητικών προσομοιώσεων πρόβλεψης της εξέλιξης του παράκτιου πυθμένα.

List of figures

List of tables

Table 6.3 Comparative grades of each wave IR method based on its performance and computational efficiency for the "Morphostatic" simulation approach. Higher grades (in bold fonts) denote the best performing method for each wave IR branch

Table 6.4 Calculated BSS values and classification score at each coastal Profile for the EFM, KM-01 and RMWH-04 wave IR methods. Bold fonts denote the best performing method in each Profile

List of abbreviations

ANN	Artificial Neural Network
BIR	Binning Input Reduction
BSS	Brier Skill Score
EFM	Energy Flux Method
FBM	Fixed Bins Method
EFMEE	Energy Flux Method with Extreme Events
KM	K-Means
Morfac	Morphological acceleration factor
MIKE21 CM FM	MIKE 21 Coupled Model Flexible Mesh
IR	Input Reduction
PMS-SP	Parabolic Mild Slope - Spectral
RMSE	Root Mean Square Error
RMWH	Representative Morphological Wave Height

List of symbols

Symbol	Definition	Units
A	Complex wave amplitude	m
C	Wave phase celerity	m/s
c_f	Bed skin friction factor	-
C_g	Wave group velocity	m/s
D	Mild slope equation parameter	
D_*	Dimensionless sediment grain size diameter	
d_{50}	Median sediment grain size diameter	m
d_{90}	Characteristic grain diameter exceeding 90% of the grain sizes	m
E_f	Wave energy flux	$kg \cdot m/s^3$
f_i	Frequency of occurrence	-
f_w	Wave skin friction factor	-
F_y	Counterforce restoring equilibrium acting of sediment	N
g	Gravity acceleration	m/s^2
h	Still water depth	m
H_b	Significant wave height at breaking	m
h_{in}	Inner depth of closure	m
H_{max}	Maximum wave height	m
H_s	Significant wave height	m
$H_{s,e}$	Equivalent significant wave height	m
$H_{s,norm}$	Normalized significant wave height	m
$H_{s,r}$	Representative significant wave height	m
k	Wavenumber	rad/m
k_s	Nikuradse equivalent sand grain roughness	-
MWD	Mean wave direction	rad
n	Sediment porosity	-
P_o	Non-dimensional cross-shore parameter	-

P	Sediment pick-up rate function	kg/m^2/s
R	Relative bed roughness	-
S	Longshore sediment transport rate	kg·m^2/s
s	Relative sediment density	-
S_{xy}	Radiation stress component in xy plane	kg·m^2/s
$t_{b,y}$	Bed shear stress	N/m^2
T_p	Peak wave period	s
$T_{p,e}$	Equivalent peak wave period	s
$T_{p,norm}$	Normalized peak wave period	s
U	Current speed	m/s
U_{cr}	Critical current speed	m/s
U_{rms}	Root mean squared wave orbital velocity	m/s
U_w	Wave orbital velocity	m/s
$U_{w,cr}$	Threshold wave orbital velocity	m/s
w_b	Wave breaking energy dissipation factor	s^{-1}
A	Wave incidence angle	rad
α_b	Wave incidence angle at breaking	rad
α_e	Equivalent wave incidence angle	°
α_{norm}	Normalized wave incidence angle	rad
γ	Breaker index	-
θ	Shields parameter	-
θ_{cr}	Critical Shields parameter	-
v_h	Kinematic viscosity of saltwater	m^2/s
ρ	Saltwater density	kg/m^3
ρ_s	Sand density	kg/m^3

Chapter 1

~Introduction

1.1. Background, motivation and research objectives

The prediction of the coastal bed evolution and ultimately the shift of the shoreline position, due to the impact of the waves has been at the forefront of coastal engineering research efforts for several decades, dating as far back as the 1950's (Pelnard-Considère, 1957). With the ever-increasing human interventions in the coastal area, the erosion of the coastal bed poses a significant threat, with strong implications to the economy, environment and community safety. Therefore, accurate predictions of the coastal bed evolution at an annual scale are mandatory to identify imminent risks and design measures to remedy the erosion problem through the form of "hard" coastal protection structures or nature-based solutions (Luijendijk et al., 2018).

With the increase of computing power in the last decades, a plethora of numerical models are available, each with different advantages and shortcomings, but all concentrating at simulating the coastal bed evolution at the engineering scales of interest, i.e. for coastal areas extending a few kilometers and timescales of 1-10 years. When dealing with coastal areas characterized by complex bathymetries with the presence of manmade structures (e.g. harbours) coastal area models (Roelvink and Reniers, 2011) are almost exclusively applied due to their ability to describe in great detail the wave, hydrodynamic and sediment transport field. However, these models are associated with a staggering computational burden rendering the morphological simulations at an annual scale a tedious task.

In addition, engineers are usually in possession of large amounts of variable offshore sea-state wave characteristics, which further increase the computational effort and render the assessment of the morphological bed evolution rather difficult due to the sheer number of simulations that have to be performed. To combat this, wave Input Reduction methods are generally employed to accelerate the demanding morphological modelling simulations, all based on the notion of selected a reduced (order of 8-24) representative wave conditions that should produce similar bed level evolution predictions compared to the full timeseries. Several wave Input Reduction methods have been developed and utilized in literature and can be vaguely divided in three branches: (a) Representative Morphological Wave Height selection methods (Borah and Balloffet, 1985; Brown and Davies, 2009; Chondros et al., 2022; Chonwattana et al., 2005; Karambas et al., 2013;

Papadimitriou et al., 2022a; Pletcha et al., 2007) (b) Binning wave Input Reduction methods (Benedet et al., 2016; de Queiroz et al., 2019; Papadimitriou et al., 2020; Van Duin et al., 2004; Walstra et al., 2013), (c) Clustering algorithms (de Queiroz et al., 2019; Papadimitriou and Tsoukala, 2022).

Despite their widespread usage, it should be noted that wave Input Reduction methods are influenced by a multitude of parameters (e.g. the number of representatives, the duration of the wave climate). Most importantly, their redeeming qualities are not so visible when the coastal area models operated by directly coupling the wave, hydrodynamic and morphodynamic modules. Consequently, a concise effort to introducing enhancements to all branches of the wave Input Reduction methods with the ultimate goal of further reducing the computational burden without compromising the reliability of the results and provide practical guidelines to the engineering community, to the best of the author's knowledge, has not been undertaken yet.

Based on the above, the specific research objectives of this thesis are:

- To expand on the concept of the wave Input Reduction methods, by introducing elimination of sea-states considered unable to initiate sediment motion in the calculation procedure, with the ultimate goal to further alleviate the required computational effort.
- To assess clustering algorithms as a viable wave input reduction method and examine possible enhancements by counterbalancing the "unsupervised" learning aspect of said algorithms.
- To incorporate machine learning in wave Input Reduction, by introducing a properly and thoroughly trained Artificial Neural Network which can further speed-up the demanding numerical simulations.
- To apply and intercompare several instances of wave Input Reduction methods in two coastal areas, to ultimately provide initial recommendations and guidelines for practical applications.

1.2. Innovative points and highlights

This thesis is based on the investigation and most notably expansion of the concept of wave Input Reduction for the acceleration morphological modelling simulations, by simultaneously aiming to retain the reliability of the model results. The following innovative aspects are highlighted:

- A novel approach is introduced to the classical Binning Input Reduction methods, concentrating on the reduction of the length of the timeseries of offshore sea-state wave characteristics by eliminating wave records that are considered unable to initiate sediment motion. The outcome of this approach is the considerable alleviation of computational effort achieved by the reduction of the numerical model run-time.
- Clustering algorithms are for the first time assessed as viable Input Reduction methods in a coastal area characterized with considerable alongshore variability. Six alternative configurations of the widely used K-Means clustering

algorithm were evaluated aiming to introduce vital aspects influencing the annual morphological bed evolution to the algorithm's procedure to calculate the representative wave conditions.

- The concept of Representative Morphological Wave Height (or Equivalent Wave Height) selection methods is revisited and further enhanced. The highlight of this investigation is the incorporation of an Artificial Neural Network tasked with eliminating lowly-energetic wave records that are considered to have inconsequential impact to the annual morphological bed evolution. The trained Artificial Neural Network was deemed capable of systematically produce reliable results and further accelerate the morphological simulations.

- A robust Parabolic Mild Slope wave model based on the work of Chondros et al., 2021, is enhanced and expanded in the framework of this thesis to treat the generation and propagation of uni-directional irregular waves. The aforementioned model is an integral part of several of the tested wave Input Reduction methods evaluated in the framework of this thesis.

- Performance evaluation of all the examined wave Input Reduction methods is undertaken in the framework of this thesis to provide practical guidelines and recommendations for coastal modellers. A sole method is also selected for each distinct branch of Input Reduction, and a comparative analysis is carried out assessing model results with available field measurements of bed elevation in a coastal area affected mostly by the impact of the waves. Comparison of coastal morphological model results with field measurements of bed elevation is in itself an innovative aspect since only a handful of research efforts have been realized on this topic.

1.3. Thesis structure

The thesis is assembled in seven distinct chapters, including the present introductory one and a brief overview of each chapter will be subsequently provided. The central focus of this thesis is the utilization of wave Input Reduction methods for the efficient numerical modelling of the morphological coastal bed evolution. The primary aspects of the morphological modelling under the combined effect of waves and currents, highlighting the ever-prevailing importance of wave Input Reduction methods is showcased by the literature review and the description of key research issues in Chapter 2.

In Chapter 3, a novel approach is realised and implemented to the widely used Binning Input Reduction methods (Benedet et al., 2016). The centerpiece of this approach is the elimination of lowly-energetic sea states which are unable to initiate sediment motion in the surf zone and are thus have a negligible effect in shaping the morphological bed evolution. Two methods developed in the framework of this dissertation are implemented. The first one is based on the calculation of the sediment Pick-up rate as a proxy quantity dictating the calculation of the wave representatives (Papadimitriou et al., 2020). The second one concentrates on the elimination of wave

records unable to initiate sediment motion based on the Threshold Current Speed concept and utilizing the wave energy flux as the main driving quantity to estimate the representative sea-states. This Chapter also presents the background of the numerical model utilized for the morphological simulations (DHI, 2014), along with the validation of an enhanced model, developed in the framework of this work (Papadimitriou et al., 2020) and considered integral to the methodologies.

In Chapter 4, the capability of the K-Means clustering algorithm in predicting the annual bed evolution is investigated. Apart from the performance evaluation of the clustering algorithm, several modifications are also examined aimed at coercing the algorithm to utilize quantities that are vital in shaping the morphological bed evolution, hence bringing the gap between the unsupervised clustering algorithm and the Binning Input Reduction methods.

In Chapter 5, performance evaluation is carried out for another widely used category of Input Reduction methods, entitled Representative Morphological Wave Height selection methods. The highlights of this Chapter concern the training and validation of an ANN, which can readily eliminate lowly-energetic sea-states that are considered to have a negligible effect on the morphological bed evolution at an annual scale.

Chapter 6 builds on the previous Chapters 3,4 and 5 and contains a comparative analysis and selection of a singular optimal method out of those examined per Chapter, based on the model performance (i.e. capability of each method to predict the morphological bed evolution reliably) and ease of implementation (i.e. computational efficiency). Then each of the selected three methods (one for each chapter) was implemented in the coastal area of Skala Eresou in Lesvos Island, Greece, to compare and evaluate model results with available field measurements, to verify the capabilities of wave Input Reduction methods in predicting coastal bed evolution in real-field cases.

Finally, Chapter 7 encapsulates the general conclusions of this thesis. In addition, suggestions for future research are also laid out. An outline of the thesis structure, showcasing the innovative points and main research objectives of each Chapter is shown in Figure 1.1.

Chapter 1: Introduction
- Process-based models used to predict coastal bed evolution are computationally demanding
- Wave Input Reduction methods can somewhat alleviate this burden

Chapter 2: Numerical modelling of coastal bed evolution and wave Input Reduction principles
- Overview of advantages and limitations of the process-based model categories to simulate annual coastal bed evolution
- Definition of the three branches of wave Input Reduction used to accelerate morphological simulations

Research Objectives	Approach	Data	Outcome
Chapter 3: A novel approach to Binning Input Reduction Methods	Develop new BIR based on the criterion of incipient sediment motion to speed-up morphological simulations	1. Eliminate lowly-energetic sea-states and develop two new BIR methods 2. Apply the methods in the coastal area in Rethymno, Crete, Greece	Regional wave hindcast data: • MEDSEA_MULTIYEAR_WAV_006_012 (Copernicus Marine Service)	The two developed BIR methods (Pick-up Rate and Threshold Current Method) showed "Excellent" performance and achieved a model run-time reduction of about 58 %.
Chapter 4: Evaluation and enhancement of the K-Means clustering algorithm	Investigate the validity of K-Means clustering algorithm as a viable IR method and overcome its "unsupervised" nature	1. Propose 5 alternatives to the K-Means algorithm to improve the morphological model performance 2. Apply the alternatives in the coastal area in Rethymno, Crete, Greece	Regional wave hindcast data: • MEDSEA_MULTIYEAR_WAV_006_012 (Copernicus Marine Service)	All the examined alternatives improve the performance of the default K-Means configuration. The clustering algorithm is a viable IR method requiring minimal user input
Chapter 5: Revisiting the concept of Representative Morphological Wave Heights	Propose enhancements to the traditional RMWH methods by introducing the influence of cross- and longshore transport and machine learning	1. Develop 5 alternatives to the K-Means algorithm to improve the morphological model performance 2. Apply the alternatives in the coastal area in Rethymno, Crete, Greece	Regional wave hindcast data: • MEDSEA_MULTIYEAR_WAV_006_012 (Copernicus Marine Service)	All the examined alternatives improve the performance of the default K-Means configuration. The clustering algorithm is a viable IR method requiring minimal user input
Chapter 6: Comparative analysis of Input Reduction Methods with field measurements	Compare the best performing IR methods with available field bed level measurements to evaluate their validity in real-field settings	1. Select an optimal method of each IR branch based on performance and computational efficiency 2. Apply the selected methods in the coastal area in Skala Eressou, Lesvos, Greece	• Available data from bathymetric, topographic and geotechnical surveys Regional wave hindcast data: • MEDSEA_MULTIYEAR_WAV_006_012 (Copernicus Marine Service)	Satisfying performance of the three selected IR methods compared to the field measurements validating their effectiveness. The RMWH-04 method incorporating an ANN was the best performing IR method

Chapter 7: Conclusions

For the prediction of coastal bed evolution using Input Reduction methods
- Filtering of lowly energetic sea-states can both improve model results and reduce the computational effort
- Incorporation of Artificial Neural Networks can enhance the model performance
- The Binning and Representative Morphological Wave Height selection methods perform consistently better

Future research objectives
- Examine the effect of Morphological Acceleration Factor in the results
- Add additional parameters to the wave Input Reduction methods, such as the wave climate "intensity"

Figure 1.1. Outline of the overall structure of the thesis including research objectives, approach, data and outcome

Ñumerical modelling of coastal bed evolution and wave Input Reduction principles

2.1. Process-based modelling of coastal bed evolution

Coastal areas are dynamic, ever-evolving systems constituting a home for various lifeforms while also concentrating a multitude of human activities. Approximately three billion people – half the world's population – live and work within a couple of hundred kilometers of a coastline. The morphological bed and shape of the coasts is altered continuously being subject to several -and often contradicting- forcing factors. Ultimately the shift of shoreline position gathers vast amounts of interest from both the public and the research community, since it has serious implications to the economy, community safety and the environment.

Of the forcing factors responsible for the morphodynamic processes, surface gravity waves are a key component since they are responsible for stirring sediments through the orbital motion observed under the wave crest and trough. As waves propagate from deep to shallower depths, they start interacting with the bottom with increased non-linear characteristics and dissipate energy mostly due to bottom friction and bathymetric breaking. Wave energy dissipation within the surf zone in turn leads to the generation of currents which are responsible for the transport of sediments in the nearshore both in the longshore (for the case of obliquely incident waves related to the shore-normal) and cross-shore (for direct wave incidence) direction. Furthermore, wave set-up gradients induced by the spatial variation in wave energy, can generate strong alongshore and cross-shore flows such as a rip-current circulations (Roelvink and Reniers, 2011). These littoral flows are notoriously capable of transporting large amounts of sediment (Komar and Miller, 1975). Obstruction of the littoral drift leads to areas of accretion followed by to beach erosion to the down-drift end, a phenomenon often observed in the vicinity of harbours and coastal protection structures. Consequently, numerical modelling of wave propagation and transformation in the nearshore, wave-generated currents, the corresponding sediment transport rates and ultimately the coastal bed evolution is of the utmost importance and has been at the forefront of research efforts of coastal engineers and scientists for the past decades (Afentoulis et al., 2019; Chondros et al., 2022; de

Vriend et al., 1993; Karambas and Samaras, 2017; Papadimitriou et al., 2020; Roelvink and Reniers, 2011).

The behaviour and response of a coastal system is dynamic and occurs on a variety of spatial and temporal scales. The spatial scale is generally determined by the dimensions (in meters) of a particular morphological element, usually indicating its extend. Similarly, a timescale is generally interpreted as the period of time (e.g. in years) required for the characteristic morphological development to take place. This timescale often refers to the total duration that a morphological system needs to reach a new equilibrium state once it has been disturbed by nature or by the humans (Roelvink and Reniers, 2011). Equilibrium in this sense denotes that the overall sediment balance of the morphological unit is maintained (no erosion and no accretion is observed). The spatial and temporal scales of a morphological feature are closely coupled, the larger the spatial scale of a specific feature the larger the corresponding timescale. Indicatively, as showcased in Figure 2.2, the timescales of interest range from a few hours for the evolution of small bedforms like bottom dunes and ripples but can reach up to decades or centuries for morphological evolution of a large tidal inlet system (Bosboom and Stive, 2022). For most practical applications, the timescale of interest (hereafter denoted as engineering timescale), usually correspond to the evolution of littoral systems at an interannual scale up to a few years (typically 1-10 years). This timescale is usually of particular interest to assess the effect of human interventions (e.g. shore protection works, construction of a harbour) to the morphological bed evolution.

Consequently, coastal engineers would generally not be interested in dynamics on very small scales (morphological changes of few meters occurring in a few hours), like the evolution of wave ripples or even breaker bars in the surf zone. The complex dynamics on these scales are mostly oscillatory, and therefore have no net effect on the engineering timescales. In contrast, the natural behaviour on these larger engineering scales generally shows a net trend. Examples are the downdrift erosion due to the construction of a harbour, the erosion or accretion of a delta, and the migration of a tidal inlet. Human interventions have timescales of years to decades and spatial scales of 1 km to 100 km. The coastal behaviour due to human intervention (harbours, coastal protection structures, land reclamation) interferes with the natural behaviour of the coastal system on these particular temporal and spatial scales. Coastal modellers often refer to morphological changes occurring on the aforementioned scales as "medium-term" coastal bed evolution (de Vriend et al., 1993; Lesser, 2009), in order to loosely distinguish it from the short-term (hours to days) and long-term (decades to centuries) changes.
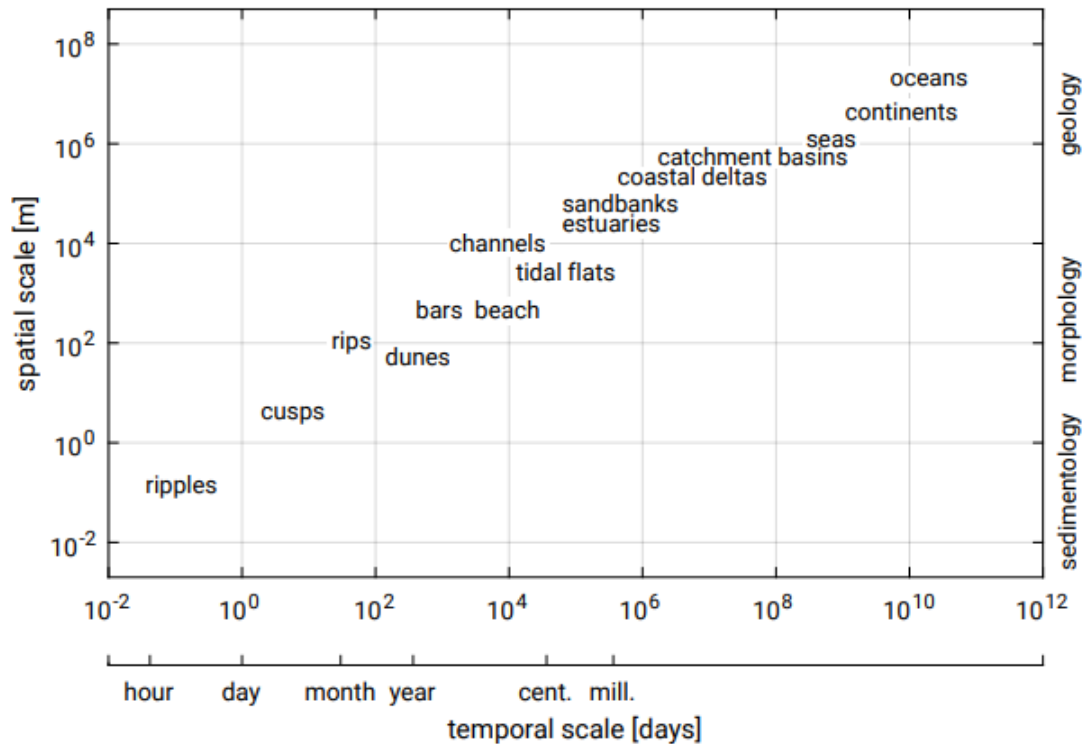
Figure 2.2. Relationship between the spatial and temporal scales of interest of various types of coastal features (Bosboom and Stive, 2022)

The complex prediction of the evolution of littoral systems to identify possible areas of erosion and establish mitigation measures is generally carried out by means of numerical simulation. Traditionally, the numerical models developed and tasked with the prediction of coastal bed evolution under the combined effect of waves and currents focus on resolving the relevant coastal processes. They are often referred to as "process-based" or "deterministic" models and can be divided in the following three large categories, each with different characteristics and based on different assumptions (Roelvink and Reniers, 2011).

- **Coastal profile models**, where the longshore variability is neglected, and the main driving factor is the cross-shore transport and the subsequent profile evolution (Roelvink and Brøker, 1993).
- **Coastline models**, where the cross-shore profiles are considered to retain their shape, whether the shoreline advances or retreats (Szmytkiewicz et al., 2000).
- **Coastal area models** (de Vriend et al., 1993), where flow variations and sediment transport gradients are resolved in both the horizontal dimensions. They can be further subdivided into two-dimensional horizontal (2DH) models which solve depth-averaged equations or three-dimensional (3D) models which resolve the vertical variations in both flow and sediment transport.

In the following subsections, the main characteristics of each category of process based numerical models will be briefly outlined. It is noted that coastal area models will be analysed in more detail, since a coastal area model was utilized to perform all the

necessary simulations in this thesis due to the alongshore and cross-shore variability of the study areas.

2.1.1. Coastal profile models

Coastal profile models are typically implemented in two types of applications: evaluation of storm events' impact on a coastal profile, with or without the presence of coastal structures, and evaluation of longer-term behaviour of sandbars and nourishment schemes, both on the beach and on the shoreface. The first profile models were essentially driven by offshore directed suspended sediment transport induced by return flows (Dally and Dean, 1984; Steetzel, 1990; Stive and Battjes, 1985). A detailed profile model for the modelling of beach erosion under a storm event was proposed by (Leont'yev, 1996), considering two distinct components of sediment transport rates contributing in the profile development and evolution, the first one caused by the wave-current interaction shoreward the surf-zone and the second one induced by run-up flow. When examining more moderate sea-states, which reshape the coastal profile, additional and more detailed transport mechanisms (e.g. aeolian transport, phase lag effects) should be considered. Watanabe and Dibajnia, 1988, utilized various empirical formulations for onshore and offshore directed sediment transport as a function of the bed shear stress. Stive and Battjes, 1985, considered contributions from wave asymmetry terms applying the energetics model of Bailard, 1981. Roelvink and Stive, 1989 introduced spatial lag effects in the prescription of the return flow, while also considering additional stirring due to wave breaking induced turbulence while also accounting for long wave effects, a concept latter expanded upon by Sato and Mitsunobu, 1991. Although profile models do not take into account alongshore variation, they capture an important part of the processes that shape the coasts and hence provide significant insights when used in conjunction with the more detailed coastline or coastal area models.

2.1.2. Coastline models

Coastline models have their origins on the "single-line" or "one-line" shoreline evolution theory, the foundation of which has been laid out by Pelnard-Considère, 1957. The main assumption of this theory is that cross-shore processes are relatively fast-evolving and are therefore able to maintain the shape of the coastal profile over a certain profile height, which runs from the so-called depth of closure (i.e. the depth shoreward which no significant bottom changes can be observed) to the top of the active profile, usually taken as the first dune landward. Hence the beach profile is considered to move parallel to itself seaward or landward depending on if the coast erodes or accretes. Due to the constant profile shape one contour-line can be used to describe changes in the beach plan shape and volume under wave forcing. Typically, in these models the computation is divided into two parts. Firstly, a profile model computes the longshore transport rates as a function of the angle of wave incidence relative to the shore-normal. Then, the coastline model updates the coastline positions and recomputes the wave incidence angles taking into account the longshore sediment transport rates calculated

previously in the profile model. Various commercial or open-source coastline models have been established with the main characteristics briefly outlined below:

- GENESIS (Hanson, 1989) which is based on the extended CERC formula (Ozasa and Brampton, 1980), including the effect of longshore gradients in wave height and has the capability of describing the impact of coastal structures on the local wave climate and shoreline evolution.

- LITPACK (DHI, 2023) which utilizes a process-based model to estimate sediment transport rates which are then used to simulate coastal response arising from the effect of natural features and considering a wide variety of coastal structures

- UNIBEST-LT/CL (Tonnon et al., 2018) which combines longshore transport (LT) calculations combining a coastal profile model approach with coastline computations on a curvilinear coastline (CL)

- UnaLinea (Stripling and Panzeri, 2015) which is based on the extended CERC formula (Ozasa and Brampton, 1980) and has special features for wave transmission through structures, bypassing of groynes and breakwaters and is capable of reproducing the effect of seawalls on sediment transport

- CEM (Ashton and Murray, 2006a, 2006b) model provides a different approach which allows the plan-view shoreline to take on arbitrary local orientations, and even fold back upon itself. This is particularly important since under certain sea-states, i.e., when waves approach the coast with certain wave incidence angles (>45°, a phenomenon known as "high-angle instability"), complex shapes such as capes and spits are formed and can be reproduced using this model.

Coastline models assume gradually varying flow conditions and approximately parallel depth contours. Under such circumstances the longshore transport can locally be treated as if it has fully adapted to the local incident wave conditions relative to the coast orientation. Since it typically takes hundreds of meters for the longshore current to spin up, coastline models should in principle be applied for large-scale applications, over alongshore distances of many kilometers in order to satisfy the assumptions associated with the "single-line" theoretical approach.

2.1.3. Coastal area models

Coastal area models have been developed since the early 1980s (see Nicholson et al., 1997 for a comprehensive review). They are applied when a separation between longshore and cross-shore scales and processes is not feasible, for instance in the vicinity of a tidal inlet, in the vicinity of a harbour, and in coastal zones with complex bathymetric features, rip channels and shoals forming varying angles with respect to the undisturbed coast orientation. The first instances of these models were essentially wave, hydrodynamic and sediment transport/morphology codes operating usually independently as a batch process and exchanging output files constantly. In the late 1980s and early 1990s, the large European institutes (Deltares, Danish Hydraulic

Institute) combined their research efforts within the EU MaST-G6M and G8M projects and carried out major developments and restructuring of their coastal area models, which led to the development of much more robust and flexible codes that are still successfully operated and used by several coastal engineers to this day, such as Delft3D (Deltares, Netherlands), Mike21 (Danish Hydraulic Institute) and Telemac (Laboratoire Nationale d'Hydraulique, France). All coastal area models consist of a wave driver model, providing the forcing input for the subsequent members of the modelling toolchain, which are a hydrodynamic model and a sediment transport/morphology model.

Wave driver models can either be based on the "phase-averaged" approach, where the wave field is averaged at the scales of over both individual waves or wave groups. The most notorious wave propagation models are based on the phase-averaged approach are the 3rd generation spectral wave models (Benoit et al., 1997; Hasselmann et al., 1988) and model the evolution of the two-dimensional wave spectrum based on the conservation of the wave-action balance. These models neglect information about the phase of the waves hence are not well-equipped for the detailed resolution of the processes of wave diffraction, despite efforts to reproduce diffraction effects behind obstacles such as detached breakwaters (Holthuijsen et al., 2003; Ilic et al., 2007; Mase et al., 2001), or wave reflection from obstacles. When wave reflection and diffraction cannot be neglected, then "phase-resolving" models are employed which can in great detail represent the wave transformation in the nearshore. To this day, few coastal-area models employ phase-resolving wave drivers (Afentoulis et al., 2022; Karambas and Samaras, 2017; Klonaris et al., 2018; Long et al., 2008; Papadimitriou et al., 2022b) due to the sheer number of elements required to resolve the wavelength, however they are gaining increasing popularity in the last decade due to the increase in computing power.

Hydrodynamic (or flow) models can either be 2DH or 3D. In the first case, the computations are based on the solution of the depth-averaged shallow water equations. This generally implies that the sediment transport direction follows that of the depth-averaged flow, although sometimes the mean return flow is taken into account. Full 3D flow models in the context of coastal area models, where horizontal scales are much larger than vertical scales, are normally based on the 3D shallow water equations. They offer a very satisfactory representation of the effects of breaking waves on the current profiles and at the same time deal with density-driven flows and deviations of the vertical due to strong curvatures. Most 3D models apply k−ε turbulence models or similar, 2-equation turbulence models, which can deal with simultaneous sources of turbulence due to e.g. wave breaking, bed shear stress, horizontal shear, buoyancy effects.

In most sediment transport/morphological models, sediment transport is split up into bed load transport and suspended load transport. Bed load transport is always treated as a direct function of the near-bed velocity or bed shear stress; in 2DH the bed shear stress follows the depth-averaged flow, whereas in 3D it follows the near-bed flow. Suspended sediment concentration in some models is only a function of the local flow and wave conditions, but in most it is solved using the advection-diffusion equation in 2DH or 3D. The largest differences between 2DH and 3D sediment transports can be

observed in the surf zone and in strongly curved areas, as well as in areas with strong density gradients in the horizontal and/or vertical. Depending on the discretization scheme of the governing equations these models can be operated in a regular grid or flexible finite element mesh. A large number of coastal area models are available in various suites either as open-source codes or as commercial software. The main characteristics of well-known and widely-used coastal area models are compiled and shown in Table 2.1 .

The general setup and procedure to perform morphological bed evolution simulations with coastal area models is briefly outlined below.

1. An initial 2D bathymetry of the study area is constructed.
2. Given certain forcing sea-states for the wave driver and boundary conditions for the hydrodynamic model, simulations are executed for both models operating in a two-way or one-way coupled mode.
3. The sediment transport field is computed based on the hydrodynamic flow field, the wave orbital motion, the sediment characteristics and the bathymetry.
4. The bathymetry is updated based on the sediment transport gradients.
5. Return to step 2 for a full update of waves, flow and sediment transport field or to step 3 for an intermediate update of the sediment transport field.
6. The model execution is terminated when all the forcing sea-states have been simulated and the final predicted bed levels are obtained.

To expand on the above, it is noteworthy to highlight two approaches of morphological modelling, one where waves, currents and morphology exchange feedback constantly and the second one where it is considered that the sediment transport and morphology evolve in a slower scale than the hydrodynamics, hence, only the sediment transport field is recomputed after the bathymetry update. The first and more detailed approach is based on the constant interaction and feedback exchange between waves hydrodynamics and sediment transport morphology. This approach is called "Morphodynamic" (Olij, 2015). On the other hand, when the wave, hydrodynamic and sediment transport/morphology simulations for each sea-state are executed considering the same initial bathymetry without updating the bed levels at each model time-step and then the final bed is obtained as a weighted average of each morphological simulation, then the approach is called "Morphostatic". It can be deduced that considering the interaction of all the feedback mechanisms between waves-currents and the sediment transport, leads to more time-consuming simulations, but is necessary when modelling complex phenomena such as the migration of a sandbar.

Coastal area models are capable of resolving most coastal processes (depending on the type of wave driver, flow and sediment transport model) and can therefore be implemented in a variety of scales and applications, from small-scale coastal engineering problems to macro-scale evolution of tidal basins. Considering the basic aspects and features of the three categories of coastal modelling tools, Table 2.2 provides an overview of the scales and typical applications where each model category is best suited to be implemented.

Table 2.1

Main characteristics of available coastal area models, adapted and updated from (Roelvink and Reniers, 2011).

Model	Wave driver	Hydrodynamic model	Sediment transport	Bed composition	Grid system	Availability
DELFT 3D (structured)	spectral wave averaged	2DH/3D	2DH/3D sand & mud	3D	structured or curvilinear grid	open source
DELFT 3D FM	spectral wave averaged	2DH/3D	2DH/3D sand & mud	3D	unstructured mesh	commercial
MIKE 21	spectral wave averaged	2DH/3D	2DH/3D sand & mud	3D	unstructured mesh	commercial
Telemac	spectral wave averaged	2DH/3D	2DH/Q3D sand & mud	3D	unstructured mesh	open source
CMS	spectral wave averaged	2DH	2DH/3D sand	2DH	structured grid	commercial (through SMS)
ROMS-SED	spectral wave averaged	3D	2DH/3D sand	3D	structured or curvilinear grid	open source
MOHID	spectral wave averaged	2DH	2DH/3D sand	2DH	structured or curvilinear grid	commercial
XBeach	phase-resolving or short-wave averaged	2DH	Q3D sand or gravel	2DH	structured or curvilinear grid	open source
FUNWAVE-TVD	phase-resolving	2DH	Q3D sand or mud	2DH	structured grid	open source
COAWST	spectral wave averaged	3D	2DH/3D sand	3D	unstructured mesh	open source
SCIENTIA MARIS	phase-resolving	2DH	2DH/Q3D sand	2DH	structured grid	commercial

Table 2.2
Spatial and temporal timescales of typical coastal engineering applications: profile models (red font), coastline models (green font), coastal area models (blue font)

Timescale/Spatial scale	1m – 1km	10m – 10km	100m – 100km
1hour – 10days	Dune erosion, bar formation due to extreme events Reset events		
1day – 10years	Effect of shoreface nourishments Evolution of beach states Impact of coastal structures	Impact of harbour extensions Mega nourishments	Longshore spreading of nourishments Coastal response to wave climate variability
1year – 1000years	Climate change impact on profile behaviour	Evolution of tidal inlets & climate change impact assessment	Evolution of tidal basins Large scale coastline evolution

Observing Table 2.2, it can be deduced that coastal area models are usually applied in the most practical applications of coastal engineering, especially spanning from coastal areas of a few meters up to large 2D areas with alongshore variability with or without the presence of coastal structures. However, at spatial scales of a few hundred meters, it is desirable to model in great detail the wave transformation and wave-driven flow patterns and the corresponding morphology changes around small structures such as groynes and detached breakwaters. This implies that small grid cell sizes are required to resolve the main processes in turn leading to small time steps to satisfy stability restrictions imposed by the hydrodynamic models. Consequently, simulating these applications is computationally intensive, especially when predictions over longer time periods than a storm event are required. Hence, although coastal area models can accurately resolve the dominant processes driving coastal bed evolution in turn they are associated with staggering computational burden, especially when desiring to obtain coastal bed evolution predictions in the medium term (1-10 years).

2.2. Morphological upscaling and acceleration techniques

To combat the excessive computational effort and time constraints of the coastal area models when simulating medium to long term changes for larger scale applications several acceleration techniques have been realized (Lesser, 2009; Jimenez & Mayerle, 2010). Most approaches take advantage of the fact that the morphological evolution of coastal features for practical engineering applications usually occurs at timescales

several order of magnitude larger than the hydrodynamic fluctuations driving sediment transport. Indicatively, de Vriend et al., 1993, highlight three distinct approaches to accelerate morphological modelling simulations.

- **Model reduction**, in which smaller-scaler processes are not described in great detail allowing for the coastal model to be reformulated.
- **Behaviour oriented modelling**, which attempts to model the phenomenon of interest without attempting to describe the underlying processes.
- **Input reduction**, which is based on the premise that the residual (long-term) effects of smaller-scale processes can be obtained by applying models of those smaller-scale processes forced with reduced "representative" inputs

Regarding model reduction, several methods have been utilized in literature and are discussed thoroughly in Cayocca, 2001, Dodd et al., 2003 and Roelvink, 2006.

The first method entitled "tide averaging" or "elongated tide" (Latteux, 1995) is based on the premise that morphological changes within a single tidal cycle are usually very small compared to the trends over a longer period, and such small changes do not affect the hydrodynamics or sediment transport patterns significantly. It is then acceptable to consider the bottom fixed during the computation of hydrodynamics and sediment transport over a tidal cycle. The rate of bed level changes is then computed from the gradients in the tidally averaged transport. Starting from an initial bathymetry, the wave–current interaction is solved over a tidal cycle, using an iterative approach. The resulting hydrodynamic and wave fields are then provided as input into a sediment transport model, which computes bed load and suspended load transports over the tidal cycle. The averaged result is then utilized to compute bed changes. The updated bathymetry is finally fed back to the hydrodynamic module and the method is repeated. The morphological time step is numerically restricted (for explicit schemes) by the Courant number and additionally the accuracy of this method depends on the time integration discretization scheme (usually an explicit Euler scheme). Because of these limitations on the morphological time step, it is necessary to update the transport rates regularly.

An improved version of the "tide-averaged" approach is the "continuity correction" method (Roelvink, 2006). It is a frequently applied method to adjust the flow field after small changes in the bathymetry given that the sediment transport rates S is a function of the current speed u and the wave orbital velocity u_{orb}:

$$\vec{S} = f(\vec{u}, u_{orb}) \tag{2.1}$$

Since the flow pattern is assumed to not vary for small bottom changes, the local flow rate q can be assumed to be constant:

$$\vec{q} = h\vec{u} \tag{2.2}$$

where h is the still-water depth and $\vec{u}$ the current speed.

The same assumption can be adopted for the wave field, the significant wave height H_s, peak wave period T_p and angle of wave incidence α_o, are kept constant and only the wave orbital velocity has to be readjusted to the local water depth.

Adaptation of the sediment transport field is hence decomposed on merely adjusting the flow-velocity and orbital velocity and recomputing the sediment transport using Eq. (2.1). The main limitation of the "continuity correction" approach is the assumption that the flow rates and patterns remain constant over time. In the case of a shallow area becoming even shallower (e.g. due to the formation of bars or increased accretion), the flow velocity keeps increasing under this approach, whereas in reality, the flow will adjust around the shallow area subject to the increasing dissipation due to bottom friction.

The need to often interpret the outcome of initial sediment transport computations without resorting to the full morphodynamic simulations led to the development of the "RAM" (Rapid Assessment of Morphology) approach. With the same assumptions as the "continuity correction" approach as a basis, i.e. that no significant changes to the flow and wave field are expected when the bottom changes are small, the tide-averaged transport rates are a function of flow and wave patterns which do not vary on the morphological time-scale, while the local depth does. Essentially, given a certain set of nearshore currents and wave characteristics, the sediment transport at a given location is only a function of the water depth.

In dynamic areas, such as estuaries and outer deltas, the RAM method may work well enough to be applied as a quick updating scheme. As soon as bottom changes become significant, a full simulation of the hydrodynamics and sediment transport is carried out for a predefined number of input conditions. A weighted average sediment transport field is then determined, which is the basis for the next RAM computation over, say, a year of morphological time. The updated bathymetry is then fed back into the detailed hydrodynamic and transport model. A flow chart indicating the operation of the "RAM" approach is given in Figure 2.3.
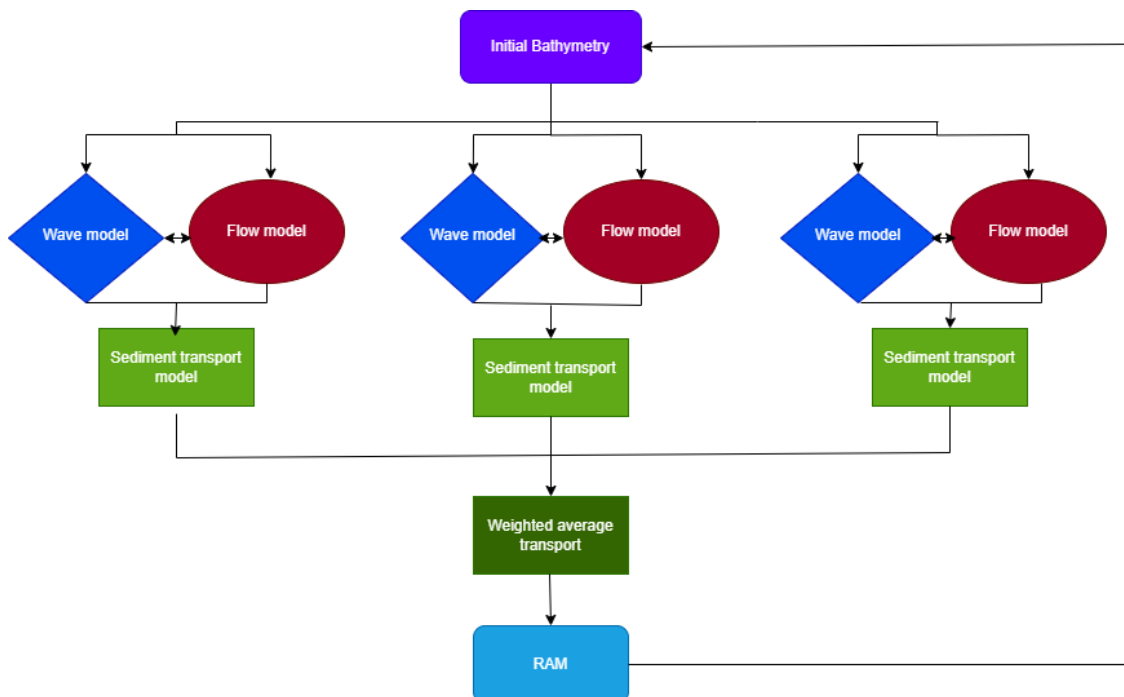
Figure 2.3. Flow chart of the operation of the RAM approach

The most widely used method of model reduction is the Morphological acceleration factor (Morfac) approach (Lesser, 2009; Lesser et al., 2004). This approach multiplies the bed level change rates, obtained in each morphological timestep by a constant factor n. Effectively, by taking advantage of the difference in the timescales of the morphological evolution of coastal features compared to the hydrodynamic fluctuations, if simulations are performed for instance for one tidal cycle, the use of the Morfac allows to simulate morphological changes after n tidal cycles. An advantage of the aforementioned method is, that short-term processes are coupled at each flow time-step level, which makes it easy to include various interactions between flow, sediment transport and morphology, and also renders the need to store large amounts of data between processes redundant (Roelvink, 2006). What clearly distinguishes this method from other model reduction techniques is that the bottom evolution is computed in much smaller time steps, even when relatively large values of n are used.

The use of Morfac has effectively overshadowed all other model reduction techniques and is offered exclusively as an option to all commercial or open-source software showcased in Table 2.1 due to its simplicity, ease of implementation and achieved model run-time reduction. However, the use of large Morfac values introduces errors in the simulations due to the non-linear response of the sediment transport to the wave forcing (Lesser, 2009). Clearly defined limits about the allowable values of the Morfac do not exist in the literature since Morfac depends upon a wide array of parameters. Lesser, 2009, stated that for the DELFT3D model and for coasts under wave attack a maximum value of 100 can be utilized for the morphodynamic simulations and argued that for extreme sea-states Morfac values should be close to unity, hence a hybrid model reduction approach should be considered. Knaapen and Joustra, 2012, assessed Morfac values in the Sisyphe model of the Telemac suite for three separate cases, a laboratory trench case, a river floodplain and an estuary and concluded that large factors can be used in stationary situations however for the more complex cases (as an estuary) using values higher than 20 introduces error in the simulations, in the form of increasing the RMSE compared to the benchmark prediction (Morfac = 1). Ranasinghe et al., 2011, extensively examined the dependencies of the Morfac and concluded that it a function of the grid cell size, the hydrodynamic time step, Froude number and the bed-level update solution scheme. They then defined a preliminary criterion to estimate a priori critical values of Morfac based on the hydrodynamic Courant number. However, in cases where waves are the main factor dricing the nearshore sediment transport it is inherently difficult to predict the critical value of Morfac. Taking the above into consideration, Morfac is a widely used morphodynamic upscaling technique, but care should be taken not to use excessively large values for energetic sea-states that may introduce errors in the morphological bed evolution predictions.

Behaviour-oriented modelling acceleration techniques essentially encompass the treatment of complex processes in a simplified manner, such as the shift of the shoreline position or computation of the sediment transport rates in the swash zone. The most commonly used methods of this kind revolve around moving shoreline boundary

conditions (Balzano, 1998; Lynett et al., 2002; Prasad and Svendsen, 2003) and erosion of dry cells (Lesser, 2009).

Input Reduction or Input Schematization methods have been utilized in the coastal engineering practice since the 1980's (Borah and Balloffet, 1985), aiming to reduce the sheer amount of input forcing conditions required to obtain a medium-term prediction of the morphological bed evolution. In essence, all Input Reduction methods lead to the selection of a few "representative" wave conditions which are deemed capable of reproducing the bed level changes induced by the full wave climate. Nowadays wave characteristics are readily available through oceanographic databases (e.g. Copernicus Marine Service, Copernicus Climate Data Store, AVISO) for the global ocean at 1 or 3-hour intervals. It can be deduced that simulations with coastal area models considering hourly changing boundary conditions is prohibitive for practical applications. Consequently, considering this rapid increase of the available sea-state wave characteristics, exploring ways to further speed up the demanding morphological simulations by further enhancing the Input Reduction Methods is especially important. Hence, this dissertation aims to systematically evaluate and develop new wave Input Reduction methods, able to reduce the required computational effort while maintaining reasonable accuracy in model results. In the following subsection the basic theoretical aspects and main branches of Input Reduction methods are briefly presented and analysed.

2.3. Basic aspects of Input Reduction

When desiring to obtain a reduced set of representative conditions from a timeseries of offshore wave characteristics or a wave climate obtained from empirical methods, it is important to define the dominant forcing/input parameters for the area of application. A typical list of input parameters for coastal area models is given below (Roelvink and Reniers, 2011):

1. tidal amplitude or phase within the spring-neap cycle
2. offshore sea-state wave characteristics (significant wave height H_s, peak wave period T_p and mean wave direction MWD)
3. wind speed and direction
4. surge level
5. river & sediment discharges

Considering microtidal coastal areas with dimensions of a few km (hence the wind effect and surge levels can be considered to have small variations along the domain) and no significant point discharges are present, it can be deduced that the main input parameter driving the sediment transport and subsequent bed evolution is the offshore sea state wave characteristics. Based on this observation, thereafter the wave Input Reduction (IR) methods which in a general sense derive a set of predefined representative wave conditions using a quantity driving the medium-term morphological evolution as a proxy, will be presented and analyzed. Many parameters affect the performance of IR methods

(Benedet et al., 2016; de Queiroz et al., 2019; Walstra et al., 2013) with the following parameters having the most prominent effect:

- method & proxy quantities to select the representative wave conditions
- number of representatives
- sequencing of the wave climate
- desired duration to be simulated

To evaluate the performance of IR methods various error statistics aiming to measure the model's accuracy or skill are commonly utilized. The usual approach (Benedet et al., 2016; de Queiroz et al., 2019; Luijendijk et al., 2019; Papadimitriou et al., 2020; Walstra et al., 2013) is to compare the results obtained by implementing an IR method to a "benchmark" simulation, containing the full set offshore sea-state characteristics or a robust wave climate (i.e. >50 cases). This benchmark simulation is often called "Brute force" or "reference" and is commonly used in practice, since in most cases no detailed field measurements of coastal bed elevation are readily available, especially in tandem with buoy measurements of wave characteristics.

The most common measures of a morphological model's accuracy are the Mean Absolute Error (MAE), Mean Square Error (MSE) and Root Mean Square Error (RMSE). Given a set Y of J forecast predictions (the results obtained by implementing the IR methods in this context) and X a set of observations (the results of the Brute force simulation) the MSE is calculated as (Sutherland et al., 2004a):

$$MSE(Y, X) = \frac{1}{J} \sum_{j=1}^{J} (y_i - x_i)^2 = \langle (Y - X)^2 \rangle \tag{2.3}$$

where the angular brackets denote averaged quantities.

The morphological model's skill is a non-dimensional measure of the accuracy of a prediction relative to the accuracy of a baseline prediction (Sutherland et al., 2004a), which could, for example, be the initial bathymetry, a random choice (from the possible range of outcomes) or a simple empirical predictor (such an equilibrium coastal profile). The most commonly used measure of skill for morphological bed evolution applications is the Brier Skill Score (BSS) which has been employed in numerous studies (de Queiroz et al., 2019; Papadimitriou et al., 2022b, 2020; Sutherland et al., 2004a, 2004b; van Rijn et al., 2003; Vousdoukas et al., 2011). The BSS is calculated as follows:

$$BSS = 1 - \frac{MSE(Y, X)}{MSE(B, X)} = 1 - \frac{\langle (Y - X)^2 \rangle}{\langle (B - X)^2 \rangle} \tag{2.4}$$

where B is a baseline prediction, usually taken as the initial bathymetry.

Perfect agreement with measurements gives a BSS of 1 whereas modeling the baseline condition gives a score of 0. If the model prediction is further away from the final measured condition compared to the baseline prediction, the skill score is negative. As shown in Eq. (2.4) these skill scores are unbounded at the lower limit. Therefore, they can be extremely sensitive to small changes when the denominator is small, as is the case with other non-dimensional skill scores derived from the ratio of two numbers.

Additionally, large negative values can be obtained even from models which a change of the correct order of magnitude when the measured change is very small. The following classification of the BSS (Sutherland et al., 2004a) is widely utilized to evaluate the performance of morphological models as shown in Table 2.3:

Table 2.3
Classification for the BSS (Sutherland et al., 2004a)

Classification	BSS
Excellent	*0.5 - 1.0*
Good	*0.2 - 0.5*
Reasonable/Fair	0.1 - 0.2
Poor	*0.0 – 0.1*
Bad	<0.0

Based on the methodology followed and corresponding proxy quantities used to select the representative wave conditions, various wave IR methods have been realised and can be divided into the following categories:

- Representative morphological wave height (RMWH) selection methods (Borah and Balloffet, 1985; Brown and Davies, 2009; Chondros et al., 2022; Chonwattana et al., 2005; Karambas et al., 2013; Karambas and Samaras, 2017; Papadimitriou et al., 2022a; Pletcha et al., 2007)
- Binning Input Reduction (BIR) methods (Benedet et al., 2016; de Queiroz et al., 2019; Papadimitriou et al., 2020; Roelvink and Reniers, 2011; Walstra et al., 2013)
- Clustering Algorithms (CA) wave schematization methods (de Queiroz et al., 2019; Papadimitriou and Tsoukala, 2022)

In the following subsections the background and methodology of the three branches of wave Input Reduction will be presented.

2.3.1. Representative morphological wave height selection methods

The oldest -but still widely used- RMWH methods divide the bivariate wave climate (significant wave height and angle of wave incidence) into directional bins of fixed size, and then for each bin a representative wave condition is obtained using a quantity considered vital in driving longshore sediment transport as a proxy. Based on this concept, Borah and Balloffet, 1985, presented a method to select annual "equivalent wave heights" based on the conservation of the alongshore component of wave power as shown below:

$$\sum (f_i) H_{s,e}^2 T_{p,e} \cos a_e \sin a_{e,b} = \sum \left(f_i H_{s,i}^2 T_{p,i} \cos a_i \sin a_{i,b} \right) \tag{2.5}$$

where: $H_{s,e}$ denotes the yearly "equivalent" significant wave height, $T_{p,e}$ the yearly equivalent peak wave period, α_e the yearly equivalent wave incidence angle, with the

subscript b denoting the value at the breaker line. In the right-hand side of the Eq. (2.5) the subscript "i" denotes individual wave events, with f_i being the frequency of occurrence of each event.

Considering identical angles of wave incidence, Eq. (2.5) can be rewritten in the following form (Karambas et al., 2013):

$$T_{p,e} = \frac{\sum (f_i T_{p,i})}{\sum f_i} \tag{2.6}$$

$$H_{s,e}^2 = \frac{\sum (f_i T_{p,i} H_{s,i}^2)}{T_{p,e} \sum f_i} \tag{2.7}$$

The frequency of occurrence of each representative condition is the sum of the individual frequencies of occurrence f_i of the members of each directional bin. This method has been used in many studies (Karambas et al., 2013; Karambas and Samaras, 2017; Tsiaras et al., 2020) and practical applications, taking advantage of its relative ease of implementation (since calculations can be usually carried out within a single spreadsheet). However, calculation of a representative incidence wave angle is not clearly defined and often can be taken as the mean value of each directional bin.

Chonwattana et al., 2005, followed a similar approach aiming to expand on the concept of representative morphological wave heights using the conservation of wave energy flux along a wave ray and coupling it with either bulk longshore or cross-shore transport formulations. Hence, conservation of wave energy flux along a wave ray orders that:

$$H_{s,1}^2 C_{g1} = H_{s,2}^2 C_{g2} \tag{2.8}$$

where H_s is the significant wave height and C_g is the wave group velocity. The subscripts "1" and "2" denote two sequential positions along the wave ray.

Substituting the value of wave group velocity for the deep water ($C_g = \frac{g T_p}{4\pi}$) in Eq. (2.6) and eliminating constants we obtain the following relationship.

$$H_{s,1}^2 T_{p,1} = H_{s,2}^2 T_{p,2} \tag{2.9}$$

Taking the component of the wave energy flux in the longshore direction one obtains:

$$H_s^2 T_p sina_o = C_1 \tag{2.10}$$

where a_o is the deepwater wave incidence angle relative to the shore-normal and C_1 a constant.

Similarly, for the cross-shore direction Eq. 2.7 takes the following form:

$$H_s^2 T_p cosa_o = C_2 \tag{2.11}$$

where C_2 is a constant.

With the assumption that longshore sediment transport rates (S) depend on the longshore component of the wave energy flux in the surf-zone (USACE, 1984), and utilizing the formula of Vongvisessomjai et al., 1993, one obtains:

$$S = 0.064208 H_s^{2.5} cos(a_o^{0.25}) sin(2a_o) \tag{2.12}$$

If the longshore sediment transport is conserved, Eq. (2.12) yields:

$$H_s^{2.5} cos(a_o^{0.25}) sin(2a_o) = C_3 \tag{2.13}$$

where C_3 is a constant.

Solving Eq. (2.10), (2.11) and (2.13) for each wave record of a given timeseries of offshore sea state characteristics the representative or "equivalent" values of the constants C_1, C_2, C_3 can be obtained as follows:

$$\begin{cases} C_{1,e} = \dfrac{\sum f_i C_{1,i}}{\sum f_i} \\ C_{2,e} = \dfrac{\sum f_i C_{2,i}}{\sum f_i} \\ C_{3,e} = \dfrac{\sum f_i C_{3,i}}{\sum f_i} \end{cases} \tag{2.14}$$

with f_i being the frequency of occurrence of each wave record.

After computing the equivalent values of the constants, the system of equations shown in Eq. (2.14) is inverted to obtain "equivalent" values of the wave characteristics $(H_{s,e}, T_{p,e}, a_e)$ as shown below.

$$\begin{cases} a_{o,e} = \tan^{-1} \dfrac{C_{1,eq}}{C_{2,eq}} \\ H_{s,e} = \left[\dfrac{C_{3,eq}}{(cos a_o)^{0.25} \sin(2a_{o,eq})} \right]^{2/5} \\ T_{p,e} = \dfrac{C_{2,eq}}{H_{s,eq}^2 cos a_{o,eq}} \end{cases} \tag{2.15}$$

Chonwattana et al., 2005 also examined an alternative approach, one based on the conservation of the cross-shore sediment transport component throughout the beach profile. The authors argued that the calculation of a reduced set of representative wave conditions should preferably be linked to offshore wave characteristics to further abet simplicity and speed. Hence, they selected the formula for offshore bar migration proposed by Kraus et al., 1991 and later modified by Dalrymple, 1992 who defined a non-dimensional parameter P directly linked to offshore wave characteristics.

$$P_o = g \frac{H_s^2}{w_f^3 T_p} \tag{2.16}$$

where w_f is the sediment settling or fall velocity.

If the cross-shore sediment transport is conserved and the sediment characteristics are considered constant throughout the beach profile, Eq. (2.16) yields:

$$\frac{H_s^2}{T_p} = C_4 \tag{2.17}$$

where C_4 is a constant.

Solving once again Eq. (2.10), (2.11) and (2.17) for each wave record of a given timeseries of offshore sea state characteristics and calculating the constants $C_{1,e}$, $C_{2,e}$, $C_{4,e}$ based on the conservation of the cross-shore sediment transport the corresponding values of the "equivalent" wave characteristics can be obtaining:

$$
\begin{cases}
a_{o,e} = \tan^{-1}\dfrac{C_{1,eq}}{C_{2,eq}} \\[2ex]
H_{s,e} = \left[\dfrac{C_{1,eq}\,C_{4,eq}}{\sin{(a_{o,eq})}}\right]^{1/4} \\[2ex]
T_{p,e} = \dfrac{C_{2,eq}}{H_{s,eq}^2 \cos a_{o,eq}}
\end{cases}
\qquad (2.18)
$$

An indicative bivariate plot of H_s and α_o indicating the equidistant directional bins and obtained representatives wave conditions utilizing the approach of Chonwattana et al., 2005 is showcased in Figure 2.3.
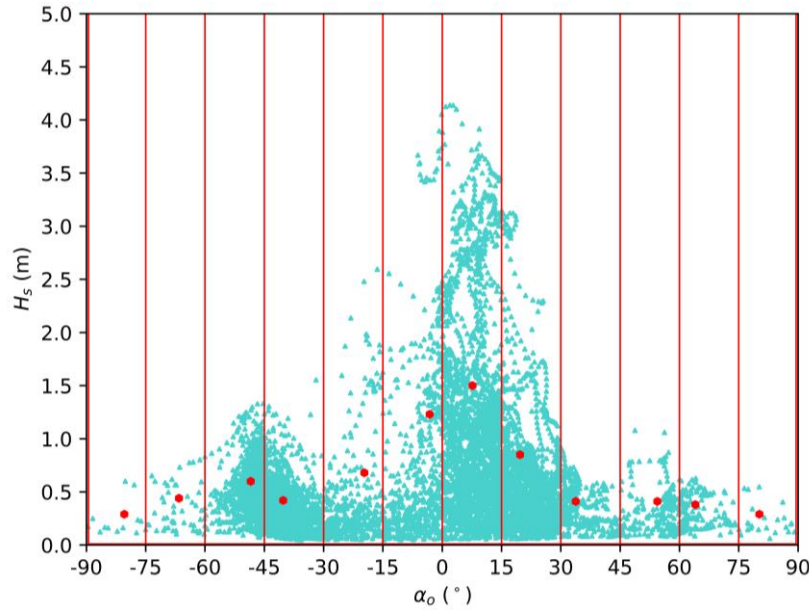
Figure 2.3. Records of offshore sea state timeseries (lightblue dots) and obtained 12 representative wave conditions (red markers). The red boundaries denote the equidistant directional bins.

Chonwattana et al., 2005 applied a coastal area model in a groyne compartment to assess the morphological evolution of the coastal bed and assess model performance. By applying either the system of Eq. (2.15) or (2.18) for a varying number of representative conditions (ranging from 1 to 16 representative inputs) they concluded that the required computational effort is reduced significantly, by a factor of 200 with a small reduction of model efficiency (order of 5%). The two alternative approaches produced similar representatives and results, with the ones calculated based on the longshore sediment transport having a slight edge. By increasing the number of representatives, the root-mean square error (RMSE) of model predictions decreased, albeit with a proportional increase in computational time. Since the wave climate is divided in directional bins of fixed size, if the wave energy is concentrated around one

dominant direction, this method can add more weight in waves generated from directions that are not so vital in shaping the morphological evolution of the specific study area.

Pletcha et al., 2007, intercompared alternative formulations for the calculation of the sediment transport rates and obtained different "equivalent" values of wave characteristics at a coastal lagoon in the Iberian Peninsula. The authors stated that a number of 8 representatives is adequate to describe the annual morphological evolution for the particular case. They concluded that the performance of the representative waves is case specific and sensitive to the longshore sediment transport formulation considered, implying that a thorough calibration of the morphological model should be undertaken.

Brown and Davies, 2009, introduced a RMWH method with the goal of maintaining the statistical properties of the wave characteristics while simultaneously retaining somewhat the chronology of the events. For that purpose, they divided the annual wave climate at 4 separate seasons and 4 directional sectors. For each directional sector and season, a mean value for the significant wave height was selected as the representative wave condition.

$$H_{s,r} = \frac{\sum f_i H_{s,i}}{\sum f_i}$$

(2.19)

The corresponding representative peak wave periods were obtained by applying the correlation of Jonswap wave prediction method. Ultimately 16 representative wave conditions were obtained, superimposed with two additional extreme sea-states introduced in the autumn and winter seasons. This RMWH selection method is the only one attempting to retain a form of wave chronology, since information about the sequencing of individual sea-states is inherently lost by grouping and then schematizing an annual wave climate. However, this method usually requires a higher number of wave representatives compared to the methods of Borah and Balloffet, 1985 and Chonwattana et al., 2005, and does not take into account the non-linear relationship between the wave height and the longshore sediment transport rates.

2.3.2. Binning Input Reduction methods

Binning Input Reduction methods have been used in numerous studies of medium-term coastal area morphological modelling (Antolínez et al., 2016; Benedet et al., 2016; de Queiroz et al., 2019; Hendrickx et al., 2023; Lesser, 2009; Papadimitriou et al., 2020; Van Duin et al., 2004; Walstra et al., 2013). The main distinction from RMWH methods is that the directional bins are not predefined and are also characterized by an uneven size. In general, the bivariate wave climate of wave height and mean wave direction (or angle of wave incidence) is divided in a predefined number of N_r bins containing an equal portion of a proxy quantity considered vital in driving the medium-term coastal bed evolution (such as the wave energy flux, or longshore sediment transport). The most widely-used BIR methods are the following (Benedet et al., 2016):

- the Fixed Bins Method (FBM), where the number of directional intervals and height intervals arbitrarily defined. Initially a given number of directional bins with

fixed degree intervals is used to divide the offshore sea-state time series and subsequently, a pre-defined number of wave height intervals is applied to each wave directional bin. It can be deduced that the wave height intervals of the subdivisions are fixed, but do not necessarily have the same range between the directional classes.

- the Energy Flux Method (EFM), in which instead of arbitrarily defining the wave directional bins with fixed intervals like in the FBM, the EFM directional bins are calculated as 'equal wave energy flux' intervals, calculating the energy flux of each sea-state as follows:

$$E_{f,i} = \frac{1}{16} \rho g H_{s,i}^2 C_{g,i} \tag{2.20}$$

Where ρ is the seawater density and g is the acceleration of gravity.

For instance, if 15 wave representatives are selected a priori, with 5 subdivisions in the wave direction and 3 in the wave heights, each bin ultimately contains 1/15 of the total wave energy flux.

- the Energy Flux Method with Extreme Events (EFMEE) is similar to the EFM, however, an extreme wave condition is added to the wave climate in order to provide a representation of a 'storm condition' in an averaged wave climate. a representation of a 'storm condition' in an averaged wave climate. The extreme wave class contains the 12 wave records with the highest wave energy in each wave directional bin (probability of yearly exceedance of 0.137%), therefore there is always one extreme wave case per directional bin in this method.

- the CERC Method is similar to the EFM however instead of the wave energy flux it uses sediment transport rates to define the wave direction and height bins. Sediment transport rates are calculated with the empirical CERC formula (USACE, 1984).

$$S_i = K \frac{\rho \sqrt{g}}{16 \gamma^{0.5} (\rho_s - \rho)(1 - n)} H_b^{2.5} \sin(2a_b) \tag{2.21}$$

The main principle of the method is the definition of wave classes that represent similar accumulated potential longshore sediment transport. The directional and wave height bins are calculated considering 'equal transport' intervals. Compared to the EFM the CERC Method yields somewhat similar wave classes with small differences (Benedet et al., 2016; de Queiroz et al., 2019) with the biggest difference between these two methods is that the wave direction is explicitly considered in the CERC Method.

Having laid the foundations of each of the 4 BIR methods, the following steps are generally undertaken to schematize timeseries of offshore sea-state wave characteristics and obtain N_r representative conditions (Benedet et al., 2016):

1. A scatter plot of significant wave height (H_s) vs mean wave direction (MWD) or wave incidence angle relative to the shore normal (a_o) is prepared.

2. The time series of offshore sea-state characteristics is divided into a pre-determined number of wave directional bins (N_d).

3. The number of wave height subdivisions (N_h) that each wave direction will be further divided into is defined.

4. Wave classes then defined as a result of N_d*N_h intersections among the wave height and directional bins using a proxy quantity depending on the BIR method. At first (Figure 2.4b), the boundaries of the directional bins are defined since each bin contained an equal portion of the proxy quantity of choice (e.g. E_f/N_d, for the wave energy flux). Then (Figure 2.4c), each directional bin is further subdivided in N_h wave height bins (e.g. each bin contains a portion of $E_f/(N_d*N_h)$ for the wave energy flux input reduction method).

5. A set of N_r representative wave characteristics, taken as the mean value of each class and the corresponding frequency of occurrence are obtained.

The procedure to define 20 classes and representative wave conditions, with 5 directional and 4 wave height bins is showcased in Figure 2.4 for the EFM.
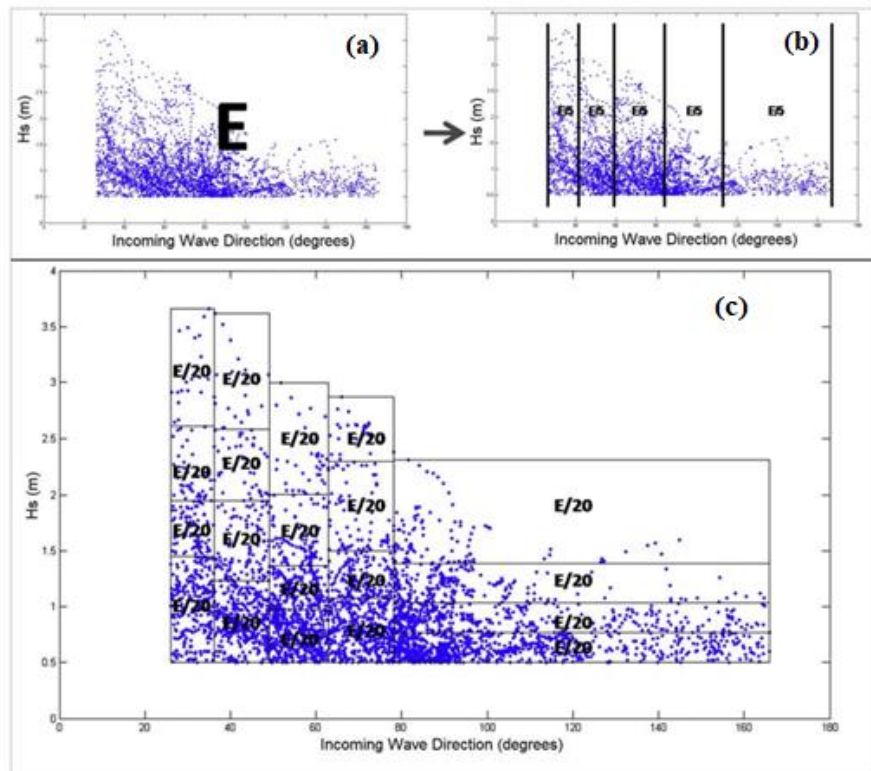
Figure 2.4. Procedure to define classes through the EFM (Benedet et al., 2016)

The difference between the classes and obtained 12 representative wave conditions obtained by implementing the FBM and the EFM for a given set of offshore sea-state characteristics is illustrated in Figure 2.5. The difference is the bin definition for the two methods is notable, since those obtained through the EFM are characterized by an uneven size and thus can better capture the concentration of wave energy around the perpendicular angle of wave incidence for the particular wave climate.
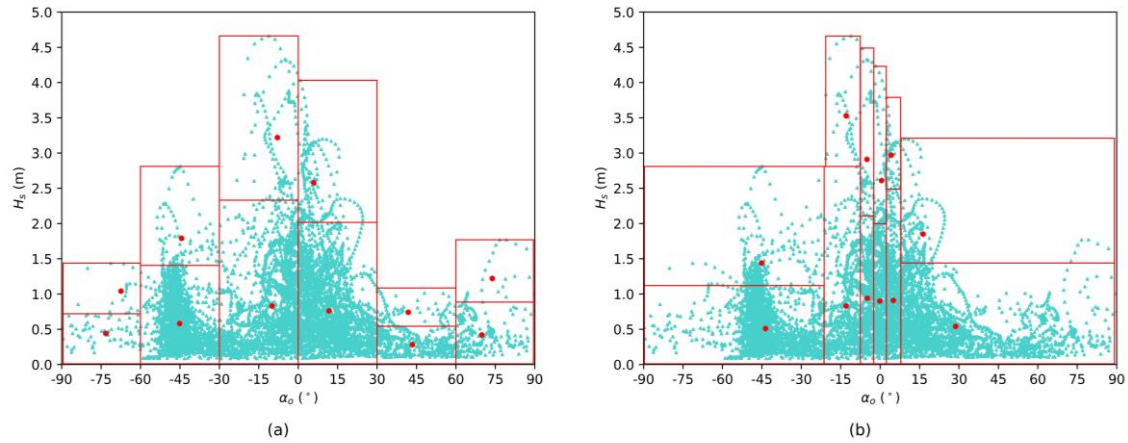
Figure 2.5. Obtained classes (bounded by the red rectangles) and 12 representative wave conditions (red markers) for an arbitrary dataset of offshore sea-state wave characteristics (light blue markers) using the (a) FBM and (b) EFM.

A more sophisticated BIR method, called the "Opti-Routine" (Roelvink and Reniers, 2011) attempts to reproduce more accurately the complete accretion/erosion patterns utilizing sequential numerical model simulations. The general outline of this method is to perform short-term simulations for each record of the full offshore sea-state wave characteristics to obtain the target sedimentation/erosion patterns and then through an automatic trial and error approach reducing the number of wave representatives by keeping sea-states with largest contribution in shaping the sediment transport regime (Roelvink and Reniers, 2011). The general steps of the "Opti-Routine" are as follows:

1. Simulations to obtain initial sedimentation/erosion patterns for the full wave climate (usually > 50 sea-states) are executed and the results are added based on the frequency of occurrence of each sea-state to obtain the weighted average target pattern.
2. A large number of "mutations" are created (usually at the order of 1000) where the frequencies of occurrence of each mutation varies within a certain range. For each of these mutations the weighted average pattern is computed and error statistics in this pattern compared to the target pattern are also kept track off.
3. The "mutation" with the smallest error is kept.
4. The "mutation" with the smallest contribution to the average pattern is removed.
5. Return to step 2 and repeat the procedure until a predefined number of representatives N_r is obtained.

By repeating this procedure, it can be deduced that the frequencies of occurrence gradually grow or reduce until they become either dominant or extinct, and that the overall pattern remains almost unchanged until a number between 5-10 representative conditions are selected. Selecting fewer representatives than 5 usually sharply increases the error and should be avoided. The "Opti routine" has a strong theoretical basis and can be applied for any coast configuration, however it is associated with significant additional computational burden compared to the other BIR methods since it requires the sequential execution of a large number of numerical simulations.

As has been previously mentioned, while the main theoretical aspects that drive the medium-term morphological bed evolution are generally universally acknowledged, in turn the unique morphological and metocean conditions of each coastal area greatly influences the performance of wave Input Reduction methods. Motivated by this, several researchers have attempted to systematically evaluate the performance of wave Input Reduction methods for interannual morphological bed evolution aiming to provide practical recommendations and guidelines about the best IR method and optimal configuration.

Walstra et al., 2013 examined in two study sites various aspects affecting the performance of the FB and EFM methods of input reductiom, i.e. the wave climate duration T_{wc}, the method to select representative wave conditions, testing the Fixed Bins and the Energy Flux method, as well as the sequencing of wave conditions. The performance of the BIR methods was compared to Brute force simulations of 3 years with wave conditions measured at 3-hour intervals. They concluded that BIR methods inherently introduce error in model predictions which are influenced by all the abovementioned parameters. They stated that the Energy Flux method performs better than the Fixed Bins method while a random ordering of wave conditions (i.e. interchanging lowly and highly energetic sea-states) also gives the best results since it resembles the variability and stochastic nature of the wave conditions in field sites. In a similar manner, Benedet et al., 2016, performed a comprehensive evaluation of the different types of BIR methods for a beach nourishment project in Florida, USA. They performed sensitivity analysis on the number of representatives performing simulations with 6,12, 20 and 30 conditions respectively, utilizing upscaling with Morfac. The performance of the BIR methods was compared to a Brute force simulation containing a detailed wave climate of 62 cases by calculating the corresponding RMSE. They concluded that the best performing methods were the Energy Flux method followed by the "Opti-Routine" when a number of 12 representatives is selected. The Energy Flux method with Extreme Events performed well when a high number of representatives is considered (>20), with a rapid deterioration of results for a lesser number. Ultimately, the authors stated that a number of 12 representatives is adequate to reproduce morphological bed evolution at an annual scale.

A disadvantage of performing simulations through the "Morphodynamic" approach (considering constant feedback between wave, hydrodynamics and morphology) is that the simulation duration has to be the same as the full wave climate (Benedet et al., 2016; Papadimitriou et al., 2020) and the biggest reduction of model run-time is due to the lower spin-up times required for the reduced amount of input conditions. de Queiroz et al., 2019 evaluated the performance of BIR methods and the RMWH method of Brown and Davies, 2009, in reproducing sandbar dynamics for the same study sites as the ones shown in Walstra et al., 2013. The main focus of the research was the evaluation of the effect of the number of representatives and the sequencing of wave conditions utilizing the coastline model UNIBEST-CL. As far as the sequencing of the wave conditions is concerned, they tested four different settings, (a) Random sequencing, (b) Markov chain,

(c) Monte Carlo Markov chain and (d) Monte Carlo Markov chain with repetition. From their evaluation for the specific study sites the authors concluded that the best performing was the CERC method followed by the EFM, while the RMWH method was the worst performing one. Despite retaining some form of the original chronology with the Markov chain & Monte Carlo methods ultimately the Random ordering of wave representatives was the best performing one. In accordance to Benedet et al., 2016, a number of 10 representatives was considered adequate to emulate inter-annual migration of a sandbar. Despite the aforementioned research efforts that focused on evaluating the performance of BIR on various study sites, clear practical guidelines about the best performing BIR methods depending on the approach followed ("Morphostatic" vs "Morphodynamic") have not been provided yet.

2.3.3. Clustering Algorithms

Cluster analysis is a machine learning method for data processing. It centers around grouping a set of objects in a way that objects in the same group (cluster) are more similar to each other than to those in other clusters. These groups may reveal underlaying patterns related to the phenomenon under investigation. Cluster analysis has many applications in psychology, biology, computer graphics, image processing & pattern recognition and machine learning. Lately, cluster analysis has been employed in various studies in ocean and coastal engineering such as storm classification (Martzikos et al., 2018), wave energy resource (Fairley et al., 2020), longshore transport rates (Splinter et al., 2011), cross-shore profile morphological evolution (Kelpšaitė-Rimkienė et al., 2021) and multivariate wave climate classification (Camus et al., 2011). Since for most of the aforementioned applications no direct relationship between the data to be grouped is available, the clustering algorithms tasked with performing the analysis belong in the branch of "unsupervised learning". Consequently, no labels and directions are given to the algorithm which is left on its own to identify the structure in the input data. Most clustering algorithms are based on the general principle of computing a distance metric as a similarity measure for a large number of variables, to ultimately assign data to different clusters. Various clustering algorithms have been developed to efficiently handle large quantities of data such as K-Means (c), Fuzzy C-Means (Bezdek, 1981) and CURE (Guha et al., 1998) among others. Particularly, K-Means is one of the most used and notorious algorithms for multivariate cluster analysis that has been proven efficient in handling wave climate datasets (Camus et al., 2011) and sediment transport gradients (Splinter et al., 2011). It belongs in the category of centroid-based partitioning clustering since it identifies the presence and boundaries of clusters by finding their centroids (the mean point of each cluster).

The K-Means (KM) clustering algorithm divides a multi-dimensional data space into a pre-determined number of clusters, each one defined by an arbitrary centroid and formed by the data for which the centroid is located the nearest to (Camus et al., 2011). Essentially, given a dataset of d-dimensional vectors $X = \{x_1, x_2, ..., x_d\}$ the KM algorithm allocates each observation to the closest cluster, using the Euclidean distance between

an observation and a cluster centroid as a metric to minimize the sum of errors obtained by the following objective function:

$$E = \sum \sum \left\| x_i^{(j)} - \bar{m}_j \right\|^2 \tag{2.22}$$

where E is the sum of the errors for all objects in the dataset, x_i is a point in cluster j, and $\bar{m}_j$ the mean of each cluster (Kelpšaitė-Rimkienė et al., 2021).

By selecting j initial centroids, usually obtained through the fast-converging K-Means++ initialization algorithm (Arthur and Vassilvitskii, 2007), each point is assigned iteratively to the cluster it is located closest to in order to effectively minimize the objective function E until a user-defined convergence criterion is satisfied and the centroids are no longer reassigned. A distinctive characteristic of the KM algorithm is that each data point belongs uniquely in each cluster.

Various alternatives to the K-Means algorithm can be utilized with the most widely-used being the following:

- K-Medians, where instead of the mean of each cluster the median is taken as the centroid of each cluster.
- K-Medoids, where the centroid of each cluster is a point belonging to the original dataset of observations.
- Fuzzy C-Means or Soft K-Means, in which each data point can belong to more than one cluster by using a soft membership function.

The a priori determination of the number of clusters and the centroid-based definition of the cluster boundaries is alluring for the purpose of schematizing a dataset of offshore sea-state wave characteristics. As in several other machine learning techniques, the data used as input to the algorithm (a multivariate wave climate of H_s, T_p, a_o for coastal engineering applications) have to be normalized.

Significant wave height values ($H_{s,i}$), are normalized utilizing a min-max normalization as follows:

$$H_{s,norm} = \frac{H_{s,i} - H_{s,i,min}}{H_{s,i,max} - H_{s,i,min}} \tag{2.23}$$

where $H_{s,i,max}$, $H_{s,i,min}$ are the maximum and minimum recorded values of the significant wave height encountered in the dataset respectively.

Similarly for the wave periods the normalized value is given through the following relationship:

$$T_{p,norm} = \frac{T_{p,i} - T_{p,i,min}}{T_{p,i,max} - T_{p,i,min}} \tag{2.24}$$

where $T_{p,i,max}$, $T_{p,i,min}$ are the maximum and minimum recorded values of the peak wave period encountered in the dataset respectively.

The angle of wave incidence is a circular variable, since the distance between two given values can be measured clockwise and counterclockwise. This implies that the maximum difference between two radial directions is π. Therefore, the distances

between two angles are normalized between [0,1] and the absolute values of the angle will be normalized between [0,2]. It is assumed that the angles are measured in radians or that sexadecimal degrees are converted to radians by multiplying them with a factor of π/180. The normalized angle $\alpha_{i,norm}$ is found by converting each observed angle α_i of the dataset:

$$\alpha_{i,norm} = \frac{a_i}{\pi} \tag{2.25}$$

Utilizing the corresponding inverse transform function, the obtained centroids are de-normalized and a set of representative wave conditions $H_{s,r}, T_{p,r}, a_r$ are obtained. Twelve obtained centroids and the corresponding clusters (denoted with different colors) are showcased as a bivariate scatter plot of H_s vs α_o in Figure 2.6 for an arbitrary annual dataset of offshore sea-state characteristics.
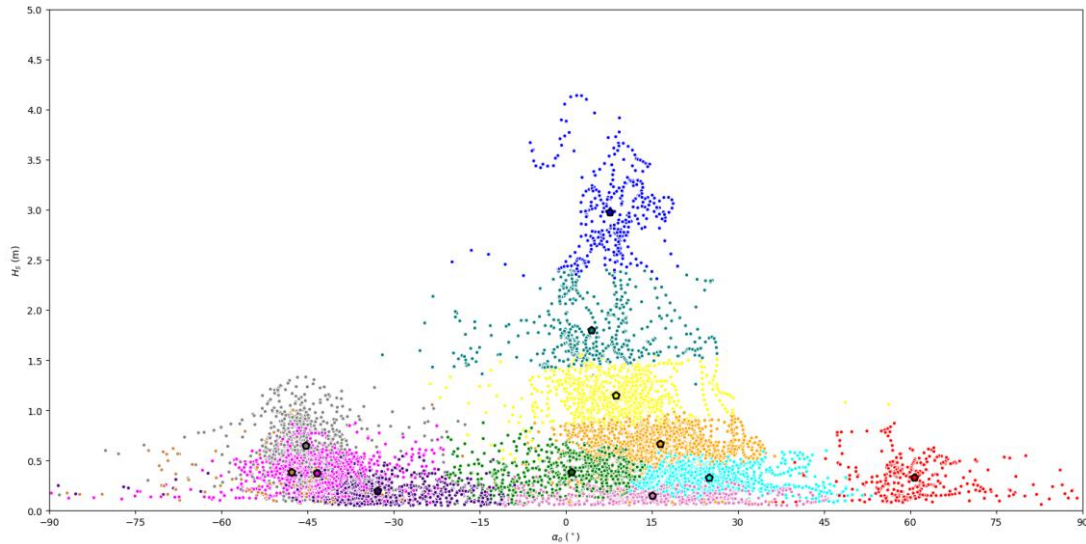
Figure 2.6. Records of offshore sea-state timeseries, corresponding clusters and obtained 12 representative wave conditions (large pentagon markers). The different colors of the data points denote separate clusters

Few research efforts which utilize and evaluate the performance of clustering algorithms as wave IR methods have been realized (de Queiroz et al., 2019; Papadimitriou and Tsoukala, 2022). In particular, de Queiroz et al., 2019, tested various clustering algorithms with different settings (K-Means, Fuzzy C-Means, Maximum Dissimilarity Algorithm, K-Harmonic Means) for the case of a sandbar migration for two field sites using the profile model UNIBEST-TC. Their investigation showed that clustering algorithms perform generally worse than the best Binning Input Reduction methods, which was attributed to the over-representation of lowly energetic sea-states in the clustering framework. The best performing CA was found to be the K-Means. However, a more detailed evaluation of clustering algorithms' performance as an alternative to the more classical Binning Input Reduction Methods for an alongshore variable 2D domain, aiming to enhance the coastal area model results by introducing proxy quantities important to the medium-term morphological bed evolution has not been undertaken yet.

Chapter 3

A novel approach to Binning Input Reduction methods[1]

Binning wave Input Reduction methods have been utilized extensively in coastal engineering studies (Benedet et al., 2016; de Queiroz et al., 2019; Walstra et al., 2013) due to their proven capability to reduce the computational burden of morphological coastal bed evolution simulations. However, when performing simulations through the "Morphodynamic" approach, it is usual to combine them with model reduction techniques to further reduce the computational effort, since the total simulation time forced with the reduced input has to be identical to that of the full set of conditions ((Benedet et al., 2016; Papadimitriou et al., 2020)). This chapter proposes a novel approach and further expands upon the concept of binning IR methods, introducing criteria for the elimination of lowly energetic sea-states, aiming to further alleviate the computational burden associated with coastal area modelling simulations.

Two different IR methods will be presented in this chapter, one based on the calculation of the sediment Pick-up rate, and one based on elimination of wave conditions based on the non-exceedance of a threshold current speed (Soulsby, 1997). The common trait of both methods is the elimination of lowly energetic sea-states considered unable to initiate sediment motion, albeit utilizing a different approach, which in turn leads to an effective reduction of the length of the dataset and subsequently the model run-time reduction.

The innovative aspects in this chapter revolve around concerting Input Reduction techniques with model reduction aspects achieving a significant model run-time reduction. A robust wave propagation numerical model based on the Parobolic Mild Slope equation (Chondros et al., 2021) has been extended and enhanced in the framework of this research and is considered an integral part of the methodologies presented herein due to complexity of the present approach.

Implementation of the developed methods is undertaken in the coastal area in the vicinity of Rethymno Port, Crete, Greece utilizing the coastal area model MIKE21 CM FM. An extensive and comprehensive evaluation of the obtained results is then carried

---

[1] Parts of this Chapter have been published in Papadimitriou et al., 2020.

out and along with the estimation of CPU times clearly highlight the advantages of the proposed methods.

3.1. Theoretical background and methodology

For flows with very low velocity over a sandy bed the sand layer generally tends to stay immovable. However, if the flow velocity slowly increases some grains begin to move. This process is called the initiation of sediment motion or incipient motion (Soulsby, 1997). A similar process occurs beneath waves, and beneath combined waves and currents. Waves are responsible for stirring sediment while the mean flow is responsible for transporting it. It follows, that when no significant movement of sediment occurs in a coastal area, the wave field is usually mild, leading to low current velocities and sediment transport rates.

For the case of a steady current, the threshold (or critical) depth-averaged speed U_{cr} required to set a grain of mean sediment diameter d_{50} into motion on an un-rippled bed with still water depth h can be predicted by a number of methods.

Van Rijn, 1984, proposed the following formula valid for freshwater at 15° C and sand of density ρ_s = 2650 kg/m^3.

$$U_{cr} = \begin{cases} 0.19d_{50}^{0.1} \log_{10}\left(\dfrac{4h}{d_{90}}\right) & for\ 100 \leq d_{50} < 500\ \mu m \\[2ex] 8.50d_{50}^{0.6} \log_{10}\left(\dfrac{4h}{d_{90}}\right) & for\ 500 \leq d_{50} \leq 2\ mm \end{cases} \tag{3.1}$$

with d_{90} being the characteristic grain diameter exceeding 90% of the grain sizes.

Soulsby, 1997, proposed the following formula, valid for any non-cohesive sediment having a dimensionless grain diameter $D_* > 0.1$.

$$U_{cr} = 7.0\left(\frac{h}{d_{90}}\right)^{1/7}\left[g(s-1)d_{50}\frac{0.30}{1+1.2D_*} + 0.055(1-e^{-0.02D_*})\right]^{1/2} \tag{3.2}$$

where s is the ratio of densities of sediment grains and water and D_* is the dimensionless grain diameter given by the following relationship.

$$D_* = \left[\frac{g(s-1)}{v^2}\right]^{1/3} d_{50} \tag{3.3}$$

where v is the kinematic viscosity of saltwater.

In the alongshore direction, the transfer of momentum from the wave motion to the mean flow generates longshore currents which are mostly responsible for the transport of sediments. Considering stationary conditions for a straight coastline and depth parallel bottom contours, the shear component of the radiation stress tensor S_{xy} acts as a driving force. The counter-force restoring equilibrium (F_y) must in turn be supplied by the bed shear stresses that develop when a longshore current is generated. The alongshore component of the momentum balance for a steady state and considering alongshore uniformity can be written as:

$$F_y = -\frac{dS_{xy}}{dx} = \bar{\tau}_{by} \tag{3.4}$$

where $\bar{\tau}_{by}$ is the time-averaged bed shear stress in the alongshore direction.

Considering a quadratic friction law for the bed shear stress due to the combined action of waves and currents leads to the following expression:

$$\vec{\tau_b} = \rho c_f |\vec{u}| \vec{u} \tag{3.5}$$

where c_f is the bed friction factor and $\vec{u}$ is the total velocity due to the combined effect of waves and currents.

Making a number of assumptions, namely the validity of the shallow water wave theory, small angles of wave incidence and also that the longshore component of the current velocity U is significantly smaller than the amplitude of the near bed wave orbital velocity signal U_w, the time-averaged bed-shear stress in the alongshore direction is given by:

$$\bar{\tau}_{by} = \frac{2}{\pi} \rho c_f U_w U \tag{3.6}$$

with U being the longshore current speed velocity magnitude.

The amplitude of the wave orbital velocity above the bed for the case of a monochromatic wave of height H and period T can be approximated through the linear wave theory as:

$$U_w = \frac{\pi H}{T \sinh(kh)} \tag{3.7}$$

For random waves, the wave field is represented by a sea-state spectrum composed of different frequencies, amplitudes and directions, the root-mean square wave orbital velocity signal near the bed (denoted as U_{rms}) can be computed by summing the velocity contributions from each district frequency component (derived from the linear wave theory) over the whole frequency range. Soulsby and Smallman, 1986, proposed the following approximate formula to compute U_{rms} :

$$U_{rms} = \frac{0.25 H_s}{T_n (1 + At^2)} \tag{3.8}$$

where $T_n = \sqrt{h/g}$ is the natural wave period, H_s is the significant wave height, and A and t are non-dimensional parameters defined as:

$$A = [6500 + (0.56 + 15.54t)^6]^{1/6} \tag{3.9}$$

$$t = \frac{T_n}{T_z} = \sqrt{\frac{h}{g}} \frac{1}{T_z} \tag{3.10}$$

where T_z is the zero-crossing wave period, taken usually as $T_z = T_p/1.28$ with T_p being the peak wave period of a Jonswap spectrum.

Thereafter, combining Eq. (3.4) and (3.6) one can obtain the value of longshore current speed as follows:

$$U = -\frac{dS_{xy}}{dx} \frac{\pi}{2 \rho c_f U_w} \tag{3.11}$$

For regular waves, the maximum value of the longshore current speed occurs at the breaking point, i.e. the point where initiation of wave breaking takes place. Irregular waves exhibit a more saturated surf zone and the maximum value is not encountered specifically at the point where initiation of breaking occurs, but still lies within the surf

zone. If the values of the longshore current speed obtained through Eq. (3.11) at a given still water depth h exceed the threshold current speed calculated through Eq. (3.2) then initiation of sediment motion is considered to take place.

The most precise and commonly used measure of the threshold of motion is expressed in terms of the ratio of the force exerted by the bed shear stress acting to move the sediment grains on the bed layer, to the submerged weight of the grain resisting to this action. This theory was initially developed by Shields, 1936 giving birth to the homonymous threshold Shields parameter θ_{cr} which can be calculated by the following expression proposed by Soulsby & Whitehouse 1997.

$$\theta_{cr} = \frac{0.24}{D_*} + 0.055(1 - e^{-0.02D_*}) \tag{3.12}$$

Near the bed, due to turbulence and friction effects, an oscillatory wave boundary layer is generated in which the wave orbital velocity rapidly increases from zero at the sea-bottom to the value of U_w at the top of the boundary layer. As has been previously mentioned the most important hydrodynamic property of waves contributing to sediment transport is the bed shear stress they produce. This stress is usually dependent on the wave orbital velocity signal near the bed U_w and the wave friction factor f_w and is computed via the following relationship:

$$\tau_{b,w} = \frac{1}{2}\rho f_w U_w^2 \tag{3.13}$$

The wave friction factor depends on the status of the flow, namely if it is laminar, smooth-turbulent or rough-turbulent, which in turn is related to the wave Reynolds number R_w and the relative roughness r. The latter quantity is calculated through:

$$r = \frac{U_w T}{2\pi k_s} \tag{3.14}$$

where k_s is the Nikuradse equivalent sand grain roughness.

For rough-turbulent flows, as is generally the case for a coastal bed under wave attack, the wave friction factor depends on the relative roughness r and the wave orbital velocity excursion near the seabed. The formulation of Swart, 1974, reads:

$$f_w = \begin{cases} 0.3 & for\ r \leq 1.57 \\ 0.00251e^{5.21r^{-0.19}} & for\ r > 1.57 \end{cases} \tag{3.15}$$

The non-dimensional Shields parameter θ is then obtained through the following relationship:

$$\theta = \frac{\tau_{b,w}}{g d_{50}(\rho_s - \rho)} \tag{3.16}$$

It can be deduced that initiation of sediment motion occurs when the values of the Shields parameter θ exceed the threshold values of θ_{cr} obtained through Eq. (3.12).

A quantification of the eroding capacity of individual sea-states can be achieved by calculating the sediment Pick-up rate P. Van Rijn, 1986, defined the pick-up process for various flow velocities (in the range of 0.5–1.5 m/s) and sand diameters (100–1500 μm). Thereafter, van Rijn et al., 2019, extended the Pick-up rate function for high flow velocities (in the range of 2–6 m/s) by introducing a damping factor f_D incorporating all the additional effects on sediment movement in high velocities, such as the damping of

turbulence (turbulence collapse) in the near-bed area where sediment concentrations are larger. Ultimately, the Pick-up rate function reads:

$$P = 0.00033\rho_s[(s-1)gd_{50}]^{1/2}D_*^{0.3}f_D\left[\left(\frac{\theta-\theta_{cr}}{\theta}\right)\right]^{1.5} \tag{3.17}$$

It can be derived from Eq. (3.17) that the Pick-up rate function becomes zero if $\theta < \theta_{cr}$.

Having laid the foundations of the criteria for initiation of sediment motion, two distinct methodologies of Binning IR methods were developed in the framework of this thesis and will be presented hereafter. The first method eliminates waves conditions based on the Shields criterion of incipient sediment motion (solely for the impact of waves) and calculates the wave representative conditions based on the Pick-up rate function (Pick-up rate method). The second method eliminates waves conditions by calculating the longshore current speed potential of each sea state (Threshold Current method) and comparing it to the threshold current speed obtained from Eq. (3.2) and obtains the representatives using the wave energy flux as a proxy. The distinct steps to obtain representative wave conditions through each method are presented in the following subsections.

3.1.1. Pick-up rate wave schematization method

In this subsection the steps to determine the representative wave conditions, utilizing the Pick-up rate wave input reduction method are presented. The larger portion of this method is rather simple in conceptualization and execution and can be reproduced either by employing a simple computer code or performing calculations in a spreadsheet. The distinct steps of this method are as follows:

1. Timeseries of offshore sea-state wave characteristics (e.g. either by buoy measurements, or hindcast simulations from oceanographic databases) are obtained for a desirable time range T_{wc}. The wave characteristics that are usually required by the binning input reduction methods are H_s, T_p (or another characteristic wave period) and MWD (Mean Wave Direction).

2. The timeseries are then filtered by disposing off records that do not contribute in shaping the bed evolution, namely sea-states exiting the computational domain.

3. The critical Shields parameter θ_{cr} through Eq. (3.12) is calculated.

4. Wave characteristics at a characteristic depth (at around h=8-10 m) are obtained. For this purpose, either a wave ray model (O'Reilly and Guza, 1991), a spectral wave model (Benoit et al., 1996), or a Mild Slope wave model (Chondros et al., 2021; Karambas and Samaras, 2017) can be used. For this implementation, a Parabolic Mild Slope model with non-linear dispersion characteristics, able to treat unidirectional random wave propagation enhanced during the scope of this thesis, entitled PMS-SP was used. The reason for utilizing this model is the accuracy in prescribing the wave field in mildly sloping beaches due to incorporation of non-linearity and the saving of considerable computational time relative to the time-dependent formulations of the hyperbolic mild slope equation. After obtaining the wave climate in the nearshore area a "1-1" correspondence

between the wave characteristics of each sea-state offshore (H_s, T_p, MWD) and the wave characteristics at the characteristic depth ($H_{s,in}$, $T_{p,in}$, MWD_{in}), is established.

5. Calculation of the inner depth of closure (h_{in}) which is defined as the seaward limit of the littoral zone for the given timeseries through the following equation (Houston, 1995):

$$h_{in} = 8.9\bar{H}_{s,in}$$

(3.18)

where h_{in} is the depth of closure and $\bar{H}_{s,in}$ is the mean significant wave height at a characteristic depth h=8-10 m, utilizing the wave characteristics calculated at step 4. The depth of closure was considered for the purpose of this research the critical depth after which no net sediment movement takes places. Consequently, this depth will be later set for the calculation of the wave orbital velocity since the larger portion of sediment transport takes place between h_{in} and the shoreline.

6. Calculation of the wave orbital velocity signal near the bed through Eq. (3.7) for monochromatic or Eq. (3.8) for irregular waves setting h=h_{in}.

7. For each wave record ($H_{s,in}$, $T_{p,in}$, MWD_{in}) the friction factor f_w (Eq. 3.15), the bed shear stress due to waves $\tau_{b,w}$ (Eq. 3.13) and ultimately the Shields parameter θ (Eq. 3.16), are calculated

8. If the $\theta < \theta_{cr}$ the wave record is eliminated since it does not contribute in setting sediments into motion. Through the "1-1" correspondence established at step 4, the respective wave record of the offshore timeseries is disposed. The total number of wave records offshore N is thus reduced using the criterion of the initiation of motion at a total of N_s (with $N_s \leq N$)

9. Calculation of the sediment Pick-up rate P through Eq. (3.17) for each wave record at the depth of closure. Also, the cumulative Pick-up rate P for the reduced time-series is determined.

10. The number of representative wave conditions N_r that will replace the full wave climate (e.g. 12 representative conditions) are determined. The number of representative conditions is based on discretion; however it is advised that a number between 6 and 30 conditions is chosen for sufficiently reproducing annual timeseries of offshore sea-state wave characteristics (Benedet et al., 2016). Then, the wave records are divided in classes with respect to the angle of wave incidence (or mean wave direction alternatively) and wave height. The boundaries of each class in both direction and wave heights are determined the same wave as the other commonly used wave schematization methods (see section 2.3.2 for details). Each representative class is characterized by an equal fraction of the cumulative Pick-up rate P (P/N_r) and can be described by a set of wave characteristics ($H_{s,in}$, $T_{p,in}$, MWD_{in}). Thus, it can be derived that each class is comprised of a different number of wave components, N_{cl}.

11. Utilizing again the "1-1" correspondence of wave characteristics offshore and nearshore, a set of representative conditions ($H_{s,r}$, $T_{p,r}$, MWD_r) can be obtained in the offshore wave boundary by considering that the bounding limits of each representative class in the depth of closure coincide with the respective ones in deep water. A small numerical extrapolation error stems from the fact that each representative class in the offshore boundary might not be characterized by exactly equal fraction of sediment Pick-up rate, since the Pick-up rate was calculated for the corresponding wave conditions at shallower water. However, since the proposed input reduction method concerns medium to long term morphological bed changes, this error is considered to have a very small effect in shaping the ultimate bed evolution and can consequently be neglected.

12. The frequency of occurrence $f = \frac{N_{cl}}{Ns}$ for each representative class is calculated, frequency of occurrence $f = \frac{N_{cl}}{Ns}$ for each representative class is calculated, based on the number of wave records of each class relative to the reduced dataset. Since N_s is the number of the reduced set of wave records, the frequencies of occurrence are rescaled, and the more energetic sea-states are associated with higher weights.

13. Finally, a simulation is executed with a 2D morphological area model using the representative wave conditions as forcing input. The total model run-time $T_{wc,r}$ is a fraction of the full time series, denoted as $T_{wc,r} = \frac{N_r}{N} T_{wc}$, since sea-states unable to initiate sediment movement are eliminated in step 8 and have little to no contribution in shaping the bed evolution.

The distinct steps of the methodology are also showcased as a flow chart in Figure 3.1.

Conversely to other widely used Binning IR methods, which are subject to a number of simplistic assumptions (i.e. straight coastline with depth-parallel contours) the Pick-up rate method incorporates numerical modelling to obtain nearshore wave characteristics and perform the binning procedure in the bi-variate wave climate of H_s and MWD. The utilization of a PMS wave model is better suited for use in the framework of this methodology since it provides accurate and robust solutions in the nearshore while minimizing the required computational effort. It is worth mentioning that the depth of closure (see step 5 of the above methodology), provides a rather strict criterion to eliminate wave conditions since at this depth the cross-shore component of sediment transport is considered by definition almost null. However, initiation of sediment motion is highly dependent on a multitude of parameters apart from the wave characteristics, such as the beach slope, sediment properties and bottom friction among others. While some sea-states considered unable to initiate sediment motion in the depth of closure may be able to set sediment into motion in shallower depths it is considered that calculation of the near bed wave orbital velocity at the depth of closure is a valid approximation within the scope of the Pick-up rate method since it depends only on the annual wave climate and is hence easy to compute for the purpose of reducing a set of offshore sea-state wave characteristics.
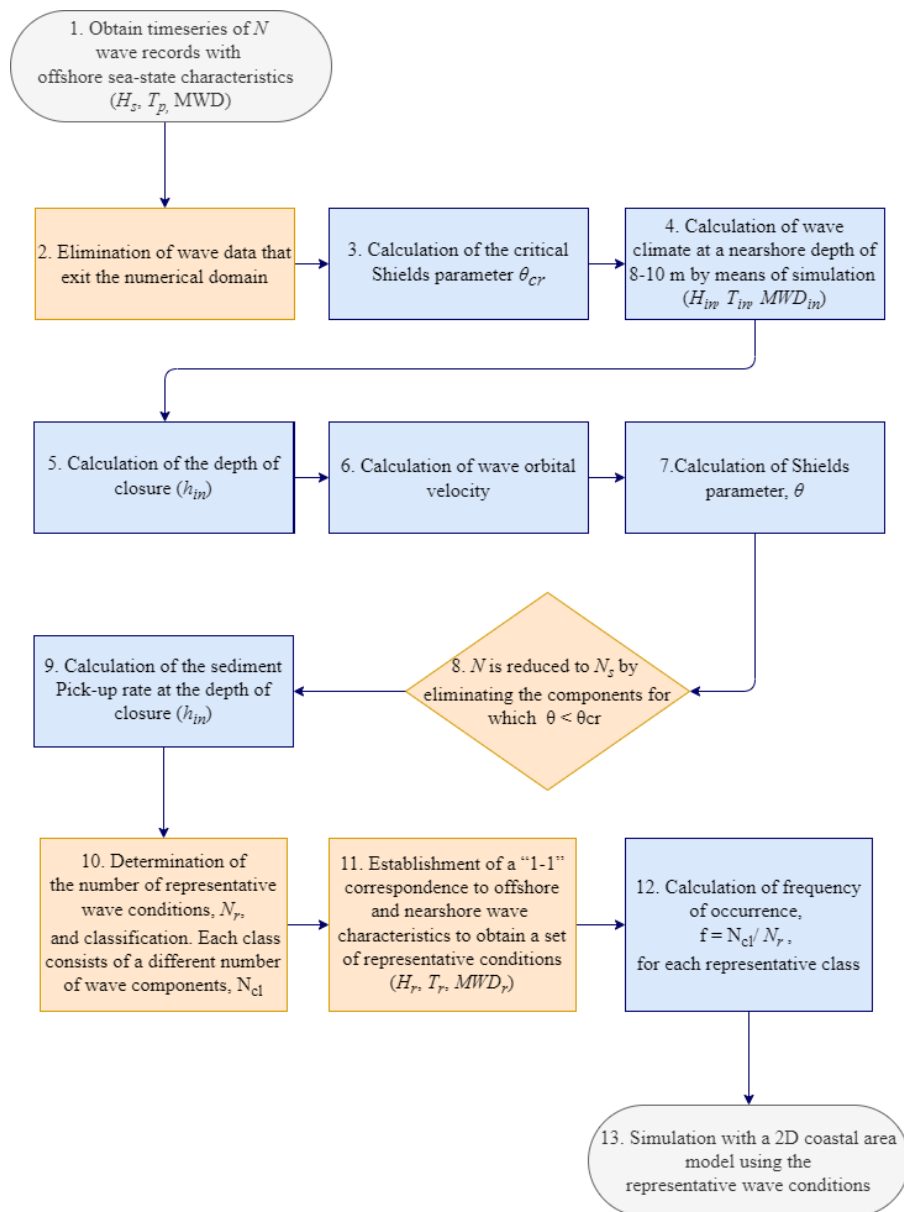
Figure 3.1. Flow chart indicating the implementation of the Pick-up rate method.

3.1.2. Threshold Current wave schematization method

The Threshold Current binning wave IR method is a slight modification to the Pick-up rate method, utilizing the calculation of longshore current velocities within the surf zone and comparing them to the value of U_{cr} as calculated through Eq. (3.2). Similarly, to the Pick-up rate method, a Parabolic Mild Slope wave model is utilized to extract wave characteristics in the nearshore in order to perform the necessary calculations. The steps undertaken to implement the Threshold Current method are the following:

1. Timeseries of offshore sea-state wave characteristics (H_s, T_p, MWD) are obtained for a desirable time range T_{wc}.

2. The timeseries are then filtered by disposing records that do not contribute in shaping the bed evolution, i.e. sea-states exiting the computational domain.

3. For each sea state, a simulation with a modified version of a Spectral Parabolic Mild Slope wave model (PMS-SP) is executed.

4. A profile cross-section considered representative of the beach geomorphology is specified. This cross-section corresponds to a particular row/column of PMS-SP model computational domain.

5. At the specified cross-section the point where initiation of breaking occurs is identified shoreward the surf-zone

6. For each wave record calculation of the maximum value of the longshore current speed U encountered in the surf-zone through Eq. (3.11) follows at the pre-determined cross section.

7. At the specific cell where the maximum value of the longshore current speed is encountered the critical value of the current speed U_{cr} is calculated

8. If $U < U_{cr}$ the wave record is eliminated since it does not contribute in setting sediments into motion. The total number of wave records offshore N is thus reduced using the threshold current criterion of incipient sediment motion at a total of N_s (with $N_s \leq N$)

9. Calculation of the wave Energy Flux through Eq. (3.17) for each wave record offshore is carried out along with the cumulative Energy flux $E_{fl,tot}$ for the reduced dataset.

10. The number of representative wave conditions N_r that will replace the full dataset of offshore sea-state characteristics is specified. Then, the wave records are divided in classes with respect to wave direction and wave height containing an equal portion of cumulative wave Energy Flux. Each class is comprised of a different number of wave components, N_{cl}.

11. The frequency of occurrence $f = \frac{N_{cl}}{Ns}$ for each representative class is calculated, based on the number of wave records of each class relative to the reduced dataset. Since N_s is the number of the reduced set of wave records, the frequencies of occurrence are rescaled, and the more energetic sea-states are associated with higher weights.

12. Finally, a simulation is executed with a 2D morphological area model using the representative wave conditions as forcing input. The total model run-time $T_{wc,r}$ is a fraction of the full time series, denoted as $T_{wc,r} = \frac{N_r}{N} T_{wc}$, since wave sea-states considered unable to initiate sediment movement and induce significant morphological changes are eliminated in step 8.

Since the Threshold Current wave schematization method eliminates sea-states based on longshore current gradients, it is expected to lead to elimination of sea-states with an almost perpendicular angle of wave incidence with respect to the shore normal, since those generally generate cross-shore currents, even if those sea-states are characterized by large H_s or T_p values.

3.2. Numerical modelling tools

In this section the numerical models utilized in the framework of this thesis, i.e. a parabolic mild slope wave model extended and enhanced in the framework of this thesis as well as a widely used coastal area model tasked with the 2D morphological bed evolution simulations are presented. For each model the main features, capabilities and governing equations are outlined.

3.2.1. The PMS-SP wave model
Governing Equations

An integral part of the methodologies presented in Section 3.1 is the utilization of a Parabolic Mild Slope wave model, taking advantage of its accuracy in prescribing the wave field in mildly sloping beds and its computational efficiency. In particular, the initial version of the model (Chondros et al., 2021), hereafter denoted as PMS-NL is based on the work of Kirby and Dalrymple, 1983, who derived a parabolic equation, in the form of a cubic Schrödinger differential equation, governing the complex amplitude, A , of the fundamental frequency component of a Stokes wave. Dalrymple and Kirby, 1988, improved the parabolic equation and its range of validity by developing approximations based on minimax principles in order to allow for large-angle propagation and rendering the approximation suitable for large scale applications, thus proposing the following governing equation:

$$C_g A_x + i(\overline{k} - a_0 k) C_g A + \frac{1}{2}\left(C_g\right)_x A + \frac{i}{\omega}\left(\alpha_1 - b_1 \frac{\overline{k}}{k}\right)\left(CC_g A_y\right)_y - \frac{b_1}{\omega k}\left(CC_g A_y\right)_{yx}$$

$$+ \frac{b_1}{\omega}\left(\frac{k_x}{k^2} + \frac{\left(C_g\right)_x}{2kC_g}\right)\left(CC_g A_y\right)_y + \frac{i\omega k^2}{2}D|A|^2 A + \frac{w}{2}A = 0 \tag{3.19}$$

where the parameter D is given by $D = \frac{(\cosh 4kh + 8 - 2\tanh^2 kh)}{8\sinh^4 kh}$, the complex amplitude A is related to the water surface displacement by $\eta = Ae^{-i(kx-\omega t)}$, k the local wave number related to the angular frequency of the waves, ω, and the water depth, h. The symbol $\overline{k}$ denotes a reference wave number taken as the average wave number along the y-axis, C is the phase celerity, C_g is the group celerity and w is a dissipation factor. Finally, coefficients a_0, α_1 and b_1 depend on the aperture width chosen to specify the minimax approximation. In the model, the combination of $a_0 = 0.994733$, $\alpha_1 = -0.890065$, and $b_1 = -0.451641$ produces reasonable results for a maximum angular range of 70º (Kirby, 1986) and is ultimately applied in the PMS-NL wave model.

The governing equation, Eq. 3.19, is solved in finite difference form and approximated according to a Crank-Nicholson implicit scheme for parabolic differential equations. The resulting tridiagonal system of equations is solved utilizing the Thomas algorithm. The solution of the governing equation is carried out in two steps. During the first step Eq. 1 is solved excluding the dissipation term (assuming factor $w = 0$) and thereafter in the next step the dissipation term is included.

Chondros et al., 2021, incorporated non-linear dispersion characteristics, in order to improve model results in the nearshore, by introducing an approximate non-linear

amplitude dispersion relationship, designated to mimic the effect of amplitude dispersion in shallow water. Several approximate non-linear dispersion relationships have been proposed (Hedges, 1987; Kirby and Dalrymple, 1986; Zhao and Anastasiou, 1993). During this thesis, the formulation of Kirby & Dalrymple, 1986 was utilized since it produces consistent results and provides a smooth transition and prediction of wave characteristics over the entire range of water depths. The non-linear dispersion relationship adopted in the PMS-NL wave model reads:

$$\omega^2 = gk(1 + f_1(kh)\varepsilon^2 D)tanh(kh + f_2(kh)\varepsilon) \tag{3.20}$$

where $f_1(kh) = tanh^5(kh)$, $f_2(kh) = [kh/\sinh kh]^4$, $\varepsilon = k|A|$.

Incorporation of non-linear dispersion characteristics is of paramount importance for the accurate prediction of wave characteristics in the nearshore and especially the point where initiation of breaking occurs which is integral for the implementation of the Threshold Current wave schematization method.

Enhancements and developments

In the scope of this dissertation, the PMS-SP model has been extended to account for generation and propagation of irregular uni-directional waves to further improve model results and enhance the accuracy of the solutions. Irregular wave generation in the wave model is treated by performing separate simulations of several regular wave components and ultimately performing linear superposition to obtain the spectral wave characteristics. The spectral energy density $S(f)$ of the wave spectrum can be interpreted by using either a Jonswap, TMA, or Pierson-Moskowitz source function. The source function for the widely used Jonswap spectrum reads:

$$S(f) = aH_{mo}^2 f_p^4 f^{-5}\exp\left[-1.25\left(\frac{f_p}{f}\right)\right]\gamma^{\exp\left[-0.5\left(\frac{\frac{f}{f_p}-1}{\sigma}\right)^2\right]} \tag{3.21}$$

where H_{mo} is the spectral wave height, f_p is the peak frequency of the wave spectrum, f is the frequency of each individual wave component, γ is a peak factor with values ranging typically from 1-7, σ is a dimensionless parameter adopting the value 0.07 if $f \leq f_p$ or 0.09 if $f > f_p$ and $a = \frac{0.0624}{0.23++0.0366\gamma-\frac{0.185}{1.9+\gamma}}$ is a scaling factor.

The wave energy spectrum is decomposed into a predefined number of discrete frequency bins at equal wave energy intervals. Then the central frequency of each bin is selected, while the wave height is the same since each bin is characterized by an equal amount of incident wave energy. Then as previously stated, a regular wave computation for each discrete wave component is carried out and through linear superposition the irregular wave characteristics are obtained. The methodology of dividing the incident wave spectrum into equal energy bands has been incorporated in other wave propagation models solving the mild slope wave equation such as ARTEMIS (EDF-R&D, 2009) or MIKE21-PMS (DHI, 2017).

Of particular importance is the estimation of wave energy dissipation due to bathymetric breaking in the wave model since apart from significantly altering wave

characteristics, the excess radiation stress gradients inside the surf-zone in the longshore direction generate longshore currents. Due to the inherent connection between wave breaking and the radiation stresses the accurate prediction of wave energy dissipation of mild sloping beds is mandatory especially in the scope of the Threshold Current wave IR method.

In the initial version of the PMS-NL model wave energy dissipation due to bathymetric breaking w_b is calculated through the bore model of Battjes and Janssen, 1979.

$$w_b = \frac{\frac{1}{4}\frac{Q_b}{T_m}H_{max}^2}{\frac{1}{8}H_{rms}^2} \tag{3.22}$$

where H_{rms} is the root mean square wave height, Q_b is the ratio of breaking waves, T_m is the mean period of the wave energy spectrum and H_{max} is the maximum wave height calculated through the criterion of Miche, 1951, as follows:

$$H_{max} = \gamma_1 k^{-1}\tanh\left(\gamma_2 kh/\gamma_1\right) \tag{3.23}$$

where γ_1 and γ_2 are parameters equal to 1.0 and 0.8 by default.

In the enhanced version PMS-SP of the wave model, an alternative formulation to calculate wave energy dissipation due to wave breaking proposed by Janssen and Battjes, 2007, which reads:

$$w_b = \frac{\frac{3\sqrt{\pi}B}{16}\frac{\bar{f}\rho g H_{rms}^3}{h}\left[1+\frac{4}{3\sqrt{\pi}}\left(R^3+\frac{3}{2}R\right)\exp(-R^2)-\mathrm{erf}\,(R)\right]}{\frac{1}{8}H_{rms}^2} \tag{3.22}$$

where B is a calibration coefficient, $R = H_{max}/H_{rms}$ and h is the still water depth.

The model of Janssen and Battjes, 2007 is based on the work of Baldock et al., 1998, improving the latter criterion's behaviour at the coastline by achieving the elimination of singularities after the point of saturation.

The code has also been parallelized using OPEN-MP and auto-parallelization directives (valid for Intel and IFX fortran compilers) to further reduce the levels of computational resources required by the model simulations.

Model Validation

To validate the performance of the PMS-SP model in simulating the transformation of waves from deep water to the nearshore, two experimental validation cases will be presented. Both cases focus mostly on the new developments of the model carried out in the framework of this thesis, with special attention given to the combined effect of refraction diffraction and the bathymetric breaking of irregular unidirectional waves.

The first validation case concerns the propagation and transformation of irregular uni-directional waves over a submerged elliptical shoal. Vincent and Briggs, 1989, conducted experiments in the U.S. Army Coastal Engineering Research Center's 29 m long by 35 m wide directional wave basin located in Vicksburg, MS, USA. The shoal was characterized by a major radius of 3.96 m, a minor radius of 3.05 m with a minimum water depth of approximately 0.15 m at the top, while the depth at the region outside the

shoal was kept constant at 0.457 m. Several tests were performed, including the generation of unidirectional and multidirectional irregular waves utilizing a TMA spectrum source function. The temporal evolution of the surface elevation was measured using an array of nine parallel-wire resistance-type sensors. The layout of the bathymetry inserted in the numerical model along with the control sections where wave characteristics were measured is depicted in Figure 3.2. This experiment is crucial in assessing the model's performance to simulate the transformation of irregular uni-directional waves in cases where the combined refraction-diffraction dominates the wave field.

A regular grid was constructed with an equal grid spacing of dx=dy=0.05 m in each direction. Hence the grid was constituted by a total of 660 cells in the y and 500 cells in the x-direction respectively.
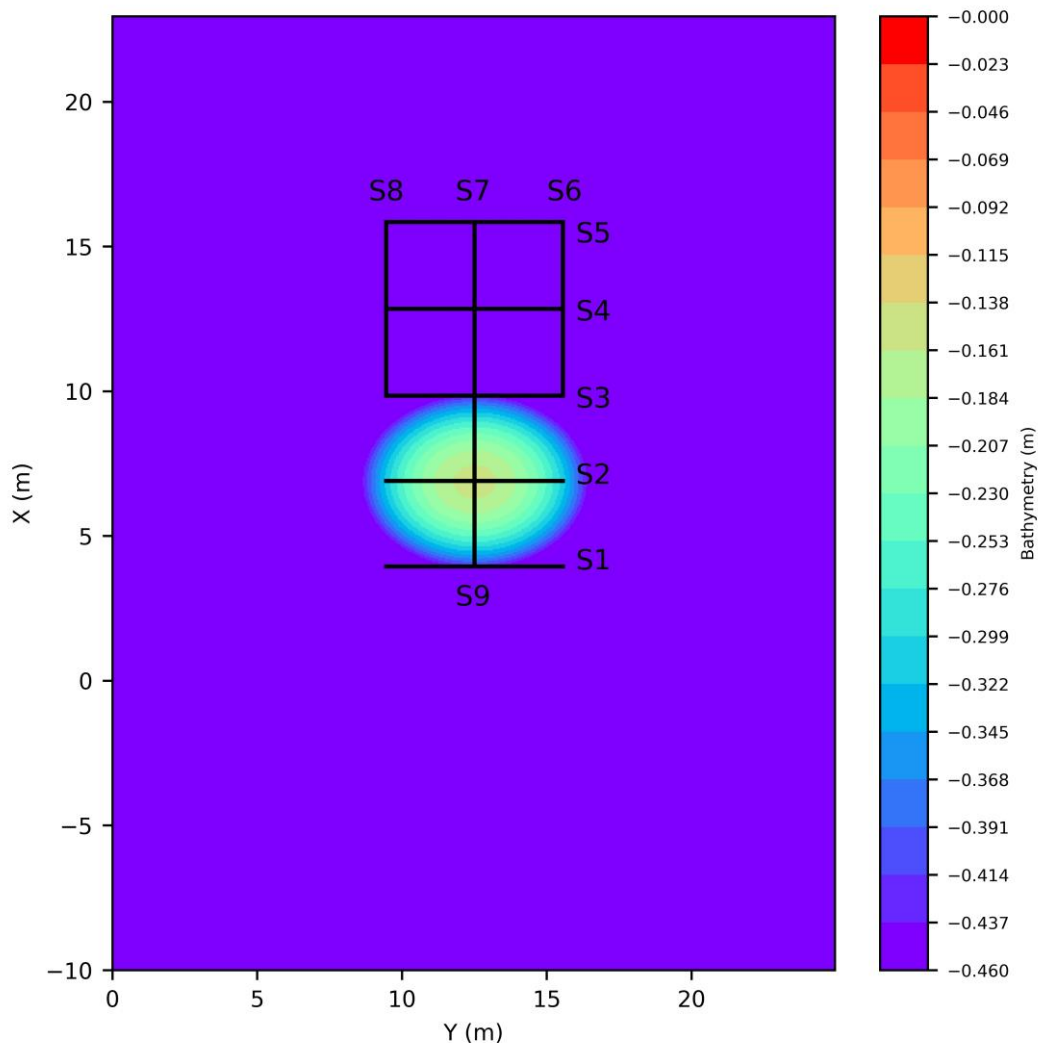
Figure 3.2. Bathymetry of the Vincent and Briggs, 1989 experiments and control sections where wave characteristics were measured.

Two uni-directional wave propagation cases were simulated with the PMS-SP wave model, case U3, corresponding to a broad frequency spectrum and case U4, corresponding to a narrow-banded frequency spectrum. The incident wave conditions of the simulated cases are shown in Table 3.1.

Table 3.1
Incident wave conditions of the Vincent and Briggs, 1989 experiments simulated with the PMS-SP

Case	H_o (cm)	T_p (s)	a	γ
U3	2.54	1.30	0.00155	2
U4	2.54	1.30	0.00047	20

The significant wave height results stemming from the simulations with the PMS-SP model extracted along control section S4 are divided by the incident wave height H_o in order to obtain normalized wave height results. The particular transect is located in the lee of the mound where the combined effect of refraction and diffraction significantly affects the wave field. Model results are plotted and compared to the experimental measurements in Figure 3.3.
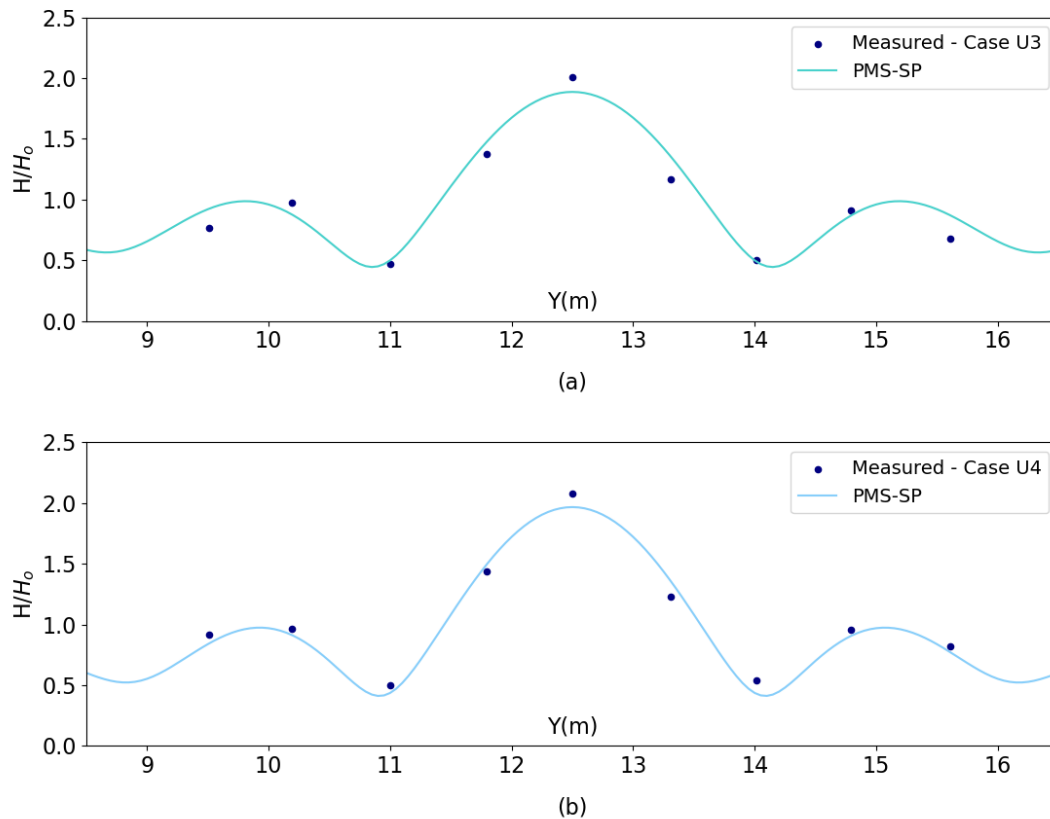
Figure 3.3. Simulated (solid line) and measured (points) normalized wave heights results for (a) case U3 and (b) case U4 of the Vincent and Briggs, 1989 experiments.

From Figure 3.3 it can be deduced that PMS-SP can very satisfactorily capture the focusing of the wave energy due to the combined effect of refraction-diffraction for uni-directional waves with a broad and narrow banded frequency spectrum respectively. The exemplary performance of the model is attributed in the inclusion of the non-linear dispersion relationship which significantly improve results for the cases where bottom irregularities are present compared to models incorporating linear dispersion characteristics. Ultimately the PMS-SP model is deemed capable of simulating wave

transformation due to the combined refraction-diffraction which dominates the shaping of the wave field in most real-field cases.

   The next validation case concerns an experiment on wave transformation and breaking on a plane sloping beach of an impermeable slope of 1:20 conducted by Mase and Kirby, 1992. In the experimental layout, shown in Figure 3.4, waves propagate for 10 m on a bed with constant water depth of 0.47 m, before propagating up a sloped beach starting at x = 0 m. The free surface was measured by 12 probes located at 0, 2.4, 3.4, 4.4, 5.4, 5.9, 6.4, 6.9, 7.4, 7.9, 8.4, 8.9 m respectively. Waves were generated through a Pierson-Moskowitz source function Two irregular unidirectional wave breaking cases entitled A & B respectively were tested with a peak frequency of f_p=0.6 Hz and f_p=1.0 Hz respectively.
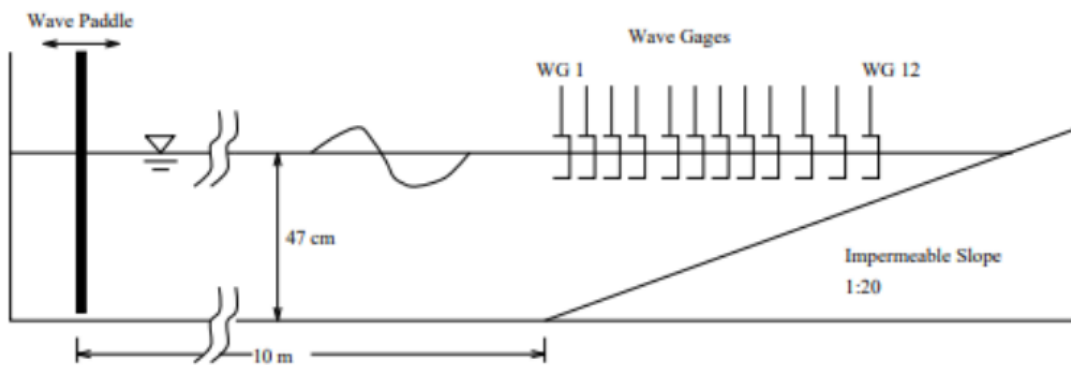
Figure 3.4. Bathymetry of the Mase and Kirby, 1992 experiments and wave gages where wave characteristics were measured

The bathymetry was discretized with an equal spatial step in both directions dx=dy=0.1 m and the spectrum divided in 50 discrete frequencies ranging from 0.2-2.0 Hz. The incident wave conditions as well as the breaking dissipation parameters are shown in Table 3.2.

Table 3.2
Incident wave conditions of the Mase and Kirby, 1992 experiments simulated with the PMS-SP

Case	H_s (m)	T_p (s)	a	γ_1	γ_2
A	0.068	1.67	1.0	1.0	0.70
B	0.06	1.00	1.0	1.0	0.70

The obtained results of significant wave height obtained by the PMS-SP simulations are compared to the measurements at the 12 placed wave gauges at the Mase and Kirby, 1992, experiment and are showcased in Figure 3.5.
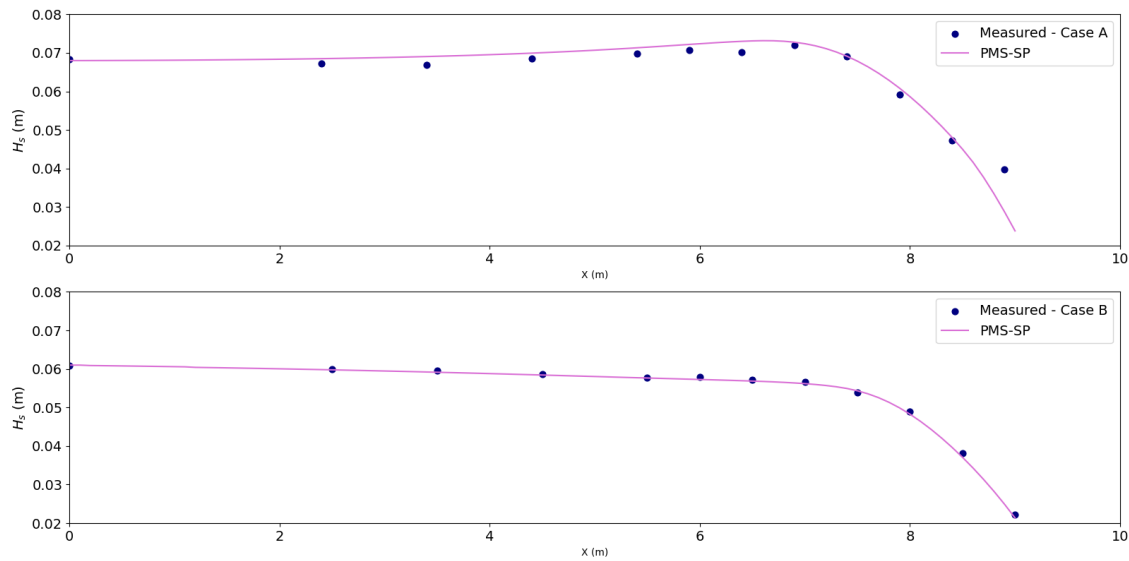
Figure 3.5. Simulated (solid line) and measured (points) significant wave heights results for case A and case B of the Mase and Kirby, 1992 experiments.

Overall, results are in excellent agreement with the experimental measurements and the model is capable of simulating wave shoaling and the subsequent decay of the waves due to bathymetric breaking. A discrepancy between measurements and model results at the last gauge for Case A is due to the presence of wave setup which is not incorporated in the model. Ultimately, the model is deemed capable of simulating irregular wave breaking in plane sloping beds and capturing the wave energy dissipation intensity. This is a particularly important feature of the model since the accurate prediction of the width of the surf zone is an integral part of the methodologies presented in this Chapter.

3.2.2. The MIKE-21 CM FM suite

The coastal area model utilized for the morphological bed evolution simulations deducted in this Chapter and throughout the thesis is the MIKE21 CM FM suite developed by DHI (DHI, 2014). The model has been used extensively in a variety of coastal engineering applications, with and without the presence of coastal protection structures (Afentoulis et al., 2017; Gad et al., 2018; Papadimitriou et al., 2020).

The MIKE21 Coupled model FM suite includes several complementary numerical models and tools three of which were used for the purpose of this research:

- MIKE21 SW, a 3rd generation spectral wave model based on the conservation of the wave action balance, suited for the propagation and transformation of waves in the coastal zone.
- MIKE21 HD, a depth-averaged hydrodynamic model based on the Reynolds averaged Navier-Stokes equations of motion (RANS), for the description of the nearshore current field.

- MIKE21 ST, a sand transport and morphology updating model, used to calculate sediment transport rates and the morphological bed evolution.

The models are directly coupled, allowing for the interaction between waves and currents and the effect of bed level changes in waves and hydrodynamics. The calculations are performed in an unstructured finite element mesh, allowing for flexibility in calculations and a more precise representation of the coastline and complex topography features.

MIKE 21 SW model is a 3rd generation spectral wave model suited for the propagation of waves in the oceanic scale and in nearshore areas. The governing equation of the model is based on the principle of conservation of the wave action-balance which reads in Cartesian coordinates:

$$\frac{\partial N}{\partial t} + c_x \frac{\partial N}{\partial x} + c_y \frac{\partial N}{\partial y} + c_\sigma \frac{\partial N}{\partial \sigma} + \sigma_\theta \frac{\partial N}{\partial \theta} = \frac{S}{\sigma} \tag{3.23}$$

where $N(x,y,\sigma,\theta,t)$ is the wave action density, c_x, c_y are the propagation wave celerities in the spatial domain, c_σ is the propagation celerity in the frequency domain and c_θ is the propagation celerity in the directional domain. All the transfer celerities are computed according to the linear wave theory. In the right-hand-side of Eq. (3.23) the term S denotes the source and sink terms of the wave action balance equation (e.g. generation due to wind, white-capping dissipation, non-linear wave interactions, depth-induced breaking, wave blocking due to a strong opposing current etc).

The discretization in the geographical and spectral domain is carried out using a finite volume cell-centered method. In frequency space, a logarithmic discretization is used, whereas in the directional space an equidistant division is used (DHI, 2009a). The time integration is performed based on a fractional step approach. The propagation step is at the first level solved without taking the source terms into account, utilizing an explicit Euler scheme. To loosen stability restrictions, a multi-sequence integration scheme is implemented based on the principles presented in Vilsmeier and Hänel, 1996, allowing for the use of large time steps for the wave propagation and spectrum evolution. On the second level the source term integration step is solved using an implicit Euler scheme.

The hydrodynamic and transport model MIKE21 HD is based on the solution of the depth-integrated shallow water equations, expressed by the continuity and momentum equations in the x and y directions in the Cartesian space:

$$\frac{\partial h}{\partial t} + \frac{\partial h\bar{u}}{\partial x} + \frac{\partial h\bar{v}}{\partial y} = hS \tag{3.24}$$

$$\frac{\partial h\bar{u}}{\partial t} + \frac{\partial h\bar{u}^2}{\partial x} + \frac{\partial h\overline{uv}}{\partial y} = f\bar{v}h - gh\frac{\partial \eta}{\partial x} - \frac{h}{\rho}\frac{\partial p_a}{\partial x} - \frac{gh^2}{2\rho}\frac{\partial \rho}{\partial x} + \frac{\tau_{sx}}{\rho} - \frac{\tau_{bx}}{\rho} - $$
$$\frac{1}{\rho}\left(\frac{\partial S_{xx}}{\partial x} + \frac{\partial S_{xy}}{\partial y}\right) + \frac{\partial}{\partial x}(hT_{xx}) + \frac{\partial}{\partial y}(hT_{xy}) + hu_s S \tag{3.25}$$

$$\frac{\partial h\bar{v}}{\partial t} + \frac{\partial h\overline{uv}}{\partial x} + \frac{\partial h\bar{v}^2}{\partial y} = f\bar{u}h - gh\frac{\partial \eta}{\partial y} - \frac{h}{\rho}\frac{\partial p_a}{\partial y} - \frac{gh^2}{2\rho}\frac{\partial \rho}{\partial y} + \frac{\tau_{sx}}{\rho} -$$
$$\frac{\tau_{bx}}{\rho}\frac{1}{\rho}\left(\frac{\partial S_{xy}}{\partial x} + \frac{\partial S_{yy}}{\partial y}\right) + \frac{\partial}{\partial x}\left(hT_{xy}\right) + \frac{\partial}{\partial y}\left(hT_{yy}\right) + hv_s S$$

(3.26)

where h is the total depth of the water column, $\bar{u}$ and $\bar{v}$ are the depth-averaged current velocity components in the x and y direction respectively, η is the free surface elevation, f is the Coriolis parameter, ρ is the water density, S_{xx}, S_{yy}, S_{xy}, are components of the radiation stress tensor, p_a is the atmospheric pressure, S the magnitude of point sources, with u_s, v_s [m/s] being the velocity vectors of the point discharge and T_{xx}, T_{yy}, T_{xy} denoting lateral stresses including viscous, turbulent friction and differential advection.

A first or a second order solution scheme can be applied for the solution of the above equations in the spatial domain using a finite-volume approach. The time integration is carried out by implementing either a low order explicit Euler scheme or a 4th order Runge-Kutta scheme. An approximate Riemann solver is applied to calculate the convective fluxes at the cell faces. Second-order accuracy is achieved by employing a linear gradient-reconstruction technique.

The MIKE 21 ST model calculates the sediment transport rates and the morphological bed evolution either in a pure current case, or under the combined effect of waves and currents. The model is valid for sand grains and often overestimates shingle-sized material transport rates (DHI, 2009b). For the case of sediment transport induced by the combined effect of waves and currents, the sediment transport rates are calculated by linear interpolation on an externally formed sediment transport table. The core of this utility is a quasi-three-dimensional sediment transport model (STPQ3D). The model ultimately calculates the instantaneous and time-averaged hydrodynamics and sediment transport in the two horizontal directions. The bed level updating is carried out by implementing an explicit first order Lax-Wendroff scheme.

3.3. Methodology implementation

3.3.1. Study area and model setup

The developed methodologies presented in Section 3.1, were implemented in the coastal area near the port of Rethymno in Crete, Greece. The area of interest, shown in Figure 3.6, includes the aforementioned port, located in the northern end of Crete within the homonymous bay and the adjacent coastal area eastward, with a coastline of approximately 4 km in length. Being a highly urbanized area, commercial, administrative, cultural and tourist activities are concentrated along the coastal zone where the city is located. The coastline of interest consists mainly of fine sand sediment, and due to the sediment transport and hydrodynamic patterns, sediment is periodically accumulated in the entrance of the port hindering navigational procedures.
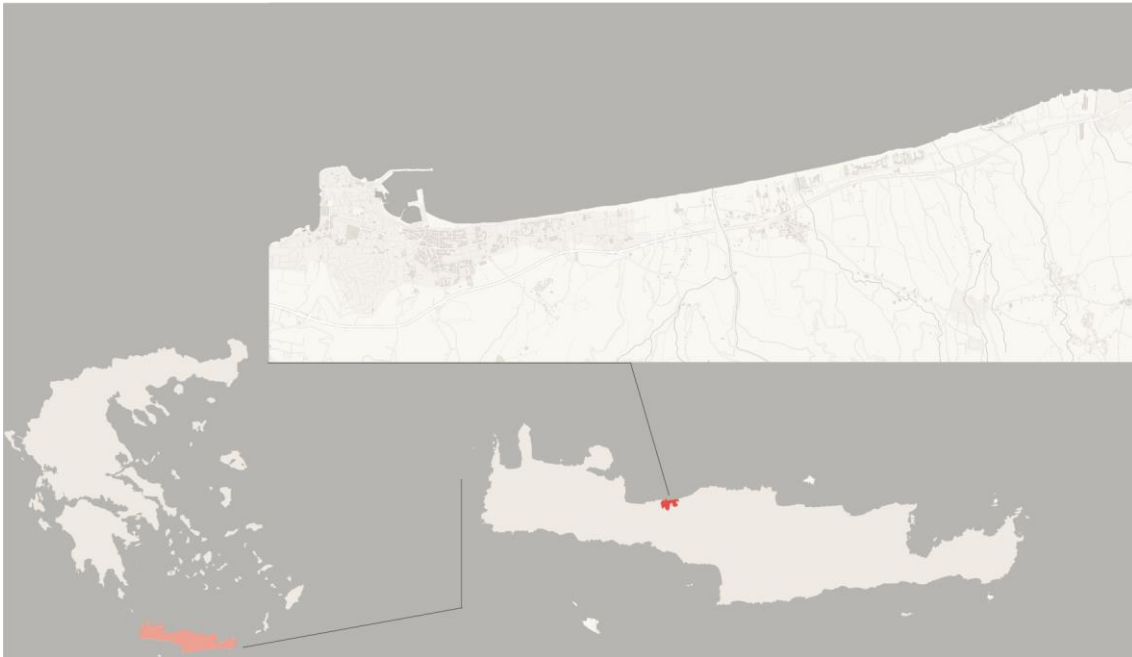
Figure 3.6. The island of Crete (bottom left), the municipality of Rethymno (bottom right) and the study area showing the port and the adjacent coastline.

An unstructured triangular finite element mesh was constructed for the purpose of performing the morphological bed evolution simulations with the MIKE21 CM FM coastal area model. Waves enter the computational domain through the north, east and west offshore boundaries. Three density levels were used for the discretization of the domain, with the finer area being near the offshore wave boundaries, and the denser one covering an extend of 3.5 km long and 10.0 km wide. A third density level was established extending at about 250 m offshore the eastern coastline of interest. For the solid boundaries, a vertice-adaptive mesh generation scheme allowed the construction of relatively small finite elements in this area, allowing for the more detailed description of the bathymetric variations in shallow waters. Regarding the dimensions of the interior triangular elements, they are comprised of a mean nominal length of about 100 m, with the largest element size being 293 m and the minimum 0.71 m. Bathymetric data in the port basin were obtained from topographical surveys conducted during the EU funded research project Preparing for Extreme And Rare events in coastal regions (PEARL) and were further populated offshore by data available in the NAVIONICS database (https://webapp.navionics.com/). After interpolating the bathymetric data, the maximum depth of the numerical domain reaches up to 180 m.

To force the 3rd generation spectral wave model MIKE21 SW and perform the wave schematization, time series of offshore sea-state characteristics, namely spectral wave height H_{mo}, peak wave period T_p and mean wave direction MWD were obtained from the Copernicus Marine Service (https://marine.copernicus.eu/) database for a time range covering 01/1993 - 01/2020. For the particular case, the regional package MEDSEA_MULTIYEAR_WAV_006_012 (Korres et al., 2019), a multi-year wave hindcast product composed of hourly wave parameters at 1/24° horizontal grid resolution was utilized. The corresponding modelling system is based on the widely used 3rd

generation spectral wave model WAM 4.6.2 and consists of a nested sequence of two computational grids (coarse and fine) to ensure that swell propagating from the North Atlantic towards the strait of Gibraltar is correctly entering the Mediterranean Sea. The offshore sea-state characteristics were extracted at a point coinciding with the center of the north offshore boundary of the computational mesh, and specifically at coordinates with a longitude of 24.5043° and a latitude of 35.4038°. A full year of wave records, selected arbitrarily to be the year 2012, was extracted for the execution of the numerical simulations. In Table 3.3, the mean values of the offshore sea-state characteristics for the year 2012 are compared to those from the period of 1993-2020 indicating that the year 2012 is valid representation of the annual wave climate at the study area.

Table 3.3
Mean values comparison for the offshore sea-state wave characteristics between the year 2012 and the period of 1993-2020

Time span	$\bar{H}_{mo}$ (m)	$\bar{T}_p$ (s)	$\overline{MWD}$
2012	1.05	5.75	335.19
1993-2020	0.98	5.60	334.39

The mean annual wave climate at the study area for the year 2012 is showcased as a rose plot in Figure 3.7. As can be seen from the wave rose and the orientation of the coastline, wave records propagating from the west, southwest, south, southeast and east sectors (with $90° < MWD < 270°$) do not contribute to the morphological bed evolution and were eliminated. Consequently, the 8761 hourly changing wave records were reduced to a total of 8219 by records.
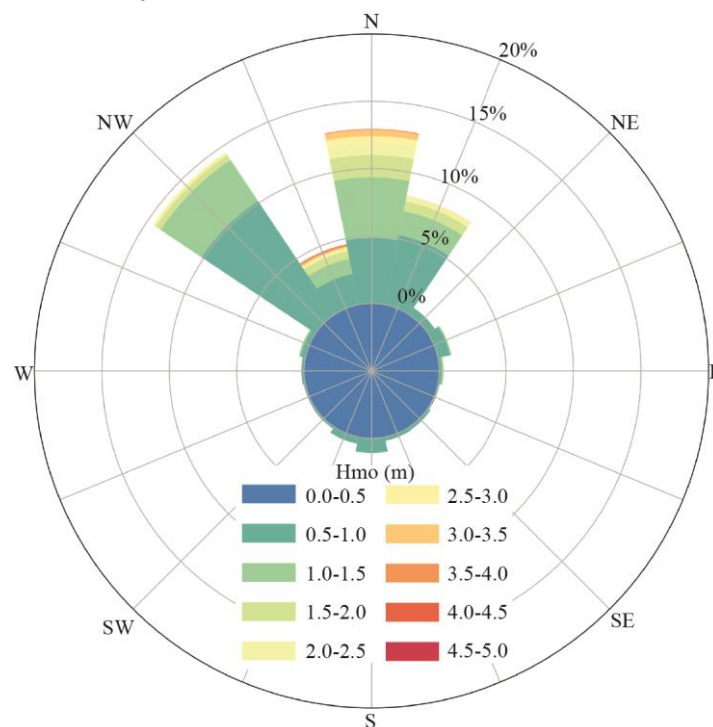
Figure 3.7. Wave rose for the year 2012 from the Copernicus database offshore the port of Retmymno.

The simulations of the MIKE21 CM FM model were conducted through the "Morphodynamic" approach allowing for the direct feedback between waves, hydrodynamics and sediment transport/morphology updating. Hence a morphological scale factor (Morfac) of 50 was utilized to keep the computational model run-time at reasonable levels. Additionally, a constant mean sediment diameter of 0.15 mm was considered throughout the numerical domain for the morphological modelling simulations.

Model performance evaluation will be carried out in an area of interest extending up to a close of 450 m offshore the eastern coastline adjacent to the port and reaching a maximum depth of about 9 m. It should be noted, that for the particular dataset the depth of closure calculated through Eq. (3.18) is about 5.5 m signifying that the largest portion of the sediment transport occurs shoreward of this depth. This area (enclosed by the polygon shown in Figure 3.8 was the main focus of the evaluations, since it consists mostly of a sandy uniform bed and is of high interest to the public due to the concatenation of tourist and economical activities at this location. The coastline of interest is relatively straight with an orientation of West to East, implying the beach is under direct wave attack (angle of incidence $\alpha_o \approx 0°$) from waves approaching from the north sector.
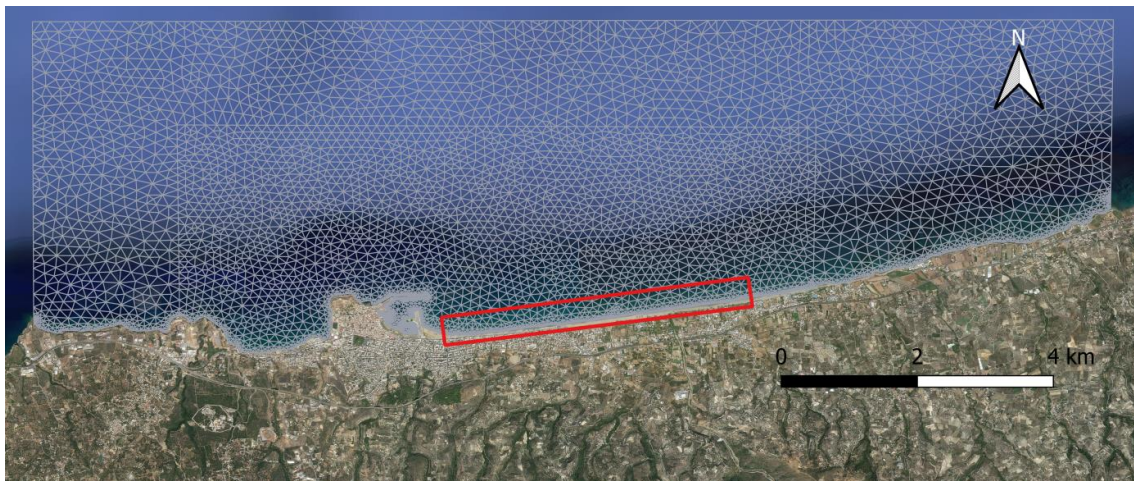
Figure 3.8. Finite element mesh showcasing the area (within the closed polygon) where the morphological model results will be evaluated

In the absence of bed level elevation measurements, the results of the simulations utilizing the Pickup Rate and the Threshold Current wave schematization method will respectively be compared to a Brute force simulation acting as a benchmark and containing the full set of 8219 hourly changing wave records. The obtained results from both the wave IR methods developed in the framework of this research will be also compared to those stemming from the widely used Energy Flux method, which as stated in numerous studies (Benedet et al., 2016; de Queiroz et al., 2019; Walstra et al., 2013) is considered to be among the best performing IR methods. For the evaluation of model skill, the commonly used in coastal morphological modelling Brier Skill Score metric (Sutherland et al., 2004a) will be calculated for the area of interest shown in Figure 3.8. For the purpose of calculating the BSS, the Brute force simulation results will be

considered as the measurement values acting as a benchmark, while the baseline condition will be the initial bathymetry. The model predictions of each simulation carried out via the IR methods tested in this Chapter will then be used to calculate the BSS values, with a value of unity declaring perfect agreement between model results and measurements.

3.3.2. Representative wave conditions

In this subsection the representative wave conditions obtained by implementing the newly developed Pick-up rate and Threshold Current wave IR methods will be presented. As has been previously stated, the methodologies presented in section 3.1, incorporate the PMS-SP model in the simulations to estimate wave characteristics at a nearshore depth of 9 m for the Pick-up rate method and estimate longshore current velocity in the Threshold Current method respectively.

Out of the 8219 wave records implementing the Shields criterion of incipient motion led to the elimination of 4699 sea-states that are considered unable to induce significant morphological changes by implementing the Pick-up rate IR method effectively reducing the input dataset. A bivariate plot of H_s and a_o presenting the obtained representative wave conditions and their respective boundaries is showcased in Figure 3.9. It should be stated that the blue scatter data denote wave records that are considered in the calculation of the representative wave conditions whereas the light blue transparent scatter data are those eliminated from the dataset.
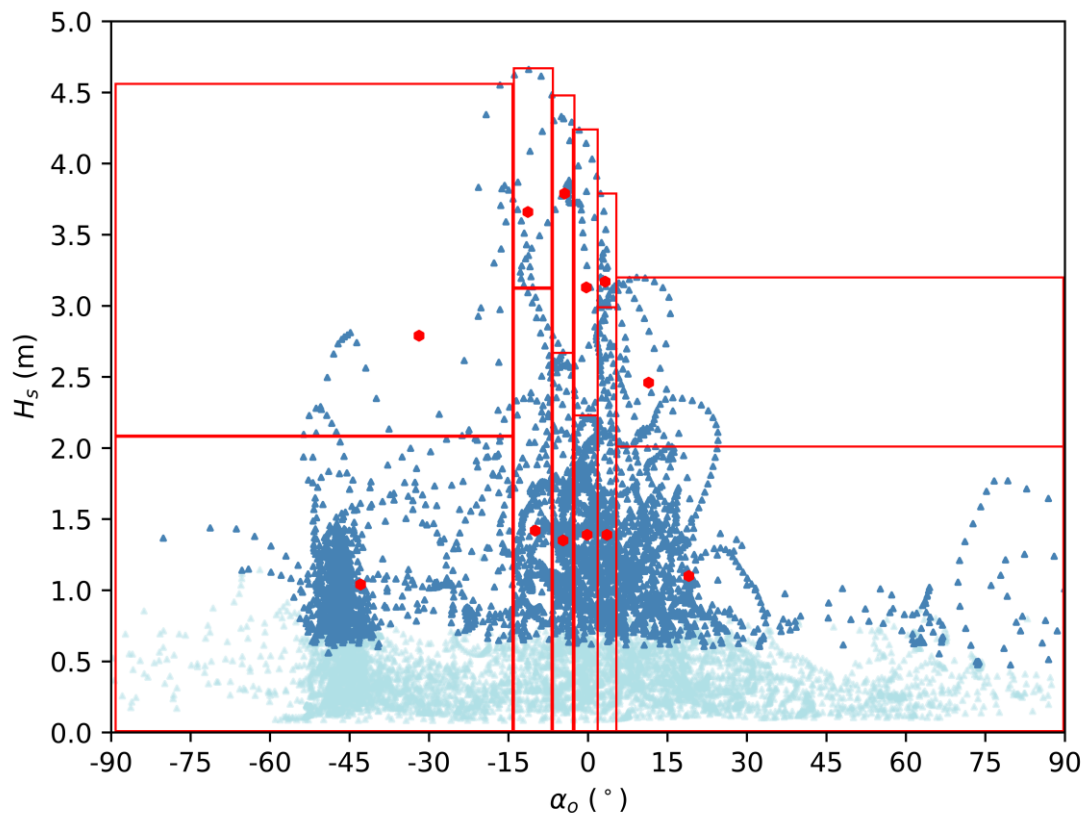
Figure 3.9. Obtained 12 representative wave conditions (red markers) by implementing the Pick-up rate wave IR method. The light blue markers denote wave records eliminated from the dataset.

Observing the obtained representative conditions and their respective bins it can be deduced that the more "energetic" sea-states are present in the north sector (at angles of wave incidence $a_o \ni [-15°, 5°]$) hence 8 bins out of the total of 12 are defined in this range. Implementing the Shields criterion of incipient motion strictly for the bed-shear stress induced by the exclusive action of waves, leads to a universal threshold for the significant wave heights under which no sediment motion takes place which is about H_s=0.52 m.

By implementing the Threshold Current wave IR method 5082 sea-states were eliminated reducing the full dataset of wave records to a total of 3137. In the same vein, Figure 3.10 shows the representative wave conditions obtained through the Threshold Current method with the light blue transparent scatter data denoting those eliminated from the dataset.
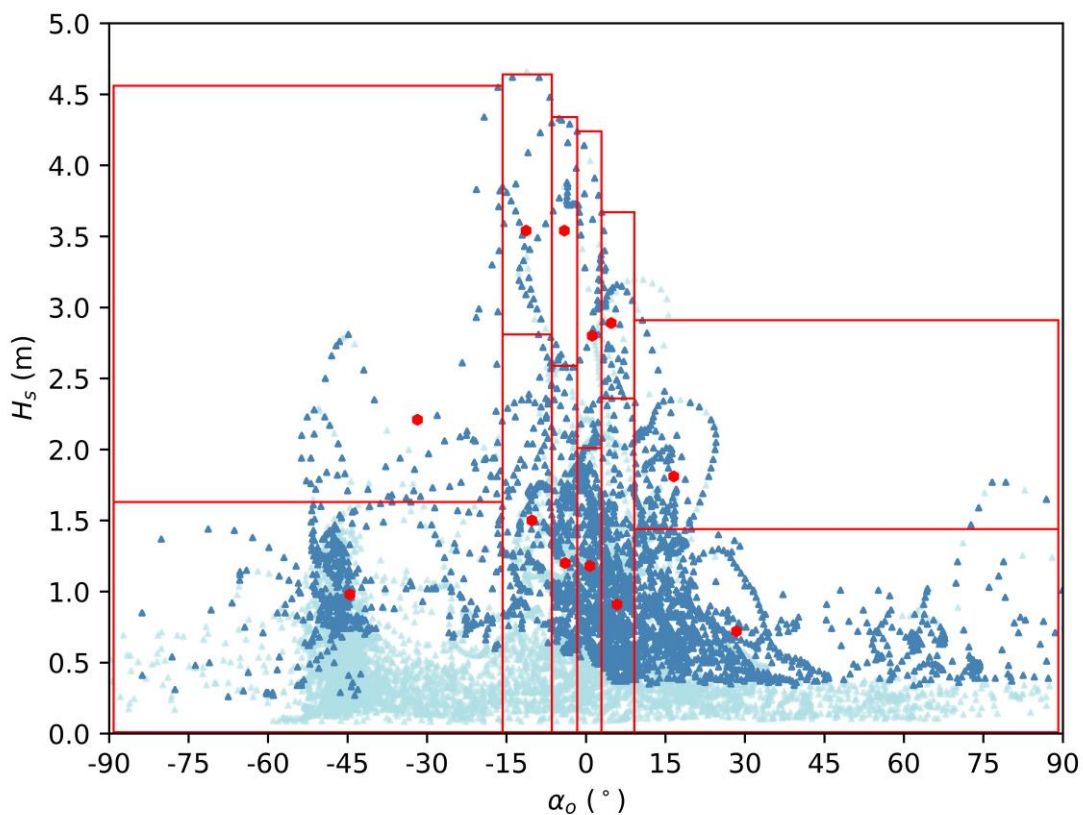
Figure 3.10. Obtained 12 representative wave conditions (red markers) by implementing the Threshold Current wave IR method. The light blue markers denote wave records eliminated from the dataset.

Similarly, to the Pick-up rate wave IR method, the more energetic representative wave conditions are concentrated in the north sector albeit the width of the respective bins is a bit wider than those formed in the Pick-up rate method (at angles of wave incidence $a_o \ni [-16°, 10°]$). It can be observed that once again for most cases, sea-states with $H_s < 0.5$ m are eliminated from the full dataset. Exceptions to this rule are wave approaching at angles of $a_o = -45°$ or $a_o = 45°$ which are coincidentally the angles where the maximum value of longshore current speed is obtained considering the case of a straight coastline and depth parallel contours. Supporting this fact, waves

approaching with an angle of incidence approaching 0° within the surf-zone produce almost null longshore current gradients hence a large number of records eliminated are present near the $a_o = 0°$ mark, even if they are associated with relatively large wave heights. In general however, the obtained bins and the respective representative wave conditions obtained by implementing both methods are nearly identical, although the quantities used as a proxy to estimate representative wave conditions (Pick-up rate vs Energy flux) as well as the applied criteria of sediment motion (bed shear stress vs Threshold Current speed) differ significantly.

To offer a comprehensive comparison of the representatives obtained by the IR methods developed during this thesis against the traditional Binning IR counterparts the representative wave conditions obtained by implementing the Energy Flux method are showcased in Figure 3.11.
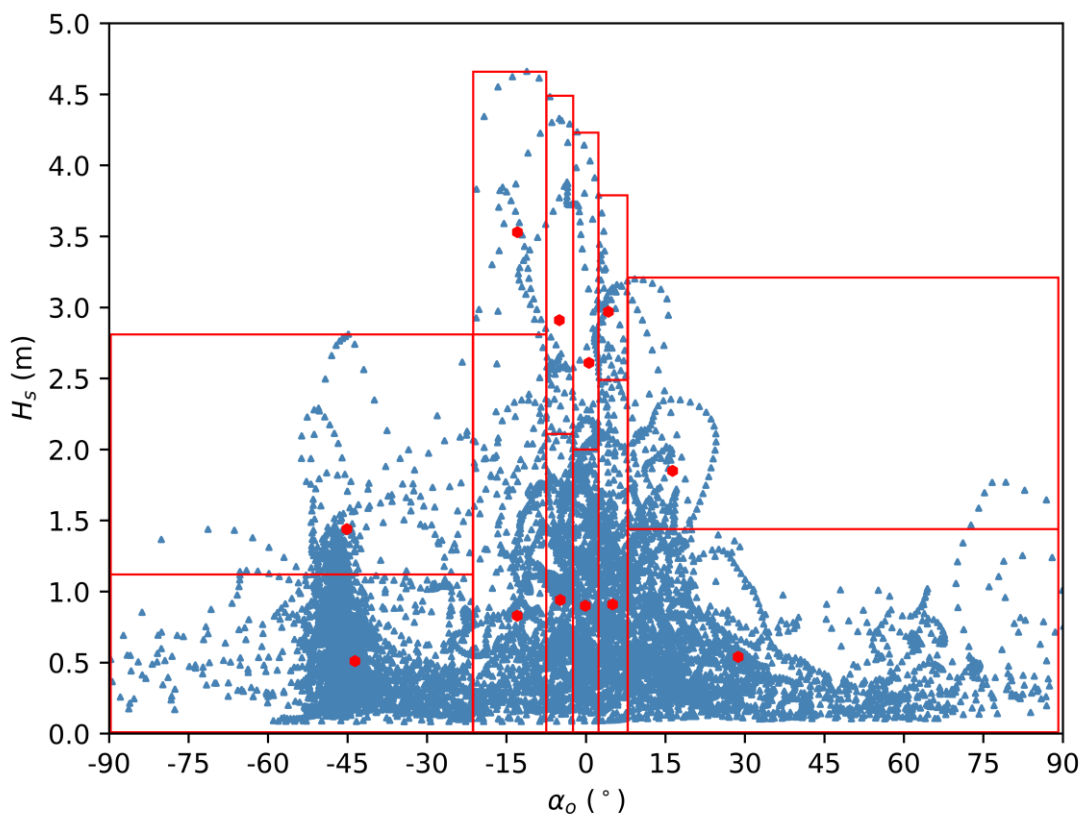
Figure 3.11. Obtained 12 representative wave conditions (red markers) by implementing the Energy Flux wave IR method.

It can be derived by observing Figure 3.9, Figure 3.10 and Figure 3.11 that the elimination of sea-states that are considered unable to induce significant morphological changes by applying the filtering procedures proposed in the Pick-up rate and Threshold Current methods significantly alters the representative wave conditions and their respective weights as expressed by the frequency of occurrence of each class. For the case in question offshore the port of Rethymno, waves with H_s <0.5 m have large frequencies of occurrence and thus shift the weights of the representative wave conditions to less "energetic" centroids as can be seen in Figure 3.9 for the Energy Flux method.

The other significant difference concerns the frequencies of occurrence f of each class and selected representative conditions. In Table 3.4 a comparison of the representative wave conditions with the corresponding frequencies of occurrence obtained by the Pick-up rate and the Energy Flux method showcases this difference for the frequencies of occurrence.

Table 3.4
Comparison of representative wave conditions and frequencies of occurrence by implementing the Pick-up rate and Energy Flux method.

Bin	Pick-up rate representatives				Energy flux representatives			
	H_s (m)	T_p (s)	a_o (°)	f (%)	H_s (m)	T_p (s)	a_o (°)	f (%)
1st	1.04	6.26	-42.93	29.29	0.51	5.05	-43.60	30.68
2nd	2.79	8.35	-31.88	1.22	1.44	6.87	-45.15	3.78
3rd	1.42	6.62	-9.98	8.64	0.83	5.20	-12.99	8.52
4th	3.66	8.88	-11.35	0.60	3.53	8.77	-12.95	0.52
5th	1.35	6.50	-4.72	10.68	0.94	5.59	-4.86	7.93
6th	3.79	8.99	-4.42	0.60	2.91	8.17	-5.02	0.78
7th	1.39	6.49	-0.19	10.94	0.90	5.43	-0.14	8.52
8th	3.13	8.41	-0.31	0.99	2.61	7.98	0.54	1.00
9th	1.39	6.37	3.57	9.03	0.91	5.39	5.00	8.22
10th	3.17	8.44	3.25	1.05	2.97	8.20	4.20	0.80
11th	1.10	5.98	19.03	24.83	0.54	4.61	28.72	26.95
12th	2.46	7.65	11.45	2.13	1.85	7.01	16.33	2.29

For the methodologies developed in the framework of this thesis, elimination of wave records from the dataset shifts the waves in more "energetic" sea-states whereas in contrast, the Energy Flux Method leads to an over-representation of lowly energetic sea-states with higher frequencies of occurrence. This particular trait of the novel Binning IR presented herein offsets the reduced duration each of the selected representative wave conditions must be simulated with the coastal area model.

3.4. Results and Discussion

In the present section the predicted bed level changes obtained by implementing the Pick-up rate, Threshold Current and Energy Flux method will be compared to the Brute Force simulation in order to comprehensively evaluate model results. The Brute force simulation containing 8219 hourly changing boundary conditions of offshore sea-state wave characteristics and with the utilization of a Morfac of 50 the total simulation time was set to about 88 hours. The morphological bed evolution obtained from the Brute force simulation is shown in Figure 3.12. Zones of accretion can be observed along the examined coastline along with some accretion at the lee breakwater of the port. Additionally, accumulation of sediment can be observed at the port entrance while a distinctive erosion zone is located southern the port entrance. Sand accumulation inside the port has been observed at the port basin of the Rethymno port requiring often dredging actions. Some erosion zones also exist at shallow depths extending from the middle of the computational mesh till the eastern boundary.
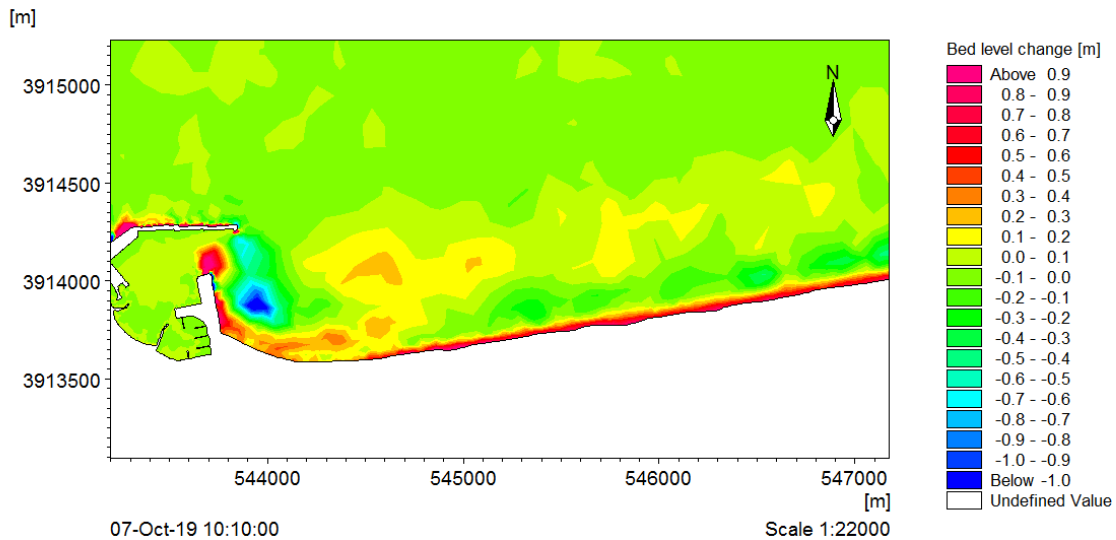
Figure 3.12. Bed level change obtained by the Brute Force simulation with MIKE21 CM FM.

For the simulations carried out with the representatives obtained from the Pick-up rate IR method, 4699 sea-states were considered unable to initiate sediment motion implementing the Shield's criterion effectively reducing the length of the dataset and the total simulation model run time by 57.2 %. In the same vein, the Threshold Current method led to the elimination of 5082 sea-states reducing the total simulation run time by 62 %. Since the Energy Flux method does not pre-emptively eliminate any wave records from the dataset it requires the model to be run prescribing the same simulation time as the Brute force simulation. The bed level change results for the area of interest obtained by implementing the three distinct IR methods are showcased in Figure 3.13.

From a visual inspection of the bed level change results obtained from the three tested binning IR methods and the Brute force simulation it can be deduced that in general the accretion/erosion patterns of the Brute force simulation are fairly captured and reproduced by the Binning IR methods. In particular, the Energy Flux method reproduces in a very satisfying manner the accumulation of sediment across the coastline of interest as well as the accretion of sand in the port entrance. The Pick-up rate and Threshold Current methods produce similar results and in general reproduce adequately the accretion and erosion patterns in the area near the port albeit they seem to systematically underpredict the magnitude of the bed level changes compared to the Brute Force simulation. This can be attributed to the reduction of the total model run-time due to the elimination of lowly energetic sea-states from the dataset, reducing the effective time the morphological bed evolution to take places, despite in turn shifting the weights to more energetic representative conditions.
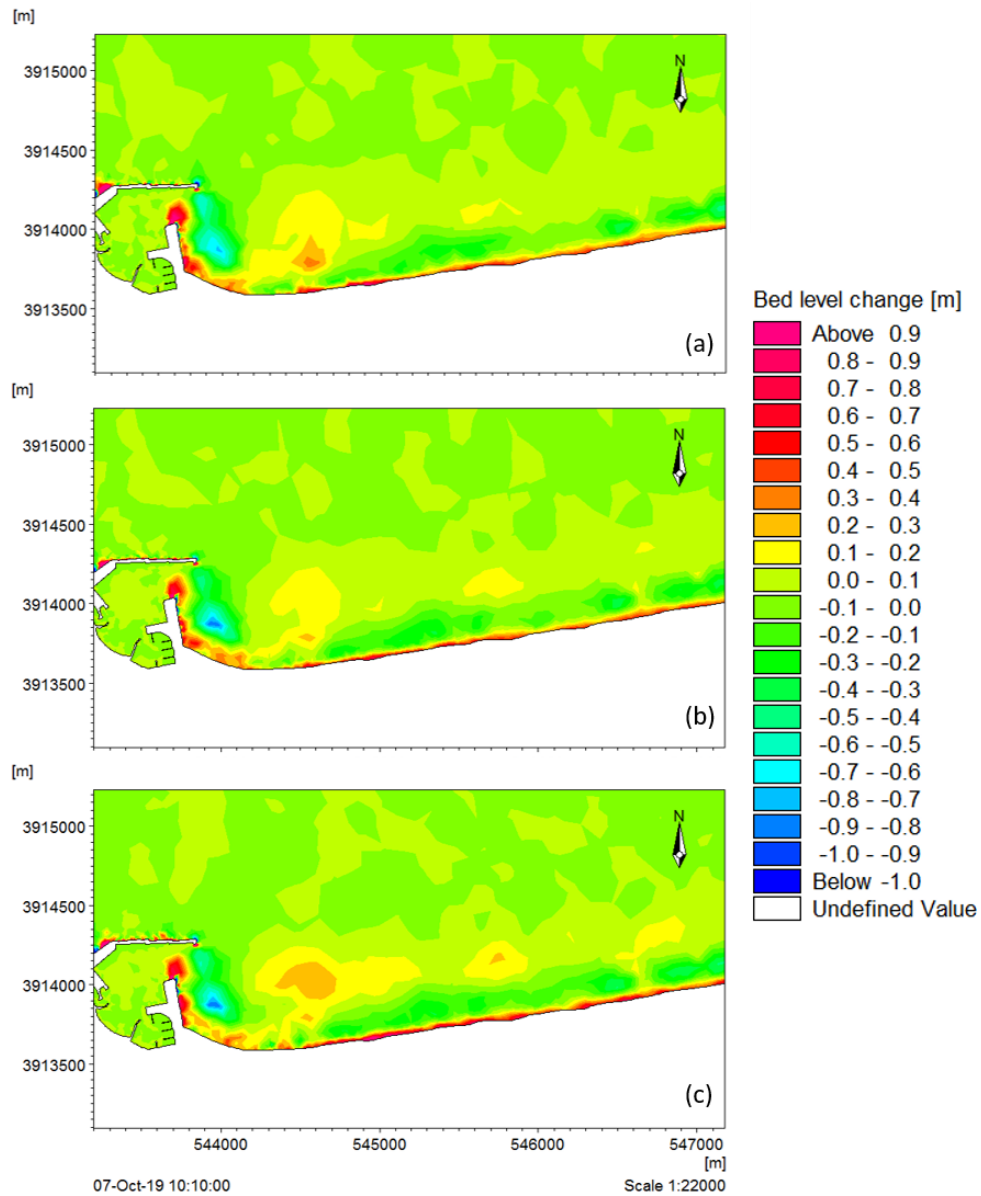
Figure 3.13. Bed level change simulation results for the (a) Pick-up rate, (b) Threshold Current, (c) Energy flux wave schematization methods.

The evaluation of the model results is ultimately assessed by computing error metrics and the BSS values for the area enclosed within the polygon shown in Figure 3.9. Bed level values were extracted from the MIKE21 CM FM simulation results for each node enclosed within this area, reaching a total of 998 nodes. The calculated Brier Skill Scores, as well as the model run time reduction compared to the Brute Force simulation are presented in Table 3.5.

117

Table 3.5
Obtained statistical parameters in the area of interest for the Pick-up rate, Threshold Current and the Energy flux method.

	Pick-up rate method	Threshold Current method	Energy flux method
BSS	0.74	0.72	0.85
Simulation time reduction (%)	57	63	13

Concerning the obtained BSS values, which is the most widely-used metric to assess the performance of morphological models (Sutherland et al., 2004a) all the simulation results are deemed as "Excellent" since the calculated values exceed 0.5. The best performing method is the Energy Flux method as was also deduced from visual inspection of the bed level change results. The Pick-up rate and Threshold Current methods are associated with similar BSS values of 0.74 and 0.72 respectively. Of paramount importance is the simulation time reduction achieved compared to the Brute Force simulation. Specifically, despite a significant reduction in computational effort the reliability and accuracy of the morphological bed evolution results is maintained with an inconsequential reduction of the BSS. Nevertheless, for simulations through the "Morphodynamic" approach both the Pick-up rate and the Threshold Current method predict very satisfactorily the annual bed level evolution while simultaneously achieving a noteworthy reduction of the model run-time.

It should be noted that model calibration for the Brute force simulation due to absence of bed level measurements in the study area is not feasible, however it is considered that the process of keeping the same model parametrization between the Brute force and the corresponding simulations with the reduced input can provide a fair evaluation of the model performance examined herein.

Chapter 4

Evaluation and enhancement of the K-Means clustering algorithm[2]

In this Chapter the validity of considering the K-Means (KM) clustering algorithm as a viable alternative to the classic Binning Input Reduction methods in thoroughly investigated. Several alternative configurations of the KM algorithm are examined, aiming to alleviate the inherent restrictions [3]associated with the unsupervised nature of the algorithm and introduce core coastal bed evolution principles in the estimation of the representative wave conditions.

In accordance with the procedure followed to evaluate the performance of the Binning IR methods presented in Chapter 3, the MIKE21 CM FM is implemented for the study area of Rethymno, Greece, performing morphological bed evolution simulations for each set of obtained representative wave conditions and comparing the results to a simulation containing the full wave climate. An integral part of the methodological approach is also the utilization of a spectral version of a Parabolic Mild Slope wave model (PMS-SP) which was also enhanced to calculate longshore sediment transport rates and energy flux at the point where initiation of depth-induced breaking takes place.

Finally, an intercomparison of the alternative tests of the KM-algorithm is undertaken to assess the optimal configuration also highlighting the advantages and disadvantages of utilizing the KM algorithm as an IR method.

4.1. Theoretical background and methodology

4.1.1. General aspects

Clustering is a branch of the unsupervised maline learning techniques, commonly used to predict patterns in unlabelled data and group them in clusters, when the expected outcome is a priori not known. A plethora of clustering algorithms exist and have been used in many scientific sectors such as biology, medicine, economy, market research and engineering. Depending on the type of input data, several categories of clustering algorithms can be distinguished:

---

[2] Parts of this Chapter have been submitted for publication in Papadimitriou & Tsoukala 2022

- Centroid-based clustering, where the data points are separated based on their squared distance from the considered centroids. The most notorious algorithm of this category is the K-Means Algorithm (MacQueen, 1967)
- Hierarchical-based clustering where cluster are organized based on a form of hierarchy following either a top-down or bottom-up approach. Agglomerative clustering algorithms are commonly offered in open-source packages of several programming languages (Python, Julia, R)
- Density-based clustering, where data are grouped with respect to areas with high concentration of data points. A widely used density-based partitioning algorithm is DBSCAN (Ester et al., 1996)

When desiring to perform input reduction on an arbitrary dataset of offshore sea-state wave characteristics the number of representative conditions is usually pre-determined by the engineer or scientist. This imposes a restriction on the clustering algorithms than can be used, prohibiting the use of hierarchical and density-based algorithms which operate without pre-defining the number of clusters. Based on this notion, centroid-based clustering is considered more alluring for the determination of representative wave conditions for morphological bed evolution simulations.

As has been mentioned in Chapter 2, several clustering algorithms belong in the centroid-based subcategory such as K-Means, K-Medians, Fuzzy C-Means and CURE among others. It was selected in the framework of this thesis to proceed with enhancing and evaluating solely the performance of the K-Means clustering algorithm for a variety of reasons the most important of which are the following:

- ✓ K-Means is a widely used clustering algorithm in coastal engineering applications (Camus et al., 2011; de Queiroz et al., 2019; Splinter et al., 2011) and is suitable for the partition of large datasets (such as hourly changing offshore sea-state wave characteristics) with low demand of computational resources.
- ✓ Each data point belongs uniquely in one cluster in contrast to other centroid-based clustering algorithms such as CURE and Fuzzy C-Means which provide a more robust definition of the frequency of occurrence of each obtained centroid.
- ✓ Robust and customizable implementations of the K-Means algorithm exist in almost all machine learning packages of the widely used programming languages. For instance, Python includes the packages of scikit-learn (Pedregosa et al., 2011) and pyclustering (Novikov, 2019).
- ✓ The principles and alternative configurations of the K-Means clustering algorithm can readily be implemented in similar centroid-based clustering algorithms, however utilizing more than one algorithm with enhanced features would render the comparison and analysis of the obtained results non-feasible within the scope of this investigation.

The KM algorithm operates firstly by specifying the desired number of clusters and then iteratively assigning each data point to the nearest cluster based on randomly selected initial centroids. The algorithm stops the iterative procedure when a user-defined number of iterations is reached, or reassignment of the data-points no longer occurs. The iterative

120

procedure followed by the KM algorithm is carried out in two steps (the Expectation and the Maximization step) hence it is called the Expectation-Maximization approach. The objective function, can be written in the following form:

$$E = \sum \sum w_{ij} \|x_i - \overline{m}_j\|^2 \tag{4.1}$$

where $w_{ij} = 1$ if data point x_i belongs to cluster j or $w_{ij} = 0$ otherwise.

In the Expectation step the objective function E in Eq. (4.1) is minimized with respect to w_{ij} treating the centroids $\overline{m}_j$ as fixed leading to:

$$w_{ij} = \begin{cases} 1, & j = argmin\|x_i - \overline{m}_j\|^2 \\ 0, & otherwise \end{cases} \tag{4.2}$$

In the Maximization step that follows the objective function E in Eq. (4.1) is minimized with respect to $\overline{m}_j$ treating the centroids w_{ij} as fixed giving:

$$\overline{m}_j = \frac{\sum w_{ij} x_i}{\sum w_{ij}} \tag{4.3}$$

Therefore, in the Expectation step each data point x_i is assigned to the closest cluster with respect to the sum of the squared distance of the cluster centroid, while the Maximization step recomputes the new cluster centroids to reflect the new assignments carried out previously in the Expectation step.

Despite the criteria to ensure convergence of the iterations the output of the clusters and consequently the centroids are greatly influenced by their initial selection the start of the algorithm execution. Random selection of the initial centroids may prove to be highly volatile since the obtained centroids may not spread out adequately. Hence the K-Means[++] centroid initialization algorithm (Arthur and Vassilvitskii, 2007) was developed aiming to overcome this shortcoming and provide more spaced-out centroids. This is carried out by specifying the first centroid in a random location and then choosing the subsequent centroids from the remaining data points based on a probability, proportional to the squared distance away from a given point's nearest existing centroid. Since its conceptualization, the K-Means[++] algorithm is almost exclusively used for the centroid initialization of the KM algorithm.

4.1.2. Alternative configurations of the K-Means algorithm

The unsupervised nature of the K-Means algorithm offers significant advantages, with the most prominent being that the user has minimal interference on the expected outcome of the obtained representative wave conditions. Conversely, it is associated with various hinderances mostly associated with the over-representation of lowly energetic sea-states (de Queiroz et al., 2019) and the fact that morphological bed evolution principles are not considered in the algorithm implementation. Hence six alternative instances of the KM algorithm (each one named KM-01 through KM-06, with the number signifying the id of each test) were realised aiming to overcome these inherent drawbacks and are presented below. All the instances of the KM algorithm were

implemented in the open source scikit-learn package (Pedregosa et al., 2011) available in the Python programming language.

1ˢᵗ test KM-01

The first examined configuration (KM-01) aims at evaluating the validity of utilizing the unsupervised K-means algorithm as a valid input reduction method for annual wave climate datasets. In the default implementation of the algorithm user interference is minimal and the obtained centroids are based solely on the iterative procedure carried out by the algorithm. The algorithm takes as input a dataset of offshore sea-state wave characteristics, consisting of significant (H_s) or spectral (H_{mo}) wave height, peak wave period (T_p) and mean wave direction (MWD) that have to be normalized in order to perform the cluster analysis, and outputs the centroids that are taken to be the representatives wave conditions and will be used as forcing input in the coastal area model. Special attention was given to prescribing a large number of iterations (1000 in this case) in order to avoid large differences in the obtained centroids due to non-convergence of the algorithm. After blindly repeating the procedure to obtain the centroids 5 times it was deduced that convergence was achieved since the obtained centroids were the same between the separate executions of the algorithm. While prescribing the number of iterations increases the computational intensity, for typical datasets of multivariate wave climates, this increase is inconsequential for practical applications (order of seconds to a few minutes). The initial centroids have been selected by utilizing the K-means⁺⁺ algorithm to ensure that the initially chosen centroids are adequately spread out.

2ⁿᵈ test KM-02

The unsupervised nature of the default implementation of the KM algorithm in KM-01 has the advantage of minimal user interference and easier inspection of the iterative procedure to select the centroids. However, when considering the nature of wave-induced hydrodynamics and sediment transport following a process-based modelling approach, this unsupervised nature of the algorithm does not ensure accurate results in bed level prediction since the algorithm considers only the Euclidean distances to assign centroids and disregards core principles of sediment transport and morphology. The next test case (hereafter denoted as KM-02) aims at counterbalancing this issue, by concerting the classic binning input reduction methods with clustering techniques. For this purpose, the widely-used Energy Flux binning method of wave schematization was implemented to obtain a set of representative wave conditions. The obtained representatives are then normalized and set as initial centroids to an instance of the KM algorithm and a new set of centroids are obtained after the iterative procedure. Effectively, the algorithm is coerced to initiate the re-assignment of clusters and centroids from initial values which are linked to the medium-term morphological bed evolution of coastal areas instead of utilizing K-Means⁺⁺.

3ʳᵈ test KM-03

In practical applications, multivariate wave climate datasets (obtained either from buoy measurements, employment of parametric models or from oceanographic databases)

are often diverse with interchangeable energetic and mildly energetic sea-states. Often, these lowly energetic sea-states are associated with large frequencies of occurrence and are present in large quantities in datasets of offshore sea-state characteristics. Cluster analysis often overestimates the contribution of these wave records in the morphological bed evolution due to the shear amount of data points concentrated at areas of low wave energy. Test KM-03 aims to enhance the contribution of the more energetic wave conditions by using the individual wave energy flux of each wave records as a weight to perform cluster analysis. After calculating the individual energy flux of each sea-state normalization follows essentially assigning the value of 1 to the wave records with the highest wave energy flux capacity. These weights are then provided as external values to the KM algorithm leading to the formation of clusters and shift of centroids to more energetic sea-states. For this case, K-Means^{++} was utilized for the cluster initialization similarly to the KM-01 test.

4th test KM-04

de Queiroz et al., 2019, swapped the input variables of the cluster analysis from H_{rms}, T_p, a_o to $H_{rms}^{2.5}$, T_p, a_o and observed a performance increase for the case of predicting sandbar migration. Essentially, the authors replaced the rms wave height values of the dataset with ones based on the premise that longshore sediment transport is the main driving factor for the medium-term morphological evolution of a coastal areas.

Consequently, an additional test case was set-up (KM-04), swapping the cluster analysis input variables from H_s, T_p, a_o to S, E_{fl}, a_o, incorporating both bulk longshore sediment transport rates and the wave energy flux which are both associated to the morphological coastal evolution. Various bulk longshore sediment transport formulations can be found in literature (Bailard, 1985; Kamphuis, 1991a; Komar and Inman, 1970; Mil-Homens et al., 2013) and most of them can be written in a general form as a function of the yx-component of the radiation stress tensor and wave celerity at breaking point. The CERC bulk longshore transport formula can be written as follows:

$$S = \frac{K}{\rho g(s-1)(1-n)} \cdot s_{yx,b} \cdot c_b \tag{4.4}$$

where K is a proportionality factor.

Assuming a straight coastline with parallel depth contours and the validity of linear wave theory, the well-known CERC formulation of bulk longshore sediment transport in deep water can be obtained from Eq. (4.4):

$$S = \frac{K}{32(s-1)(1-n)} \cdot \sin(2a_o) \cdot c_b \cdot H_s^2 \tag{4.5}$$

where a_o is the deep-water wave incidence angle with respect to the shore-normal and H_o is the deep-water wave height. Even in the expression containing deep-water wave characteristics the wave celerity at the breaker line must be calculated.

It can be deduced from both Eqs (4.4) and (4.5) that for a bed where sediment characteristics can be considered homogenous and constant, then the bulk longshore

transport rate for each sea-state ultimately depends on the product of the shear component of the radiation stress tensor and the wave celerity at breaker line.

For the particular test case, S values were calculated as the product of $s_{yx,b} \cdot c_b$ utilizing the PMS-SP model presented in Section 3.2.1 in order to obtain said values for each wave record in the dataset. The use of an accurate and detailed wave model can contribute to alleviating the inconsistencies and assumptions by implementing Eq. (4.5) for coastal areas with complex bed formations and non-straight coastlines. A cross-section, which can be considered representative of the coastal bathymetry is specified for the calculation of $s_{yx,b} \cdot c_b$ shoreward the point where initiation of breaking occurs. At this point, it should be noted that for regular waves the maximum value of $s_{yx,b} \cdot c_b$ is encountered at the breaking point whereas that is not always the case for irregular waves. Hence, when treating irregular waves, the maximum value of $s_{yx,b} \cdot c_b$ encountered within the surf-zone is utilized the calculate the value of the longshore sediment transport rate. By performing separate simulations for each wave record of the offshore sea-state timeseries a unique "1-1" correspondence is established between H_s, T_p, a_o and S, E_{fl}, a_o. Having calculated the values of S and E_{fl} for each wave record the KM algorithm is executed with input variables S, E_{fl}, a_o to obtain the clusters and the corresponding centroids. Taking advantage of the "1-1" correspondence mentioned previously the representative wave conditions $H_{s,r}$, $T_{p,r}$, $a_{o,r}$ are extrapolated and provided to the coastal area model to perform the morphological simulations.

5th test KM-05

The penultimate test case, namely KM-05, concentrates at incorporating results obtained from the binning input reduction methods while simultaneously counterbalancing the issue associated with the over-representation of low-energetic sea-states, in the wave climate (de Queiroz et al., 2019). For this purpose, the KM algorithm is coerced to initiate centroid initialization from the more "energetic" wave characteristics as obtained by the Pick-up rate wave schematization method presented in Section 3.1.1.

6th test KM-06

Lastly, a test case denoted as KM-06, comprised of a modification to test KM-04, was setup. The centerpiece of this modified test was the application of a comprehensive filtering procedure taking advantage of the employment of the PMS wave model for the propagation of individual wave characteristics and estimation of longshore transport rates and the wave energy flux at the breaking point. The distinct steps of the methodology applied in KM-06 are shown below and illustrated as a flow chart in Figure 4.1:

1. A dataset consisting of offshore sea state wave characteristics is obtained.
2. A simulation utilizing a PMS wave model is executed for each wave condition.
3. A particular section (row or column) of the computation domain considered representative of the coastline geometry and bathymetry of the study area is predefined.

4. The point where initiation of breaking occurs is located for the predefined row/column of the computational grid specified at the previous step.

5. Non-breaking waves are noted since they are considered unable to produce adequate longshore transport for sediment motion and then eliminated, effectively reducing the total amount of wave characteristics. It should be stated that non-breaking waves denote sea-states with particularly small values of significant wave height, which given the specific numerical grid resolution do not dissipate their energy due to bathymetric breaking.

6. Inside the breaker zone, and specifically shoreward the depth where wave breaking is initiated (see step 4), the maximum product of the shear radiation stress component $s_{yx,b}$ and wave celerity c_b is computed and then the longshore sediment transport S through Eq. (3) and wave energy flux E_{fl} through Eq. (2) are calculated.

7. A reduced dataset of S, E_{fl}, MWD is provided as input to the KM algorithm in order to obtain the resulting centroids.

8. The centroids obtained at step 7 are transformed to H_{mo}, T_p, MWD taking into consideration that each individual wave record belongs uniquely in each cluster.

9. The representatives calculated in the previous step are used as initial centroids for the non-reduced dataset of offshore sea-state wave characteristics (see step 1) and another instance of KM algorithm is utilized to obtain new centroids.

10. The centroids obtained at step 9, corresponding to the final representative wave conditions are obtained.

11. The wave representatives are set as input to the coastal area numerical model, to perform the morphological evolution simulation.

The particular test case aims at alleviating the inconsistency inherently present in KM-05 concerning waves approaching the coastline perpendicularly. It can be deduced that these sea-states can be associated with high energy flux values but produce little to no longshore sediment transport rates, effectively skewing the results. It should also be stated that "non-breaking waves" refer to waves with inconsequential values of H_s or T_p that do not dissipate energy due to bathymetric breaking given a typical resolution of the bathymetric grid since in nature all waves break as they approach the shoreline.
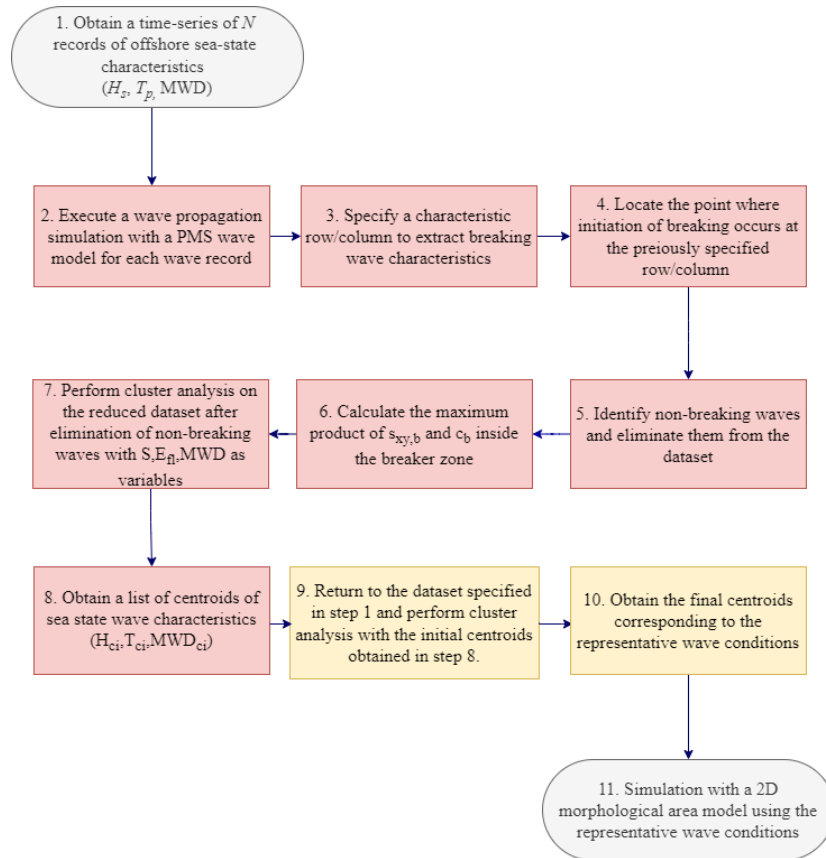
Figure 4.1. Flow chart of the methodological procedure applied in KM-06 to obtain the representative wave conditions.

Concatenated overview of the examined tests

A complete list of the examined tests carried out for the purpose of this research, signifying important aspects of the KM algorithm configuration is compiled and shown in Table 4.1. Moreover the maximum number of iterations was set at 1000 for all the tests, a number which is adequate to ensure convergence. The execution time for each instance of the algorithm ranges between 10-50 s and depends on the initial centroid selection.

Table 4.1
Overview of the examined Input Reduction cases and applied configurations for the cluster analysis.

Test	Input Variables	Cluster Initialization Method	Applied weights
KM-01	H_s, T_p, a_o	K-Means^{++}	-
KM-02	H_s, T_p, a_o	Energy Flux method centroids	-
KM-03	H_s, T_p, a_o	K-Means^{++}	Energy flux of each wave record
KM-04	S, E_{fl}, a_o	K-Means^{++}	-
KM-05	H_s, T_p, a_o	Pick-up rate method centroids	-
KM-06	S, E_{fl}, a_o H_s, T_p, a_o	K-Means^{++} Centroids from previous instance of the algorithm	-

4.2. Methodology implementation

The obtained representative wave conditions obtained from each examined test, corresponding to an alternative configuration of the KM algorithm will be used as forcing input for the MIKE21 CM FM in the study area in the vicinity of Rethymno port, as presented previously in section 3.3.1. Hence, an identical numerical mesh was utilized for the simulations with the same parametrizations in the wave, flow and sediment transport model to ensure consistency between the examined tests. For all simulation sets, as was the case with the Binning Input Reduction simulations, a number of 12 representatives was considered and kept constant throughout each corresponding simulation set.

4.2.1. Representative wave conditions

In this section an overview of the 12 representative wave conditions obtained through the cluster analysis will be given. Although clustering algorithms utilize three variables as input for the purpose of wave schematization, a 2-D scatter plot in terms of wave height and wave incidence angle for all tests is shown in Figure 4.2 for a more comprehensible representation. It should be noted that in Figure 4.2 wave incidence angles are given with respect to the shore normal, with -90˚ denoting waves generated from the west sector and 90˚ denoting waves generated from the east.

Regarding the obtained representatives for KM-01 it can be observed that due to the form of the dataset, some obtained centroids are closely located (e.g. at angles of wave incidence located near -40˚). For tests KM-02, KM-05 and KM-06, which use previously obtained representatives as initial centers, cluster centroids are distributed in a broader area, and a shift is observed to more energetic wave representatives. Special attention should be given to test KM-03, namely the one introducing weights related to the wave energy flux during the algorithm execution, which as seen in Figure 4.2, leads to a

significant shift of all the obtained centroids to more energetic representatives compared to all the other tests. Clusters in KM-04 are more clearly defined which can be attributed to the shift of clustering variables from H_{mo}, T_p, a_0 to S, E_{fl}, a_0. Finally, tests KM-05 and KM-06, in which two filtering methodologies for low-energetic sea-states were applied, lead to a similar pattern regarding the distribution of wave representatives in the wave height/wave incidence angle plane.

Although not evident directly in Figure 4.2, a major parameter influencing the final bed level change results is the frequency of occurrence of each representative sea-state, which is calculated by dividing the number of members of each cluster with the total amount of data points in the dataset. As an indicative example showcase, in Table 4.2, the representatives obtained through KM-02 and the respective ones through KM-05 are presented.

Table 4.2
Comparison of the obtained representatives from KM-02 and KM-05 cases.

Cluster	KM-02				KM-05			
	H_{mo} (m)	T_p (s)	a_0 (°)	fi (%)	H_{mo} (m)	T_p (s)	a_0 (°)	fi (%)
1st	0.58	3.88	-45.35	19.36	0.52	3.18	-43.32	11.62
2nd	0.63	6.75	-45.12	11.77	0.64	5.40	-46.73	15.06
3rd	0.38	4.92	-14.41	8.65	0.65	7.78	-43.06	5.15
4th	2.40	3.18	-0.94	1.70	2.32	3.37	-1.94	2.08
5th	0.39	3.52	5.36	11.23	0.41	3.61	6.73	11.86
6th	3.46	6.83	-2.48	1.39	3.20	6.75	-5.38	1.98
7th	0.41	5.83	23.80	11.50	0.42	5.86	23.88	11.33
8th	0.91	4.34	2.36	9.83	1.02	4.36	1.29	9.78
9th	2.11	6.60	-4.34	3.21	0.40	4.84	-12.93	9.27
10th	1.57	5.17	-3.46	7.12	1.74	5.79	-2.62	7.73
11th	0.43	5.92	62.88	5.57	0.43	5.92	62.88	5.57
12th	1.07	6.87	6.47	8.68	1.07	6.84	6.65	8.57
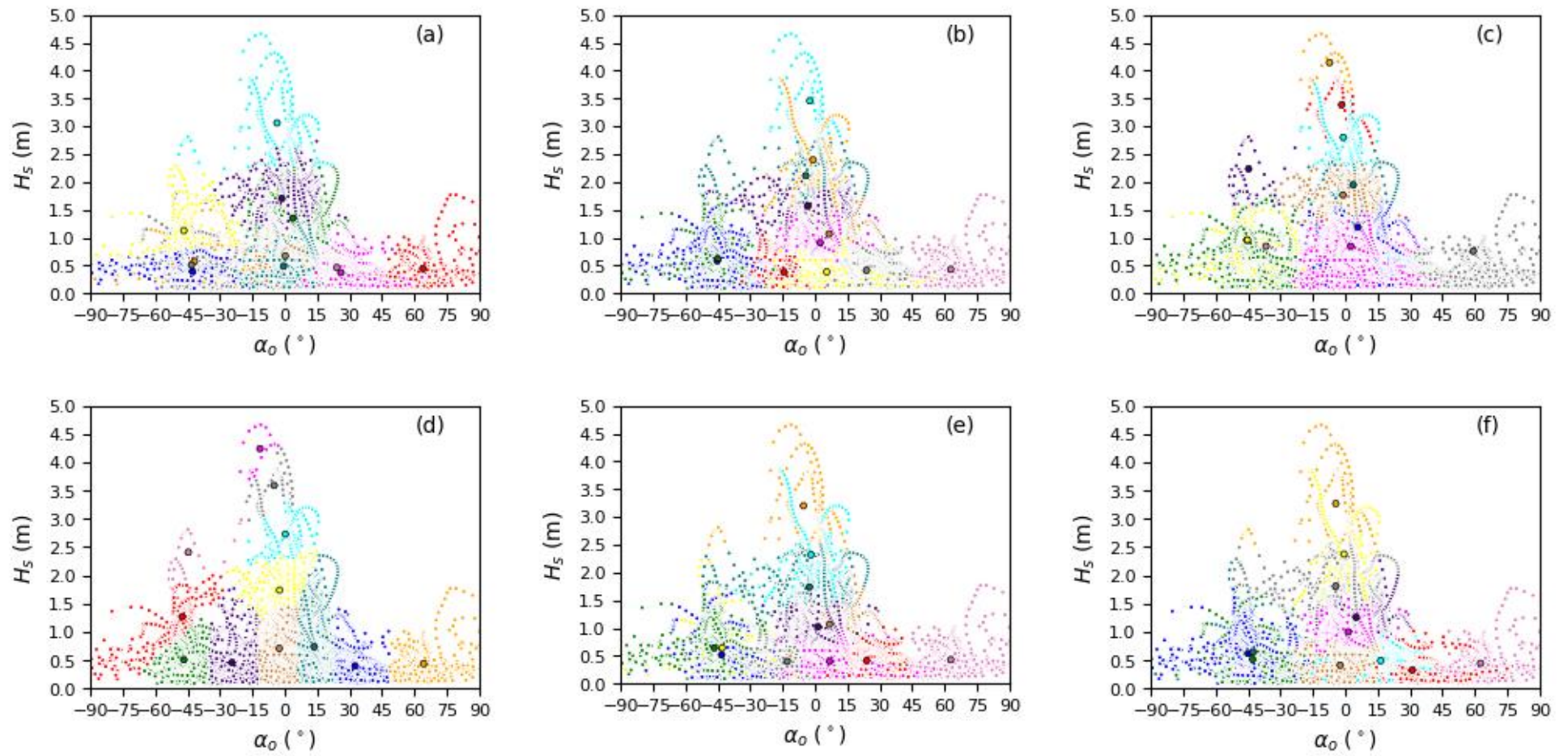
Figure 4.2. Obtained clusters and representative wave conditions for the (a):KM-01, (b):KM-02, (c):KM-03, (d):KM-04, (e):KM-05, (f):KM-06 test cases.

It can be observed that most respective representatives of the two tests showcased in Table 4.2 above are quite similar (with the more major difference observed at cluster 9). However, in general the KM-05 representatives are characterized by higher frequency of occurrence for the more energetic sea-states (e.g. cluster 6) compared to KM-02 and in turn milder wave conditions have a lower frequency of occurrence (e.g. cluster 1). This can in part be attributed to the elimination of low-energetic wave sea-states due to the criterion of incipient motion, integral to the implementation of the Pick-up rate method, which coerces the KM algorithm to initiate the iterative procedure from essentially more energetic centroids. Therefore, tests that include a filtering procedure and utilize previously calculated initial centroids tend to have increased frequency of occurrence for more energetic wave events. Hence, it is considered that the frequency of occurrence is a parameter directly influencing the composite model (i.e. MIKE 21 CM FM) performance and accuracy of the results.

At this point, it is noteworthy to make mention of a systematic way undertaken to eliminate as much as possible the effect of wave chronology and sequencing of representatives. When performing simulations through the "Morphodynamic" approach, sequencing of the reduced set of wave records influences the results and subsequent performance evaluation (Benedet et al., 2016; de Queiroz et al., 2019; Walstra et al., 2013). Regarding the sequencing of the reduced set of wave conditions obtained through cluster analysis, a random ordering was undertaken, known to give a good representation of the natural variability of the wave climate (de Queiroz et al., 2019). It can be easily deduced that the sheer amount of sequencing combinations for 12 representatives would add both another factor of complexity and significantly increase the computational burden required for a comparison between the respective KM tests due to corresponding sensitivity analysis. Recognizing however, that random perturbation of the cluster centroids obtained through tests KM-01 to KM-06 can lead to a majorly different ordering of the representatives and significantly affect model performance evaluation, an effort to minimize this effect was undertaken. Performing a random ordering of the obtained representatives for case KM-01, for the subsequent tests the ordering with the closest similarity between the examined test and KM-01 was obtained by implementing the well-known Kuhn-Munkres optimization algorithm (Munkres, 1957) typically used for the assignment problem. Specifically, the most similar centroids with regards to the normalized H_{mo}, T_p, a_0 values with respect to the KM-01 case were calculated for each test KM-02 through KM-06 and then ordered accordingly. Although the representatives obtained through the different tests still possess differences, the implementation of the Kuhn-Munkres algorithm can ultimately minimize the effect of sequencing between the consecutive tests and ensure that the performance evaluation of model results can largely be attributed to the enhancements to the KM algorithm examined in the framework of this thesis.

4.3. Results and Discussion

In this section the results obtained by the MIKE21 CM-FM composite model will be presented and analyzed for all the examined tests with respect to the different configurations of the KM algorithm.

The morphological bed evolution obtained from the Brute force simulation is shown in Figure 4.3. Zones of accretion can be distinguished along the examined coastline along with some accretion at the lee breakwater of the port. Additionally, accumulation of sediment is shown at the port entrance while a distinctive erosion zone is located south of the port entrance. Some erosion zones also exist at shallow depths extending from the middle of the computational mesh till the eastern boundary. It should be noted that model calibration for the Brute force simulation due to absence of bed level measurements in the study area is not feasible, however it is considered that the process of keeping the same model parametrization between the Brute force and test simulations can provide a fair evaluation of the performance of the KM algorithm examined herein.
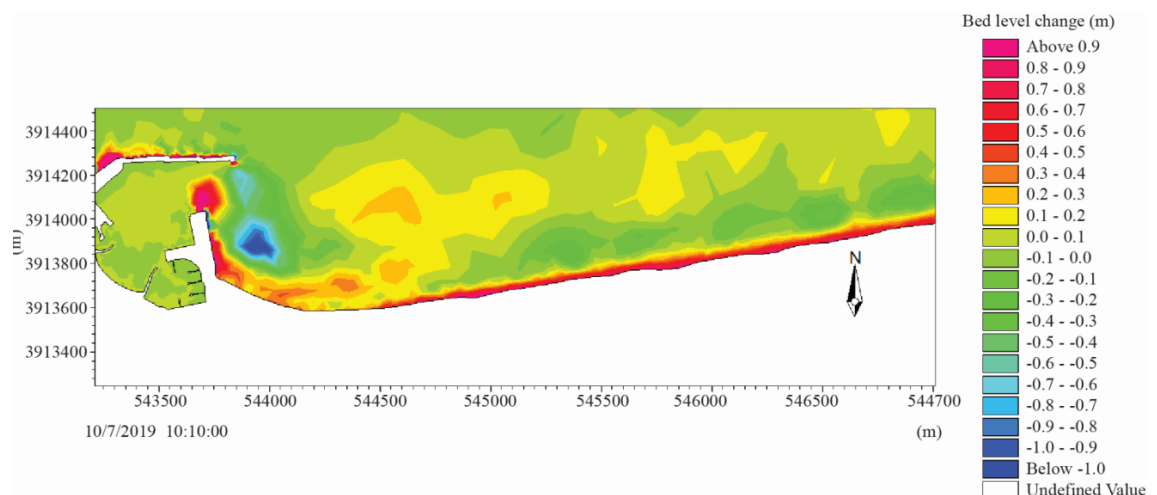
Figure 4.3. Relative bed level change obtained from the Brute force simulation containing the full dataset of wave records.

The bed evolution at an annual time scale, obtained at the end of the numerical simulations for tests KM-01 through KM-06 is depicted in Figure 4.4. The results will firstly be visually compared to the Brute force simulation to evaluate the capability of each test in reproducing the morphological changes induced by the full wave climate.

Regarding case KM-01, the general morphological response is deemed similar to the one obtained from the Brute force simulation. Although the accretion at the coastline of interest is reproduced, the magnitude of the bed level changes is underestimated, whilst the erosion areas just a few meters offshore are overestimated both in length and magnitude. Additionally, the erosion zone southward of the port entrance is present in the process-model results, albeit it is once again underestimated in magnitude. The same conclusions can be drawn for case KM-02, although more alternating zones between erosion and accretion are observed throughout the shallow areas of the computational mesh.

KM-03 test seems to lead to the best results regarding the visual inspection of the morphological evolution related to the Brute force simulation results. Interestingly, despite the fact that this test is associated with the more energetic representatives, in turn the morphological changes are generally milder than the previously analyzed tests. This can be attributed to the fact that the extreme sea-states have small frequencies of occurrence and that the morphological response of the particular study area is not driven exclusively by these events. To expand on this, the obtained representatives of the particular KM-03 test shown in Figure 4.2, do not correspond to the best representation of the cluster members throughout, since the centroids are shifted to unrealistically large values for the milder sea-states.
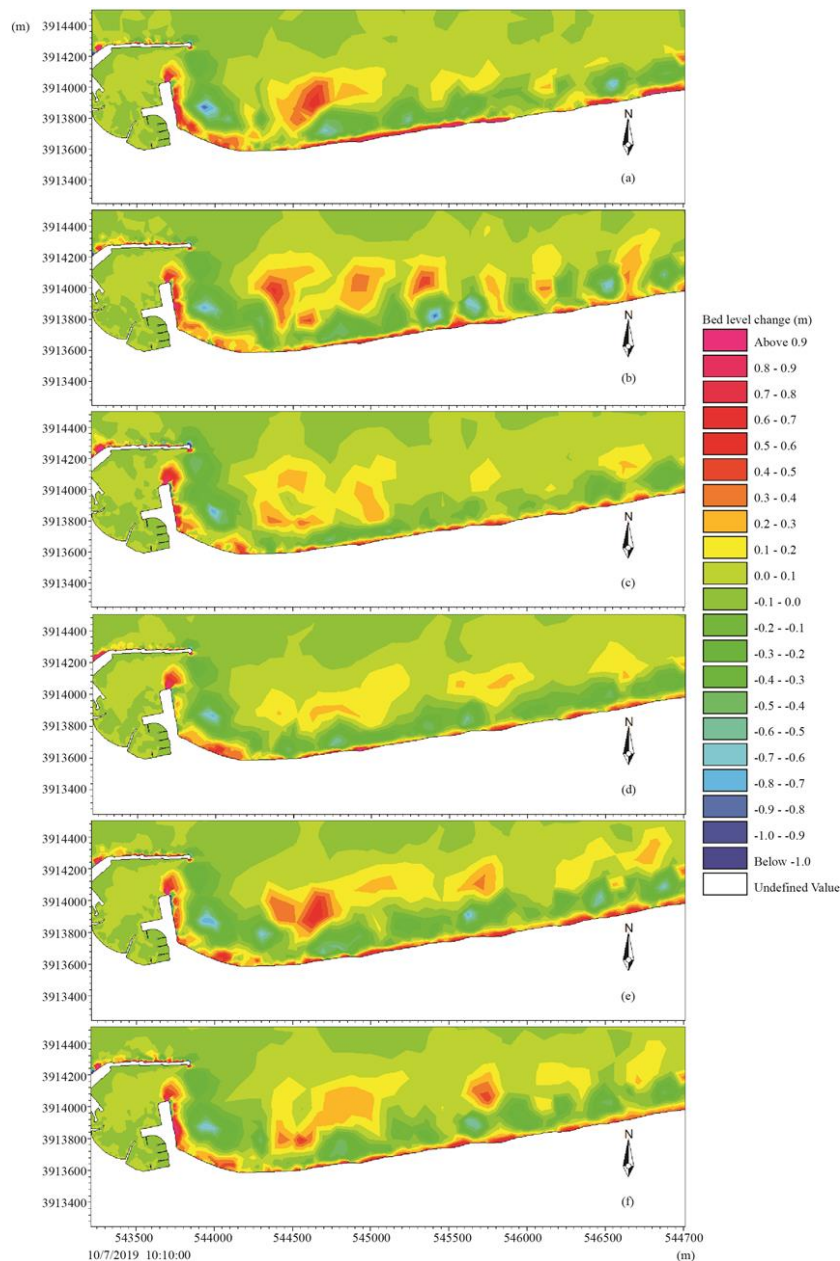
Figure 4.4. Morphological bed evolution simulation results for tests (a) KM-01, (b) KM-02, (c) KM-03, (d) KM-04, (e) KM-05, (f) KM-06.

Concerning case KM-04 a persistent underestimation of the intensity of the morphological changes is present throughout the computational mesh. Particularly evident is the absence of an elongated accretion zone at the port's lee breakwater. The transformation of clustering variables can be the cause of this effect, since non-breaking waves that have oblique incidence with respect to the coastline normal, can significantly affect the clustering analysis results. In general though, the morphological patterns of KM-04 are deemed acceptable compared to the reference simulation.

KM-05 seems to offer a good reproduction of the morphological evolution obtained from the full wave climate. Specifically, this test is associated with morphological changes of the same magnitude as the Brute force simulation, capturing the intensity of the accretion zone at the coast of interest quite satisfactorily. As with the previously examined scenarios though, the erosion zone near the port entrance is once again underestimated. Similar morphological bed evolution results are obtained in the KM-06 case which operates in a similar manner, i.e. centroid initialization specified by a thorough methodological approach and filtering of lowly-energetic sea-states. Small differences in the accretion/erosion patterns can be observed in which each test is superior to the other, for example KM-05 gives a better reproduction of the results along the sandy coastline whereas KM-06 captures the accretion at the lee breakwater in a more satisfying manner.

As has been previously mentioned, model evaluation will be carried out for the area enclosed within the polygon shown in Figure 3.7, to ultimately assess in a more precise manner the performance of each test and evaluate the efficiency of the KM clustering algorithm as an input reduction technique. A compiled list of the calculated BSS values is shown in Table 4.3.

Table 4.3
Calculated BSS values for all the examined test cases.

	KM-01	KM-02	KM-03	KM-04	KM-05	KM-06
BSS	0.63	0.64	0.65	0.66	0.71	0.68

All tests that were examined for the purpose of this research are deemed as "Excellent" with respect to the BSS classification (Sutherland et al., 2004a) which further validates the findings from visual inspection of the morphological bed evolution analysed above. Test KM-02 leads to a rather inconsequential improvement in terms of BSS compared to the default setup of the KM algorithm presented in KM-01. Both tests essentially perform similarly since they overly estimate the contribution of lowly-energetic sea-states, signified by relatively large frequencies of occurrence for the corresponding clusters. KM-03 test offers a slight improvement in the statistical metrics compared to the previous two tests, which should in part be attributed to the increased weights of the highly-energetic sea-states.

Test KM-04 shows a marginal improvement of performance, which signifies that for the particular study area, swapping clustering variables from H_{mo}, T_p, MWD to S, E_{fl},

MWD leads to an improvement of model results. Additionally, a further improvement is achieved in KM-06, which operates using the same clustering variables, albeit utilizing a filtering procedure to eliminate non-breaking waves from the dataset, considered unable to produce significant morphological changes. It should be noted that for the study area in question and the particular dataset, non-breaking waves corresponded to about 23% of the total amount of data, a percentage which is regarded to affect cluster formation significantly. To further support this, the best performing test was found to be KM-05 which once again utilizes cluster initialization obtained from a binning input reduction method in conjunction with a filtering methodology based on the criterion of incipient sediment motion.

In both KM-05 and KM-06, the effective reduction of the dataset ultimately leads to a shift of higher frequencies of occurrence for the more energetic representative wave conditions. This parameter is considered to be vital in obtaining more accurate results, since even a small percentile increase significantly affects the obtained morphological evolution at an annual scale. By applying a filtering methodology, the issue inherently present in clustering algorithms, related to the overestimation of mild sea-states' contribution to the morphological bed evolution (de Queiroz et al., 2019) is somewhat alleviated, leading to a significant performance increase of the process-based model. Finally, it should be stated that model performance can also be affected using a Morfac to speed up simulations associated with the non-linear response of the morphology to each wave forcing condition.

Due to the complexity of the Pick-up rate method, integral for test KM-05, it is considered and proposed that the methodological approach of KM-06 can be safely applied in coastal engineering applications producing satisfying results of bed level evolution for coasts where waves are the main forcing factor driving the sediment transport. Despite the lower obtained BSS values in relation to the proposed enhancements, the use of the default implementation of the K-Means algorithm (KM-01 test) is justified for use in coastal engineering applications. The minimal interference required for the selection of the representative sea-states is especially alluring, since it requires minimal user input and interference compared to the more complex tests of KM-02 through KM-06.

Chapter 5

Revisiting the concept of Representative Morphological Wave Height[1]

Representative Morphological Wave Height (RMWH) selection approaches constitute the oldest branch of wave input reduction methods that is to this day used in numerous studies (Borah and Balloffet, 1985; Chondros et al., 2022; Chonwattana et al., 2005; Karambas et al., 2013; Karambas and Samaras, 2017; Papadimitriou et al., 2022b; Pletcha et al., 2007; Tsiaras et al., 2020) due to the relative ease of implementation and sound theoretical background. It is quite similar in conceptualization and operation to the Binning IR methods, with the main difference being the consideration of fixed directional bins that are not characterized by an equal fraction of a "morphologically significant" proxy quantity. In the framework of this thesis the concept of RMWH methods is revisited and various modifications to the initially proposed method of Chonwattana et al., 2005, aiming to improve model performance are examined.

To that end, three alternative (often used in tandem) approaches are examined in addition to the default case revolving around the following: (a) subdivision in wave height bins per each directional class, (b) considering transitional zones where longshore and cross-shore sediment transport dominate the sediment transport regime interchangeably and (c) elimination of lowly energetic sea-states by employing an Artificial Neural Network (ANN) developed and trained in the framework of this thesis.

The innovative aspects in this chapter revolve around considering the effect of both longshore and cross-shore sediment transport in the specification of the representative wave conditions. Noteworthy is also the employment of an Artificial Neural Network to provide concise and rapid elimination of wave records unable to initiate sediment motion overriding the utilization of time-consuming numerical simulations for that purpose.

The alternative configurations of the RMWH method of Chonwattana et al., 2005, were once again implemented and intercompared in the coastal area in the vicinity of Rethymno Port, Crete, Greece by performing simulations with MIKE21 CM FM, to select the optimal configuration with respect to the predicted bed levels.

---

[1] Parts of this Chapter have been published in Papadimitriou et al., 2022.

5.1. Theoretical background and methodology

5.1.1. General aspects

In the framework of this PhD thesis the method to select RMWH proposed by Chonwattana et al., 2005 was utilized, specifically the one pertaining to the conservation of the longshore sediment transport in each directional bin. As has been previously mentioned, in order to obtain a pre-defined number of representatives, firstly one has to divide the dataset of offshore sea-state characteristics in directional bins of fixed size, with the number of directional bins being identical to the desired number of representative wave conditions. Then, for each directional bin and each distinct wave record the constants C_1, C_2, C_3 are calculated through Eqs. (2.10), (2.11) and (2.13) respectively. Then the equivalent value of each constant is obtained as the mean value in each directional bin. Finally, the representative wave characteristics are obtained by implementing the system of equations shown in Eq. (2.15).

In order to justify elimination of sea-states unable to induce incipient sediment motion, which is an integral part of one the examined configurations, the wave orbital velocity signal near the bed is compared to the critical values as proposed by van Rijn, 2007:

$$U_{cr,w} = \begin{cases} 0.24[g(s-1)]^{0.66}d_{50}^{0.33}T_p^{0.33} \ for \ 0.05 \leq d_{50} < 0.5 \ mm \\ 0.95[g(s-1)]^{0.57}d_{50}^{0.43}T_p^{0.14} \ for \ 0.5 \leq d_{50} \leq 2.0 \ mm \end{cases} \tag{5.1}$$

In the following subsection the examined alternative configurations considered to investigate possible room for improvements of the more traditional approach will be presented.

5.1.2. Examined alternative configurations

The alternative configurations examined herein can be generally implemented for any arbitrary number of sea-states chosen to represent a mean annual wave climate, however for the purpose of this research this number was chosen to be constant at 12 for all cases.

1st test RMWH-01

The first test corresponds to the default implementation of the morphological wave height selection method of Chonwattana et al., 2005. A dataset of offshore wave characteristics of H_{mo}, T_p, MWD is transformed to H_{mo}, T_p, a_0. Given that the offshore wave incidence angle with respect to the shore normal is within the range of [-90˚, 90˚] and the number of representatives is 12, it follows that 12 corresponding directional bins at 15 degree intervals are formed. Then for each directional bin, with the sequential utilization of Eqs. (2.10), (2.11), (2.13), (2.14) and (2.15) a set of 12 representative offshore wave characteristics (H_e, T_e, a_e) are obtained which then can be used to force the coastal area model.

2nd test RMWH-02

As has been previously mentioned, representative wave characteristics are obtained by dividing the wave climate in a predefined number of directional bins and obtaining solely one representative sea-state for each bin. Most coastal zones are subject to a diverse wave climate, containing both mild (usually associated with higher frequencies of

occurrence) and extreme wave conditions. For these cases, prescribing only one wave representative for each directional bin, tends to be inadequate to describe the variations of the wave height. Test RMWH-02 aims to counterbalance this issue by providing an additional subdivision in the wave heights sector, depending on if the wave energy flux of a particular wave record exceeds the average energy flux of the particular directional sector. The distinct steps of this methodology have as follows:

1. Obtain a timeseries of offshore sea-state characteristics.
2. Define the desired number of representative conditions N_r. An even number of N_r should be specified.
3. Divide the wave records into $N_r/2$ directional bins.
4. For each directional sector calculate the individual wave energy flux of each wave record (eliminating constants), through the following relationship.

$$E_{f,i} = \frac{1}{32\pi} H_{s,i}^2 T_{p,i}$$

(5.2)

where the subscript "i" denotes each wave record.

5. Calculate the average wave energy flux of each directional bin as follows:

$$E_{f,eq} = \frac{\sum E_{f,i} f_i}{\sum f_i}$$

(5.3)

6. Using the value calculated through Eq. (5.3) as a boundary, two subsectors in each directional bin are formed. Each wave record is assigned to a sole subsector, depending on if its individual wave energy flux exceeds or subceeds the average value calculated in Eq. (5.3).
7. Effectively a total of N_r subsectors (with $N_r/2$ subdivisions in wave direction and 2 subdivisions in the wave height) are obtained.
8. Calculate the representative wave characteristics at each subsector by implementing the system of Eq. (2.15).

This test aims to bring the RMWH method closer to the Energy flux binning IR method (Benedet et al., 2016) by implementing similar principles, albeit the Energy flux bins do not contain the same fraction of the cumulative energy flux of the timeseries. By defining "subcritical" and "supercritical" subdivisions in the wave height sector based on the average wave energy flux, the interplay between mild and more energetic sea-states is more adequately prescribed.

3rd test RMWH-03

The previously presented tests are all based on the premise that longshore sediment transport is the main driving force responsible for the medium-term bed level evolution. Considering an ideally straight coastline with parallel depth contours and assuming that waves approach the coastline with small angles of incidence (almost perpendicularly) then cross-shore sediment transport is an important factor influencing the morphological evolution and should be considered in the calculations. To that end, a new RMWH method, hereafter called the "Transition Zone" method has been developed and

implemented in the framework of this research defining influence zones where longshore and cross-shore transport drive the morphological bed evolution interchangeably.

Observing a wave ray and applying the principles of wave energy conservation in deep water and eliminating constant quantities, the longshore and cross-shore component of the wave energy flux can be calculated as follows:

$$\begin{cases} E_{ls} = H_s^2 T_p \sin a_0 \\ E_{cs} = H_s^2 T_p \cos a_0 \end{cases} \tag{5.4}$$

where E_{ls} is the alongshore and E_{cs} the cross-shore component of the wave energy flux respectively.

Given a pair of significant wave height H_s and peak wave period T_p and solving Eq. (5.4) for several values of the wave incidence angle a_0, zones with interchange dominance of longshore and cross-shore sediment transport gradients are distinguished, with the following boundaries, as chosen in the framework of this thesis:

$$\begin{cases} |E_{ls}| \geq 2|E_{cs}|, & longshore\ transport\ dominates \\ |E_{cs}| \geq 2|E_{ls}|, & cross-shore\ transport\ dominates \\ else, & interchangeable\ dominance \end{cases} \tag{5.5}$$

Considering once again the idealized case of a straight coastline with depth parallel contours, the following five zones can be distinguished with respect to the angle of wave attack relative to the shore normal, as shown in Table 5.1.

Table 5.1
Zones of interchangeable influence of longshore and cross-shore transport gradients depending on the angle of wave incidence for an idealized straight coastline.

Zone	Angle of wave incidence intervals	Influencing factor
Z1	[-90.0, -63.5)	Longshore transport
Z2	[-63.5, -26.5)	Longshore & Cross-shore transport
Z3	[-26.5, 0.0)	Cross-shore transport
Z4	[0.0, 26.5)	Cross-shore transport
Z5	[26.5, 63.5)	Longshore & Cross-shore transport
Z6	[63.5, 90.0]	Longshore transport

Having defined these influence zones, a separate driving quantity is selected for each one and considered vital in shaping the morphological changes and therefore the selection of representatives. Hence the following rules are applied:

- For zones Z1 and Z6 the main driving quantity is the wave energy flux which can readily be calculated through Eq. (2.20).

- For zones Z2 and Z5 the main driving quantity is the bulk longshore sediment transport, and coincidentally takes the maximum value in this angular range.
- For zones Z3 and Z4 the influence of the cross-shore transport can be calculated through Eq. (2.16).

Based on the above assumptions the steps taken to reproduce and implement this methodology have as follows:

1. Obtain timeseries of offshore sea-state characteristics.
2. Define the desired number of representative conditions N_r. An even number of N_r should be specified.
3. One representative wave is calculated for all the dataset by solving the system of Eqs. (2.15).
4. Specify the angle between the orientation of the shoreline of interest and the representative angle of wave incidence as calculated in step 3 above. Considering the value of this angle the mean wave direction of each wave record should be transformed accordingly with respect to the shore normal at the range of [-90˚, 90˚].
5. Divide the wave records into the 6 directional bins, forming the Zones Z1 to Z6 by implementing the principles of Eq. (5.5)
6. Subdivide further the directional bins defined in step 2, prioritizing the directional bins possessing waves with the higher frequencies of occurrence until a number of N$_r$/2 directional bins is obtained.
7. Depending on the influence zone each directional bin falls into, calculate a driving quantity for each individual wave records as follows:
   - Z1 and Z6: calculate the wave energy flux $E_{f,i}$ through Eq. (2.20)
   - Z2 and Z5: calculate the longshore sediment transport rate S_i through Eq. (4.3)
   - Z3 and Z4: calculate the P parameter through Eq. (2.16)
8. For each directional bin calculate the "equivalent" values of each driving quantity (taken as the mean value of each bin) as follows:

$$\begin{cases} E_{f,eq} = \dfrac{\sum E_{f,i} f_i}{\sum f_i} \\ S_{eq} = \dfrac{\sum S_i f_i}{\sum f_i} \\ P_{eq} = \dfrac{\sum P_i f_i}{\sum f_i} \end{cases} \tag{5.6}$$

9. Using the value calculated through Eq. (5.6) as a boundary, two subsectors in each directional bin are formed. Each wave record is assigned to one subsector, depending on if its individual wave energy flux exceeds or subceeds the "equivalent" value calculated in Eq. (5.6).
10. Thereafter a total of N_r subsectors (with N_r/2 subdivisions in wave direction and 2 subdivisions in the wave height) are obtained.

11. Calculation of the representative wave characteristics at each subsector by implementing the system of Eq. (2.15) follows. The representatives are then used to force the coastal area model.

It should be mentioned that the presented "Transition Zone" method, which is the backbone of test RMWH-03, is subject to a number of assumptions, the most important of which is that the coastline is considered relatively straight in the derivation of the quantities. This is not always the case in nature, which implies that the angle of wave incidence can rapidly change even between adjacent segments of the coastline. Hence, for two coastline segments with differing orientation and the same offshore sea-state characteristics, one can be influenced mainly by longshore and the other by the cross-shore sediment transport. The underlying complexity of the coastline geometry is inherently not treated by most input reduction methods which aim to retain a level of simplicity (de Queiroz et al., 2019; Pletcha et al., 2007). However, despite the limitations in the theoretical aspects of the methodology, once again the use of a parabolic mild slope wave model modified to calculate longshore sediment transport gradients at the point where initiation of breaking occurs, offers a more thorough approach compared to the analytical expressions.

4th test RMWH-04

The 4th test aims to revisit a common practice implemented in tandem with wave input reduction methods which revolves around the disposal of sea-states from the dataset if they do not exceed a certain threshold in the significant wave height (Benedet et al., 2016; Walstra et al., 2013). However, this approach is loosely defined, and the threshold is both site specific and if set too high can sometimes lead to deterioration of results (Walstra et al., 2013). The particular test aims to systematically eliminate of wave records if they are unable to initiate sediment motion, adopting the principles of the Pick-up rate binning Input Reduction method (Papadimitriou et al., 2020) but further expanding the ease of implementation and applicability range.

To that end, a methodology incorporating several simulations conducted with the PMS-SP model that were used to train an Artificial Neural Network (ANN) on the premise of eliminating wave records unable to initate sediment motion was developed. The layout of the methodology as well as the parametrization and training of the ANN is showcased below.

Methodology Layout

Observing Eq. (3.13) it can be readily deduced that the following dependencies can be distinguished for the bed shear stress under the effect of the waves.

$$\tau_{b,w} = f(U_w, f_w) \tag{5.7}$$

Considering the near-bed wave orbital velocity signal setting sediment grains into motion depends on the wave characteristics inside the surf-zone, Eq. (5.7) can be rewritten with the following dependencies.

$$\tau_{b,w} = f(H_{s,b}, T_{p,b}, a_b, f_w) \tag{5.8}$$

where the subscript "b" denotes values inside the surf-zone.

Estimation of breaking wave characteristics depends mainly on the offshore sea-state wave characteristics as well as the bed slope as ordered by a plethora of analytical wave breaking models (e.g. Kamphuis, 1991b; Weggel, 1972). Additionally, the wave friction factor can be substituted with a sole dependency on the median sediment grain diameter d_{50} by specifying a Nikuradse roughness k_s=2.5d_{50} considering that the turbulence conditions within the surf-zone can be safely approximated as rough and the bed considered flat. Hence the bed shear stress due to waves, is rewritten with the following dependencies:

$$\tau_{b,w} = f(\text{H}_\text{s}, \text{T}_\text{p}, a_o, d_{50}, tan\beta) \tag{5.8}$$

The same dependencies also apply in the calculation of the near-bed wave orbital velocity signal. The correspondence between offshore sea-state characteristics and the values within the surf-zone is obtained by implementing the PMS-SP wave model, developed and enhanced in the framework of the present thesis. Given an annual dataset of hourly varying offshore sea-state wave characteristics, the estimation of $\tau_{b,w}$ would be a tedious task, requiring intense computational resources and compromising the acceleration aspect of Input Reduction Methods when applied in coastal zones with vastly different characteristics. Hence, a thorough methodology has been developed to systematically eliminate sea-states considered unable to initiate sand motion by combining numerical modelling simulations and the training and implementation of an Artificial Neural Network (ANN) to accelerate morphological modelling simulations and enhance the reliability of model results for a wide application range. The distinct steps comprising the methodology are the following:

1. Three idealized alongshore uniform bathymetries are constructed, each characterized by a different value of the bed slope tanβ, namely 1:5, 1:25 and 1:50. A spatial discretization step of 2.5 m was utilized to discretize the bathymetry with a total of 2800 cells in the cross-shore and 100 cells in the alongshore direction.

2. This step concerns the definition of a preset number of combinations of the Input Parameters (IP) of {H$_\text{s}$, T$_\text{p}$, a_o, d_{50}, $tan\beta$}. It was desirable to define many combinations of the IP in order to cover the wide array of possible values in an arbitrary dataset of offshore sea-state characteristics and coastal bed composition. Hence the lower and upper boundaries of the IP were defined and are shown in Table 5.2, and a Saltelli sampling method (Saltelli, 2002) typically used in Global Sensitivity Analysis applications was utilized to obtain a set of 14168 possible combinations of the IP. To ensure realistic pairs of H_s and T_p an additional restriction was imposed on the values of peak wave period, which was to satisfy the Jonswap correlation between H_s and T_p. To reduce the sheer number of combinations, the K-Means clustering algorithm was implemented to reduce the combinations of the IP to 3000. Finally, 250 additional scenarios were considered to account for bounding values of the IP not directly accounted for by the cluster analysis, raising the final number to 3250.

Table 5.2
Boundaries of the Input Parameters specified in the analysis

	H_s (m)	T_p (s)	a_o $(°)$	d_{50} (mm)	$tan\beta$ $(-)$
minimum	0	0	-90	0.06	1:50
maximum	7	15	90	2.0	1:5

3. For each combination of the IP, simulations were carried out through the PMS-SP wave model. The model outputs are given in the form of maps of significant wave height and mean wave direction.

4. Taking advantage of the alongshore uniformity of the bathymetries, the mean value of the near-bed wave orbital velocity shoreward the depth where initiation of breaking takes place is calculated at a cross-section in the middle of the domain in the alongshore direction.

5. The set of IP $\{H_s, T_p, a_o, d_{50}, tan\beta\}$ are therefore linked to a unique value of the Output Parameter (OP) $\{U_w\}$. The corresponding values of IP and OP are provided for the training and validation of an ANN, which will predict U_w for any values within the ranges defined in Table 5.2.

6. The trained ANN can then be implemented for any dataset containing offshore sea-state wave characteristics by specifying corresponding values of the median sediment diameter and mean bed slope and then predict values of U_w.

7. The predicted values of U_w are then compared to the critical values of $U_{cr,w}$ as calculated by Eq. (5.1). If $U_w < U_{w,cr}$ the sea-state is considered unable to initiate sediment motion and is eliminated from the dataset. All the eliminated sea-states are considered to contribute to the "calm" conditions, which also contain sea-states that exit the numerical domain and do not induce morphological changes in the coastline of interest.

8. With the completion of step 7, a reduced set of "morphologically significant" offshore sea-state characteristics is obtained containing the sea-states that are considered capable of initiating sediment motion.

9. A pre-defined number of wave representative conditions are obtained by solving the system of equations in Eq. (2.15) for each desired directional bin.

10. The representatives obtained at step 9 are then used to force the coastal area model.

The proposed methodology developed in the framework of test RMWH-04 is valid for real-field conditions (and not for experimental scale) and for any combination of the parameters within the ranges presented in Table 5.2, considering the effect of the waves in stirring the sediment. It is a natural evolution of the filtering methodology presented in section 3.1.1 in the framework of the Pick-up Rate binning IR method but has the following distinguishing qualities:

- Through the training of an ANN, the added computational burden is inconsequential (the ANN produces results within seconds) further enabling the concept of acceleration of morphological modelling simulations.

- Considering the mean value of the wave orbital velocity within the surf-zone ensures a concise filtering of relatively low-energetic sea-states. Strictly speaking, all sea-states at a certain point are subject to wave breaking and initiate sediment motion, the proposed methodology however aims to define wave records that would produce significant morphological changes for an extended area within the surf-zone.

Training and validation of the ANN

The basic aspects and procedure to train and validate the developed ANN will be presented herein. In general, two datasets are needed when training an ANN, in particular the training and the validation dataset. The combination of the two sets composes the generalization set which contains the necessary data for the construction of the ANN. In the present study, the generalization dataset is comprised of 3250 combinations of the IP as shown in the subsection above, which are divided into 2925 events for the training dataset and 325 randomly selected events for the validation dataset, leading to a training / validation split of 90% / 10%.

A Multilayer feed-forward ANN was chosen to predict the wave orbital velocity signal near the bed, for a given set of offshore sea state wave characteristics and a representative value of the bed slope and sediment mean diameter. The number of units (neurons) and hidden layers composing the ANN architecture is vital for its performance. In essence, fewer neurons and hidden layers will result in low accuracy whereas too many neurons and hidden layers will increase complexity and significantly increase the computational effort required for the training procedure. The most employed methods of determining the number of hidden neurons are experimentation and trial and error.

The ANN architecture that was implemented herein was chosen after experimenting with various architectures and parametrizations, with the goal to minimize the Mean Squared Error (MSE) between the generalization dataset target values and the ANN predictions. The ANN was set-up in the python programming language using the open source TensorFlow machine learning library (https://www.tensorflow.org/). After the trials, it is comprised of the following architecture.

- An input layer (IL) sending input data to the network.
- A hidden layer (HL1) composed of 32 units and a rectified linear unit (relu) activation function.
- A hidden layer (HL2) composed of 64 units also using a relu activation function.
- An output layer (OL) with a linear identity activation function.

The relu activation function is commonly applied in the hidden layers of Machine Learning and Deep Learning models. The function returns zero if it receives any negative input, but for any positive value it defaults to a linear identity function as follows:

$$f(x) = \max(0, x) \tag{5.9}$$

For the output layer a linear identity transfer function $(x) = x$ is used.

Input and output parameters are normalized so that they always fall within a specified range [0,1] in order to reduce errors associated with the specific characteristics and magnitudes of the data. Any value of the IP:$\{H_s, T_p, a_o, d_{50}, \tan\beta\}$ is normalized through

a minmax normalization based on the bounding limits shown in Table 5.2. For the OP a minmax normalization is also implemented based on the maximum and minimum values of U_w calculated through the set of 3250 distinct simulation scenarios. Given a specific value of parameter (p) the normalized value (p^n) is obtained as:

$$p^n = \frac{p - P_{min}}{P_{max} - P_{min}} \tag{5.10}$$

where p is a particular input/output parameter, P_{min} and P_{max} are the minimum and the maximum values of the parameter encountered in the entire dataset, and the superscript n denotes a normalized value.

The normalized values of the input parameters propagate from the input layer (IL) through the hidden layers (HL1, HL2) to the output layer (OL). The final and intermediate values are calculated as follows:

$$x_j^{HL1} = F\left[\left(\sum_{i=1}^{N1} w_{ij}^{HL1} x_i^{IL}\right) - \theta_j^{HL1}\right] \qquad j=1,...,N1 \tag{5.11}$$

$$x_j^{HL2} = F\left[\left(\sum_{i=1}^{N2} w_{ij}^{HL2} x_i^{HL1}\right) - \theta_j^{HL2}\right] \qquad j=1,...,N2 \tag{5.12}$$

$$\left(x_j^{OL}\right)^n = F\left[\left(\sum_{i=1}^{5} w_{ij}^{OL} x_i^{HL2}\right) - \theta_j^{OL}\right] \qquad j=1,1 \tag{5.13}$$

where $N1$ and $N2$ is the number of units in the hidden layers HL1 and HL2 respectively, subscript j denotes a particular data point of the generalization dataset, w_{ij} are numerical weights (between the input and hidden layers w_{ij}^{HL1}, w_{ij}^{HL2}), θ_j are the biases, and F is the activation function considered on each layer.

The initial weights and biases are randomly assigned, and the ANN is trained using the IP to assign the optimum weights and biases. As has been previously mentioned, the performance of the training procedure is assessed by calculating the Mean Squared Error (MSE) between the output and the target values as follows:

$$MSE = \frac{1}{N}\sum_{i=1}^{N}\left[\left(x_j^{OL}\right)^n - \left(x_j^{target}\right)^n\right]^2 \tag{5.14}$$

where N is the amount of generalization data points i.e. 3250 for the particular case.

The MSE is then utilized to adjust weights and biases using the gradient descent method:

$$w_{ij}' = w_{ij} - \kappa\frac{\partial MSE}{\partial w_{ij}} \tag{5.15}$$

$$\theta_{ij}' = \theta_{ij} - \kappa\frac{\partial MSE}{\partial \theta_{ij}} \tag{5.16}$$

where w_{ij}' and θ_{ij}' are the updated weights and biases after each epoch and κ is the learning rate set equal to 0.001, while setting 100 epochs (passes) was found sufficient to obtain the optimal values of the MSE. Ultimately, an $MSE = 9.2$ E-5 was obtained after completing the training and validation of the ANN. The error and performance metrics of the training of the ANN are showcased in Figure 5.1.
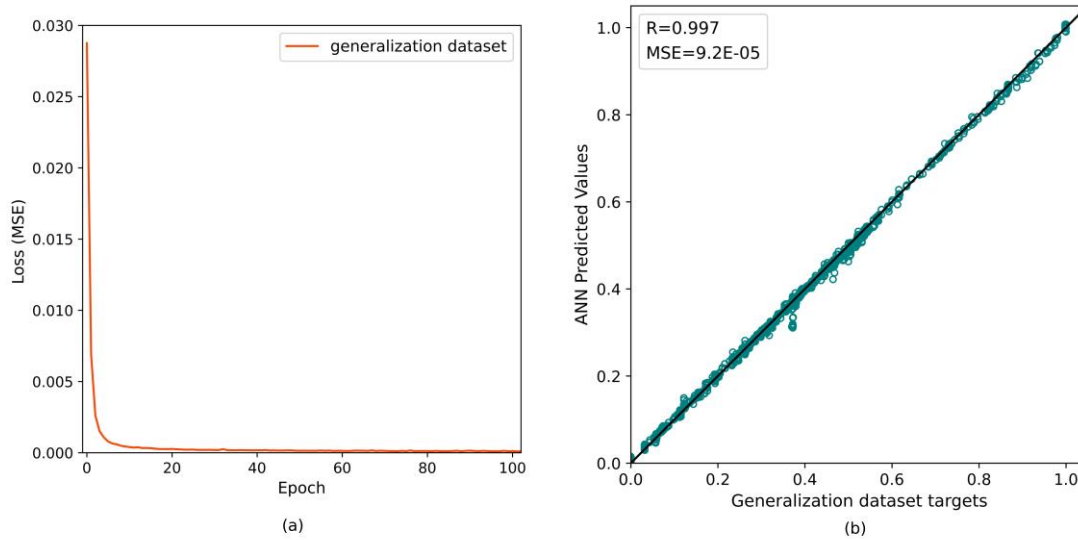
Figure 5.1. Error and performance metrics of the training procedure of the ANN: (**a**) Evolution of the MSE during the training and validation of the generalization dataset (**b**) ANN predicted values against the respective targets of the generalization dataset (normalized values).

The implemented ANN is valid for sand sediment grains and for all the values within the ranges shown in Table 5.2. The following assumptions and restrictions were considered:

- The sole effect of the waves on stirring up sediment is taken into account. This assumption is made on the basis that in essence the bed shear stress due to waves is orders of magnitude greater than the respective one due to current only (Soulsby, 1997).
- The training of the ANN was carried out with simulations of uni-directional waves through a Parabolic Mild Slope wave model. For multidirectional waves an alternative model should be used for the training procedure, since the parabolic approximation of the mild slope equations pertains mostly to waves with small directional spreading.

Despite the above considerations, the ANN covers a wide array of coast configurations and offshore sea-state wave characteristics and is a useful and valid complementary tool for the RMWH selection method examined herein.

5.2. Methodology implementation

5.2.1. Study area and model setup

In a similar manner to Chapters 3 and 4, the simulation sets corresponding to the alternative RMWH configurations will be implemented in the coastal area of Rethymno, Crete, Greece. However, in contrast to the evaluation the Binning Input Reduction methods and the K-Means clustering algorithm, which were carried out through the "Morphodynamic" approach, the simulations in this Chapter will be performed as dictated by the "Morphostatic" approach. Hence, each representative wave condition will use the same initial bathymetry from the simulations and the final bed level will be obtained by combining the respective results. As has been previously mentioned, although the

"Morphostatic" approach omits some principles on the constant feedback between waves and hydrodynamics and the sequencing of sea-states, it is in turn used very oftern in engineering practice since it is several orders of magnitude faster and easier for the assessment of results compared to the "Morphodynamic" approach, so it is worth examining in the framework of this dissertation.

A slightly altered finite element mesh was utilized for the simulations of the alternative RMWH configurations, considering a circular offshore boundary and is showcased in Figure 5.2. The circular boundary is considered to better accommodate sea-states with relatively large angles of wave incidence with respect to the shore-normal, which are more prevalent in the RMWH selection methods compared to the Binning wave schematization methods. The nominal length of the finite elements and the mesh density levels were kept consistent with the previous instance of the mesh utilized for the simulations presented in Chapters 3 and 4. In Figure 5.2, the area where model results will be evaluated by calculating the BSS values, is also showcased.
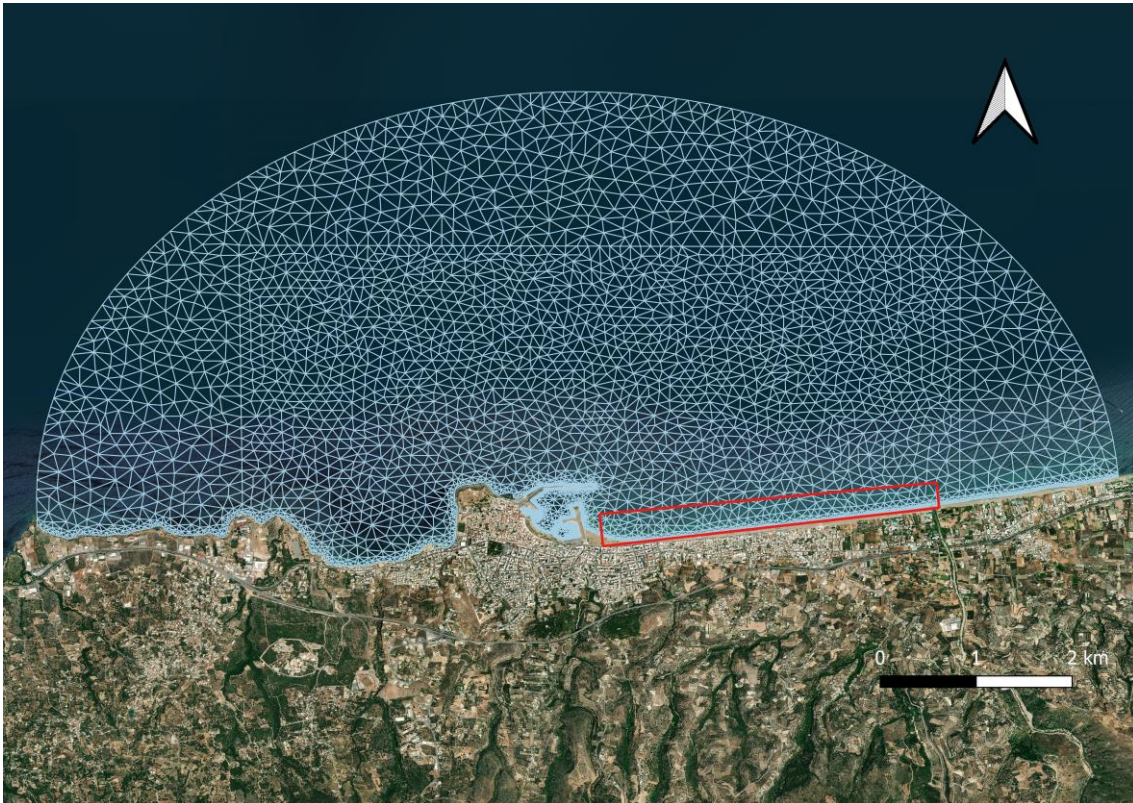
Figure 5.2. Finite element mesh with circular open boundary, showcasing the area (within the closed polygon) where the morphological model results will be evaluated for the RMWH tests

Once again, offshore sea-state wave characteristics extracted for the year 2012 from the MEDSEA_MULTIYEAR_WAV_006_012 (Korres et al., 2019) product was used to force the 3rd generation spectral wave model MIKE21 SW. It should be stated that it is not feasible to perform a simulation with 8219 hourly changing wave records that influence the study area (as can be seen in the wave rose plot in Figure 3.6) through the "Morphostatic" approach, since that would require an excessive amount of computational

resources. Hence, for the purpose of conducting a Brute force simulation a detailed -yet schematized- wave climate was considered in line with similar studies on this subject (e.g. Benedet et al., 2016; Walstra et al., 2013). Hence the offshore wave climate was divided in wave height bins of constant intervals of 0.5m and for angles of wave incidence ranging from -90° (generated from the west sector) to 90° (generated from the east sector) a constant step of 15° was considered. A histogram of the significant wave height and the wave incidence angle is showcased in Table 5.3.

Table 5.3
Histogram of significant wave height and wave incidence angle for the year 2012.

H_s [m]	[-90,-75)	[-75,-60)	[-60,-45)	[-45,-30)	[-30,-15)	[-15,0)	[0,15)	[15,30)	[30-45)	[45,60)	[60-75)	[75-90)	Percentage
(0.0-0.5]													41.212%
(0.5-1.0]	0.183%	0.219%	7.303%	3.834%	1.473%	5.806%	6.658%	3.846%	0.682%	0.414%	0.828%	0.122%	31.366%
(1.0-1.5]	0.012%	0.110%	3.323%	0.694%	0.609%	4.674%	5.599%	1.071%	0.049%	0.024%	0.073%	0.073%	16.310%
(1.5-2.0]	-	-	0.243%	0.316%	0.316%	2.726%	2.118%	0.426%	-	-	0.012%	0.061%	6.220%
(2.0-2.5]	-	-	0.134%	0.024%	0.146%	0.694%	1.144%	0.170%	-	-	-	-	2.313%
(2.5-3.0]	-	-	0.061%	0.037%	0.061%	0.414%	0.572%	0.012%	-	-	-	-	1.156%
(3.0-3.5]	-	-	-	-	0.024%	0.207%	0.523%	0.012%	-	-	-	-	0.767%
(3.5-4.0]	-	-	-	-	0.061%	0.341%	0.061%	-	-	-	-	-	0.463%
(4.0-4.5]	-	-	-	-	0.012%	0.122%	0.012%	-	-	-	-	-	0.146%
(4.5-5.0]	-	-	-	-	0.012%	0.037%	-	-	-	-	-	-	0.049%
	0.195%	0.329%	11.064%	4.905%	2.714%	15.019%	16.687%	5.538%	0.730%	0.438%	0.913%	0.256%	100.000%

Observing the frequencies of occurrence of the histogram it can be deduced that 68 sea-states are considered to compose the Brute force simulation with each sea-state represented by the mean value of the corresponding significant wave height, incident wave angle and peak period bins.

The following procedure is adopted to obtain the final bed level for the Brute Force simulations. Each distinct sea-state simulation is executed utilizing the MIKE21 SW, HD and ST models in direct coupling. Furthermore, the SW and HD models are utilized in quasi-stationary mode to ensure faster convergence, allowing to prescribe relatively shorter total simulation times. The simulation is completed after an "equilibrium" state is obtained in the morphological model, signifying small variations on the rates of bed level change in each time step, practically no longer altering the coastal bed. The appropriate time depends on the incident wave characteristics and computational domain size and was determined by implementing a trial-and-error approach, concluding that setting a total time of 86,400s was sufficient to reach an equilibrium state in the morphological bed evolution. To avoid unrealistic fluctuations in the bed level update calculations the model

was allowed to "spin-up", meaning that the morphological calculations were initialized after 30,000 s.

The computed bed level change obtained from each distinct sea-state simulation is then multiplied by the corresponding frequency of occurrence (as shown in Table 5.3). Ultimately, the respective results are summed together to obtain the integrated annual bed level change from the Brute Force simulation. The same procedure is followed for the RMWH tests, but instead of using 68, 12 wave representative sea-states are considered.

5.2.2. Representative wave conditions

In this subsection the representative wave conditions obtained from the distinct tests RMWH-01, RMWH-02, RMWH-03 and RMWH-04 will be showcased.

In Figure 5.3 the representatives of the RMWH-01 method, constituting the classical approach to select representative "annual equivalent" wave heights are showcased as a bivariate scatter plot of significant wave height and wave incidence angle.
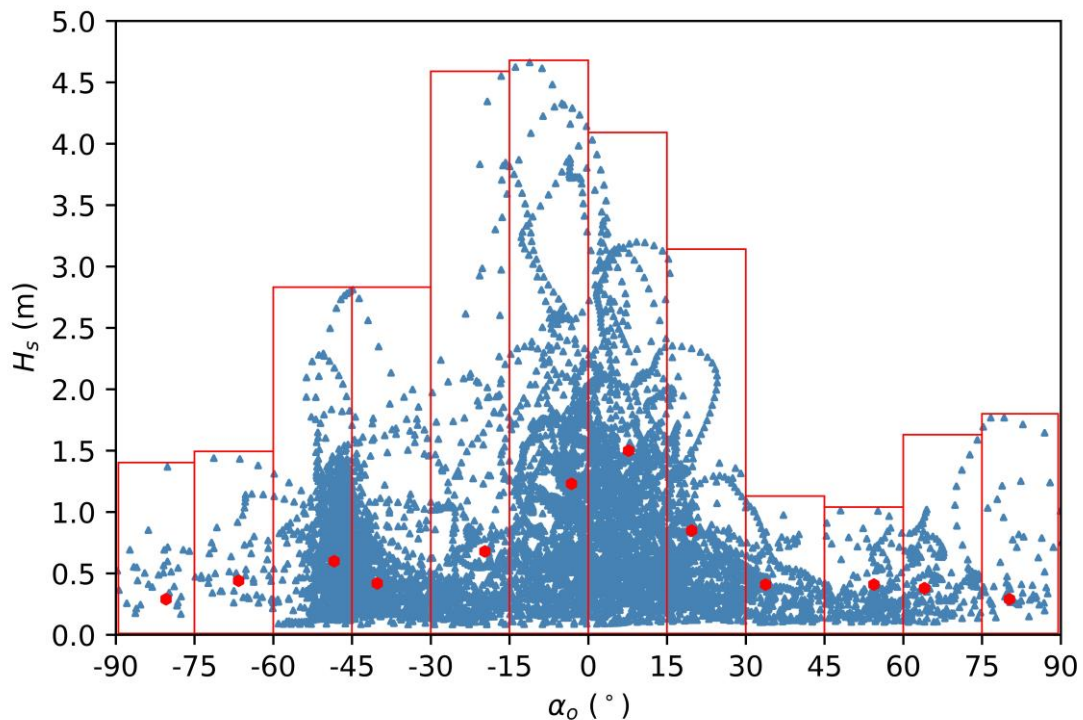
Figure 5.3. Obtained 12 representative wave conditions (red markers) by implementing the RMWH-01 test. The boundaries of the rectangles denote the constant directional bins.

As can be seen in Figure 5.3, the high frequencies of occurrence of the lowly energetic sea-states shift the representative wave conditions to relatively lower values. In contrast to the binning IR methods, the divisions strictly concern the directional and not the wave heights bins, and for the particular case the description of the more extreme sea-states that are present in the directional bins with $a_o \ni [-15°, 30°]$ is not well posed.

The abovementioned issue is somewhat alleviated in test RMWH-02, which considers 6 directional bins and 2 subdivisions in the wave height bins. Each subdivision in the wave heights contains half of the cumulative energy flux of the wave records present in

each of the 6 directional bins. The obtained representatives and respective bins are shown in Figure 5.4.
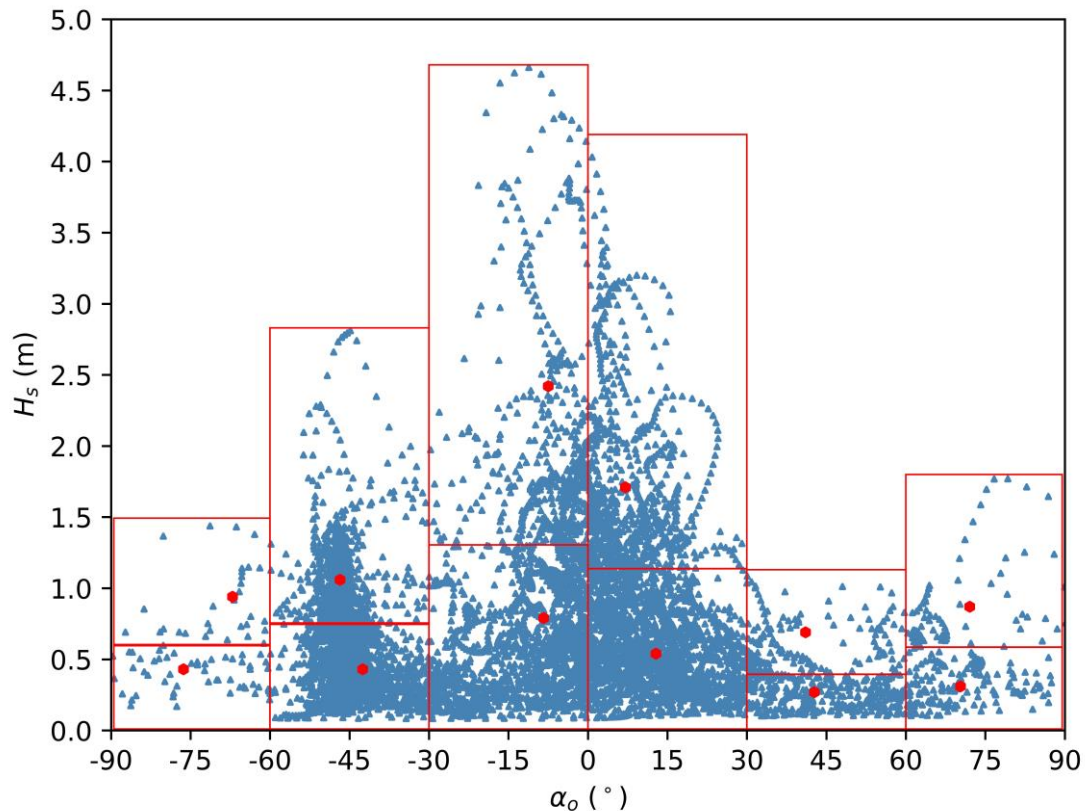
Figure 5.4. Obtained 12 representative wave conditions (red markers) by implementing the RMWH-02 test. The boundaries of the rectangles denote the defined bins.

The relatively simple approach of providing additional divisions in the wave height -at least visually- leads to a better prescription of the diversity of the full offshore wave dataset of the particular study area. Effectively, test RMWH-02 brings the RMWH methods closer to their binning IR counterparts, with the main difference is that binning IR methods do not consider a constant interval in the directional bins.

The next test (RMWH-03) requires a preliminary estimation of a singular representative set of significant wave height and peak wave period in order to define the transition zones where longshore and cross-shore transport interchangeably drive the calculation of the representatives. Implementing the system of Eqs. (2.15) a sea-state with $H_{s,r}$=1.04m and $T_{p,r}$=5.12s was calculated. Thereafter following the methodology of RMWH-03, the "transition zones" for this set of wave characteristics were defined and are shown in Figure 5.5.
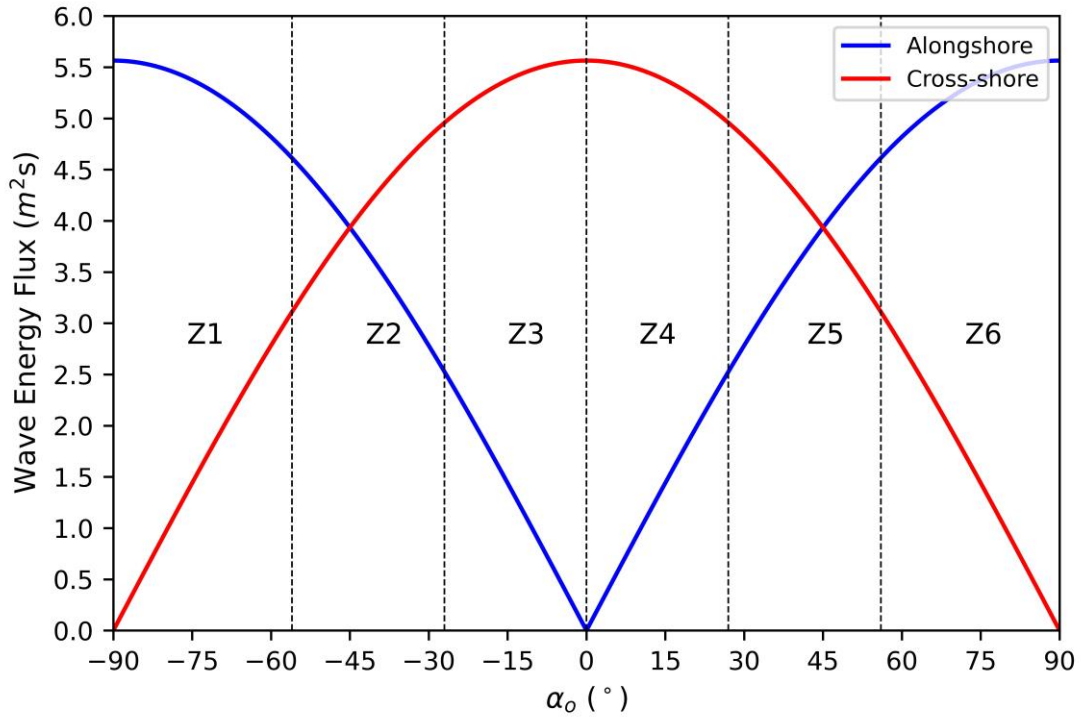
Figure 5.5. "Transition zones" of interchangeable dominance of the alongshore (blue line) and cross-shore (red line) component of the wave energy flux (defined by the perpendicular dashed lines).

The obtained representative wave conditions of test RMWH-03 is shown in Figure 5.6.
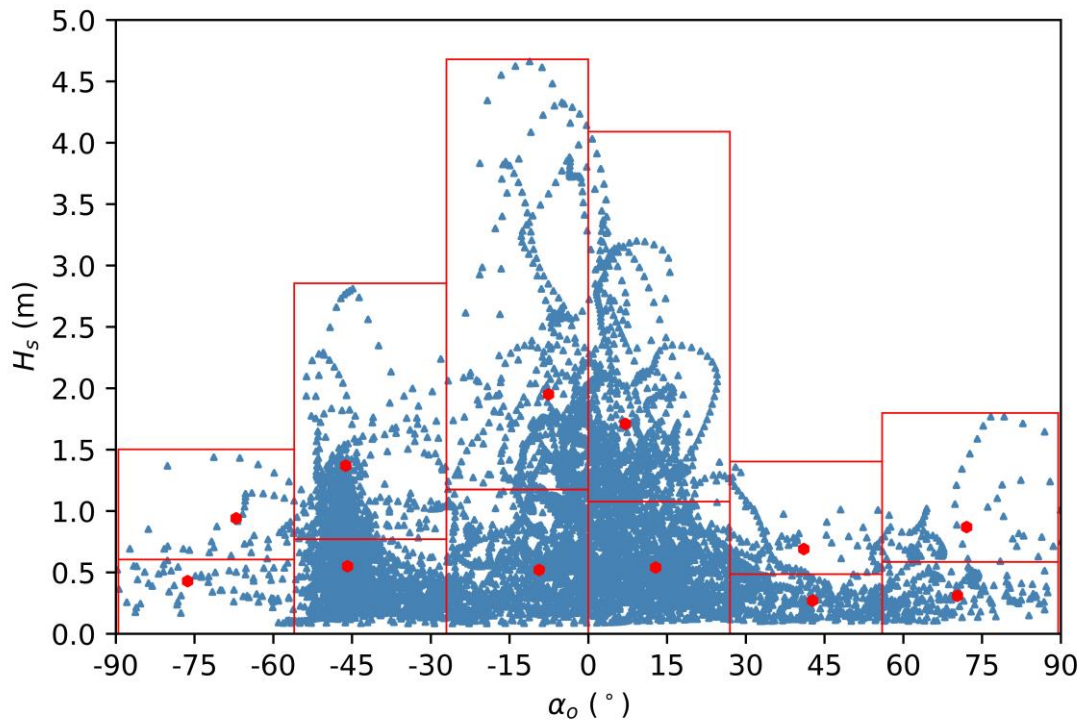
Figure 5.6. Obtained 12 representative wave conditions (red markers) by implementing the RMWH-03 test. The boundaries of the rectangles denote the defined bins corresponding to the "transition zones".

150

Comparing the obtained respective representatives between RMWH-02 and RMWH-03 it can be deduced that they are quite similar. In particular, for zones 3 and 4, where cross-shore transport drives the selection of representatives, RMWH-03 shifts the representatives to lesser wave heights. This can be attributed to the use of H_s^2/T_p as a proxy quantity instead of $H_s^2 T_p$ which pertains to test RMWH-02. Nevertheless, the representative sea-states ultimately selected by the two tests are quite similar in values and frequencies of occurrence.

Test RMWH-04 utilizes the trained ANN to estimate wave orbital velocities for each combination of offshore sea-state wave characteristics and then systematically eliminate those that do not exceed the threshold value of the near-bed orbital velocity calculated through Eq. (5.1). As has been previously mentioned, a median sediment diameter of 0.15mm and bed slope of 1:50 was set as input to the ANN. Out of the 8219 wave records, 4060 are considered unable to initiate sediment motion and are therefore eliminated from the dataset. A scatter plot showcasing the obtained representative conditions of test RMWH-04, as well as the retained and eliminated sea-states are shown in Figure 5.7.
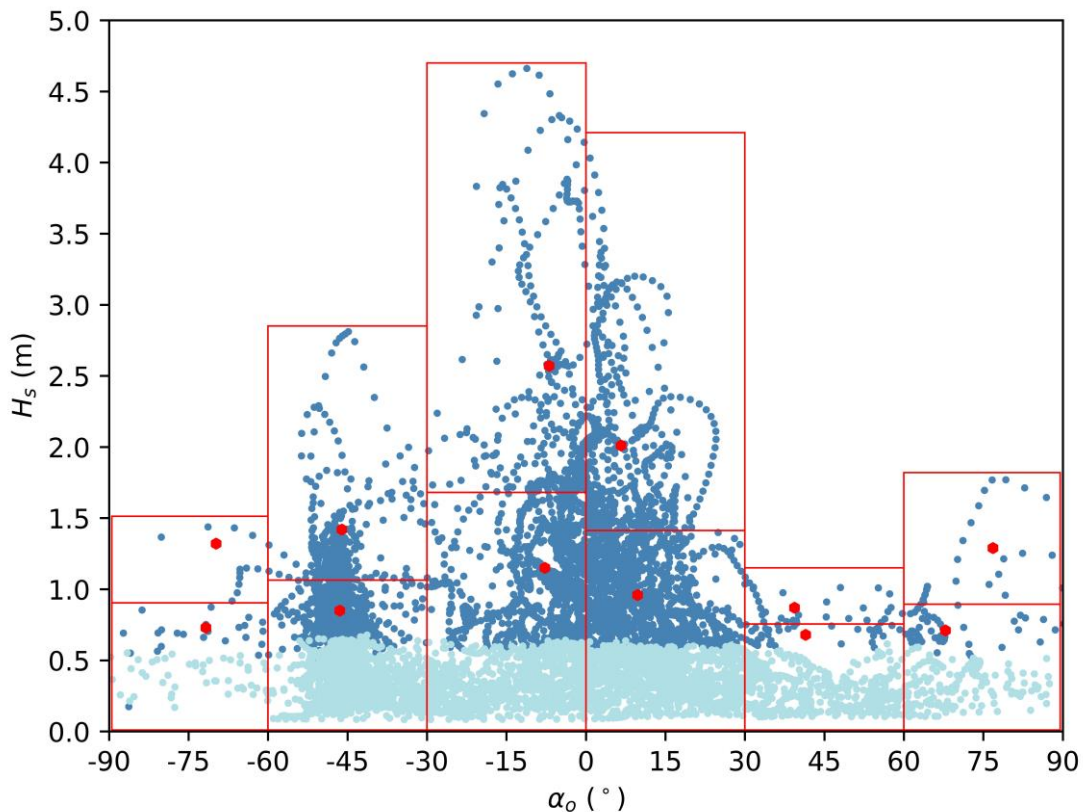
Figure 5.7. Obtained 12 representative wave conditions (red markers) by implementing the RMWH-04 test. The light blue markers denote sea-states eliminated by the ANN whereas dark blue markers denote those retained in the dataset.

Observing Figure 5.7 it can be derived that the elimination of lowly energetic sea-states shifts the results to more energetic representative waves conditions. To better assess the differences, the representatives obtained by the RMWH-04 test are compared to

those obtained by the similar RMWH-02 test and are shown in Table 5.4. As it has already been mentioned, the sea-states that are eliminated through the implementation of the ANN in RMWH-04, are considered to contribute to the "calm conditions", i.e. they retain their frequency of occurrence but are considered to have no contribution in shaping the morphological bed evolution. This is articulately shown in Table 5.4, as the total frequency of occurrence for the 12 representatives of RMWH-04 sums up to 56% and not 100%. Ultimately, the interplay between the more energetic wave characteristics obtained through RMWH-04 and their lowest frequencies of occurrence is considered to significantly influence the reliability and accuracy of the morphological model results.

Table 5.4
Representative wave conditions obtained by the RMWH-02 and RMWH-04 test respectively.

Bin	RMHW-02				RMWH-04			
	H_{mo} (m)	T_p (s)	a_0 (°)	fi (%)	H_{mo} (m)	T_p (s)	a_0 (°)	fi (%)
1st	0.43	5.71	-76.33	0.69	0.73	5.02	-71.75	0.32
2nd	0.43	4.45	-42.54	17.55	0.85	5.21	-46.48	8.97
3rd	0.79	4.63	-8.39	21.39	1.15	5.23	-7.74	11.12
4th	0.54	5.16	12.82	21.81	0.96	5.76	9.74	14.13
5th	0.27	5.74	42.71	4.92	0.68	5.5	41.45	0.45
6th	0.31	5.96	70.29	1.93	0.71	6.02	67.84	0.82
7th	0.94	4.33	-67.08	0.34	1.32	6.76	-69.8	0.11
8th	1.06	5.05	-46.8	12.13	1.42	5.88	-46.07	4.33
9th	2.42	5.22	-7.49	5.17	2.57	5.74	-6.97	4.31
10th	1.71	5.68	7.04	11.72	2.01	6.33	6.61	5.44
11th	0.69	5.91	41.05	1.17	0.87	6.62	39.33	0.37
12th	0.87	5.98	72.06	1.17	1.29	5.8	76.79	0.24
Total				100.00				50.61

5.3. Results and Discussion

In a similar manner to Chapter 2 and 3, in this section the results obtained by the MIKE21 CM-FM coastal area model will be presented and analyzed for all the examined RMWH tests. An advantage of the "Morphostatic" approach to model morphological bed evolution is that it is easier to observe the impact of individual sea-states in shaping the hydrodynamic and sediment transport field and assess the results compared to the "Morphodynamic" approach where the forcing sea-states consecutively succeed one another and hence it is considerably more difficult to assess the impact of each sea-state

individually. In Figure 5.8, the wave and hydrodynamic field after steady state conditions are achieved for the sea-state of the Brute force simulation with the following characteristics H_s=3.06m, T_p=5.81s and MWD=15.27° are presented.

(a)

(b)
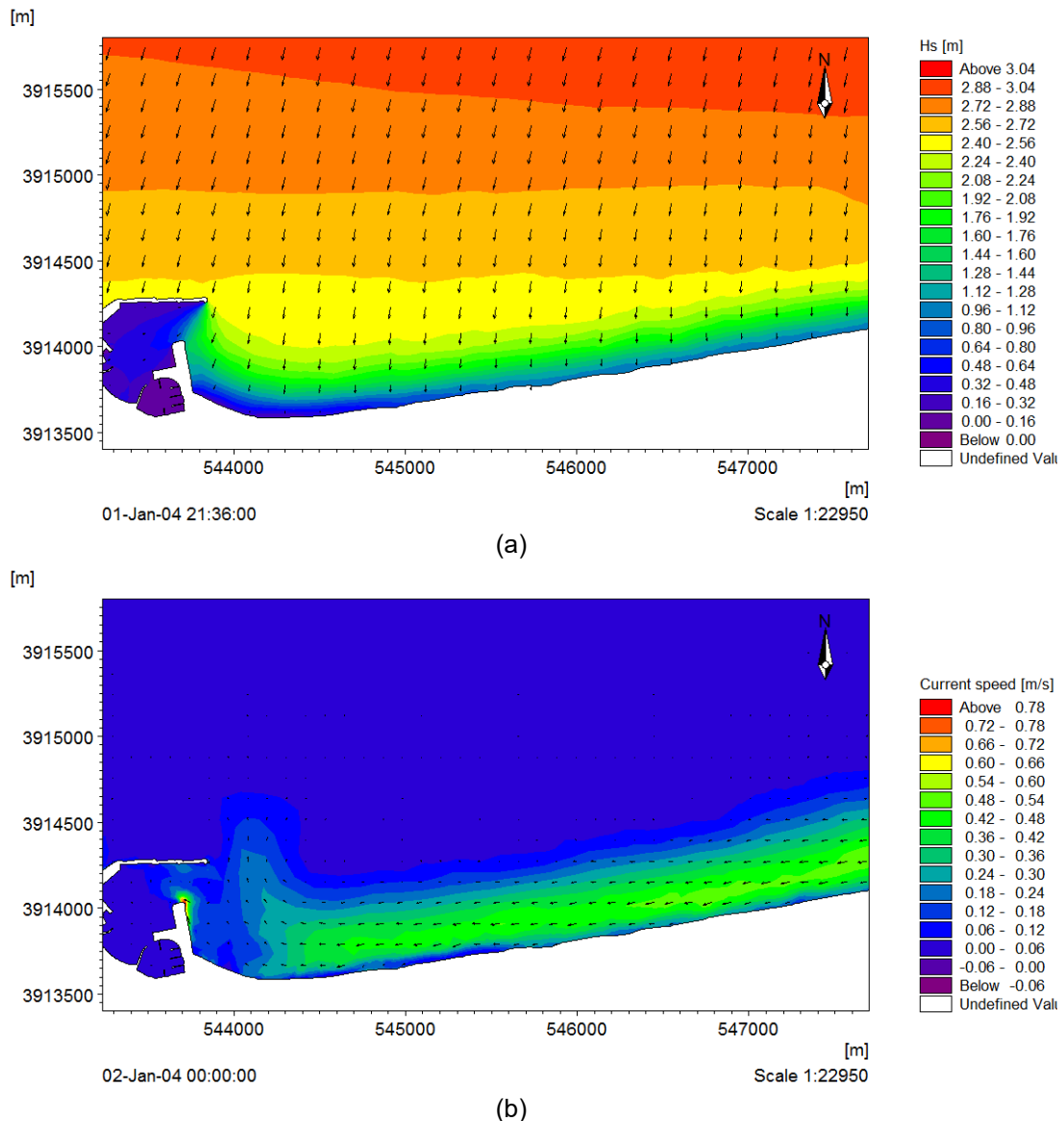
Figure 5.8. Obtained wave (a) and hydrodynamic field (b) for a sea-state with H_s=3.06m, T_p=5.81s and MWD=15.27°.

As can be seen in Figure 5.8, waves refract as they reach the shoreline, with almost perpendicular directions of wave incidence, relative to the shore-normal. The "diffraction patterns" that are observed at the shadow area of the port's main breakwater, are caused by the directional turning of the waves when they reach an obstacle and not by the effect of wave diffraction which was not enabled in the wave simulations. Consequently, phase averaged models such as MIKE 21 SW are not suitable to describe the diffracted waves inside port basins, especially when wave reflection is dominant.

In Figure 5.9 the results of the bed level changes obtained by the Brute force simulation consisting of the 68 sea-states shown in Table 5.3 are presented.
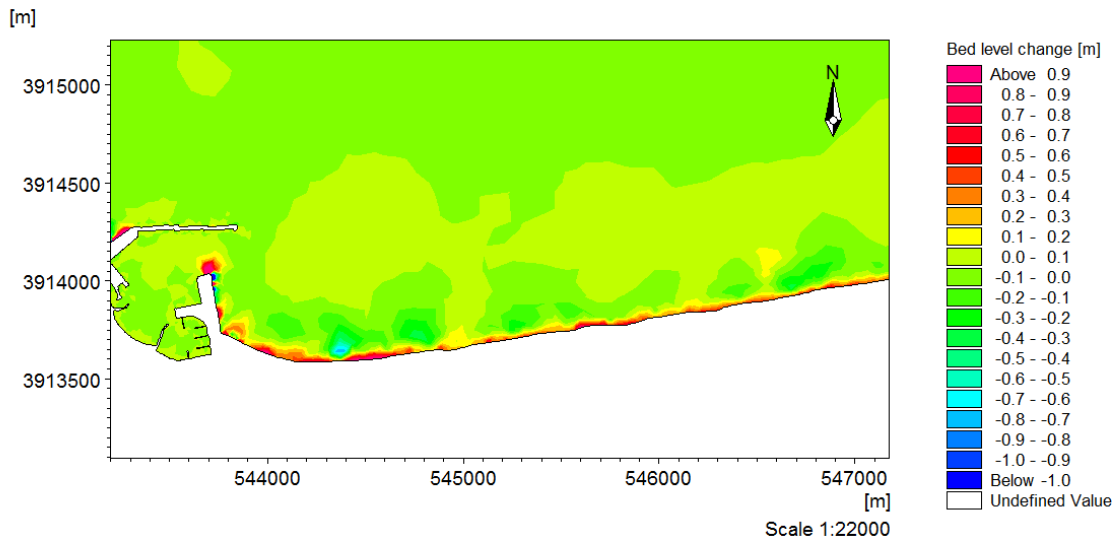
Figure 5.9. Bed level changes obtained by the Brute force simulation.

Observing the results of Figure 5.9, an area of accretion can be distinguished across the shoreline, followed by eroding zones just seaward this zone. The erosion areas are more spatially extended (denoted by the green and light-green colors in the colormap), albeit with smaller intensity compared to the accretion. In the port entrance accumulation of sediment is also observed. Comparing the results to the ones obtained through the Brute force simulation for the same study area and time period performed through the "Morphodynamic" approach in Chapters 3 and 4 (i.e. Figure 4.3), it can be deduced that the two simulations produce similar results as far as the patterns of sedimentation/erosion are concerned. The Brute force simulation of the "Moprhostatic" approach slightly underpredicts the magnitude of the bed level changes, especially for the eroding areas, and the changes occur mainly at shallower depths. The last part can be attributed to the constant feedback between the hydrodynamics and morphology in the "Morphostatic" approach, constantly altering the depths at each morphological time step, hence shifting the breaker zone position for each sea-state and affecting the hydrodynamic and morphological results.

The obtained bed level changes for each alternative simulation sets (RMWH-01 to RMWH-04) examined are shown in Figure 5.10.
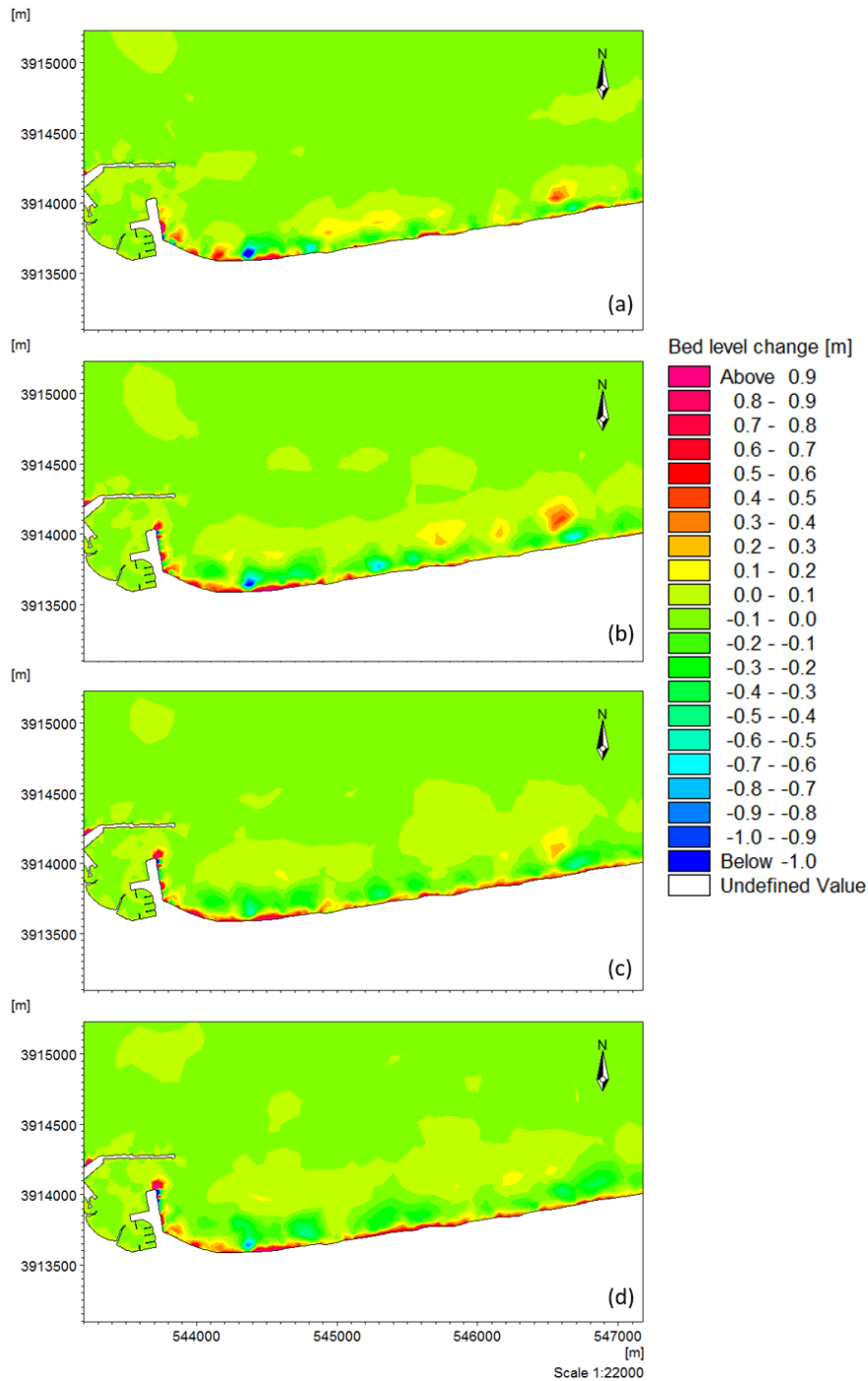
Figure 5.10. Bed level change simulation results for tests (a) RMWH-01, (b) RMWH-02, (c) RMWH-03 and (d) RMWH-04.

Inspecting the results for all the RMWH test simulations, it can be observed that the general morphological features and patterns are adequately reproduced. However, the visual inspection of the obtained results from RMWH-01 identifies significant discrepancies compared to the Brute force simulation. In particular, the erosion at x = 544500 m and y=3913700 m is overpredicted and the accumulation of sediment in the port entrance is not present at all in test RMWH-01. This can be attributed to the shifting of the centroids to less energetic sea-states since division in classes is only undertaken

155

in the directional bins whereas the hydrodynamic patterns leading to deposition of sediment in this are my be caused by more energetic sea-states.

In contrast, test RMWH-02 offers a distinction in overcritical and subcritical classes based on the cumulative energy flux of each directional bin, achieving a better description of the diversity of the wave characteristics in the annual dataset. This seems to lead a significant improvement of model results compared to the benchmark Brute force simulation, where it is noteworthy to mention that all the dominant morphological features can be observed in both the results of both the Brute force and RMWH-01 test. Hence, the simple modification of altering the form of the bins where representative waves will be thereafter calculated improves the results for the specific case study.

Test RMWH-03 expands on the concept of RMWH-02 but utilizes different proxy quantities to define the bins in the wave height based on if the longshore or cross-shore sediment transport influences the morphological evolution. The obtained results are very close to those obtained in RMWH-02, and adequately reproduce the morphological bed evolution of the Brute force simulation. From the visual inspection of the results, test RMWH-04, which utilizes a trained ANN to eliminate sea-states that are considered incapable of initiating sediment motion in the nearshore seems to provide the best reproduction of the morphological changes observed in the Brute force simulation. To further support this assessment, in Table 5.5 the obtained BSS values for the evaluation area shown in Figure 5.2 along with the percentage model run-time reduction compared to the Brute Force simulation are shown.

Table 5.5
Obtained Brier Skill Scores (BSS) in the evaluation area and model run-time reduction compared to the Brute Force simulation for the RMWH simulation sets.

	RMWH-01	RMWH-02	RMWH-03	RMWH-04
BSS	0.24	0.56	0.58	0.65
Simulation time reduction (%)	485	470	462	468

The obtained BSS values for tests RMWH-02, RMWH-03 and RMWH-04 are classified as "Excellent" with respect to the classification proposed by Sutherland et al., 2004a, while the default implementation of Chonwattana et al., 2005, (RMWH-01) is classified as "Good". Consequently, the enhancements to the default method examined in the framework of this thesis lead to a significant improvement of model results validating their use for the annual prediction of coastal bed evolution. Particularly, test RMWH-04, which takes advantage of an ANN to eliminate sea-states that are unable to produce significant morphological changes seems to be the best performing method out of those examined herein. When performing simulations through the "Morphostatic" approach, a significant reduction in model run-time can be observed mostly due to the fact that the forcing wave conditions are reduced from 68 for the Brute force to 12 for the RMWH tests. Some small fluctuations between the model run-time reduction between the

RMWH simulation sets are attributed to the required time to achieve convergence in the MIKE21 wave and hydrodynamic modules, which is not constant for all sea-states, but depends mainly on the wave period and wave height boundary conditions at the offshore boundary.

Chapter **6**

Comparative analysis of Input Reduction methods with field measurements

The assessment of the performance of wave Input Reduction methods is a tedious task, usually requiring conducting a "brute force" simulation (Benedet et al., 2016; Luijendijk et al., 2019; Papadimitriou et al., 2020; Walstra et al., 2013) containing the full offshore sea-state timeseries of wave characteristics. Utilizing "brute force" simulations as the ground truth for validation of model results, obtained by implementing wave input reduction methods, is carried out due to the inherent difficulty of performing detailed field measurements of bed evolution at an annual and inter-annual scale. Recognizing this, in this Chapter an attempt to evaluate the reliability of the wave IR methods examined at the framework of this thesis and compare them with field measurements of beach morphology is undertaken.

It should be noted that obtaining accurate and reliable measurements of the bed evolution of an elongated coastal area (or even individual beach profiles) at these temporal scales is a daunting task. First and foremost, simultaneous and frequent measurements (at least for a full 6-month period and periodically every month up until a year is reached) of offshore wave characteristics, nearshore hydrodynamics and morphology are required to be able to accurately calibrate each driver composing the coastal area model. Ideally, additional measurements of beach morphology & topography should be carried out before and after storm events to assess their impact on the morphological evolution of the upper and lower shoreface. It is obvious that these issues have both economic implications and also add a varying degree of uncertainty if the measuring instrumentation is not properly adjusted and calibrated.

Therefore, due to these restrictions few research efforts (Chonwattana et al., 2005; de Schipper et al., 2016) have been realized to assess the performance of morphological models against field measurements of 2D coastal areas in the medium term (months to a few years). In particular, most research efforts focus on the process-based modelling of the Sand Engine (Stive et al., 2013) mega nourishment project established along the Delfland coast by depositing about 21 million m^3 of sand. The initial annual spreading and morphological response of the mega nourishment has been simulated with the Delft3D coastal area model (Luijendijk et al., 2017a, 2017b). The authors conducted

"brute force" simulations containing the full annul dataset of measured offshore sea-state characteristics and considering the effect of tide and wind and concluded that the default parametrizations of the Delft3D model did not produce a satisfactory morphological response. The need to parametrize the coastal area models to meet the site-specific needs staggeringly increases both the complexity of the simulations and most importantly the computational resources. In addition, the lack of available field measurements of waves and bed elevation in most coasts worldwide, leads most researchers to evaluate the performance of input reduction methods considering brute force simulations containing the full or a detailed representation of the full wave climate as a benchmark and replacement to the measurements (Benedet et al., 2016; de Queiroz et al., 2019; Papadimitriou et al., 2020; Papadimitriou and Tsoukala, 2022; Walstra et al., 2013).

In this chapter, the best-performing input reduction methods were identified by inter-comparing results against detailed bed evolution field measurements of the coastal area at the coast of Skala Eresou in Lesvos Island, Greece. For this reason, a single method for each branch was selected from all of the alternative configurations presented in Chapters 3, 4 and 5 (i.e. binning IR methods, K-Means algorithm and RMWH methods), based not only on the performance and obtained BSS, but also the ease of implementation and computational effort requirements. The three selected methods were then implemented to assess the capability of the MIKE21 CM model to capture the observed coastal bed evolution after a 9-month period and thus provide some initial insights for the optimal wave input reduction method for practical applications.

6.1. Study area and model set-up

In this subsection the main characteristics of the area of interest (i.e. overview, geometry of the coastal bed, sediment characteristics) are presented along with the offshore wave characteristics chosen to force the MIKE21 CM FM. Also, the thought process for selecting the best method for each branch of wave IR methods, presented in Chapters 3,4 and 5 respectively, are laid out.

6.1.1. Area of interest and available data

The coastal area of interest is located in Skala Eresou in Lesvos Island, Greece. The homonymous village has a population of 349 residents according to the census of 2011. The main activities in the village revolve around tourism due to the popularity of the beach of Skala Eresou which is contained within the study area, leading to an increase in the population of up to 6000 people (Velegrakis et al., 2008). It is a barred pocket beach with a length of about 2.2 km bounded in the east by an existing fishing shelter and in the west by the cape of Kofinas. A general overview of the study area is shown in Figure 6.1.

Figure 6.1. The study area of Skala Eresou and its relative position in Lesvos Island (within the red rectangle at the top right picture)

Regarding the geomorphological characteristics of the study area, the sea-bottom contours are relatively parallel to the shoreline in shallower depths, especially in the western part of the study area with the bed slopes reaching about 6.5%, with the presence of bars at depths between 3-5 m. The relative alongshore uniformity of the beach is disturbed to the east and especially close to the fishing harbour. Of particular interest is the presence of the stream "Chalandra" with its outflow situated at the center of the beach which resupplies the coastal zone with sediment. However, the construction of the Chalandra dam in 1999 significantly altered the sediment balance in the coastal zone, withholding up to 52%-55 of the total sediment yield of the catchment area upstream (Velegrakis et al., 2008). The eastern-most part of the coastline has experienced the vast majority of development due to seasonal tourism, with the construction of seawalls and promenades along the coastline. However, these manmade constructions inadvertently have intensified the beach erosion in their vicinity (Karambas, 2010). In general, the coastline of Skala Eresou is retreating at the easternmost part, however it is characterized by high spatial variability due to both the impact of waves and potential resupply of sediment by the "Chalandra" stream.

Detailed bathymetric surveys were conducted at the coastal zone of Chalandra for the time period between 2013-2017, at 6 specific dates (03/11/2013, 26/04/2014, 14/02/2015, 19/11/2015, 29/12/2015 and 22/06/2017). The bathymetric surveys extended between depths of -1.0 to -22.0 m utilizing a singlebeam Hi-Target HD 370 hydrographic eco sounder, at a dense grid of survey lines. In depths shallower than 1.0

m, an RTK DGPS (TopCon Hipper II) was employed to record backshore beach profiles and were combined with the bathymetric measurements (Andreadis O et al., 2017).

Additionally, sediment characteristics were measured at 19 sampling positions, both in shallow and intermediate water depths which are shown in Figure 6.2.
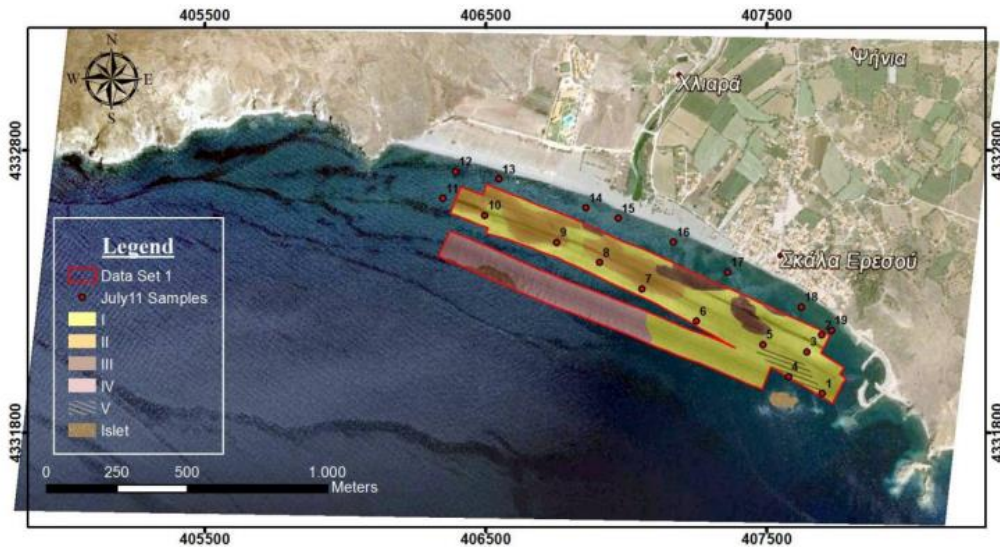
Figure 6.2. Sampling positions where sediment characteristics were obtained (Andreadis, 2022, reproduced with permission from the author)

The median grain diameter (d_{50}) and standard deviation (σ_m) for each sampling position is presented in Table 6.1.

Table 6.1

Mean grain diameters and standard deviation of the sampled sediments at the positions shown in Figure 6.2 (Andreadis, 2022, reproduced with permission from the author).

Sampling ID	d_{50} (mm)	σ_m (Ø)
1	0.44	0.62
2	0.40	0.53
3	0.27	0.58
4	0.36	0.53
5	0.25	0.62
6	0.24	0.77
7	0.27	0.66
8	0.34	0.69
9	0.42	0.68
10	0.41	0.55
11	0.51	0.55
12	0.63	0.65
13	0.59	0.57
14	0.37	0.53
15	1.06	0.85
16	0.41	0.5
17	0.37	0.4
18	0.36	0.47
19	0.44	0.62

As can be observed from Table 6.1, the sediments at the study area mostly consist of medium to coarse sand (Andreadis, 2021). It is also noted that from the conducted surveys, the finer grains were encountered at shallower water depths (h<2.5 m). Finer grain sizes are also present eastward the "Chalandra" stream, with the coarser grains situated westward.

In order to evaluate the morphological model predictions utilizing input reduction methods, it is desirable to compare consecutive bed level field measurements covering almost an entire year. Since this prerequisite was not satisfied in the study area, from the six available dates of conducted bathymetric and topographic surveys, it was selected to evaluate the performance of the morphological model for a period of 9 months between 14/02/2015 and 19/11/2015. The main reason for this selection was to avoid spans larger than one year between consecutive measurements, hence 03/11/2013 to 26/04/2014 and 29/12/2015 to 22/06/2017 were not considered, while simultaneously avoiding evaluating results in dates close to the winter season, where the presence of possible storm events close to the measuring date can distort the evaluation procedure for the extended period.

Due to the absence of offshore wave measurements at the study area, offshore sea-state characteristics were obtained from the CMEMS database at a point showcased in Figure 6.3, using the regional package MEDSEA_MULTIYEAR_ WAV_006_012 (Korres et al., 2019) for the period between 14/02/2015 and 19/11/2015. The wave rose plot for the aforementioned time period is also shown in Figure 6.3.
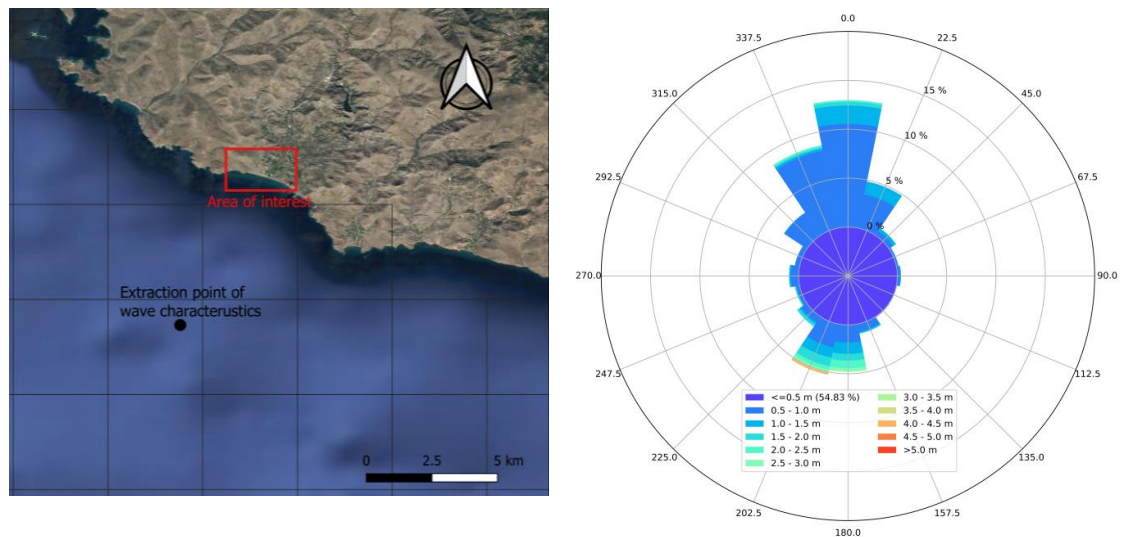
Figure 6.3. Extraction point (a) of wave characteristics and (b) wave rose plot offshore the study area of Skala Eresou, Lesvos Island.

As can be seen in Figure 6.3, with respect to the coastline orientation of the study area (i.e. the shore-normal forms an angle of 202.5° measured clockwise from the true north), waves generated with mean wave direction between [292.5°, 112.5°], i.e. from the WNW, NW, NNW, N, NNE, NE, ENE, E and ESE sectors, are excluded from the analysis since

they are not considered to produce morphological changes in the area of interest. Consequently, from the 8017 wave records 2052 were retained since they propagate towards the study area, i.e. from [112.5°, 292.5°] measured clockwise. The waves with the highest energy capacity are predominantly propagating from the south sectors. To support this, the largest wave encountered in the dataset, in terms of significant wave height propagated from the south sector with the following characteristics: H_s=4.45 m, T_p=8.39 s and MWD=197.26°.

6.1.2. Computational mesh and model parametrization

For the simulation of the wave propagation, hydrodynamics and morphological evolution the MIKE21 CM FM was once again utilized. It was selected to proceed with the "Morphostatic" approach, where each simulation with the respective representative wave forcing input is executed considering the same initial bathymetry. This approach was selected since it is easier to calibrate the model parameters and assess the morphological response of each representative simulation compared to the more complex "Morphodynamic" approach (Olij, 2015). Additionally, since all simulations are based on the same initial bathymetry, the effect of wave chronology has no effect on the integrated result.

The initial bathymetry contained data from the conducted bathymetric and topographic surveys in 14/02/2015. It should be mentioned that the coastline position was extracted by digitizing points with zero elevation, after performing linear interpolation on the original bathymetric and land elevation points. A finite element mesh was constructed based on the above, containing three density levels, a sparser area covering the offshore domain (with a local maximum area of 2500 m^2 per element), a finer, which extended from the intermediate waters up to depths of about 4.0 m at the (with a local maximum area of 300 m^2 per element) and a very detailed dense area, extending from 4 m deep up to the west shoreline (with a local maximum area of 80 m^2 per element). Furthermore, a circular offshore wave generation boundary was considered. The finite element mesh and the initial bathymetry, with the corresponding three distinct mesh density levels, is shown in Figure 6.4.
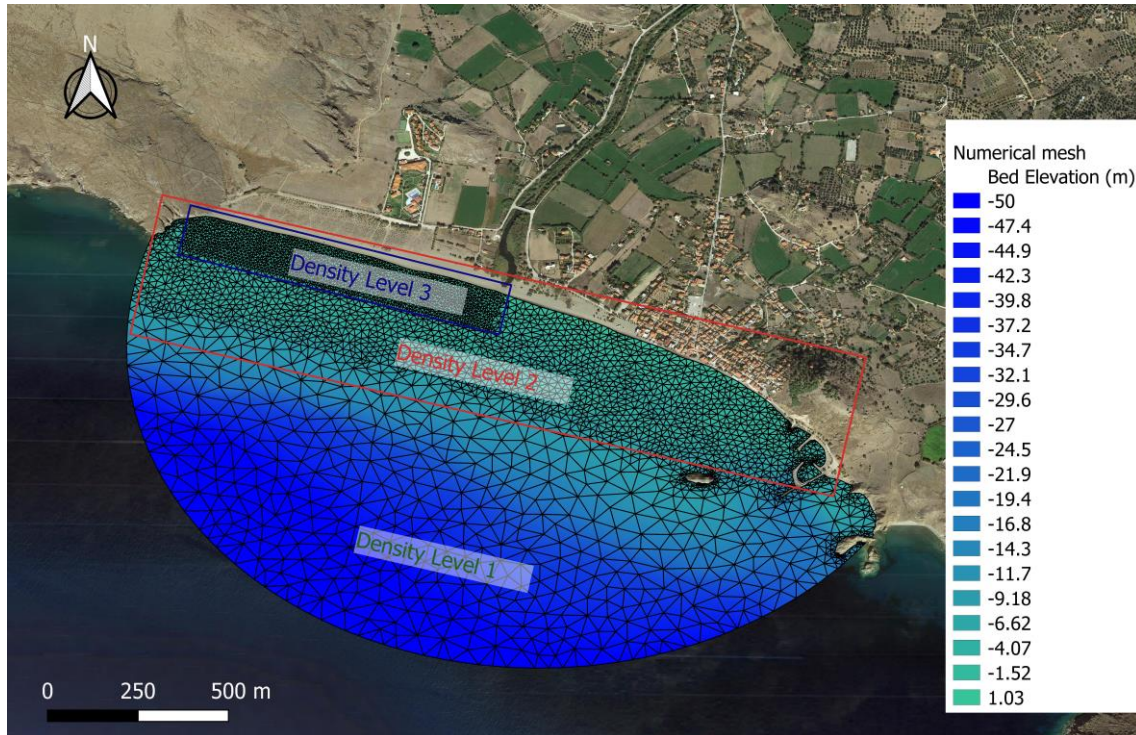
Figure 6.4. Computational mesh and initial bathymetry of the study area for the date of 14/2/2015.

To evaluate and validate the morphological model results the coastal area situated eastward the Chalandra stream was excluded from the calculations, since the presence of manmade construction works (such as seawalls and the port infrastructure) in this highly urbanized area render the inclusion of wave reflection and diffraction in the wave driver mandatory. Since MIKE21 SW is a spectral wave model, it is not capable of resolving the processes of wave reflection and diffraction, it is not deemed suitable for the purpose of evaluating results in this area. Consequently, morphological model evaluation focused in the coastal area situated west of the "Chalandra" stream at the area described in Figure 6.4 located within the mesh "Density Level 3", where there is not significant presence of reflecting walls or rocky foreshores.

The performance of the morphological model was evaluated by calculating the BSS values by considering the bathymetry of 14/2/2015 as the baseline and the bathymetry of 19/11/2015 as the measured quantity. The BSS values were evaluated in 4 distinct coastal profiles (extending up to 4 m deep), shown in Figure 6.5, and superimposed with the measured bathymetry of 19/11/2015, extracted from the bathymetric surveys.

Figure 6.5 shows that the profiles where model results were evaluated are concentrated in an area where the sediment characteristics are mainly constant (as shown in the sampling points 10, 11, 12, 13 in Figure 6.2 and Table 6.1). Taking this into consideration, a mean value of the median sediment grain diameter and grading from the abovementioned 4 sampling points was considered and set as a constant through the whole numerical domain.
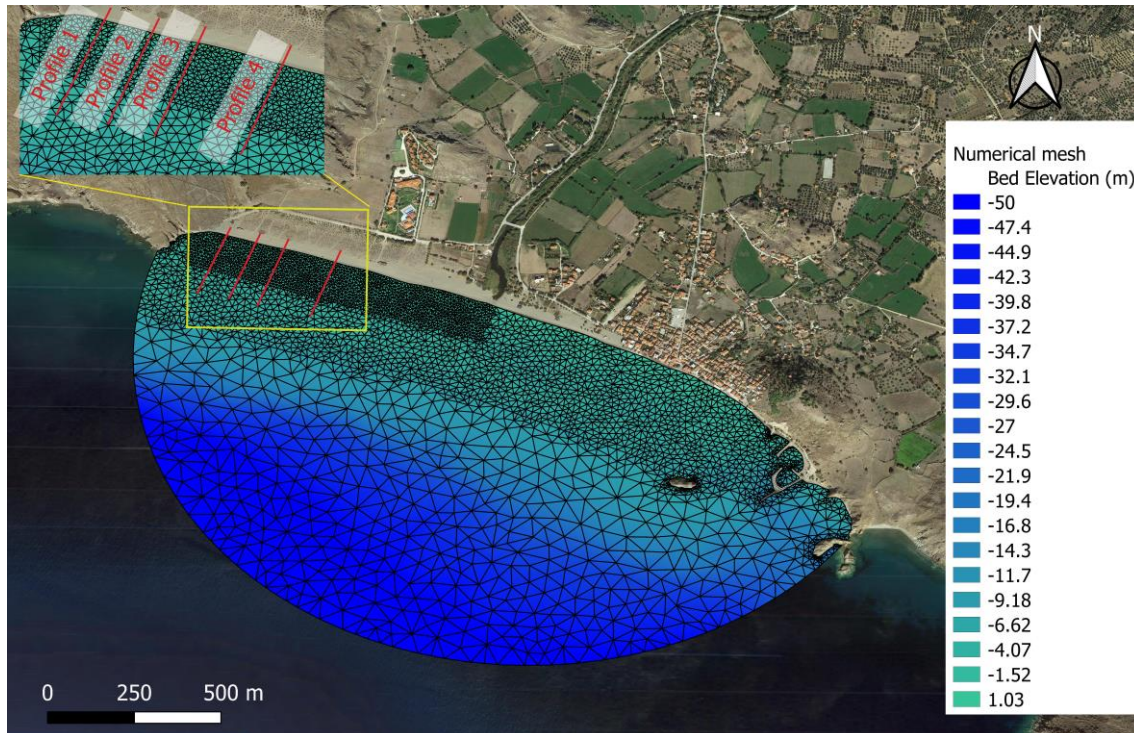
Figure 6.5. Computational mesh and measured bathymetry of the study area for the date of 19/11/2015 and control sections where model results were evaluated.

After constructing the mesh, calibration of the necessary model parameters to produce correct and consistent order of magnitude of the bed level predictions was undertaken. Observing that the offshore waves (Figure 6.3) are generated predominantly from the S (MWD=180˚) and SSW (MWD=202.5˚) sectors, accounting for about 76% of the waves propagating towards the study area, a single representative "equivalent wave" was calculated for each of those sectors though the system of Eq. (2.15). The subsequent task concerns conducting several trial-and-error simulations to determine the appropriate simulation time for the composite model and the values of important calibration parameters. Usually, a good indication of the appropriate simulation time is when the bed level changes are inconsequential (order of magnitude less than 1-2 mm between two plotting model time steps), and the coastal bed reaches an "equilibrium" state.

Due to the absence of wave measurements in the study area, the calibration parameters of the wave breaking criterion were set at their default values. Since the sediment median diameter was obtained from in-situ measurements the most important calibration parameter is the Manning friction coefficient which significantly affects the results of the hydrodynamic and sediment transport models. Summarily, the trial-and-error simulations were mostly aimed at capturing the correct order of magnitude of the bed level changes at the section of "Profile 4" (Figure 6.5), by specifying the total time of each representative simulation and the value of the Manning's coefficient. In Table 6.2, the most important parametrizations set in the MIKE21 SW, MIKE21 HD and MIKE21 ST models are compiled and shown.

Table 6.2
Significant model parameters determined through a trial-and-error set of simulations.

Model parametrizations	
Simulation time (s)	132600
Time step (s)	30
Staring time for the morphological simulation	36000
Manning coefficient ($m^{1/3}/s$)	39
d_{50} (mm)	0.535
σ_m ($\varnothing$)	0.58

The parameters shown in Table 6.2 were then consistently set in all the necessary simulations conducted for each representative of the selected IR methods.

6.1.3. Selection of the optimal input reduction methods

In this subsection a sole wave input reduction method out of those presented and evaluated from each branch, i.e. Binning IR methods (Chapter 3), K-Means clustering algorithm (Chapter 4) and RMWH selection approaches (Chapter 5), will be selected based on the accumulated experience obtained by implementing them in the coastal area of Rethymno, Greece. It is noted that apart from choosing the best performing method with regards to the calculated BSS values, significant consideration was given to the relative complexity of each method's implementation and possible additional requirements of computational resources.

The Binning IR methods examined in Chapter 3 were the Energy Flux Method, and two methods developed in the framework of this thesis, the Pick-up rate (Papadimitriou et al., 2020) and Threshold Current method. From the intercomparison of the three methods in the coastal area of Rethymno, the best performing one with respect to the BSS values was the Energy flux method, followed by the Pick-up rate and Threshold Current methods, which were similar in performance. The most alluring aspect of the newly developed methods is the significant model run-time reduction achieved by eliminating wave records unable to initiate sediment motion and thus reducing the length of the dataset of offshore sea-state wave characteristics, when following the "Morphodynamic" approach. However, this is not the case when performing simulations through the "Morphostatic" approach, where each representative is assigned the same simulation time. Inadvertently, in this case the utilization of a robust -yet complementary- PMS wave model to estimate wave characteristics in the nearshore for those two methods can increase the required computational effort. Based on its reduced complexity and ease of implementation, the fact that it was the best performing one in the case study of the Rethymno coastal area, and that it has been used consistently with satisfactory results in numerous research efforts (Benedet et al., 2016; de Queiroz et al., 2019;

Papadimitriou et al., 2020; Walstra et al., 2013), it was chosen to proceed with the Energy Flux wave schematization method as the representative of the Binning IR methods.

In Chapter 5, six different alternative configurations of the K-Means clustering algorithm were implemented, to evaluate its viability as a wave input reduction method. With regards to the obtained BSS values the best performing tests were found to be KM-05, which initiates the centroid selection based on the representative wave conditions obtained by implementing the Pick-up Rate wave IR method and KM-06, which combined the swap of the input clustering variables and filtering of wave records producing minimal (close to zero) longshore sediment transport rates. The default implementation of the clustering algorithm (test KM-01), as shown by the visual inspection of the bed level change results (Subsection 4.3) and the obtained BSS produced a satisfying reproduction of the benchmark Brute force simulation. It should be noted that test KM-05 and KM-06 exhibited a marginal improvement of performance compared to the KM-01 test, however they are rather complex for implementation in practical applications considering that they require additional numerical simulations through the PMS-SP wave model. This increases the requirements for computational effort, especially when the "Morphostatic" approach is followed. Additionally, the conceptualization and methodology of these tests is rather complex and hence more difficult to implement for practical applications. On the other hand, even though test KM-01 produced slightly worse BSS compared to the other examined tests, it is far easier to implement and requires minimal user interference. To further support this, it is noted that only the total required number of representatives has to be specified before the algorithm execution, without providing the number of subdivisions in the wave height and direction bins, which is a prerequisite for the traditional Binning IR methods. Ultimately, based on the above assessment the default implementation of the clustering algorithm (KM-01) was selected and utilized to assess the bed level evolution at the coastal front of Skala Eresou.

Regarding the RMWH selection methods examined in Chapter 5, the best performing one, with respect to the obtained BSS values was RMWH-04 closely followed by RMWH-03. The former test incorporated the use of a properly trained ANN tasked with the calculation of the wave orbital velocity and elimination of wave records unable to initiate sediment motion, while the latter was based on the definition of transition zones with interchanging influence of longshore and cross-shore sediment transport. RMWH-03 is very computationally efficient since the implementation of the ANN considerably speeds up the elimination of the lowly energetic sea-states. On the contrary the transition zone method, despite including relatively simplified calculations, is more taxing computationally for practical applications, due to the complexity of distinguishing the transition zones. The classical RMWH-01 method is relatively easy to implement, however for the analysis carried out in Chapter 5 it was the worst performing one in tests of the morphological response and obtained BSS values. A relatively simple modification to RMWH-01, namely test RMWH-02, which creates subdivisions in both the wave height and direction sectors lead to a significant performance increase. Summarily, based on the very low requirements in computational resources and the fact that it was the best

performing method with regards to the BSS for the case study of Chapter 5, the RMWH-04 method was chosen as the optimal one out of all the tested Representative Morphological Wave Height selection methods.

To provide a more comprehensible overview of the comparative analysis carried above, Table 6.3 presents a grading system of all the different methods and tests to support the selection of the three representative methods out of the prevalent branches of wave input reduction. The two criteria considered were model performance (judged mostly by the obtained BSS values for the case studies of Chapters 3,4 and 5) and computational efficiency (mostly revolving around ease of implementation and requirements of computational resources). The minimum and maximum values of the available grades are 1 and 5, signifying the worst and best behaviour respectively. The method with the highest total score was the one ultimately selected. It is imperative to note that the grading system is based on the experience obtained from the analysis carried out in the previous Chapters for the study area of Rethymno, Greece and should not be interpreted as universal criteria.

Table 6.3
Comparative grades of each wave IR method based on its performance and computational efficiency for the "Morphostatic" simulation approach. Higher grades (in bold fonts) denote the best performing method for each wave IR branch.

wave IR branch	wave IR method	Performance /Skill	Computational Efficiency	Total score
Binning IR methods	**EF method**	5	4	**9**
	PR method	4	3	7
	TC method	4	3	7
K-Means clustering	**KM-01**	3	5	**8**
	KM-02	3	4	7
	KM-03	3	4	7
	KM-04	3	3	6
	KM-05	4	3	7
	KM-06	4	3	7
RMWH selection methods	RMWH-01	2	4	6
	RMWH-02	3	4	7
	RMWH-03	4	3	7
	RMWH-04	4	5	**9**

As a disclaimer, the grades shown in Table 6.3 concern simulations conducted through the "Morphostatic" approach which is the focus of this Chapter. For instance, when performing simulations through the "Morphodynamic" approach, the grades of the computational efficiency category for the Pick-up rate and Threshold Current Binning IR methods are expected to reach higher values, while the corresponding ones for the EFM will be considerably reduced.

6.1.4. Representative wave conditions

In this section, the representative wave conditions obtained by implementing the Energy Flux, K-MEANS (KM-01) and RMWH-04, i.e. the representative morphological wave height selection method incorporating an ANN tasked with elimination of sea-states considered unable to initiate sediment motion. As has been previously mentioned, the shore-normal forms an angle of 202.5° measured clockwise from the true north, hence waves approaching the coastline with incidence angles larger than |90°| relative to the shore-normal were eliminated from the dataset since these waves do not influence the morphological bed evolution. It is noted that wave incidence angles of -90° denote waves propagating from the East sector, whereas angles of 90° denote waves propagating from the West sector respectively. Consequently, for the examined time period, 2052 hourly changing wave records approached the shoreline with angles of wave incidence capable of producing longshore sediment transport and inducing morphological changes. It should be mentioned that in a similar manner to the previous Chapters, 12 wave representative conditions were considered and kept constant for the three examined wave schematization methods examined herein.

The representative wave conditions obtained by implementing the Energy flux method of wave schematization are showcased in Figure 6.6.
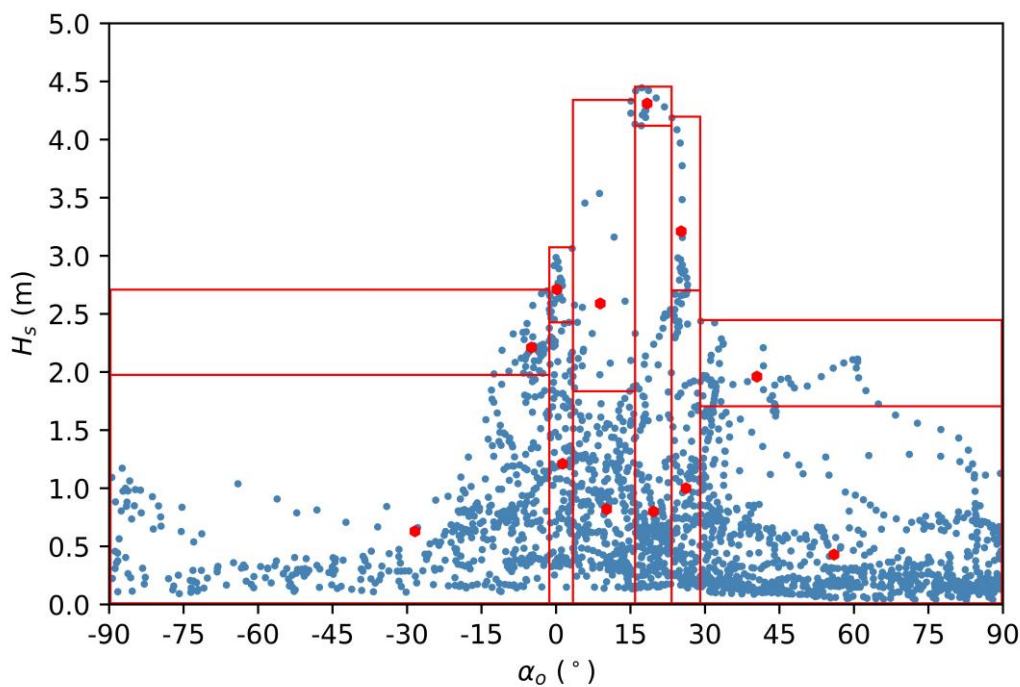
Figure 6.6. Obtained 12 representative wave conditions (red markers) by implementing the Energy Flux wave schematization method.

As expected, since the waves with the highest energy flux capacity have wave incidence angles with $a_0=[0°, 30°]$, six out of the possible twelve representative conditions fall within this range. The representative wave condition with the highest energy flux capacity has the following characteristics: H_s=4.31 m, T_p=8.39 s, MWD=198.37° with a frequency of occurrence f_i=0.44 %.

Subsequently, the wave representatives obtained by implementing the K-Means algorithm (KM-01), utilizing the K-Means++ centroid initialization algorithm and setting the maximum number of iterations to 1000 are showcased in Figure 6.7.
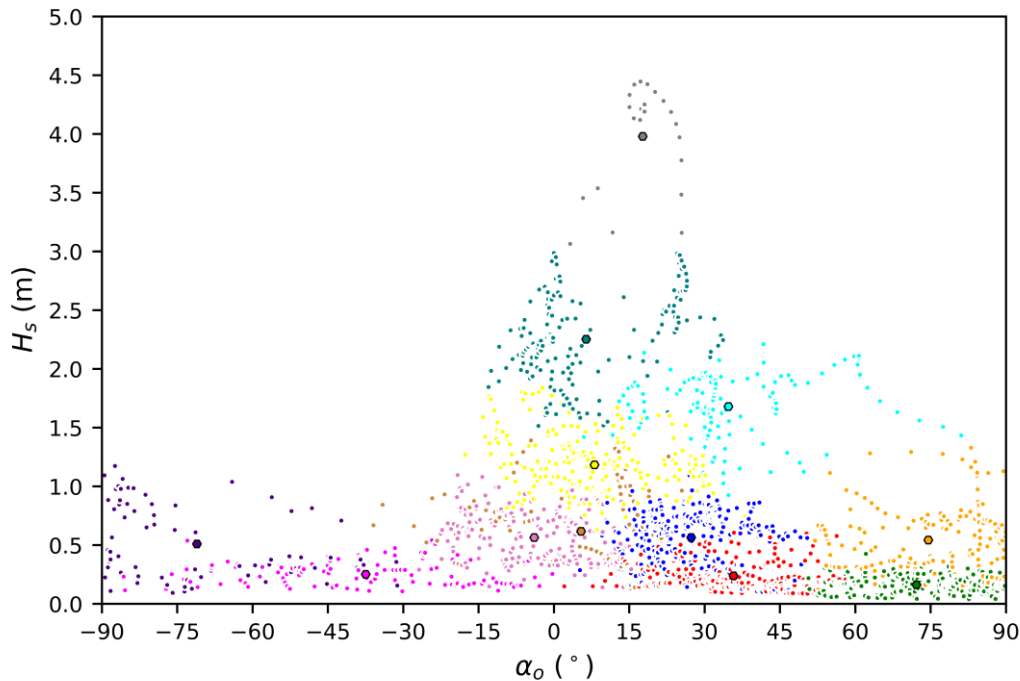
Figure 6.7. Obtained 12 representative conditions (larger pentagon markers) and respective clusters, by implementing the KM-01 wave schematization method.

Due to the nature of the offshore wave climate at the study area, implementation of the KM-01 wave schematization method leads to the formation of 5 representative sea-states within the range of $a_0=[0°, 30°]$, in a similar manner to the Energy Flux wave input reduction method. In contrast to the Energy flux wave schematization method, KM-01 calculates centroids with higher representative angles of wave incidence for the sea-states located further from the shore normal. The representative sea-state with the highest energy capacity has the following characteristics: H_s=3.98 m, T_p=8.36 s, MWD=197.70° with a frequency of occurrence f_i=1.12 %.

In order to implement the RMWH-04 method the following parameters were supplied as input to the ANN regarding the mean sediment grain size and beach slope were supplied: d_{50}=0.535 mm and $\tan\beta$=1/50. The ANN led to the elimination of 1455 sea-states, effectively reducing the length of the dataset by about 70%. The representative wave conditions, by implementing the RMWH-04 wave schematization method are presented in Figure 6.8.
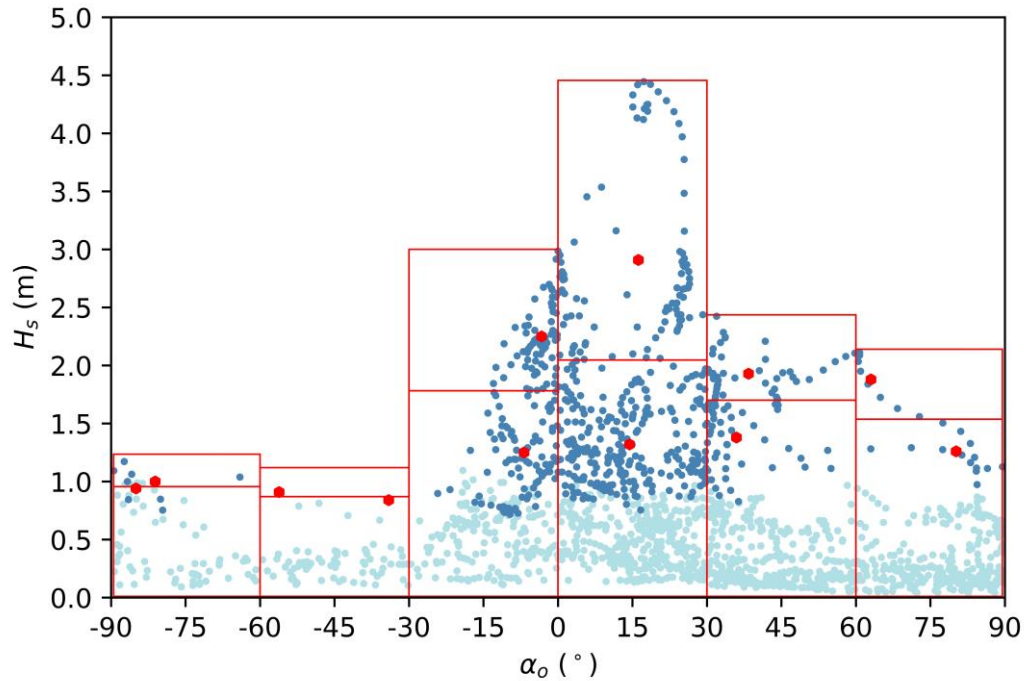
Figure 6.8. Obtained 12 representative conditions (red markers) and bin boundaries (red rectangles) by implementing the RMWH-04 method. The light blue markers denote sea-states eliminated by the ANN whereas dark blue markers denote those retained in the dataset.

The elimination of sea-states considered unable to initiate sediment motion leads to a major altering of the obtained representatives and the corresponding frequencies of occurrence. Of particular interest is the directional bin of $a_0=[-60°,-30°]$, where only two sea-states were retained in the dataset after the implementation of the ANN, hence they are considered as two of the obtained twelve representative conditions. The elimination of lowly energetic sea-states leads to the shift of the wave representatives to more energetic centroids, with the less energetic representative sea-state having the following characteristics: H_s=0.91 m, T_p=5.21 s, MWD=123.85° with a frequency of occurrence f_i=0.5 %. In contrast, the representative wave conditions with the highest energy flux capacity (H_s=2.91 m, T_p=7.49 s, MWD=196.17°) is significantly milder than the corresponding ones obtained through the Energy Flux and KM-01 wave schematization methods, however it is associated with a significantly higher frequency of occurrence f_i=4.87 %.

6.2. Results and intercomparison of input reduction methods

In this section the results of the predicted bed levels after obtaining a weighted average of the simulations with the 12 representative wave conditions obtained with the EFM, KM-01 and RMWH-04 wave schematization methods are presented and compared to the measured values from the bathymetric survey conducted in 19/11/2015 in the study area. As has been previously mentioned, the evaluation of results was carried out in four coastal profile sections Figure 6.5) focusing on part of the study area where the sediment grains are comprised mostly of fine and medium sand.

The computed bed levels from each wave IR method along with the measured values of the Initial (14/2/2015) and Final (19/11/2015) bathymetry are shown in Figure 6.9 for Profiles 1 and 2 and Figure 6.10 for Profiles 3 and 4 respectively. Observing the Initial and the Final bathymetry for all sections, significant accretion volumes are distinguished extending from the shoreline up to the bed elevation of -4 m. The largest proportion of sand is accumulated up to the bed level of -2.5 m, signifying that the coastal processes take place shoreward this depth. However, especially in Profile 3 the formation of an elongated bar can be observed, extending up to 250 m from the initial shoreline position and reaching bed levels of about -4.5 to -5.0 m.

In general, the three examined Input Reduction methods are capable of reproducing the observed accretion patterns especially between bed levels of -1.0 and -2.5 m in all the examined Profile Sections. However, the model forced with the representative wave conditions for all three methods seems unable to capture the accretion of the shoreface (the model consistently predicts erosion at depths less than 0.5 m) and at depths >3.0 m for most Profile sections.
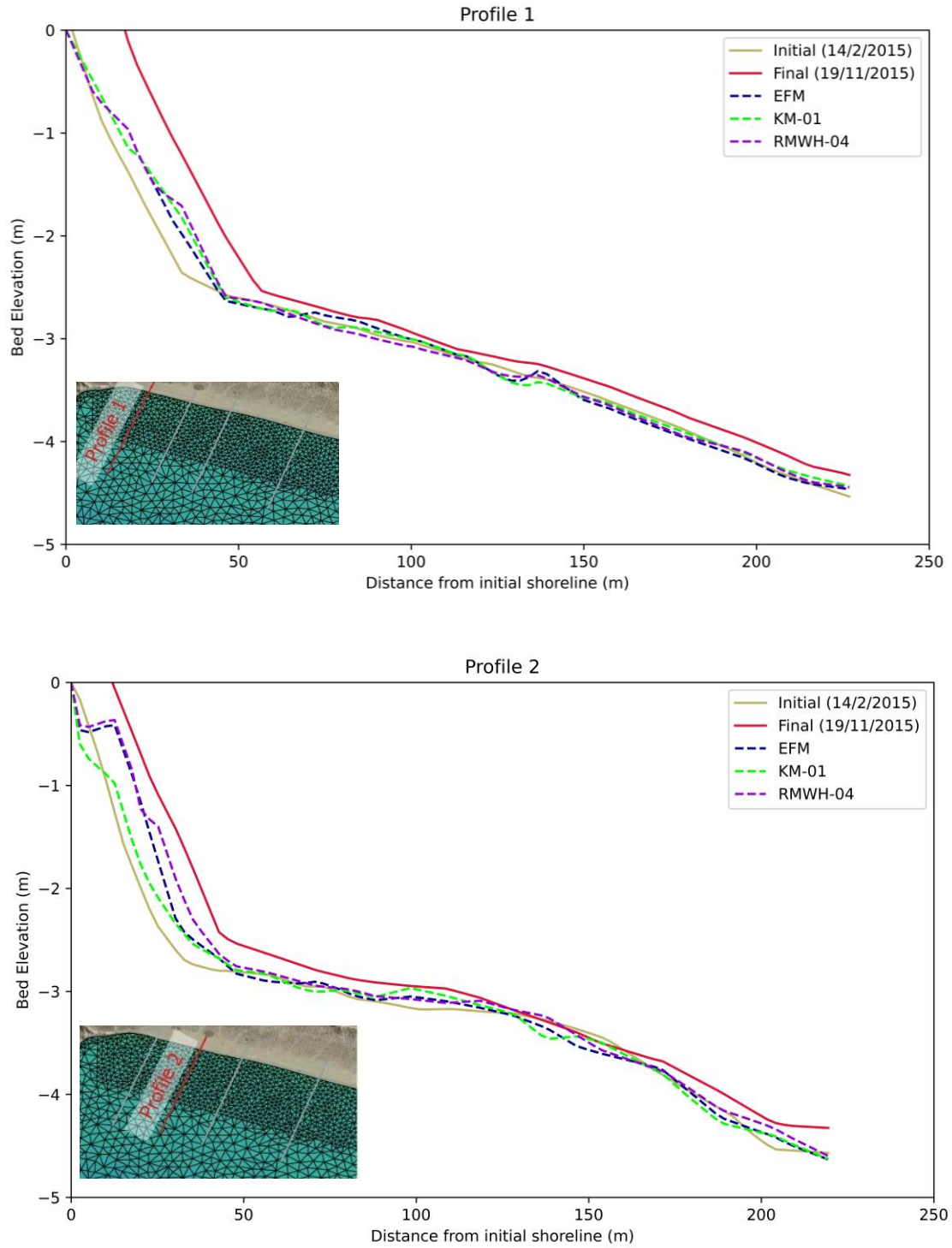
Figure 6.9. Measured and simulated bed elevation at Profile 1 (top) and Profile 2 (bottom) by implementing the EFM, KM-01 and RMWH-04 wave input reduction methods.
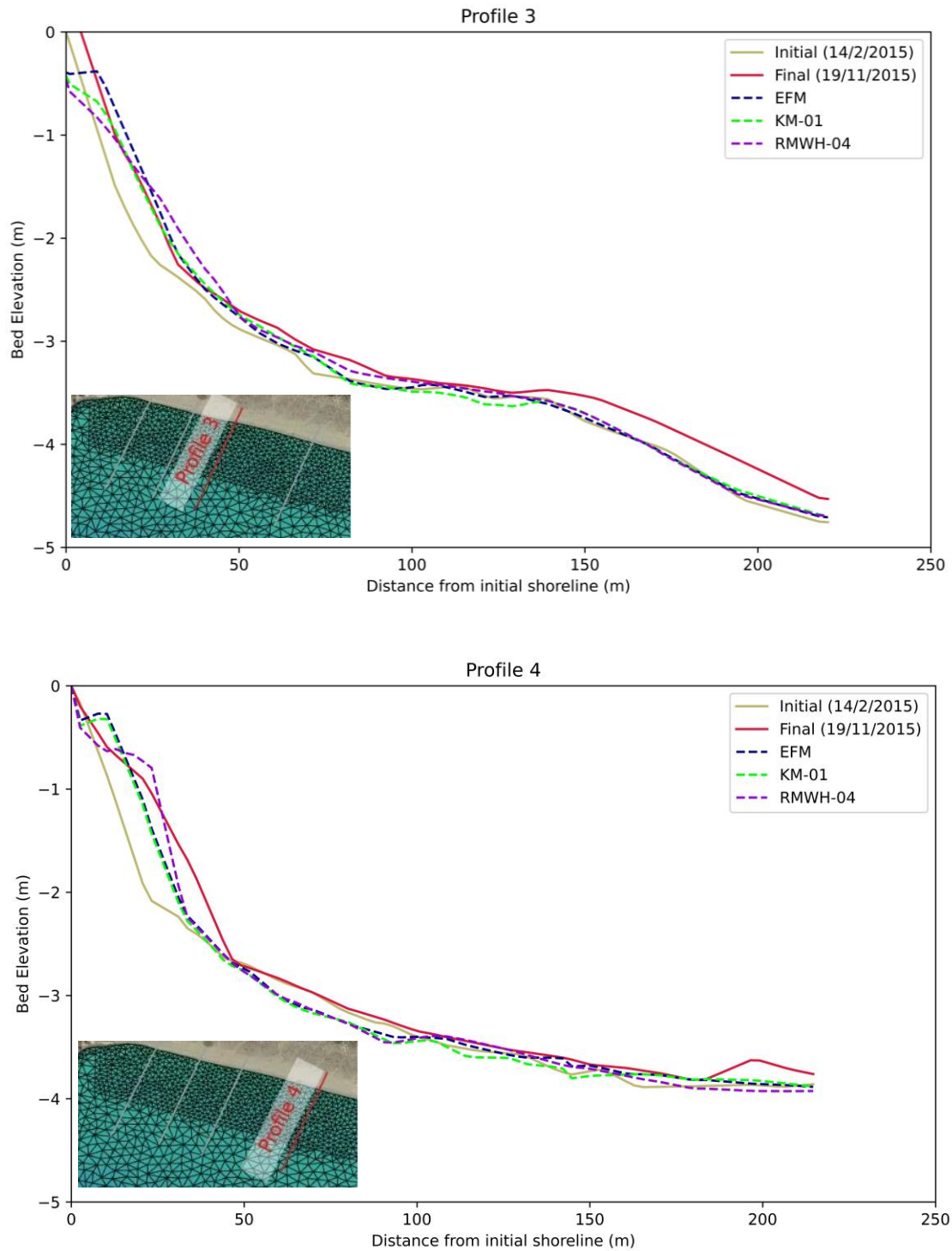
Figure 6.10. Measured and simulated bed elevation at Profile 3 (top) and Profile 4 (bottom) by implementing the EFM, KM-01 and RMWH-04 wave input reduction methods.

For Profile 1, large discrepancies are observed between the final measured bed level of 19/11/2015 and the computed one from each of the EFM, KM-01 and RMWH-04 methods. At this Profile a large volume of sand was accumulated at the shoreface, with the largest observed relative bed level change between the two measurement dates

174

being 1.68 m. Out of the three examined wave IR methods, no clear distinction can be made on the best performing one visually, since the obtained patterns are similar for all three. It is noteworthy that at shallow depths < 0.5 m the EFM and RMWH-04 methods give almost identical results. It should be noted that this Profile is located the furthest from the boreholes that measurements of sediment characteristics were available, which can in part explain the deviations between the coastal area model and measurements.

Observing Profile 2, the computed bed levels of RMWH-04 and EFM are similar, with the KM-01 method deviating the most from the final measurements. In particular, RMWH-04 seems to be the best performing one, predicting largest accretion volumes between 25 and 50 m offshore the initial shoreline position and once again between 130-142 m.

In Profile 3, all three examined methods capture the correct order of magnitude of bed level changes between 20-40 m from the initial shoreline position, with the RMWH-04 and KM-01 method giving almost identical predictions with the measured values at the distances between 22-32 m. All three methods are unable to reproduce the bar formation which is present at distances between 130-250 m from the initial shoreline position. This implies coastal processes at relatively large depths, which can be attributed to long-waves with wider surf-zones, which cannot be reproduced with the wave representative inputs, since no significant swell signal was present in the wave records obtained from the Copernicus Service database for the given time period.

Finally, in Profile 4, at the end of the 9 month period, the coastal profile takes a bilinear form, with two distinct bed slopes forming and separated at bed level of about -2.6 m due to the significant accumulation of sand in the shoreface. The RMWH-04 method seems to perform better at this section, capturing the order of magnitude of the observed bed level changes in a more satisfying manner. Once again, when the depth is higher than 2.5 m no significant bed level changes relative to the initial bathymetry are observed to the coastal area model prediction, whereas that is not the case in the measured profile.

In general, all coastal profiles exhibit increased accretion volumes throughout the upper and lower shoreface. Since an equilibrium of erosion accretion is not identified in the coastal profile, this implies that sand is transported longshore from the east to the west, which verifies the observed erosion at the easternmost area (Karambas, 2010).

To ultimately assess the performance of the morphological model forced with the three examined wave IR methods, the computed BSS values are computed for the four coastal Profiles and shown in Table 6.4. It is noted that within the brackets, the classification scores of each simulation according to Sutherland et al., 2004a, is also shown, with E, G, R/F, P, B denoting Excellent, Good, Reasonable/Fair, Poor and Bad model performance respectively.

Table 6.4
Calculated BSS values and classification score at each coastal Profile for the EFM, KM-01 and RMWH-04 wave IR methods. Bold fonts denote the best performing method in each Profile.

	EFM	KM-01	RMWH-04
Profile 1	0.25 (G)	**0.29** (G)	0.28 (G)
Profile 2	0.54 (E)	0.19 (R/F)	**0.69** (E)
Profile 3	**0.23** (G)	0.2 (R/F)	0.22 (G)
Profile 4	0.66 (E)	0.42 (G)	**0.68** (E)

Overall, the best performing method is the RMWH-04, achieving the highest BSS values at two (Profile 2 and Profile 4) of the four coastal Profiles, with the respective simulations classified as "Excellent". The EFM closely follows with an "Excellent" performance the abovementioned Profiles, albeit with smaller BSS values. The KM-01 seems to consistently perform worse, with performance ranging from "Reasonable/Fair" to "Good", although it achieved the highest BSS value at Profile 1.

From the comparative analysis of the three wave IR examined in this Chapter, it is deduced that all three can be applied in coastal areas and produce acceptable results for the monthly to annual prediction of bed level changes. Given the overall very satisfactory performance and also considering its ease of implementation, it is proposed that the **method RMWH-04 with 12 representative conditions** be applied in coastal areas when desiring to obtain reliable predictions of the coastal bed evolution, predominantly induced by waves and currents.

6.3. Discussion

Despite the overall satisfactory performance of the examined wave IR methods, compared to real field measurements, a large number of uncertainties are present in the analysis of this Chapter, concerning mostly the conduction the availability of the measurements and data. Consequently, the most important uncertainties associated with the conducted analysis are hereafter denoted.

As has been previously mentioned, in the four examined Profile sections significant accretion was observed at the shoreface between February and November of 2015. It is noteworthy that for most cross-sections, a positive balance of sediment volume was observed (predominantly in Profile 1), which signifies the presence of external sediment sources, supplying nearshore area with large quantities of sediment. As stated in Velegrakis et al., 2008, the construction of the Chalandra dam in 1999 significantly altered the sediment balance in the coastal zone, withholding on average up to 52%-55 of the total sediment yield of the catchment area upstream, however the measurements suggest that close to the last measuring date (19/11/2015), and possibly to avoid overflow, the spillway of the dam could have opened and thus provided an external source of sediment in the coastal area.

In the same vein, no intermediate bed level measurements were conducted between the two examined dates. Carrying out bed level measurements at intermediate dates would further aid in understanding the underlying processes driving coastal bed evolution

and help eliminate the possibility that the last measurement could be a snapshot of the impact of recent storm events in the study area. Although the presence of storm events close to the measuring date cannot be excluded, the general model and measured patterns suggest that for the particular timespan the two measured bathymetries represent the impact of the sea-states between February and November of 2015. Additionally, the momentary sea-level elevation in the shoreline due to storm surge and astronomical tide at the measuring dates can inadvertently influence the measurements of the bathymetry and topography especially altering the exact shoreline position.

Due to the absence of wave and current measurements, the thorough calibration of the wave and hydrodynamic modules of the coastal area model was not feasible. Of particular importance is the absence of wave measurements offshore the study area. This resulted in utilization of the Copernicus database for the acquirement of hourly wave characteristics from hindcast simulations for the desirable 9-month time period. Although the Copernicus database is one of the most esteemed and thoroughly validated databases, the absence of information on the exact wave climate at the study area, obtained by measurements, introduces a level of uncertainty on the prediction of the bed level changes induced predominantly by the effect of the waves. Specifically, the measured morphological patters at the examined Profiles (especially in Profiles 1 and 3), imply the presence of swell systems affecting the study area, which might be responsible for the formation of bars at depths > 3 m. Due to the absence of swell signal in the obtained dataset of offshore sea-state wave characteristics, the coastal area model cannot reproduce the observed changes, and ultimately, despite the very good model performance in the shallower areas, the calculated BSS values are lower than expected. Some of the errors in the calculations can be attributed to the selection of the "Morphostatic" simulation approach, which does not take into account the constant feedback between waves, hydrodynamics and morphodynamics. It should be noted however, that a "Morphodynamic" simulation approach with a Morfac value of 1, which is the more accurate approach, would be prohibitive for this field case-study in terms of required computational time & resources.

Finally, the MIKE21 model is based on a spectral wave driver and fails to reproduce the formation of the upper shoreface and hence cannot simulate the hydrodynamic and moprhodynamic processes in the swash zone. The selection of an appropriate phase resolving model (e.g. Afentoulis et al., 2022; Chondros et al., 2021; Karambas and Samaras, 2017) which can simulate the morphodynamic evolution in the swash zone, could further improve the morphological model results, although it would inadvertently increase the required level of computational effort.

Summarily, the following factors introduce uncertainties in the analysis of comparing the morphological model results with real-field measurements of bed elevation:

> ➢ The presence of possible external sediment sources, supplying the nearshore with large volumes of sediment combined with lack of information on the operation of the "Chalandra" dam at the examined time period.

➢ Absence of intermediate bed level measurements, to ensure that the model evaluation is not skewed by the possible occurrence of storm events near the measuring dates.

➢ Absence of measurements of wave-induced current nearshore and wave charactristics offshore the study area to calibrate the hydrodynamic and wave model.

➢ Due to the absence of wave measurements, hindcast data from oceanographic databases were utilized to obtain the initial forcing dataset of the coastal area model, which affects the undertaken analysis and evaluation.

➢ Utilization of a linear model, which is not capable of simulating hydro-morphodynamic processes in the swash zone and thus not able to adequately reproduce the observed bed level changes in the upper shoreface.

Despite the above factors, that induce varying levels of uncertainty in the analysis and model performance evaluation, the performance of the examined IR methods is considered satisfactory and overall, the general morphological patters in the study area were reproduced by the numerical model. Consequently, for practical applications, where detailed wave, hydrodynamic and bed level measurements are not readily available, wave IR methods can be safely applied to significantly reduce the computational effort required by coastal area model simulations and produce reliable predictions of the coastal bed evolution in the medium term.

Conclusions

7.1. Summary and Concluding remarks

Due to the sheer amount of available offshore sea-state characteristics and the taxing levels of the required computational resources, wave Input Reduction methods are an indispensable tool for coastal engineers and scientists, desiring to obtain reliable prediction of the coastal bed evolution at an annual scale, while simultaneously reducing the required computational effort.

Several Input Reduction methods have been encountered and used in practice, the large majority of which are based on the notion that longshore sediment transport is the main parameter driving the coastal bed evolution at an annual scale. According to the literature review in Section 2.3, the following main branches (each containing several Input Reduction methods) were distinguished:

- o Binning methods
- o Clustering Algorithms
- o Representative Morphological Wave Height selection methods

A clear distinction was also made on the way the wave, flow and sediment transport models, composing a coastal area model, are coupled. When said models are directly coupled with the bathymetry updating undertaken at each morphological time step, the approach is called "Morphodynamic", whereas when each representative simulation is initialized from the same bathymetry, with no direct feedback between waves-hydrodynamics and morphology, the approach followed is called "Morphostatic". Each approach has different implications on the results and the computational efficiency of the wave Input Reduction methods selected. The present thesis focused on expanding and proposing enhancements to all three branches of wave Input Reduction achieving to both (a) accelerate morphological modelling and (b) improve model results. Furthermore, through the thorough intercomparison of the several alternative wave Input Reduction methods, practical guidelines and initial recommendations were given on the optimal method of each branch. Importantly, the best performing methods are validated against available field measurements of bed elevation.

In the context of this thesis, a novel approach to the classical Binning Input Reduction methods was presented, based on the elimination of sea-states considered unable to initiate sediment motion. Based on this notion, two binning Input Reduction methods

were developed and tested, the Pick-up rate method and Threshold Current method. Both methods were tested in the coastal area of the port of Rethymno, Greece and simulations were performed with the MIKE21 CM FM coastal area model. Evaluation of the model results was undertaken by calculating the Brier Skill Score (BSS) metric (Sutherland et al., 2004a), often utilized in morphological modelling evaluation.

Overall, the main conclusions drawn from the analysis carried out for the binning Input Reduction methods can be summarised as follows:

- The Pick-up rate method led to the elimination of 57.2% of the wave records of the annual dataset of offshore sea-state characteristics and ultimately leading to the same percentage of model run-time reduction, compared to the Brute force simulation containing the full timeseries. A BSS value of 0.74 was achieved classifying the simulation as "Excellent" with regards to the BSS classification.

- The Threshold Current method exhibited a similar performance with the model run-time reduction achieving about 62 % albeit with a minor penalty in the obtained BSS, which was 0.72.

- The best performing method with regards to the morphological response compared to a Brute force simulation containing the full set of conditions was the Energy Flux method, with a BSS of 0.85. However, the model run-time reduction achieved following the "Morphodynamic" approach was only 11 %.

- When performing simulations through the "Moprhodynamic" approach implementing a form of filtering and elimination of lowly energetic sea-states can significantly reduce the required computational effort with a small compromise on the accuracy of the results. It is important to note, that in order to counterbalance the reduction of the model run time, the frequencies of occurrence of each representative, should have the same sum as the full dataset and therefore should be rescaled accordingly.

Thereafter the K-Means clustering algorithm, which has been utilized in a plethora of ocean and coastal engineering applications was thoroughly evaluated as a viable alternative to the classical binning Input Reduction methods for the prediction of annual morphological bed evolution by selecting a predefined number of representative sea-states. To overcome the unsupervised nature of the algorithm, 5 alternative configurations to the default implementation of the K-Means algorithm were examined, and the six tests in total can be vaguely divided in the following categories: (a) a default case of the algorithm with minimal user intervention (test KM-01), (b) two cases concerting binning input reduction methods with clustering techniques (test KM-02 and KM-05), (c) utilization of weights in the clustering analysis (test KM-03), (d) alteration of clustering input variables (test KM-04 and KM-06) and (e) two cases concerning the application of initial filtration of sea-states unable to induce substantial morphological changes and thus reducing the contribution of less energetic sea-states (test KM-05 and test KM-06). The six distinct tests were implemented in the study area of Rethymno port

and model evaluation was carried out by comparing the obtained BSS values in the sandy coastline adjacent to the port infrastructure.

The main conclusions drawn from the intercomparison of the alternative K-Means clustering configurations are the following:

- All the tests (KM-01 through KM-06) are classified as "Excellent" with respect to the BSS classification. Each enhancement to the default test KM-01 marginally improves the calculated scores validating the performance increase by introducing quantities responsible for the longshore sediment transport in the algorithm's iterative procedure.

- The tests were intercompared by performing simulations through the "Morphodynamic" approach and simulations times were reduced by 25-30% compared to the brute force simulation, since no filtration of the initial dataset was performed for these tests.

- For the study area in question, the KM-clustering algorithm performs slightly worse than the binning Input Reduction methods examined in Chapter 3. Additionally, most tests are inherently complex and require either the initial determination of representative conditions through binning Input Reduction methods and the utilization of an additional complementary PMS wave model developed in the framework of this thesis.

- However, in direct relation to the above, the default implementation of the K-Means algorithm showcased an "Excellent" performance requiring minimal user input and interference, hence it is recommended for application when desiring to obtain a fast yet adequately accurate prediction of the annual morphological bed evolution.

In the next step, performance evaluation and possible enhancements of the third branch of wave input reduction methods, entitled the Representative Morphological Wave Height selection methods, was carried out. These methods share similar principles with binning Input Reduction, in that they use proxy quantities to divide the tri-variate wave climate in bins, albeit the directional bins are equidistant. In total 4 alternative configurations were examined centered around the following: (a) test RMWH-01 which is the default method presented by Chonwattana et al., 2005, (b) test RMWH-02 which proposed a further subdivision in the wave heights in each directional bin, (c) test RMWH-03 where "transition" zones where longshore and cross-shore sediment transport interchangeably dominate the morphological evolution are defined and the corresponding driving proxy quantities are different on each zone and (d) a test incorporating a trained Artificial Neural Network (ANN) which eliminates sea-states that are unable to initiate sediment motion. The four distinct tests were implemented once again in the coastal area of Rethymno, Greece, and simulations were carried out with the MIKE21 CM FM model in a "Morphostatic" setting. Results for each test were compared to a Brute force simulation containing a detailed wave climate of 68 sea-states which acted as a benchmark.

The main conclusions drawn from the evaluation of the RMWH selection method of Chonwattana et al., 2005 are the following:

- The "Morphostatic" approach is significantly faster than the "Morphodynamic" simulation due to the sheer reduction of sea-states that need to be simulated. For the particular case study and coastal area model applied, simulation times were reduced by about 400-450% with respect to the corresponding ones required for the Brute force simulation.

- The default implementation of the RMWH approach (test RMWH-01) showed the worse performance compared to the other tests with a BSS value of 0.24, classifying the simulation results as "Good", albeit at the lower boundary of the range of values presented in Sutherland et al., 2004.

- The further subdivision in two wave height bins for each directional bin (test RMWH-02) is relatively simple but proved effective and significantly improved model results, classifying the simulation as "Excellent".

- Test RMWH-03 further led to a performance increase by achieving larger BSS values. However, this method is rather complex in implementation and for complex geomorphological features (highly irregular bathymetries and curved coastlines) the definition of the transition zones can vary significantly for each coastline segment.

- Test RMWH-04 showcased the best performance and since it incorporates an ANN requires minimal computational resources. The exemplary performance of said test, verifies that for both "Morphostatic" and "Morphodynamic" settings the elimination of lowly energetic sea-states can lead to improved model results with a simultaneous reduction of computational burden.

Ultimately, based on the obtained BSS values and also considering the computational efficiency of all the alternative input reduction methods examined in this thesis, one method was selected as the optimal for each branch of wave Input Reduction when executing the simulations through the "Morphostatic" approach. The Energy flux method was selected as the best binning method since it achieved the highest observed BSS, the default implementation of the K-Means clustering algorithm (KM-01) was selected out of the clustering branch since it achieved a good balance of good model performance and computational efficiency and test RMWH-04, which combined numerical modelling with the use of an ANN, was chosen since it achieved the best BSS values and was less demanding computationally due to the developed ANN. The three selected methods were then implemented and intercompared for the coastal waterfront of the Eressos beach in Lesvos Island, Greece, using as benchmark available bed elevation measurements at the area for 4 profile cross sections, extending up to the depth of closure of the particular study area. In total about 9 months of wave action were simulated using the MIKE21 CM FM coastal area model and the corresponding simulations were carried out utilizing the "Morphostatic" approach.

Overall, the main conclusions drawn from the comparison of the selected three wave input reduction methods with real-field measurements are the following:

- Given the complexity of calibrating the coastal area models for morphological bed level prediction all three methods perform in a satisfying manner achieving BSS values ranging from "Good" to "Excellent" for most cross sections.

- The best performing method was found out to be the RMWH-04 which combined the utilization of an ANN tasked with the elimination of sea-states that are unable to initiate sediment motion, followed by the Energy flux binning method. In general, all three of the methods capture the correct morphological patterns (i.e. the adequately predict the accretion at the larger part of the profile), validating the use of all three input reduction methods to predict the morphological bed evolution at an annual scale.

- The model results with all three methods consistently predict erosion at the upper shoreface which is inconsistent with the measurements which showcase accumulation of sediment at the shoreface. This discrepancy is attributed mainly to the phase-averaged wave model used as a driver which neglects the hydrodynamic and sediment transport processes in the swash zone that are vital in shaping the upper shoreface and the possibility of external supply of sediment for the particular dates from the "Chalandra" stream which outflows inside the study area. It should also be noted that this discrepancy can situationally be significantly punishing for the BSS assessment.

- Discrepancies between measurements and model results can be attributed to a wide array of factors, such as the lack of wave and current measurements to estimate the appropriate orders of magnitude, the possible influx of sediment from the external sources and the lack of wave measurements from wave buoys at the offshore boundary of the computational domain. This led to the utilization of hindcast wave prediction from the Copernicus Marine Service database which may be associated with inaccuracies compared to the real wave climate transferring these levels of inaccuracies to the numerical model simulations.

Overall, the results of this dissertation are primarily useful for coastal engineers and scientists desiring to obtain reliable and accurate predictions of coastal bed evolution at an annual scale and significantly reduce the excessive computational burden. Several wave input reduction methods were tested and compared to both a benchmark detailed Brute force simulations and available field measurements. In total, 10 new wave Input Reduction methods were conceptualized and tested, each associated with advantages, disadvantages and limitations. Considering the different tested methods and the subsequent analysis, it is concluded that filtration of sea-states that are unable to initiate sediment motion consistently led to either an outright improvement of the obtained results or to a significant model run-time reduction albeit with a small penalty in model performance. From the intercomparison of the methods with the benchmark Brute force simulations and available field measurements conducted in the framework of this thesis,

it is concluded that the optimal Input Reduction method is RMWH-04. Said method achieved both the best performance and was deemed extremely computationally efficient since it incorporates a trained ANN tasked with the elimination of lowly energetic sea-states.

7.2 Suggestions for future research

The investigation on the efficiency and capability of the wave input reduction methods for the prediction of the annual coastal bed level evolution can be further expanded and investigated. Some suggestions for future research are summarized below:

- o Implementation of the wave IR methods developed and examined in the present research in more coastal area configurations to examine if their performance is consistent.

- o For simulations conducted through the "Morphodynamic" approach, more investigation of the effect of wave chronology can be undertaken. To this end, wave input reduction methods can be realised that retain a form of sequencing (de Queiroz et al., 2019). Additionally, the effect of the morphological acceleration factor (Morfac) and how it affects the performance of wave schematization methods can be further examined. Of particular importance would be to define critical values of the Morfac, depending on the offshore wave characteristics and the geomorphological properties of the coast (e.g. sediment properties, bed slope).

- o An interesting topic would be to investigate another parameter that could possibly affect the performance of wave schematization methods, related to the "intensity" of the wave climate. For instance, it would be noteworthy to investigate whether the performance of wave IR methods, especially those introducing filtering of lowly energetic sea-states (Pick-up rate method, Threshold current method, RMWH-04) are significantly affected by the intensity and frequency of storm events on the dataset of offshore sea-state wave characteristics.

References

Afentoulis, V., Eleftheria, K., Eleni, S., Evangelos, M., Archontia, L., Christos, M., Vasiliki, T., 2017. Coastal Processes Assessment Under Extreme Storm Events Using Numerical Modelling Approaches. Environ. Process. 4, 731–747. https://doi.org/10.1007/s40710-017-0253-8

Afentoulis, V., Papadimitriou, A., Belibassakis, K., Tsoukala, V., 2022. A coupled model for sediment transport dynamics and prediction of seabed morphology with application to 1DH/2DH coastal engineering problems. Oceanologia 64, 514–534. https://doi.org/10.1016/j.oceano.2022.03.007

Afentoulis, V., Papadimitriou, A., Benoit, M., Tsoukala, V.K., 2019. Numerical Approaches for the Evaluation of Sediment Transport Mechanisms on a Shallow Sloping Sea Bottom, in: 1st International Conference DESIGN AND MANAGEMENT OF PORT, COASTAL AND OFFSHORE WORKS (DMPCO), Athens, Greece, 8 - 11 May.

Andreadis, O., 2021. Ευπάθεια στη διάβρωση Ελληνικών νησιωτικών παραλιών: Παραδείγματα από τη Λεσβο και Χίο (in greek). University of the Aegean. Mytilene, Greece

Andreadis O, Hasiotis T, Psarros F, Chatzipavlis A, Velegrakis A, 2017. Erosion and sediment transport processes along Eresos coastal zone (Lesvos, Greece), in: 15th International Conference on Environmental Science and Technology. Rhodes, Greece, 31 August-2 September 2017.

Antolínez, J.A.A., Méndez, F.J., Camus, P., Vitousek, S., González, E.M., Ruggiero, P., Barnard, P., 2016. A multiscale climate emulator for long-term morphodynamics (MUSCLE-morpho). J. Geophys. Res. Ocean. 121, 775–791. https://doi.org/10.1002/2015JC011107

Arthur, D., Vassilvitskii, S., 2007. K-means++: The advantages of careful seeding, in: Proceedings of the Annual ACM-SIAM Symposium on Discrete Algorithms. pp. 1027–1035, Philadelphia, PA, USA,.

Ashton, A.D., Murray, A.B., 2006a. High-angle wave instability and emergent shoreline shapes: 1. Modeling of sand waves, flying spits, and capes. J. Geophys. Res. Earth Surf. 111, 4011. https://doi.org/10.1029/2005JF000422

Ashton, A.D., Murray, A.B., 2006b. High-angle wave instability and emergent shoreline shapes: 2. Wave climate analysis and comparisons to nature. J. Geophys. Res. Earth Surf. 111. https://doi.org/10.1029/2005JF000423

Bailard, J.A., 1985. Simplified Model For Longshore Sediment Transport., in: Proceedings of the Coastal Engineering Conference. ASCE, pp. 1454–1470. https://doi.org/10.9753/icce.v19.99

Bailard, J.A., 1981. An energetics total load sediment transport model for a plane sloping beach. J. Geophys. Res. Ocean. 86, 10938–10954. https://doi.org/10.1029/JC086IC11P10938

Baldock, T.E., Holmes, P., Bunker, S., Van Weert, P., 1998. Cross-shore hydrodynamics within an unsaturated surf zone. Coast. Eng. 34, 173–196. https://doi.org/10.1016/S0378-3839(98)00017-9

Balzano, A., 1998. Evaluation of methods for numerical simulation of wetting and drying in shallow water flow models. Coast. Eng. 34, 83–107. https://doi.org/10.1016/S0378-3839(98)00015-5

Battjes, J.A., Janssen, J.P.F.M., 1979. Energy Loss and Set-Up Due To Breaking of Random Waves. Proc. Coast. Eng. Conf.Hamburg,Germany, 27 August - 3 September.

Benedet, L., Dobrochinski, J.P.F., Walstra, D.J.R., Klein, A.H.F., Ranasinghe, R., 2016. A morphological modeling study to compare different methods of wave climate schematization and evaluate strategies to reduce erosion losses from a beach nourishment project. Coast. Eng. 112, 69-86. https://doi.org/10.1016/j.coastaleng.2016.02.005

Benoit, M., Marcos, F., Becq, F., 1997. TOMAWAC: A prediction model for offshore and

nearshore storm waves, in: Proceedings of the Congress of the International Association of Hydraulic Research, IAHR, San Francisco, CA, United States, August 10-15.

Benoit, M., Marcos, F., Becq, F., 1996. Development of a third generation shallow-water wave model with unstructured spatial meshing, in: Proceedings of the Coastal Engineering Conference, Orlando, FL, USA, 2–6 September

Bezdek, J.C., 1981. Pattern Recognition with Fuzzy Objective Function Algorithms, Pattern Recognition with Fuzzy Objective Function Algorithms. Springer US. https://doi.org/10.1007/978-1-4757-0450-1

Borah, D.K., Balloffet, A., 1985. Beach Evolution Caused by Littoral Drift Barrier. J. Waterw. Port, Coastal, Ocean Eng. 111, 645–660. https://doi.org/10.1061/(ASCE)0733-950X(1985)111:4(645)

Bosboom, J., Stive, M.J.F., 2022. Coastal Dynamics, TU Delft Open. https://doi.org/10.5074/T.2021.001

Brown, J.M., Davies, A.G., 2009. Methods for medium-term prediction of the net sediment transport by waves and currents in complex coastal regions. Cont. Shelf Res. 29, 1502–1514. https://doi.org/10.1016/j.csr.2009.03.018

Camus, P., Mendez, F.J., Medina, R., Cofiño, A.S., 2011. Analysis of clustering and selection algorithms for the study of multivariate wave climate. Coast. Eng. 58, 453–462. https://doi.org/10.1016/j.coastaleng.2011.02.003

Cayocca, F., 2001. Long-term morphological modeling of a tidal inlet: The Arcachon Basin, France. Coast. Eng. 42, 115–142. https://doi.org/10.1016/S0378-3839(00)00053-3

Chondros, M., Metallinos, A., Papadimitriou, A., Tsoukala, V., 2022. Sediment Transport Equivalent Waves for Estimating Annually Averaged Sedimentation and Erosion Trends in Sandy Coastal Areas. J. Mar. Sci. Eng. 2022, 10, 1726. https://doi.org/10.3390/JMSE10111726

Chondros, M.K., Metallinos, A.S., Memos, C.D., Karambas, T. V., Papadimitriou, A.G., 2021. Concerted nonlinear mild-slope wave models for enhanced simulation of coastal processes. Appl. Math. Model. 91, 508–529. https://doi.org/10.1016/j.apm.2020.08.027

Chonwattana, S., Weesakul, S., Vongvisessomjai, S., 2005. 3D modeling of morphological changes using representative waves. Coast. Eng. J. 47, 205–229. https://doi.org/10.1142/S0578563405001240

Dally, W.R., Dean, R.G., 1984. Suspended Sediment Transport and Beach Profile Evolution. J. Waterw. Port, Coastal, Ocean Eng. 110, 15–33. https://doi.org/10.1061/(ASCE)0733-950X(1984)110:1(15)

Dalrymple, R.A., 1992. Prediction of StormNormal Beach Profiles. J. Waterw. Port, Coastal, Ocean Eng. 118, 193–200. https://doi.org/10.1061/(ASCE)0733-950X(1992)118:2(193)

Dalrymple, R.A., Kirby, J.T., 1988. Models for very wide-angle water waves and wave diffraction. J. Fluid Mech. 201, 299–322. https://doi.org/10.1017/S0022112088001776

de Queiroz, B., Scheel, F., Caires, S., Walstra, D.J., Olij, D., Yoo, J., Reniers, A., de Boer, W., 2019. Performance evaluation of wave input reduction techniques for modeling inter-annual sandbar dynamics. J. Mar. Sci. Eng. 7. https://doi.org/10.3390/jmse7050148

de Schipper, M.A., de Vries, S., Ruessink, G., de Zeeuw, R.C., Rutten, J., van Gelder-Maas, C., Stive, M.J.F., 2016. Initial spreading of a mega feeder nourishment: Observations of the Sand Engine pilot project. Coast. Eng. 111, 23–38. https://doi.org/10.1016/J.COASTALENG.2015.10.011

de Vriend, H.J., Zyserman, J., Nicholson, J., Roelvink, J.A., Péchon, P., Southgate, H.N., 1993. Medium-term 2DH coastal area modelling. Coast. Eng. https://doi.org/10.1016/0378-3839(93)90050-I

DHI, 2023. LITPACK FM.User Guide. Copenhagen, Denmark.

DHI, 2017. MIKE21 PMS User Guide. Copenhagen, Denmark.

DHI, 2014. Coupled Model FM (MIKE 21/3 FM). User Guide. Copenhagen, Denmark.

DHI, 2009a. Spectral Wave Module Scientific Documentation. Copenhagen, Denmark.

DHI, 2009b. Flow Model FM Sand Transport Module Scientific Documentation. Copenhagen, Denmark.

Dodd, N., Blondeaux, P., Calvete, D., De Swart, H.E., Falqués, A., Hulscher, S.J.M.H., Rózyński, G., Vittori, G., 2003. Understanding Coastal Morphodynamics Using Stability Methods. J. Coast. Res. 19, 849–865.

EDF-R&D, 2009. ARTEMIS User Manual.

Ester, M., Kriegel, H.-P., Sander, J., Xu, X., 1996. A Density-Based Algorithm for Discovering Clusters in Large Spatial Databases with Noise, in: Proceedings of the 2nd International

Conference on Knowledge Discovery and Data Mining. pp. 226–231, Portland Oregon August 2 - 4.

Fairley, I., Lewis, M., Robertson, B., Hemer, M., Masters, I., Horrillo-Caraballo, J., Karunarathna, H., Reeve, D.E., 2020. A classification system for global wave energy resources based on multivariate clustering. Appl. Energy 262, 114515. https://doi.org/10.1016/j.apenergy.2020.114515

Gad, F.-K., Hatiris, G.-A., Loukaidi, V., Dimitriadou, S., Drakopoulou, P., Sioulas, A., Kapsimalis, V., 2018. Long-Term Shoreline Displacements and Coastal Morphodynamic Pattern of North Rhodes Island, Greece. Water 10, 849. https://doi.org/10.3390/w10070849

Guha, S., Rastogi, R., Shim, K., 1998. CURE: An efficient clustering algorithm for large databases. SIGMOD Rec. 27, 73–84. https://doi.org/10.1145/276305.276312

Hanson, H., 1989. GENESIS - a generalized shoreline change numerical model. J. Coast. Res. 5, 1–27.

Hasselmann, K., Hasselmann, S., Bauer, E., Janssen, P.A.E.M., Komen, G.J., Bertotti, L., Lionello, P., Guillaume, A., Cardone, V.C., Greenwood, J.A., Reistad, M., Zambresky, L., Ewing, J.A., 1988. The WAM model - a third generation ocean wave prediction model. J. Phys. Ocean.

Hedges, T.S., 1987. An approximate model for nonlinear dispersion in monochromatic wave propagation models, by J.T. Kirby and R.A. Dalrymple. Discussion. Coast. Eng. 11, 87–89. https://doi.org/10.1016/0378-3839(87)90040-8

Hendrickx, G.G., Antolínez, J.A.A., Herman, P.M.J., 2023. Predicting the response of complex systems for coastal management. Coast. Eng. 182, 104289. https://doi.org/10.1016/j.coastaleng.2023.104289

Holthuijsen, L.H., Herman, A., Booij, N., 2003. Phase-decoupled refraction-diffraction for spectral wave models. Coast. Eng. 49, 291–305. https://doi.org/10.1016/S0378-3839(03)00065-6

Houston, J.R., 1995. Beach-fill volume required to produce specific dry beach width. Coast. Eng. Tech. Note CETN II-32, US Army Corps Eng. Waterw. Exp. Station. Vicksburg, Mississippi 32.

Ilic, S., van der Westhuysen, A.J., Roelvink, J.A., Chadwick, A.J., 2007. Multidirectional wave transformation around detached breakwaters. Coast. Eng. 54, 775–789. https://doi.org/10.1016/J.COASTALENG.2007.05.002

Janssen, T.T., Battjes, J.A., 2007. A note on wave energy dissipation over steep beaches. Coast. Eng. 54, 711–716. https://doi.org/10.1016/j.coastaleng.2007.05.006

Kamphuis, J.W., 1991a. Alongshore Sediment Transport Rate. J. Waterw. Port, Coastal, Ocean Eng. 117, 624–640. https://doi.org/10.1061/(asce)0733-950x(1991)117:6(624)

Kamphuis, J.W., 1991b. Incipient wave breaking. Coast. Eng. 15, 185–203. https://doi.org/10.1016/0378-3839(91)90002-X

Karambas, T., 2010. Study of eroding phenomena of Scala Eresos (in Greek). Mytilene, Greece.

Karambas, T. V., Koutandos, E. V., Kampanis, N.A., 2013. Numerical simulation of wave-induced morphology evolution. Proc. Inst. Civ. Eng. Marit. Eng. 166, 113–124. https://doi.org/10.1680/MAEN.07.00008

Karambas, T. V., Samaras, A.G., 2017. An integrated numerical model for the design of coastal protection structures. J. Mar. Sci. Eng. https://doi.org/10.3390/jmse5040050

Kelpšaitė-Rimkienė, L., Parnell, K.E., Žaromskis, R., Kondrat, V., 2021. Cross-shore profile evolution after an extreme erosion event—Palanga, Lithuania. J. Mar. Sci. Eng. 9, 1–15. https://doi.org/10.3390/jmse9010038

Kirby, J.T., 1986. Rational approximations in the parabolic equation method for water waves. Coast. Eng. 10, 355-378. https://doi.org/10.1016/0378-3839(86)90021-9

Kirby, J.T., Dalrymple, R.A., 1986. An approximate model for nonlinear dispersion in monochromatic wave propagation models. Coast. Eng. 9, 545-561. https://doi.org/10.1016/0378-3839(86)90003-7

Kirby, J.T., Dalrymple, R.A., 1983. A parabolic equation for the combined refraction diffraction of Stokes waves by mildly varying topography. J. Fluid Mech. 136, 453–466. https://doi.org/10.1017/S0022112083002232

Klonaris, G.T., Memos, C.D., Drønen, N.K., Deigaard, R., 2018. Simulating 2DH coastal morphodynamics with a Boussinesq-type model. https://doi.org/10.1080/21664250.2018.1462300 60, 159–179.

Knaapen, M.A.F., Joustra, R., 2012. Morphological acceleration factor : usability , accuracy and run time reductions, in: XIXth TELEMAC-MASCARET User Conference Proceedings, Oxford and Wallingford, United Kingdom, 18 - 19 October.

Komar, P., Inman, D., 1970. Longshore sand transport on beaches. J. Geophys. Res. 75, 5914–5927. https://doi.org/10.1029/jc075i030p05914

Komar, P.D., Miller, M.C., 1975. On the comparison between the threshold of sediment motion under waves and unidirectional currents with a discussion of the practical evaluation of the threshold. J. Sediment. Res. 45, 362–367. https://doi.org/10.1306/212F6D66-2B24-11D7-8648000102C1865D

Korres, G., Ravdas, M., Zacharioudaki, A., 2019. [dataset] Mediterranean Sea Waves Hindcast (CMEMSMED-Waves). https://doi.org/https://doi.org/10.25423/CMCC/MEDSEA_HINDCAST_WAV_006_012

Kraus, N.C., Larson, M., Kriebel, D.L., 1991. Evaluation of beach erosion and accretion predictors, in Proceedings of the Coastal Sediments '91 Conference. pp. 572–587.

Latteux, B., 1995. Techniques for long-term morphological simulation under tidal action. Mar. Geol. 126, 129–141. https://doi.org/10.1016/0025-3227(95)00069-B

Leont'yev, I.O., 1996. Numerical modelling of beach erosion during storm event. Coast. Eng. 29, 187–200. https://doi.org/10.1016/S0378-3839(96)00029-4

Lesser, G.R., 2009. An Approach to Medium-term Coastal Morphological Modelling. PhD thesis. Delft University of Technology, Delft, Netherlands.

Lesser, G.R., Roelvink, J.A., van Kester, J.A.T.M., Stelling, G.S., 2004. Development and validation of a three-dimensional morphological model. Coast. Eng. https://doi.org/10.1016/j.coastaleng.2004.07.014

Long, W., Kirby, J.T., Shao, Z., 2008. A numerical scheme for morphological bed level calculations. Coast. Eng. 55, 167–180. https://doi.org/10.1016/J.COASTALENG.2007.09.009

Luijendijk, A., Hagenaars, G., Ranasinghe, R., Baart, F., Donchyts, G., Aarninkhof, S., 2018. The State of the World's Beaches. Sci. Rep. 8, 1–11. https://doi.org/10.1038/s41598-018-24630-6

Luijendijk, A., Ranasinghe, R., de Schipper, M.A., Huisman, B.A., Swinkels, C.M., Walstra, D.J.R., Stive, M.J.F., 2017a. The initial morphological response of the Sand Engine: A process-based modelling study. Coast. Eng. 119, 1–14. https://doi.org/10.1016/j.coastaleng.2016.09.005

Luijendijk, A., Velhorst, R., Hoonhout, B., de Vries, S., Ranasinghe, R., 2017b. Integrated Modelling of the Morphological Evolution of the Sand Engine Mega-Nourishment, in: Proceedings of Coastal Dynamics Conference. pp. 1874–1885.

Luijendijk, A.P., de Schipper, M.A., Ranasinghe, R., 2019. Morphodynamic Acceleration Techniques for Multi-Timescale Predictions of Complex Sandy Interventions. J. Mar. Sci. Eng. 7, 78. https://doi.org/10.3390/JMSE7030078

Lynett, P.J., Wu, T.R., Liu, P.L.F., 2002. Modeling wave runup with depth-integrated equations. Coast. Eng. 46, 89–107. https://doi.org/10.1016/S0378-3839(02)00043-1

MacQueen, J., 1967. Some methods for classification and analysis of multivariate observations. Proc. fifth Berkeley Symp. Math. Stat. Probab. 1, 281–297.

Martzikos, N., Afentoulis, V., Tsoukala, V., 2018. Storm clustering and classification for the port of Rethymno in Greece. Water Util. J. 20, 67–79.

Mase, H., Kirby, J.T., 1992. Hybrid frequency-domain KdV equation for random wave transformation, in: Proceedings of the Coastal Engineering Conference, pp. 474–487. https://doi.org/10.1061/9780872629332.035

Mase, H., Takayama, T., Kitano, T., 2001. Spectral Wave Transformation Model with Wave Diffraction Effect. Proceedings of the International Symposium of Ocean Wave Meaurements and Analysis 1, 814–823. https://doi.org/10.1061/40604(273)83

Miche, M., 1951. Le pouvoir réfléchissant des ouvrages maritimes exposés à l'action de la houle (in French). Technical Report, Annales de Ponts et Chaussées.

Mil-Homens, J., Ranasinghe, R., van Thiel de Vries, J.S.M., Stive, M.J.F., 2013. Re-evaluation and improvement of three commonly used bulk longshore sediment transport formulas. Coast. Eng. 75, 29–39. https://doi.org/10.1016/J.COASTALENG.2013.01.004

Munkres, J., 1957. Algorithms for the Assignment and Transportation Problems. J. Soc. Ind. Appl. Math. 5, 32–38. https://doi.org/10.1137/0105003

Nicholson, J., Broker, I., Roelvink, J.A., Price, D., Tanguy, J.M., Moreno, L., 1997. Intercomparison of coastal area morphodynamic models. Coast. Eng. 31, 97–123. https://doi.org/10.1016/S0378-3839(96)00054-3

Novikov, A., 2019. PyClustering: Data Mining Library. J. Open Source Softw. 4, 1230. https://doi.org/10.21105/joss.01230

O'Reilly, W.C., Guza, R.T., 1991. Comparison of spectral refraction and refraction-diffraction wave models. J. Waterw. Port, Coast. Ocean Eng. https://doi.org/10.1061/(ASCE)0733-950X(1991)117:3(199)

Olij, D.J.C., 2015. Wave climate reduction for medium term process based morphodynamic simulations with application to the Durban Coast. Delft University of Technology.

Ozasa, H., Brampton, A.H., 1980. Mathematical modelling of beaches backed by seawalls. Coast. Eng. 4, 47–63. https://doi.org/10.1016/0378-3839(80)90005-8

Papadimitriou, A., Chondros, M., Metallinos, A., Tsoukala, V., 2022a. Accelerating coastal bed evolution predictions utilizing Numerical Modelling and Artificial Neural Networks, in: 7th IAHR Europe Congress. pp. 159–160, Athens, Greece, 7 - 9 September.

Papadimitriou, A., Chondros, M., Metallinos, A., Tsoukala, V., 2022b. Accelerating Predictions of Morphological Bed Evolution by Combining Numerical Modelling and Artificial Neural Networks. J. Mar. Sci. Eng. 10, 1621. https://doi.org/10.3390/JMSE10111621

Papadimitriou, A., Panagopoulos, L., Chondros, M., Tsoukala, V., 2020. A wave input-reduction method incorporating initiation of sediment motion. J. Mar. Sci. Eng. 8. https://doi.org/10.3390/JMSE8080597

Papadimitriou, A., Tsoukala, V., 2022. Performance evaluation of the K-Means clustering algorithm for the prediction of annual bed morphological evolution, in: 7th IAHR Europe Congress. pp. 161–162, Athens, Greece, 7 - 9 September.

Pedregosa, F., Michel, V., Grisel, O., Blondel, M., Prettenhofer, P., Weiss, R., Vanderplas, J., Cournapeau, D., Pedregosa, F., Varoquaux, G., Gramfort, A., Thirion, B., Grisel, O., Dubourg, V., Passos, A., Brucher, M., Perrot, Édouardand, M., Duchesnay, A. 2011. Scikit-learn: Machine Learning in Python. JMLR 12, 2825-2830.

Pelnard-Considère, R., 1957. Essai de théorie de l'évolution des formes de rivage en plages de sable et de galets (in French). Journées de l'hydraulique 4, 289–298.

Pletcha, S., Sancho, F., Silva, P., Dias, J.M., 2007. Representative Waves for Morphological Simulations. J. Coast. Res. 995–999.

Prasad, R.S., Svendsen, I.A., 2003. Moving shoreline boundary condition for nearshore models. Coast. Eng. 49, 239–261. https://doi.org/10.1016/S0378-3839(03)00050-4

Ranasinghe, R., Swinkels, C., Luijendijk, A., Roelvink, D., Bosboom, J., Stive, M., Walstra, D.J., 2011. Morphodynamic upscaling with the MORFAC approach: Dependencies and sensitivities. Coast. Eng. 58, 806-811. https://doi.org/10.1016/j.coastaleng.2011.03.010

Roelvink, D., Reniers, A., 2011. A guide to modeling coastal morphology, Advances in Coastal and Ocean Engineering. World Scientific, Singapore, Singapore. https://doi.org/10.1142/9789814304269

Roelvink, J.A., 2006. Coastal morphodynamic evolution techniques. Coast. Eng. 53, 277-287. https://doi.org/10.1016/j.coastaleng.2005.10.015

Roelvink, J.A., Brøker, I., 1993. Cross-shore profile models. Coast. Eng. 21, 163–191. https://doi.org/10.1016/0378-3839(93)90049-E

Roelvink, J.A., Stive, M.F.J., 1989. Bar-generating cross-shore flow mechanisms on a beach. J. Geophys. Res. Ocean. 94, 4785–4800. https://doi.org/10.1029/JC094IC04P04785

Saltelli, A., 2002. Sensitivity Analysis for Importance Assessment. Risk Anal. 22, 579–590. https://doi.org/10.1111/0272-4332.00040

Sato, S., Mitsunobu, N., 1991. Numerical model of beach profile change due to random waves. CEJ. 34, 191-204. https://doi.org/10.1080/05785634.1991.11924549

Shields, I.A., 1936. Application of similarity principles and turbulence research to bed-load movement, U.S. Soil Conservation Service Coop. Lab., in: Ott, W.P., van Uchelen, J.C. (Eds.), (Translators), Hydrodynamics Laboratory Publication, Vol. 167. California Institute of Technology, Pasadena.

Soulsby, R., 1997. Dynamics of marine sands: a manual for practical applications. Thomas Telford, London, UK

Soulsby, R.L., Smallman, J.V., 1986. A direct method of calculating bottom orbital velocity under waves. Technical Report No SR 76; Hydraulics Research Limited: Wallingford, Oxfordshire, UK.

Soulsby, R.L., Whitehouse, R.J.., 1997. Threshold of sediment motion in coastal environments. Proc. Pacific Coasts Ports 1997 Conf, Christchurch, New Zealand, 7-11 September.

Splinter, K.D., Golshani, A., Stuart, G., Tomlinson, R., 2011. Spatial and Temporal Variability of Longshore Transport Along Gold Coast, Australia. Coast. Eng. Proc. 1, 95. https://doi.org/10.9753/icce.v32.sediment.95

Steetzel, H.J., 1990. Cross-Shore Transport during Storm Surges. Proceedings of the 22nd

International Conference on Coastal Engineering, Delft, The Netherlands 2-6 July. https://doi.org/10.1061/9780872627765.147

Stive, M.J.F., Battjes, J.A., 1985. A Model for Offshore Sediment Transport. Proceedings of the 19th International Conference on Coastal Engineering, Houston, TX, United States, September 3-7. https://doi.org/10.1061/9780872624382.098

Stive, M.J.F., De Schipper, M.A., Luijendijk, A.P., Aarninkhof, S.G.J., Van Gelder-Maas, C., Van Thiel De Vries, J.S.M., De Vries, S., Henriquez, M., Marx, S., Ranasinghe, R., 2013. A new alternative to saving our beaches from sea-level rise: The sand engine. J. Coast. Res. 29, 1001–1008. https://doi.org/10.2112/JCOASTRES-D-13-00070.1

Stripling, S., Panzeri, M., 2015. Modelling shoreline evolution to enhance flood risk assessment. Proceedings of the Institution of Civil Engineers-Maritime Engineering Conference, 162, 137–144. https://doi.org/10.1680/MAEN.2009.162.3.137

Sutherland, Peet, A.., Soulsby, R.L., 2004a. Evaluating the performance of morphological models. Coast. Eng. 51, 917–939.

Sutherland, Walstra, D.J.R., Chesher, T.J., van Rijn, L.C., Southgate, H.N., 2004b. Evaluation of coastal area modelling systems at an estuary mouth. Coast. Eng. 51, 119–142. https://doi.org/10.1016/j.coastaleng.2003.12.003

Swart, D.H., 1974. Offshore sediment transport and equilibrium beach profiles. Ph.D. Thesis, Delft University of Technology, Delft, Netherlands.

Szmytkiewicz, M., Biegowski, J.X., Kaczmarek, L.M., Okrój, T., Ostrowski, R.X., Pruszak, Z., Różyńsky, G., Skaja, M., 2000. Coastline changes nearby harbour structures: comparative analysis of one-line models versus field data. Coast. Eng. 40, 119–139. https://doi.org/10.1016/S0378-3839(00)00008-9

Tonnon, P.K., Huisman, B.J.A., Stam, G.N., van Rijn, L.C., 2018. Numerical modelling of erosion rates, life span and maintenance volumes of mega nourishments. Coast. Eng. 131, 51–69. https://doi.org/10.1016/J.COASTALENG.2017.10.001

Tsiaras, A.-C., Karambas, T., Koutsouvela, D., 2020. Design of Detached Emerged and Submerged Breakwaters for Coastal Protection: Development and Application of an Advanced Numerical Model. J. Waterw. Port, Coastal, Ocean Eng. 146, 04020012. https://doi.org/10.1061/(asce)ww.1943-5460.0000566

USACE, 1984. Shore protection manual. Dept. of the Army, Waterways Experiment Station, Corps of Engineers, Coastal Engineering Research Center, Vicksburg, Missouri.

Van Duin, M.J.P., Wiersma, N.R., Walstra, D.J.R., Van Rijn, L.C., Stive, M.J.F., 2004. Nourishing the shoreface: observations and hindcasting of the Egmond case, The Netherlands. https://doi.org/10.1016/j.coastaleng.2004.07.011

van Rijn, L.C., 2007. Unified View of Sediment Transport by Currents and Waves. II: Suspended Transport. J. Hydraul. Eng. 133, 668–689. https://doi.org/10.1061/(ASCE)0733-9429(2007)133:6(668)

van Rijn, L.C., 1986. Sediment pick-up functions. Applications of sediment pick-up function. DELFT, NETHERLANDS, DELFT Hydraul. LAB., OCT. 1986.

van Rijn, L.C., 1984. Sediment Pick-Up Functions. J. Hydraul. Eng. 110, 1494–1502. https://doi.org/10.1061/(ASCE)0733-9429(1984)110:10(1494)

van Rijn, L.C., Bisschop, R., Rhee, C. van, 2019. Modified Sediment Pick-Up Function. J. Hydraul. Eng. 145, 06018017. https://doi.org/10.1061/(ASCE)HY.1943-7900.0001549

van Rijn, L.C., Wasltra, D.J.R., Grasmeijer, B., Sutherland, J., Pan, S., Sierra, J.P., 2003. The predictability of cross-shore bed evolution of sandy beaches at the time scale of storms and seasons using process-based profile models. Coast. Eng. 47, 295–327. https://doi.org/10.1016/S0378-3839(02)00120-5

Velegrakis, A.F., Vousdoukas, M.I., Andreadis, O., Adamakis, G., Pasakalidou, E., Meligonitis, R., Kokolatos, G., 2008. Influence of dams on downstream beaches: Eressos, Lesbos, Eastern Mediterranean. Mar. Georesources Geotechnol. 26, 350–371. https://doi.org/10.1080/10641190802425598

Vilsmeier, R., Hänel, D., 1996. Adaptive solutions for unsteady laminar flows on unstructured grids. Int. J. Numer. Methods Fluids 22, 85–101. https://doi.org/10.1002/(SICI)1097-0363(19960130)22:2<85::AID-FLD264>3.0.CO;2-M

Vincent, C.L., Briggs, M.J., 1989. Refraction—diffraction of irregular waves over a mound. J. Waterw. Port, Coast. Ocean Eng. https://doi.org/10.1061/(ASCE)0733-950X(1989)115:2(269)

Vongvisessomjai, S., Chowdhury, S.H., Huq, M.A., 1993. Monitoring of shoreline and seabed of Map Ta Phut port. AIT Research Report No. 262, Bangkok, Thailand.

Vousdoukas, M.I., Almeida, L.P., Ferreira, Ó., 2011. Modelling storm-induced beach morphological change in a meso-tidal, reflective beach using XBeach, J. of Coast.Res., 1916–1920.

Walstra, D.J.R., Hoekstra, R., Tonnon, P.K., Ruessink, B.G., 2013. Input reduction for long-term morphodynamic simulations in wave-dominated coastal settings. Coast. Eng. https://doi.org/10.1016/j.coastaleng.2013.02.001

Watanabe, A., Dibajnia, M., 1988. Numerical modelling of nearshore waves, cross-shore sediment transport and beach profile change, in: IAHR Symposium on Mathematical Modelling of Sediment Transport in the Coastal Zone. Copenhagen, Denmark, May 30-June 1.

Weggel, J.R., 1972. Maximum Breaker Height for Design. Coast. Eng. Proc. 1, 21. https://doi.org/10.9753/icce.v13.21

Zhao, Y., Anastasiou, K., 1993. Economical random wave propagation modelling taking into account non-linear amplitude dispersion. Coast. Eng. 20, 59-83. https://doi.org/10.1016/0378-3839(93)90055-D

Appendix

In the present thesis several numerical codes have been developed in the Fortran and python programming languages. The following Table A.1 presents the majority of these codes.

Table A.1
Developed numerical codes/scrips

No	Name	Description
1	spejon.f	Subroutine to generate wave components for a Jonswap wave spectrum in PMS-SP model
2	PR.f	Calculation of representative wave conditions with the Pick-up Rate Input Reduction method
3	EF.f	Calculation of representative wave conditions with the Energy Flux Input Reduction method
4	KM-01.py	Calculation of representative wave conditions with the KM-01 Input Reduction method
5	KM-02.py	Calculation of representative wave conditions with the KM-02 Input Reduction method
6	KM-03.py	Calculation of representative wave conditions with the KM-03 Input Reduction method
7	KM-04.py	Calculation of representative wave conditions with the KM-04 Input Reduction method
8	KM-05.py	Calculation of representative wave conditions with the KM-05 Input Reduction method
9	KM-06.py	Calculation of representative wave conditions with the KM-06 Input Reduction method
10	RMWH-01.f	Calculation of representative wave conditions with the RMWH-01 Input Reduction method
11	RMWH-02.f	Calculation of representative wave conditions with the RMWH-02 Input Reduction method
12	RMWH-03.f	Calculation of representative wave conditions with the RMWH-03 Input Reduction method
13	RMWH-04.f	Calculation of representative wave conditions with the RMWH-04 Input Reduction method